Design of the Calibration Trajectory and 3D-Printed Warm Gas Propulsion System for an Auxiliary CubeSat for the NASA JPL Europa Clipper Mission

A senior design project submitted in partial fulfillment of the requirements for the degree of Bachelor of Science at Harvard University

Jaxson Hill
S.B. Degree Candidate in Mechanical Engineering

Jason Martel
S.B. Degree Candidate in Mechanical Engineering

Faculty Advisor: Dr. Frank Keutsch
Advisor: Adrian Arteaga Garcia
Thesis Reader: Dr. Frank Keutsch

Harvard John A. Paulson School of Engineering and Applied Sciences
Allston, MA

March, 2023

Table of Contents

Acknowledgements **1**
Abstract **2**
List of Figures **3**
List of Tables **6**
1. Introduction **7**
1.1. Context and Motivation 7
1.1.1. CubeSat History 7
1.1.2. Europa Clipper Background 8
1.1.3. Previous CaliPER Work 9
2. Background Research **10**
2.1. CubeSat Propulsion 10
2.1.1. Propulsion Theory 10
2.1.1.1. Propulsion Physics Summary 10
2.1.1.2. Isentropic Flow 12
2.1.2. Types of Propulsion 16
2.1.2.1. Chemical Propulsion 16
2.1.2.2. Electric Propulsion 17
2.1.2.3. Cold Gas Propulsion 18
2.2. Past Missions 18
2.2.1. MarCO 18
2.2.2. Lunar Flashlight 19
2.2.3. Bevo-2 20
2.2.4. INSPIRE 22
2.2.5. BioSentinel 23
2.2.6. SunRISE 24
3. Design Goals and Technical Specifications **26**
3.1. Verification Standards 26
3.2. Mission Design Independent Requirements, Justifications, and Verification Plan 26
3.3. Propulsion System Requirements, Justifications, and Verification Plan 30
3.3.1. Design Independent Technical Specifications 30
3.3.2. Design Dependent Technical Specifications 34
4. Mission Design **36**
4.1. Mission Overview 36
4.2. Trajectory Planning 38
4.2.1. Deployment Phase Design 38
4.2.2. Chase Phase Design 39
4.2.3. Calibration Path Planning 39
4.2.4. Disposal Phase 41

4.2.5. Other Delta-V Expenditures 41
4.3. Delta-V Budget 42
5. Propulsion System Design 43
5.1. System Overview 43
5.1.1. System Selection 43
5.1.2. Propellant Considerations 44
5.1.3. System Map 46
5.1.4. Manufacturing Methods 47
5.2. Mechanical Design 48
5.2.1. Body Design 48
5.2.1.1. Body Overview 48
5.2.1.2. Internal Storage Tank and Tubing 49
5.2.1.3. Body to Bus Integration 51
5.2.1.4. Exclusion Zones 52
5.2.2. Nozzles 53
5.2.2.1. Nozzle Design 53
5.2.2.2. Nozzle Placement 58
5.2.3. Flow Control 61
5.2.3.1. Port-Manifold Interface 61
5.2.3.2. Valve Selection 62
5.2.3.3. Valve Assembly 62
5.2.3.4. Fill Valve 64
5.2.4. Thermal Consideration 64
5.2.4.1. Thermal Expansion 64
5.2.4.2. Propellant Heating 65
5.3. Electrical Design 66
5.3.1. Control System 66
5.3.2. Additional Electrical Component Selection 67
5.3.2.1. Pressure Sensor 67
5.3.2.2. Wire Passthrough 68
5.3.2.3. Temperature Sensor 69
5.3.2.4. Heater selection 69
5.3.3. Power 70
5.4. Overall Size 71
6. Build 73
6.1. Building Constraints 73
6.1.1. 3D Printing Material and Capabilities 73
6.1.2. Budget 73
6.1.3. Propellant 73

6.2. Prototype Build 74
6.2.1. Test Propellant Selection 74
6.2.2. Test 3D Printing Material and Methodology 74
6.2.3. Alternate COTS Components 74
6.2.3.1. Valves 74
6.2.3.2. Pressure Sensor 75
6.2.3.3. Temperature Sensor 76
6.2.3.4. Heater 76
6.2.4. CAD 77
6.2.4.1. Test Body Design 77
6.2.4.2. Test Nozzles Design 79
6.2.4.3. Complete Test Assembly 80
6.3. Build Execution 81
6.3.1. Manifolds 81
6.3.2. 3D Print 82
6.3.3. Assembly 84
6.3.4. Leaks 85
6.3.5. Propellant Loading 88
7. Test **90**
7.1. Overview 90
7.2. Data Collection Methodology and Basic Set Up 90
7.3. Testing 93
7.3.1. Test 1: Benchtop Single Nozzle 93
7.3.1.1. Summary and Setup 93
7.3.1.2. Measurements 93
7.3.1.3. Procedure 94
7.3.2. Test 2: Benchtop Dual-Nozzle 94
7.3.2.1. Summary and Setup 94
7.3.2.2. Measurements 95
7.3.2.3. Procedure 95
7.3.3. Test 3: Prototype Single Nozzle 96
7.3.3.1. Summary and Setup 96
7.3.3.2. Measurements 97
7.3.3.3. Procedure 97
7.3.4. Test 4: Prototype Quad-Nozzle 98
7.3.4.1. Summary and Setup 98
7.3.4.2. Measurements 98
7.3.4.3. Procedure 99
7.3.5. Test 5: Prototype Quad-Nozzle Long Duration 99

7.3.5.1. Summary and Setup 99
7.3.5.2. Measurements 99
7.3.5.3. Procedure 99
8. Results and Analysis 100
8.1. Specific Impulse 100
8.2. Dual Nozzle Tests 105
8.3. Long Duration Thrust over Time 108
8.4. Sources of Error 112
8.4.1. Manufacturing Errors and Leaks 112
8.4.2. Human Error 113
8.4.3. Scale Errors 114
8.4.4. Propulsion System Behavior 115
9. Tech Spec Verification 117
9.1. Mission Design Independent Tech Specs 117
9.1.1. MR1 118
9.1.2. MR2 118
9.1.3. MR3 118
9.1.4. MR4 118
9.1.5. MR5 118
9.1.6. MR6 118
9.2. Propulsion System Design Independent Tech Specs 119
9.2.1. PR1.1 119
9.2.2. PR1.2 120
9.2.3. PR1.3 120
9.2.4. PR1.4 120
9.2.5. PR1.5 120
9.2.6. PR1.6 120
9.2.7. PR1.7 120
9.2.8. PR1.8 120
9.2.9. PR1.9 121
9.2.10. PR1.10 121
9.2.11. PR1.11 121
9.3. Propulsion System Design Dependent Tech Specs 121
9.3.1. PR2.1 122
9.3.2. PR2.2 122
9.3.3. PR2.3 122
9.3.4. PR2.4 122
9.3.5. PR2.5 122
10. Conclusion and Future Work 123

10.1. Future Work 123
10.1.1. Discovered Issues 123
10.1.1.1. Propellant Loading 123
10.1.1.2. Testing Parameters 123
10.1.1.3. Measurement Strategy 124
10.1.1.4. Fluid Issues 124
10.1.2. Expanding Project Scope 125
10.1.2.1. Orbit Analysis 125
10.1.2.2. Thermal 126
10.1.2.3. Controls 126
10.1.2.4. Mechanical Optimization 127
10.2. Impact and Conclusion 127
11. References **129**
12. Appendix **132**
A. Delta-V Budget Calculations 132
B. Thrust and Delta-V Relationship 136
C. Isentropic Flow Analytical Modeling 137
D. Test Arduino Code 145
E. Budget 155
F. Non-Technical Considerations 158
G. Product Data Sheets 159

Acknowledgements

The work of this project could not have been accomplished without the immense support of so many friends, families, coworkers, and more.

Thank you to all those who advised our project, including Elaine Kristant, Benjamin Brown, Adrian Arteaga Garcia, Steve Cortesa, Hanna Quigley, Joe Kile, Ted Sirota, Dr. Panahi, Prof. Wordsworth

A special thanks to the rest of the ES100 JPL team for being such amazing teammates and making this project as enjoyable as it could be: Kian Abbot, Richard Amankwaa, David Andrade, Adam McMullin, Grace Kim, Jeff Short, Jonathan Collins, Jack Goodwin, Kaylee Cornelius, Will Sorensen.

Thank you to all of the ES100 teaching staff for supporting all of students as we navigate our crazy projects, including Frank Keutsch, Salma Abu Ayyash, and Leo Gomezall

Thank you so much to all of the members of the Keutch lab who graciously gave their time to support our project and try to use their TVAC, including Craig Mascarenhas, Mike Litchfield, Marco Rivero, and John Dykema

Thank you to those we spoke to about your work as it relates to this project, including John Essmiller at JPL, David Sternberg at JPL, Terry Stevenson at NASA Ames, and Prof. Glenn Lightsey at Georgia Tech

Thank you to last year's ES100 JPL team for providing the amazing foundation for this project: Jordan Daigle, Jonathan Hintz, Matthew LoPresti, Spencer Rolland, Obinna Ejikeme, and Jacob Johnson.

Thank you so so much to all of our amazing, wonderful friends who kept each other sane and laughing through the late nights with stupid jokes, spontaneous adventures, and general tomfoolery. Everyone on the JPL team, Bianca, Tran, Ariel, Sydney, Catherine, Cloud, Megan, Mirian, Oskar, Eugene, Umar, Josh, Seb, Fouzia, Dakota, and so many more. You are so special to us.

An extra special thank you to my partner in crime, Jason! Thank you for being the best friend, partner, fireman carrier, and eater of popcorn around. This project would not have been the same without you. - Jaxson

No, thank you! Throughout this entire process, you've somehow managed to keep us on track while also making every single work session an absolute blast with your upbeat attitude. I really couldn't have asked for a better project partner or friend. - Jason

Abstract

NASA Jet Propulsion Laboratory (JPL) is developing Europa Clipper, a spacecraft intent on studying the inner structure of Europa for signs of life. One of its primary instruments, the Radar for Europa Assessment and Sounding: Ocean to Near-surface (REASON) Antenna, is extremely difficult to calibrate on Earth, and consequently must be calibrated while en route to Jupiter by a small, auxiliary satellite.

In Spring 2022, ES100 students proposed a Cube Satellite (CubeSat) mission, dubbed Calibration Post-Earth for REASON (CaliPER), to perform this calibration while en route. This report proposes a 3D-printed warm gas propulsion system to accomplish CaliPER mission objectives. Initial test results for specific impulse and thrust agree with theoretical predictions, which therefore support the theoretical success and performance of the full 56 m/s delta-V propulsion system. Further testing and iteration is required to produce a flight capable unit, and this report lays the foundation for this design and supports its validity.

List of Figures

1.1: Length of Europa Clipper compared to a basketball court
2.1: Various propulsion technologies plotted on a thrust vs specific impulse graph
2.2: Block diagram of the MarCO Micropulsion System
2.3: Comparison of three possible Lunar Flashlight propulsion systems
2.4: Characteristic propulsion values for the Bevo-2 satellite
2.5: System map of the Bevo-2 propulsion system
2.6: Two iterations of the Bevo-2 propulsion system
2.7: INSPIRE thruster flight units prior to delivery
2.8: INSPIRE engineering design unit with manifold and valves highlighted
2.9: A cross section of the BioSentinel propulsion system.
2.10: The SunRISE propulsion system
2.11: The valve manifold system developed by researchers in Glenn Lightsey's lab
3.1: Representation of points ±60° with respect to Clipper for Calibration
4.1: Clipper launch trajectory
4.3a: "Connected Cross" calibration path
4.3b: Front view of calibration trajectory
5.1: Various propulsion technologies plotted on a thrust vs specific impulse graph
5.2: System diagram of propulsion system
5.3: Full Propulsion system CAD
5.4: Cross sectional view of propulsion system CAD
5.5a: Isometric view of the internal volume of the storage tank
5.5b: Isometric view of the isolated negative volume of the storage tank
5.6a: Section view of FEA stress results
5.6b: Section view of FEA stress results, opposite view to 5.6a
5.7: Cross sectional and translucent view of the body, displaying internal tubing
5.8: CAD of the propulsion system and the bus
5.9: Body exclusion zones
5.10: Illustration of a simple converging-diverging nozzle
5.11: Illustration of common nozzle types
5.12: Data on conical and bell-shaped nozzles
5.13: Graph of Isp and delta-V vs Area Ratio
5.14: Graph of the derivative of Isp vs Area Ratio
5.15: Cross section of nozzle
5.16: Location of all 8 nozzles
5.17: Nozzles fired for +Z axial motion
5.18: Nozzles fired for +X rotation
5.19: Nozzles fired for +Y rotation
5.20: Nozzles fired for -Z rotation

5.21: Diagram of a port
5.22: Transparent manifold over port
5.23: Chosen solenoid valve
5.24a: Side section view of the outlet manifold
5.24b: Top section view of connector manifold
5.25: Flow Diagram of Valve Assembly
5.26: Fill valve and manifold
5.27: COMSOL stress results for thermal expansion of plastic into steel
5.28: Graph of thrust and temp vs time
5.29: CAD of the wire passthrough, pressure transducer, fill valve, and manifolds
5.30: Chosen pressure transducer near a pencil
5.31: Wire Passthrough
5.32: RTD casing options
5.33: Polyimide Thermofoil™ Heater
5.34: Overall dimensions of propulsion system
6.1: Solenoid Valve
6.2: Pressure sensor
6.3: RTD probe
6.4: Screw-Plug Immersion Heater
6.5: Test body
6.6: Cross section of test body that shows internal tubing
6.7 a: Isometric view of the internal volume of the storage tank
6.7b: Section view of the storage tank
6.8: Cross section of FEA results
6.9: Cross section of the test nozzle
6.10: CAD of test system assembly
6.11: Machining a manifold in a CNC mill
6.12: Completed manifolds
6.13: 3D print
6.14: 3D print without nozzles
6.15: Assembled test system
6.16: Crack in the system
6.17: Crack misses the storage tank
6.18: Hot glue in storage tank
6.19: Finding leaks with bubbles
6.20: Storage tank gauge pressure vs time
6.21: Propellant loading setup
6.22: Liquid propellant in storage tank
7.1: Five loading cases on the OHAUS TAJ 4001 scale
7.2: Electrical wiring diagram of Arduino MKR Zero

7.3: 3D-Printed nozzle for benchtop testing
7.4: Test 1 setup with all major components labeled
7.5: Dual-nozzle set up for Test 2
7.6: Added inline manual shut-off valve
7.7: Labeled test setup for Test 3
7.8: Labeled test rig setup for Test 3
7.9: Test rig set up for Test 4 with all nozzles connected
8.1: Distribution of calculated specific impulse values from n = 243 trials
8.2: Distribution of calculated specific impulse values from n = 156 benchtop trials.
8.3: Distribution of calculated specific impulse values from n = 87 test rig trials.
8.4a: A representative thrust vs time trial from a quad-nozzle test rig test
8.4b: A representative thrust vs time trial from a single nozzle benchtop test.
8.5a: All trials from Set 1 of Test 1 Nozzle 4
8.5b: All trials from Set 2 of Test 1 Nozzle 4
8.6: Distribution of calculated specific impulse values from n = 69 filtered trials.
8.7: Average peak normalized thrust
8.8: Average peak normalized thrust
8.9: Average peak normalized thrust
8.10: Ratio of the average peak normalized thrust
8.11: Thrust and Temperature vs time
8.12: Pressure and thrust data
8.13: Pressure and thrust data
8.14: Pressure and thrust data
8.15: Pressure and thrust data
8.16: Pressure and thrust data
8.17: Pressure and thrust data
8.18: Propellant canister mass data
8.19: Sputtering of a nozzle

List of Tables

4.1: Delta-V Budget
5.1: A comparison of the properties of various propellants
5.2: Table of predicted thrust values for given temperatures
5.3: Estimated power budget

1. Introduction

1.1. Context and Motivation

NASA Jet Propulsion Laboratory (JPL) is developing Europa Clipper, a spacecraft intent on studying the inner structure of Europa, one of the Galilean moons of Jupiter, for signs of life. One of its primary instruments, the Radar for Europa Assessment and Sounding: Ocean to Near-surface (REASON) Antenna, is extremely difficult to calibrate on Earth, and consequently must be calibrated while en route to Jupiter. However, Clipper cannot easily face back toward Earth for this calibration without risking radiation and thermal damage to the internal hardware. Therefore, an alternative calibration method is needed.

In Spring 2022, ES100 students proposed a Cube Satellite (CubeSat) mission, dubbed Calibration Post-Earth for REASON (CaliPER), to perform this calibration while en route. This year, eleven ES100 students were tasked with designing, prototyping, and testing individual subsystems to achieve the proposed mission requirements. In order to collect the necessary calibration data for REASON, CaliPER must have the ability to maneuver through space relative to Clipper. This two-person subteam was tasked with determining the calibration and chase trajectory and designing a propulsion system to enable CaliPER to follow said trajectory.

1.1.1. CubeSat History

CubeSats are a highly standardized class of nanosatellite, typically with a mass between 1 kg and 20 kg. CubeSats come in standard “U” sizes, with 1U defined as a 10 cm x 10 cm x 10 cm cube typically weighing less than 1.33 kg. Due to the standardization and modularity of design, CubeSats can be developed in a range of U sizes by attaching individual cubes together. Typically, CubeSats will be designed to 1U, 2U, 3U, or 6U sizes, though more specific mission requirements may demand CubeSats in a 12U or 24U configuration.

The CubeSat standard was collaboratively developed by Prof. Jordi Puig-Suari at California Polytechnic State University and San Luis Obispo and Prof. Bob Twiggs at Stanford University’s Space Systems Development Laboratory (SSDL) in an effort to help make Low Earth Orbit (LEO) satellite missions cheaper, more accessible, and have a shorter development time. Their result was the release of a design standard document in 1999 by which satellites could be designed, built, and tested on a budget between 5 and 7 figures, rather than the typical NASA satellite mission that could cost in the tens or hundreds of millions of dollars. Between 1999 and August 2022, there have been nearly 1900 CubeSats launches to date, with hundreds more in the works [1]. The CubeSat design standard has enabled universities and even undergraduate students to access space and deliver high-risk, low-cost payloads to launch providers.

As CubeSats have gained more usage since their inception in 1999 [2], their missions

have become more and more complex and many now require more advanced propulsion systems to meet orbital and trajectory requirements. As recently as 2018, the first interplanetary CubeSat mission was successfully carried out by NASA JPL to support the InSight lander on Mars. As will be discussed in further detail in Section 2.2.1, these two interplanetary CubeSats were named MarCO-A and MarCO-B. Each used a cold gas propulsion system developed by VACCO Industries for basic orbital correction burns and attitude determination and control [3] [4] [5]. Since then, many others have flown with fully realized propulsion systems, such as the Canadian CanX-4 and CanX-5 missions [6]. Propulsion systems for general, large-scale satellites have been around almost as long as satellites have, but the compact propulsion technology used in these nanosatellites is still new and evolving as CubeSat missions grow in complexity and frequency.

1.1.2. Europa Clipper Background

Europa is one of Jupiter's moons, and the sixth-largest moon in the solar system. It is covered completely by ice, but scientists suspect that a large, salty ocean lies beneath the surface In 2012, the Hubble Space Telescope spotted what may have been a water plume erupting from Europa, further supporting the idea of liquid water's presence on the icy moon [7]. In addition to water, scientists believe that Europa produces a significant amount of thermal energy, and likely has organic materials under its surface. The combination of these three ingredients means that Europa may even be able to sustain life.

To gather more information about the icy moon, NASA JPL is managing the Europa Clipper mission, planning to launch in 2024. Clipper is a Jupiter-orbiting spacecraft that will utilize its many scientific instruments to collect a wide variety of data. Among them is REASON, which will help scientists learn more about the ice shell and the possible ocean below.

Clipper is the largest planetary spacecraft ever made by NASA, stretching out over 100 feet in length. Figure 1.1 shows Europa laid over a basketball court for reference. While this size is impressive, it presents challenges for NASA's engineers and makes it nearly impossible to calibrate the REASON antennas on Earth.

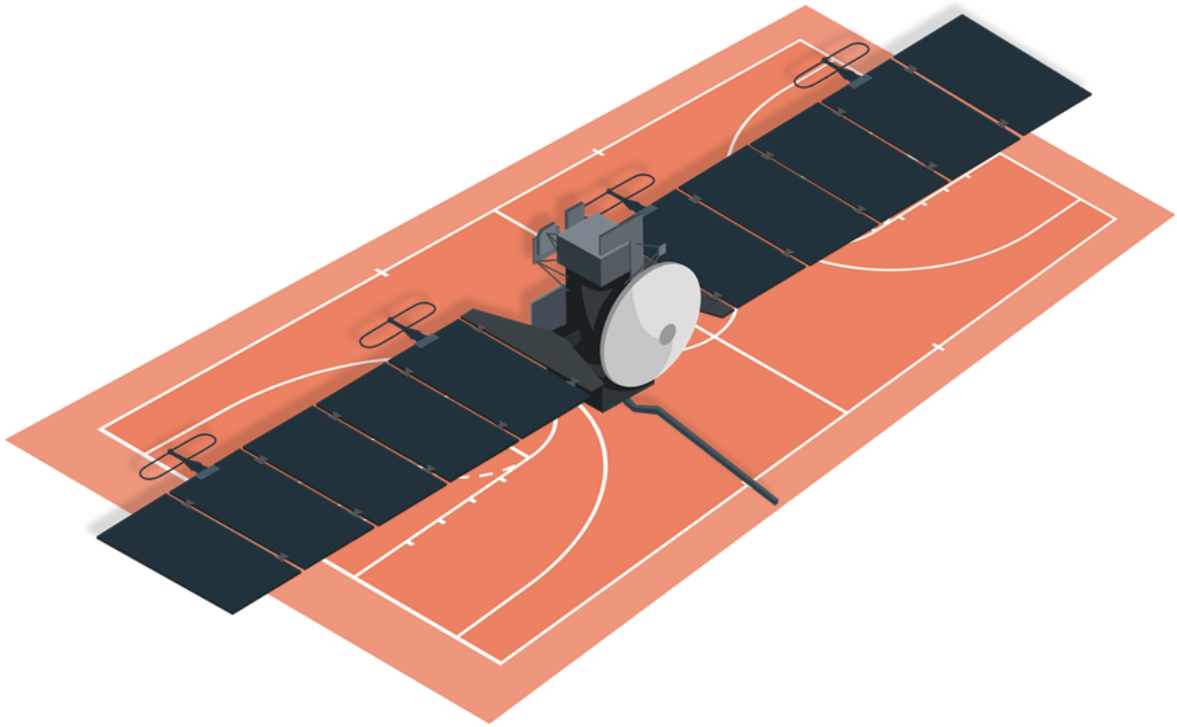

Figure 1.1: Length of Europa Clipper compared to a basketball court

To avoid the problems caused by Earth's intense gravity, NASA plans to calibrate Clipper once it is deployed in space. In near zero gravity, the spacecraft could fully deploy without deformation. Normally, this calibration method would require pointing the antennas back toward Earth and communicating with ground stations. However, doing so would expose sensitive electronics onboard Clipper to the Sun's harmful radiation.

1.1.3. Previous CaliPER Work

Extensive work in planning the CaliPER mission as a whole has been done by the 2021-2022 ES100 JPL Project Team [8]. These authors include Jordan Daigle, Jonathan Hintz, Matthew LoPresti, Spencer Rolland, Obinna Ejikeme, and Jacob Johnson. For their thesis, these students worked alongside mentors at JPL to propose CaliPER, a 12U CubeSat, to fly alongside Europa Clipper to collect data to calibrate the REASON instrument. CaliPER would maneuver around Clipper, collecting data at various spatial locations, then transmit this data back to Earth for full analysis to calibrate REASON. In their final report, the team outlined and defined requirements for the overall mission, as well as each subsystem, including the guidance, navigation, and control (GNC) system, the propulsion system, the telemetry and communication system, the power collection and storage system, as well as the thermal and structural analysis for the overall bus structure. The vast majority of this project, as well as the other subsystems this year, was built upon their work and research. While their work last year focused on

theoretical mission design and outlining of requirements, our work this year as a larger ES100 cohort focused on refining mission requirements and designing, building, and prototyping different subsystems. This report will be focused on designing, building, and testing a propulsion system to enable CaliPER's spatial movement.

2. Background Research

2.1. CubeSat Propulsion

2.1.1. Propulsion Theory

2.1.1.1. Propulsion Physics Summary

Spacecraft propulsion systems are, at the end of the day, a technological means to enact a force or torque on the spacecraft to change the spacecraft's linear or angular momentum. In other words, the propulsion system's only job is to impart impulse onto the spacecraft. Impulse is simply the change in momentum, and we can then define total impulse of a propulsion system to be:

$$I_t = \int_0^{t_{end}} F_t(t)dt$$

Eq. 2.1

where t_{end} is the time at which the system would run out of fuel and $F(t)$ is the instantaneous thrust produced by the system. Thrust can in turn be calculated by the following formula given in Eq. 2.2:

$$F_t = \dot{m}_p \cdot v_{eff}$$

Eq. 2.2

Where $\dot{m}_p$ is the mass flow rate of the propellant and v_{eff} is the effective exhaust velocity defined in Eq. 2.3 as:

$$v_{eff} = v_e + \frac{(P_e - P_o) \cdot A_e}{\dot{m}_p}$$

Eq. 2.3

where P_e is the exit pressure, P_o is the ambient pressure which is 0 in the vacuum of space, A_e

is the exit nozzle area, and v_e is the exit velocity of the propellant.

In order to differentiate and compare various propulsion systems and propellants, a measure of how mass-efficient propellants are able to be used is extremely useful. This characteristic, known as specific impulse, measures how much force can be exerted per the weight flow rate of the propellant used. Specific impulse is more explicitly defined in Eq. 2.4 below:

$$I_{sp} = \frac{F_t}{\dot{m}_p \cdot g_0}$$

Eq. 2.4

Where g_0 is the gravitational acceleration on Earth. Dividing by gravitational acceleration is simply a convention used to give the units of seconds to specific impulse and is always Earth's gravitational constant, no matter if the system subject to analysis is on Earth's surface, LEO, interplanetary space, or some other gravitational body. It is important to note that though I_{sp} is defined in terms of F_t, a higher thrust does not mean a higher I_{sp} when comparing two different types of propulsion systems. In fact, some systems have an extremely high I_{sp}, like ion propulsion, paired with an extremely low thrust and other systems have a low I_{sp}, like chemical rocket engines, but high thrust. Specific impulse and thrust are not interchangeable properties and should not be conflated. Combining Eq. 2.4 with Eq. 2.1 and Eq. 2.2 and assuming that $\dot{m}$ is constant in time yields the important relation between specific impulse and total impulse:

$$I_t = I_{sp} m_p g_0$$

Eq. 2.5

It should also be noted that one can define a volumetric specific impulse as the impulse gained per unit volume of propellant expelled:

$$I_{vol} = \frac{I_t}{V g_o} = \frac{I_t}{m_p \rho g_0} = I_{sp} g_0 \rho$$

Eq. 2.6

This is an extremely useful comparison metric as the volume on board a spacecraft is extremely limited and valuable, so the choice of propellant must also satisfy volumetric constraints.

However, no matter the choice of propellant or propulsion system, all spacecraft are equally subject to the Tsiolkovsky rocket equation, as seen in Eq. 2.7:

$$\Delta V = v_{eff} \ln \frac{m_0}{m_0 - m_p} = I_{sp} g_0 \ln \frac{m_0}{m_0 - m_p}$$

Eq. 2.7

where m_0 is initial mass, and ΔV, also written as delta-V, is an extremely important quantity used to characterize the ability and total capacity of propulsion systems. Delta-V is defined as the impulse per unit mass of the spacecraft, and without the influence of gravity, is simply the change in speed of the spacecraft. Delta-V is sometimes described as the currency of space travel, as every attitude control maneuver, transfer orbit, and correction burn expends fuel remaining total impulse available. Delta-V is therefore a mass-independent property, so a given transfer orbit will require the same delta-V no matter the mass of the spacecraft. Given Eq. 2.5, delta-V can be related to total impulse under the following relation:

$$\Delta V = \frac{I_t}{m_p} \ln \frac{m_0}{m_0 - m_p}$$

Eq. 2.8

It should be noted that sometimes the initial mass, m_0 will be referred to as the wet mass and the quantity $m_0 - m_p$ will be referred to as the dry mass. In other words, dry mass is the mass of the spacecraft without including the propellant, whereas wet mass is the mass of the actual spacecraft plus the mass of the propellant.

Ultimately, external mission parameters will determine how much delta-V the spacecraft must possess to fulfill all mission objectives. Moreover, the initial mass of the spacecraft often will have also been independently set. Therefore, one can rearrange Eq. 2.7 to find that:

$$m_p = m_0 (1 - e^{-\frac{\Delta V}{I_{sp} g_0}})$$

Eq. 2.9

which will set a hard requirement for the mass of fuel required as a function only of the mission wet mass, delta-V, and specific impulse.

2.1.1.2. Isentropic Flow

Derivations of the governing physics of gas flow through a nozzle to produce thrust can be found in most introductory fluid mechanics or thermodynamics textbooks. This section will not rederive these physics, but merely summarize the conceptual background and basic equations necessary for an understanding of ideal propulsion systems.

Propulsion systems produce thrust via the conservation of momentum by the controlled supersonic expulsion of a gaseous propellant through a nozzle. Because these systems inherently

involve complex turbulent flow, accurate predictions are only achieved through numerical methods and advanced computer simulations. Analytical solutions only exist when idealized assumptions are made. To quote from the foundational rocket propulsion textbook, *Rocket Propulsion Elements* [9]:

> In designing new rocket propulsion systems, it has become accepted practice to use such ideal rocket parameters… defined as one for which the following assumptions are valid:
>
> 1. The working fluid (which usually consists of chemical reaction products) is homogeneous in composition.
> 2. All the species of the working fluid are treated as gaseous. Any condensed phases (liquid or solid) add a negligible amount to the total mass.
> 3. The working fluid obeys the perfect gas law.
> 4. There is no heat transfer across any and all gas‐enclosure walls; therefore, the flow is adiabatic.
> 5. There is no appreciable wall friction and all boundary layer effects may be neglected.
> 6. There are no shock waves or other discontinuities within the nozzle flow.
> 7. The propellant flow rate is steady and constant. The expansion of the working fluid is uniform and steady, without gas pulsations or significant turbulence.
> 8. Transient effects (i.e., start‐up and shutdown) are of such short duration that may they be neglected.
> 9. All exhaust gases leaving the rocket nozzles travel with a velocity parallel to the nozzle axis.
> 10. The gas velocity, pressure, temperature, and density are all uniform across any section normal to the nozzle axis.
> 11. Chemical equilibrium is established within the preceding combustion chamber and gas composition does not change in the nozzle (i.e., frozen composition flow).
> 12. Ordinary propellants are stored at ambient temperatures. Cryogenic propellants are at their boiling points.

In other words, the flow of gas through the nozzle is assumed to be isentropic (no entropy generation) and follow the ideal gas law. From these physical assumptions one can solve for all parameters in the system. The mass flow rate can be calculated from Eq. 2.10:

$$\dot{m}_p = \frac{A_t P_c}{\sqrt{T_c}} \sqrt{\frac{\gamma}{R}} \left(\frac{\gamma + 1}{2} \right)^{\frac{1-\gamma}{2(\gamma-2)}}$$

Eq 2.10

where $\dot{m}_p$ is mass flow rate of propellant, A_t is the area of the throat of the nozzle, P_c is the chamber pressure, T_c is the chamber temperature, γ is the ratio of specific heats for the propellant, and R is the specific gas constant.

As seen in Eq. 2.11, one can also relate the exit mach number, or the speed of the gas as a fraction of the speed of sound in the medium, to the ratio of area of the nozzle exit to the area of the nozzle throat:

$$\frac{A_e}{A_t} = \left(\frac{\gamma+1}{2}\right)^{\frac{1-\gamma}{2(\gamma-1)}} \frac{\left(1+\frac{\gamma-1}{2}{M_e}^2\right)^{\frac{\gamma+1}{2(\gamma-1)}}}{M_e}$$

Eq. 2.11

Where A_e is the exit area and M_e is the mach number of the gas after exiting the nozzle.

As seen in Eq. 2.12, one can also solve for the temperature ratio as a function of the exit mach number:

$$\frac{T_e}{T_c} = \left(1+\frac{\gamma-1}{2}{M_e}^2\right)^{-1}$$

Eq 2.12

Where T_e is the exit temperature.

As seen in Eq. 2.13, one can also solve for the pressure ratio as a function of the exit mach number:

$$\frac{P_e}{P_c} = \left(1+\frac{\gamma-1}{2}{M_e}^2\right)^{\frac{-\gamma}{\gamma-1}}$$

Eq. 2.13

Where P_e is the exit pressure.

As seen in Eq. 2.14, one can rearrange the definition of the exit Mach number to solve for the exit velocity:

$$v_e = M_e\sqrt{e}$$

Eq. 2.14

Where v_e is the exit velocity.

Finally, as seen in Eq. 2.15, one can write the Newton's 2nd law of motion to find the thrust force:

$$F_t = \dot{m}_p v_e + (P_e - P_0) A_e$$

Eq. 2.15

Where F_t is the thrust force and P_0 is the external pressure, which is 0 in the vacuum of space.

Though these equations provide decent approximate answers, the fundamental assumptions are unrealistic. It is possible to modify these equations with theoretical or empirical correction factors for more accurate predictions based on the design.

The first correction factor, λ, accounts for non-ideal nozzle shapes. For conical nozzles with a half angle of θ, the correction factor is defined in Eq. 2.16 below:

$$\lambda = \frac{1}{2}(1 + cos\theta)$$

Eq. 2.16

This factor accounts for non-ideal expansion as the result of divergent flows of the gas and modifies Eq. 2.15 to become Eq. 2.17:

$$F_t = \lambda \dot{m}_p v_e + (p_e - p_0) A_e$$

Eq. 2.17

The 2nd correction factor, ζ_v, is measured empirically and accounts for inefficiencies in kinetic energy conversion. It modifies Eq. 2.4 to become Eq. 2.18:

$$I_{sp,actual} = \zeta_v I_{sp,theory} = \zeta_v \frac{F_t}{\dot{m}_p \cdot g_0}$$

Eq. 2.18

This correction factor typically takes on values between 0.85 and 0.99 [10].

The 3rd correction factor, ζ_d, is also measured empirically and accounts for differences in the measured mass flow rate compared to the ideal as seen in Eq. 2.19:

$$\dot{m}_{p,actual} = \zeta_d \dot{m}_{p,actual}$$

Eq. 2.19

This correction factor typically takes on values between 1 and 1.15 [10]

The final correction factor to be incorporated into predictions is ζ_F which is measured empirically and accounts for differences in measured and predicted thrust. It is therefore defined in Eq. 2.20 as:

$$F_{t,actual} = \zeta_F F_{t,theory}$$

Eq. 2.20

This correction factor is equal to the product of ζ_d and ζ_v and therefore typically takes on values between 0.92 and 1 and [10].

2.1.2. Types of Propulsion

Because fewer than 10 CubeSats have successfully flown with propulsion systems [11], it is worth examining all types of available in-space propulsion systems. As seen in Figure 2.1, different propulsion technologies vary in their performance characteristics by orders of magnitude [12]. An ideal propulsion system would lie in the upper right corner, having an extremely high thrust and specific impulse.

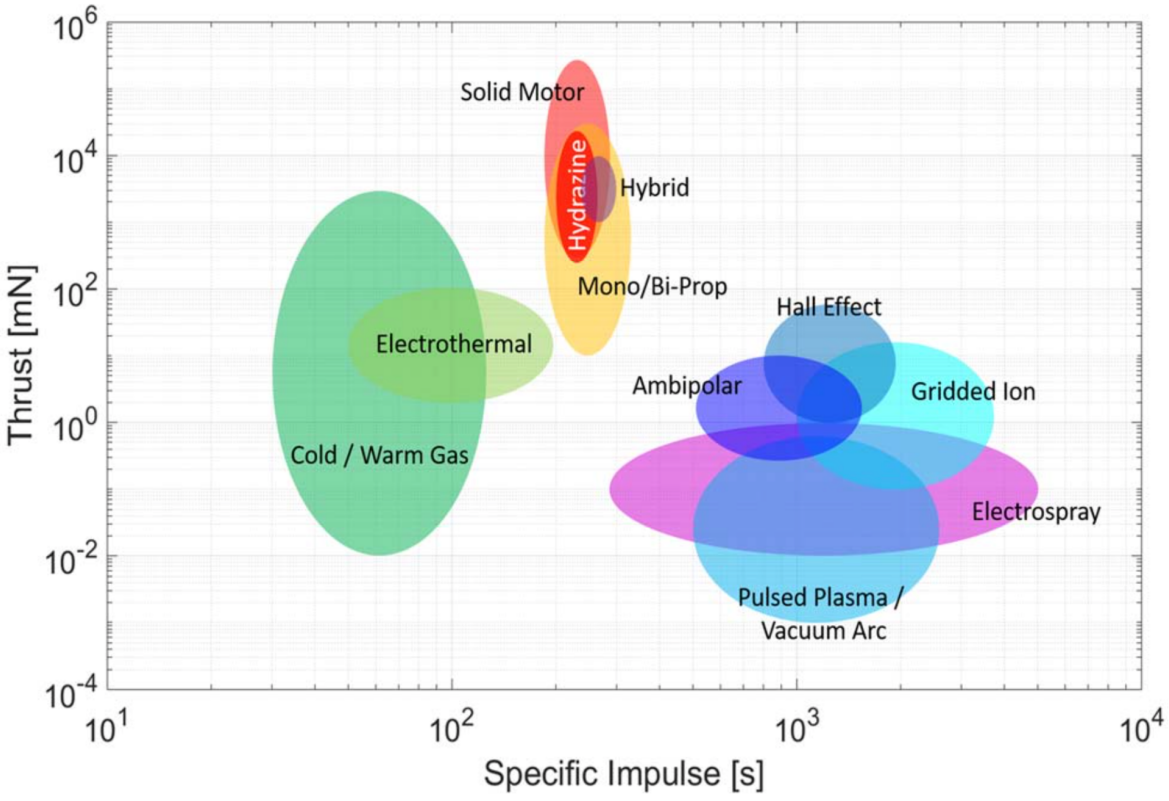

Figure 2.1: Various propulsion technologies plotted on a thrust vs specific impulse graph [12]

2.1.2.1. Chemical Propulsion

Three distinct groups emerge in Figure 2.1, each of which share similar base

characteristics. The uppermost group, consisting of Solid Motor, Hydrazine, Hybrid, and Mono/Bi-Prop systems are chemical propulsion systems. These systems rely on combustion reactions to release chemical potential energy stored in bonds to produce high pressure, supersonic gas in order to generate thrust.

The most common chemical propulsion system is the bi-propellant system, which has immense flight heritage. Throughout the history of space exploration, rockets and large spacecraft have used bi-propellant propulsion due to the system's high thrust and specific impulse. These systems are named "bi-propellant" because they require two components to react: the fuel and the oxidizer. These components are fed into the same chamber, and then ignited. They then combust, releasing an extreme amount of energy in a short period of time, creating a large thrust to move the spacecraft. Since so much energy is required to escape Earth's gravity, rockets are mostly comprised of large propellant storage tanks.

There are also monopropellant systems, the most common of which is Hydrazine. These systems combine a propellant with a solid catalyst, causing an extremely exothermic chemical reaction. Unfortunately, Hydrazine is extremely toxic, and the productive life of these systems is limited by the relatively short life of the catalyst. More recently, scientists have been trying to harness the large power production of monopropellant propulsion, without having to accept the dangerous nature of Hydrazine. These new developments have been dubbed "green monopropellants" since they are much less toxic. Two of the most developed green monopropellants are hydroxylammonium nitrate (HAN)-based, and ammonium dinitramide (AND)-based propellants. These green monopropellants have a greater density, thrust, and specific impulse than Hydrazine. However, they require higher temperatures and a more durable catalyst. Green monopropellants still require much development, but they are exciting possibilities for the future [11].

As of 2017, no CubeSats have launched with a chemical propulsion system [11]. This is due to the generally high toxicity, complexity, risk, and operating costs associated with these chemical systems. Additionally, bipropellant systems are difficult to scale down since they require two storage tanks, a mixing chamber, and an igniter. Some monopropellant systems exist for CubeSats, with a few having been developed by VACCO Industries, but have yet to see flight [13].

2.1.2.2. Electric Propulsion

The rightmost grouping of propulsion systems in Figure 2.1, including Hall Effect, Ambipolar, Gridded Ion, Electrospray, and Pulsed Plasma/Vacuum Arc, are types of electric propulsion systems. These systems utilize diverse methods of converting electrical energy into kinetic energy to generate thrust. This can range from ionizing propellant and ejecting these ions, to manipulating magnetic fields to eject plasma [11]. These technologies have low thrust, but extremely high specific impulse. This type of propulsion has seen an increased level of research and development in recent years as current electric propulsion systems have proven successful

and have the potential to promise even greater performance.

2.1.2.3. Cold Gas Propulsion

The leftmost group, consisting of Cold/Warm Gas and Electrothermal propulsions systems, do not undergo any exothermic chemical reactions to provide thrust. Instead, they exhaust a pressurized gas to produce thrust. This extremely simple design makes them useful for a wide range of applications that require a low thrust, such as attitude control for rockets and satellites. In warm gas and electrothermal systems, this gas is heated prior to release in order to increase the pressure and therefore the thrust. This can be done in a variety of methods, from simple resistor heaters to arcing electricity. Cold gas propulsion systems have the most heritage and maturity in CubeSats, as these systems have flown on the majority of CubeSat missions with a propulsion system [11].

2.2. Past Missions

2.2.1. MarCO

In 2018, NASA launched the Mars InSight lander, along with two identical CubeSats, dubbed MarCO-A and MarCO-B (henceforth referred to as the singular MarCO). As InSight was landing on Mars, MarCO was relaying live communications back to Earth. MarCO was not mission-critical for the InSight landing. In fact, MarCO was mainly used as a proof of concept for interplanetary CubeSats. MarCO performed excellently and proved the CubeSats certainly have a role in future deep space missions.

MarCO was similar to CaliPER in size, making it a very good analog. It was a 6U CubeSat with a mass of 13.7 kg [5], which is extremely close to the 6U, 12 kg plan for CaliPER (as further discussed in Section 3.2). MarCO utilized a cold gas propulsion system, called the Micro Propulsion System (MiPS), custom developed by VACCO industries. A block diagram of this system is seen below in Figure 2.2. MiPS achieved 755 N-sec of total impulse and 40 sec of specific impulse, with a wet mass of only 3.49 kg. It used R-236fa as a propellant, which was stored in a 2-phase tank that was vaporized and expelled through eight thrusters. Four thrusters were axial for trajectory control, and four were canted for attitude control. All eight achieved 25 mN of thrust [3]. The system required 15 Watts to operate, and its usage was mainly constrained by its power draw [14]. MarCO Trajectory maneuvers were planned to take less than ten minutes in order to keep battery charge at safe levels [5].

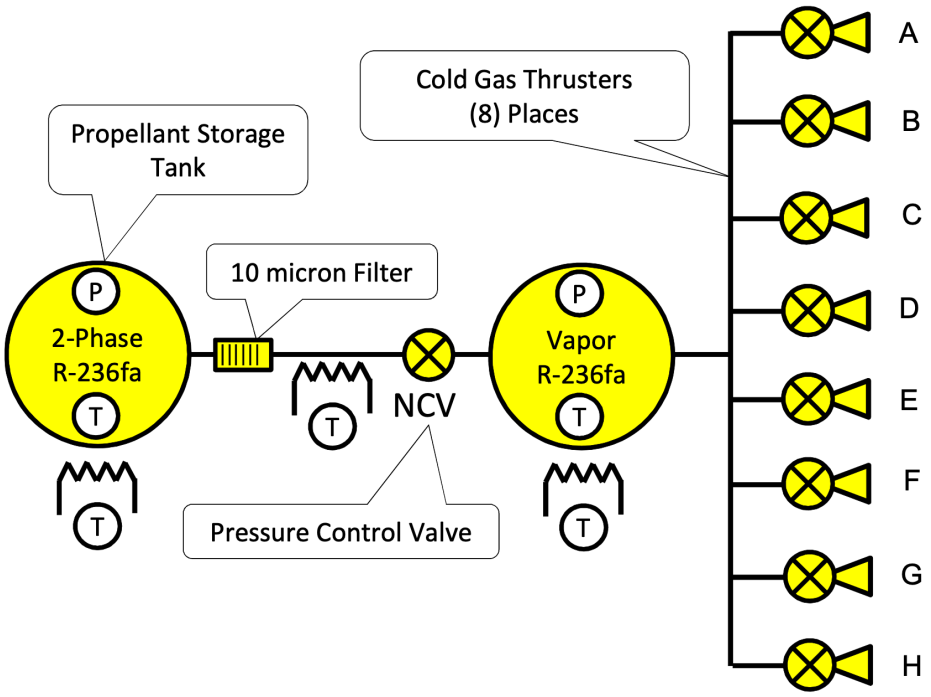

Figure 2.2: Block diagram of the MarCO Micropulsion System [3]

2.2.2. Lunar Flashlight

Lunar Flashlight is a 6U, 14 kg CubeSat developed by NASA JPL to orbit the Moon launched in December of 2022. Lunar Flashlight uses near-infrared lasers to map the ice at the Moon's south pole, passing as close as 12.6 km to the surface. Information about the presence of water near the pole may prove vital for future missions to the lunar surface [15].

Such a mission requires a robust propulsion system with a large total impulse in order to complete the many necessary trajectory corrections. A trade study was conducted between three different systems: pressure-fed monopropellant LMP-103S, pump-fed monopropellant AF-M315E, and cold gas R-236fa. Each system was designed to a rudimentary, yet fully functional state, with their characteristic being shown below in Figure 2.3.

	Pressure-Fed LMP-103S	Pump-Fed AF-M315E	Cold Gas R236fa	
Propellant Volume	1463	1562	2500	cc
Pressurant Volume	220	–	–	cc
Dry Mass	2752	3238	1260	g
Propellant Mass	1814	2296	3175	g
Auxiliary Component Mass	900	1360	650	g
Total Wet Mass	5466	6894	4206	g
Total Impulse Estimate	>3000	>3000	1713	g
Most Difficult "Constraint to Beat"	Volume	Mass	Performance	–

Figure 2.3: Comparison of three possible Lunar Flashlight propulsion systems [16]

Ultimately, the Pump-Fed AF-M315E system was chosen. AF-M315E is a HAN-based propellant with a higher specific impulse than Hydrazine, yet without the many dangers of Hydrazine. This means that Lunar Flashlight is the first CubeSat ever propelled by a green monopropellant propulsion system. The system utilizes four thrusters to provide a total impulse of over 3000 N-s [16]. Knowing that the total mass of Lunar Flashlight is 14 kg and the propellant mass is 3.175 kg, Eq. 2.8 can be used to calculate that this system provides a delta-V of 234 m/s.

2.2.3. Bevo-2

Bevo-2 was a 3U CubeSat deployed from the ISS in January 2016 and developed by the Satellite Design Lab at the University of Texas (UT) at Austin, then headed by Prof. Glenn Lighstey [17] [1]. The mission was launched alongside AggieSat-4 developed by Texas A&M University as part of the LONESTAR-2 mission to demonstrate inter-CubeSat communication, precision pointing, and autonomous rendezvous and docking. Unfortunately, communications were never established with Bevo-2 after its deployment. However, there is still value in studying the novel, custom-designed cold gas micropropulsion system designed by the team in the Satellite Design Lab.

This propulsion system used DuPont R-236fa propellant to provide at least 10 m/s delta-V to this system. A table of technical specifications of the Bevo-2 propulsion system is seen below in Figure 2.4.

Thruster System Characteristic	Value
Total dry mass	290 grams
Propellant mass	90 grams
Total thruster system mass	380 grams
Minimum power	0 W
Maximum power	1.5 W
Maximum valve operation pressure	800 psig
Valve actuation rate	500 Hz
Dimensions	10 x 9 x 4.4 cm

Figure 2.4: Characteristic propulsion values for the Bevo-2 satellite [17]

What makes Bevo-2 unique is that it is an additively manufactured, modular propulsion system. All major components of the system, including the main propellant storage tank, control plenums, output nozzle, and all connecting tubes, are printed as a single part. Accura Bluestone, an outgas-resistant resin, was used as the resin for this stereolithographically (SLA) printed part [17]. Figure 2.5 shows the basic systems diagram, including a 90 cm^3 tank to store the saturated mixture of R-236fa propellant, as well as two plenums to ensure vaporization and pressurization of the refrigerant before it is funneled into the converging-diverging nozzle.

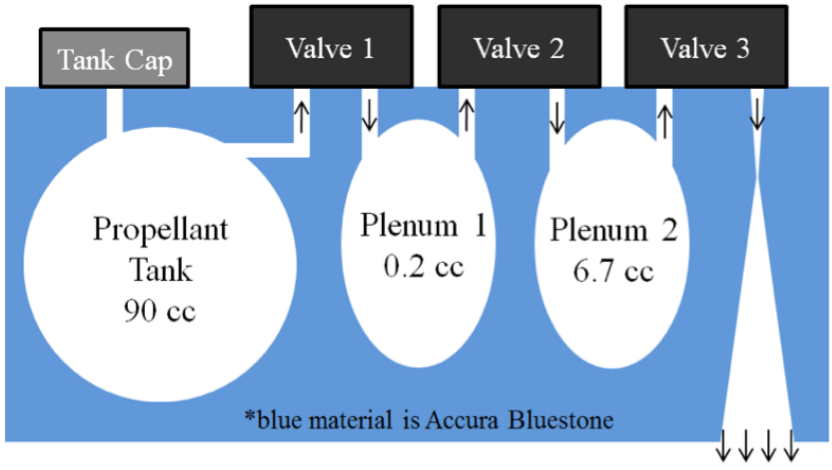

Figure 2.5: System map of the Bevo-2 propulsion system [17]

The system is entirely pressure fed and only takes two inputs to operate: the desired delta-V and the current temperature. As will be discussed further in Section 5.1.2, the UT lab decided to use R-236fa as a propellant due to its high volumetric specific impulse and vapor pressure of 100 psia at 56℃. This first proof of concept design set the groundwork for future

investigation and development of additively manufactured propulsion systems. Since additive manufacturing grants the ability to rapidly prototype and manufacture components with complex shapes, one can utilize all available space for propellant storage and minimize the misallocation of volume due to tubing and adapters associated with using commercial-off-the-shelf parts. Figure 2.6 shows images of different iterations of this 3D printed design.

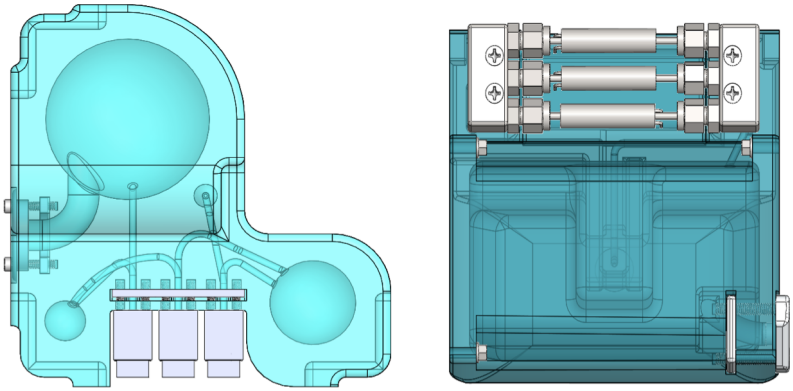

Figure 2.6: Two iterations of the Bevo-2 propulsion system [17]

2.2.4. INSPIRE

INSPIRE is the name of an unlaunched interplanetary 3U CubeSat developed for JPL in part by the Texas Spacecraft Laboratory at University of Texas at Austin led by Glenn Lightsey [18]. The INSPIRE propulsion system, which is an iteration upon Bevo-2's propulsion system, demonstrated the continued research and development of the feasibility of 3D printed propulsion units. Both flight units are seen below in Figure 2.7.

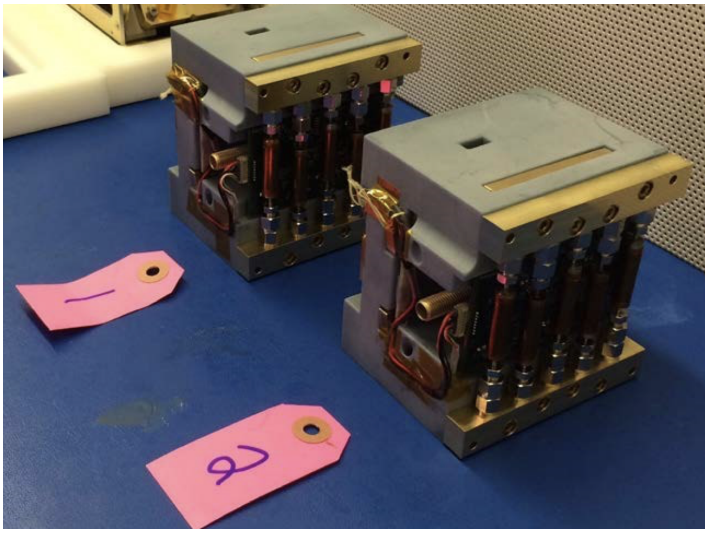

Figure 2.7: INSPIRE thruster flight units prior to delivery [18]

Since this particular propulsion system was only designed to fulfill the reaction control system (RCS) needs, the INSPIRE system only has 4 nozzles, each canted at 10 degrees. The unit is once again manufactured with an SLA printer using Accura Bluestone. The system uses 180 grams of R-236fa stored as a saturated liquid-vapor mixture as propellant. As was the case with Bevo-2, the system is designed to never operate above 100 psia. However, they designed the tank with a safety factor of 2.5 and verified this using finite element analysis. Traditionally machined manifolds were used to connect the solenoid valves and standardized ports with the plastic tanks. These manifolds were face sealed to the plastic with an o-ring in compression and connected to the valves using standard fittings threaded into the manifolds. A wire frame view of the unit can be seen in Figure 2.8.

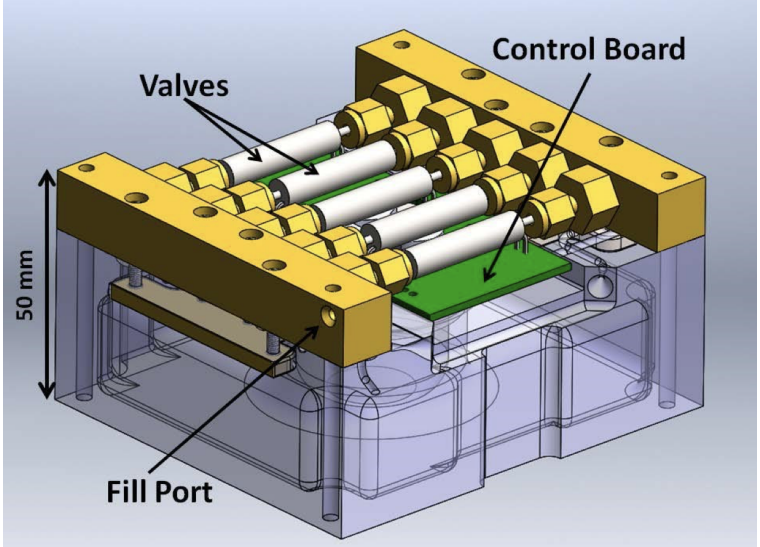

Figure 2.8: INSPIRE engineering design unit with manifold and valves highlighted [18]

2.2.5. BioSentinel

BioSentinel is a 6U CubeSat that was recently launched on Artemis-I. The spacecraft's propulsion system was developed by Georgia Tech's Space Systems Laboratory headed by Prof. Glenn Lightsey, who moved to Georgia Tech from University of Texas at Austin. Based on the designs from the Bevo-2 and INSPIRE missions, the propulsion system used 0.1 mm resolution SLA printing with Accura Bluestone to house the R-236fa propellant, nozzles, and tubing [19]. BioSentinel, being twice as large as the previous two missions, required a larger and more capable propulsion system that is roughly 2U in size.

As seen in Figure 2.9, the structure contained one main tank to hold the propellant in a saturated liquid-vapor mixture, and a separate, smaller plenum to house the gas before release through the nozzles. The system is not symmetric across the displayed cross section in Figure 2.9 - the internal geometry is too complex to show with a single cross section. BioSentinel used

the same steel manifold interface design to mount the commercial-off-the-shelf (COTS) valves to control the flow through the 3D printed structure.

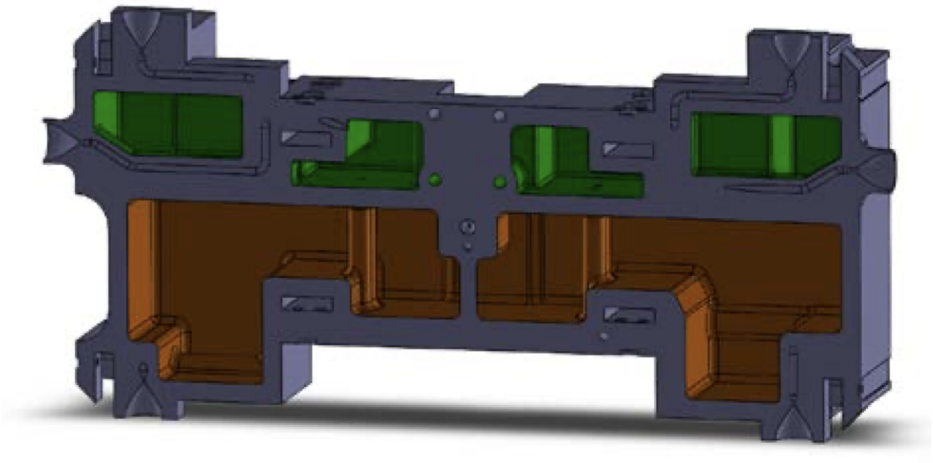

Figure 2.9: A cross section of the BioSentinel propulsion system. The green sections are the plenum, and the orange section is the tank. Note that there is only one continuous tank and one continuous plenum, this cross section view just does not show this continuity as the internal geometry is complex. [19]

2.2.6. SunRISE

The SunRISE mission will comprise six identical 6U CubeSats to study the Sun and is scheduled to launch no earlier than 2024 [20]. Managed by JPL, this satellite's propulsion system was developed by Glenn Lightsey's group in Georgia Tech's Space Systems Design Laboratory [21]. Seen in Figure 2.10, the SunRISE propulsion system provides both attitude and positional control for the spacecraft.

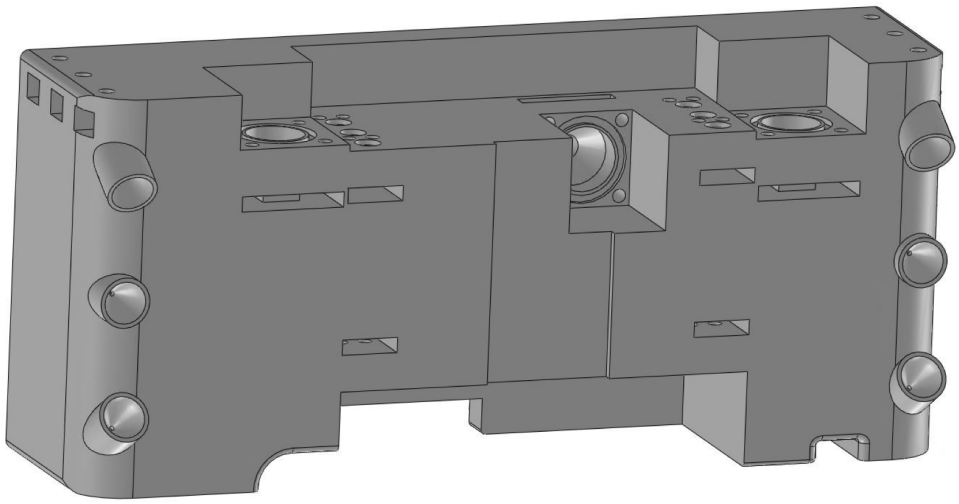

Figure 2.10: The SunRISE propulsion system [21]

Like the previous three missions, this cold gas propulsion system is an additively manufactured system that uses R-236fa refrigerant as its propellant and a similar manifold interface, seen in Figure 2.11.

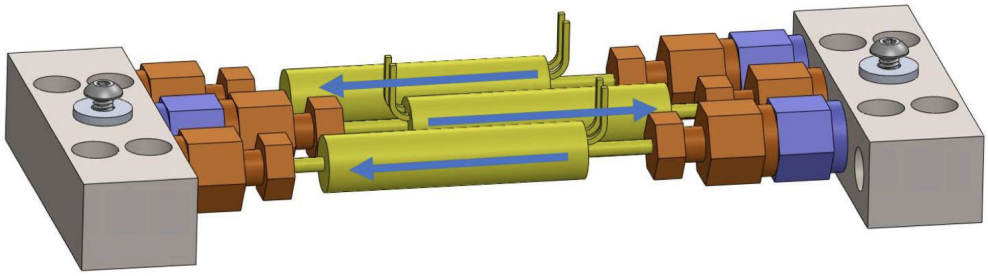

Figure 2.11: The valve manifold system developed by researchers in Glenn Lightsey's lab. In yellow are the solenoid valves, in orange are the compression fittings, and in purple are filters.

The team at Georgia Tech was able to work with their additively manufacturing team to design this tank to require no internal support structures, meaning the entire internal volume is available for use for propellant storage. They designed their system to handle their expected temperature extremes, -30℃ and 50℃.

As will be seen further in Section 5, much of the work of this paper was based on the available information on the work of Prof. Glenn Lightsey.

3. Design Goals and Technical Specifications

3.1. Verification Standards

Each requirement must meet verification standards to show it was successfully met. As defined by the NASA Systems Engineering Handbook, verification is a formal process consisting of four methods [22]:

1. **Analysis**: The use of mathematical modeling and analytical techniques to predict the suitability of a design to stakeholder expectations based on calculated data or data derived from lower system structure end product verification. Analysis is generally used when a prototype; engineering model; or fabricated, assembled, and integrated product is not available. Analysis includes the use of modeling and simulation as analytical tools.

2. **Demonstration:** Showing that the use of an end product achieves the individual specified requirement. It is generally a basic confirmation of performance capability, differentiated from testing by the lack of detailed data gathering. Demonstrations can involve the use of physical models or mock-ups. A demonstration could also be the actual operation of the end product by highly qualified personnel.

3. **Inspection:** The visual examination of a realized end product. Inspection is generally used to verify physical design features or specific manufacturer identification. Inspection can include inspection of drawings, documents, or other records.

4. **Test:** The use of an end product to obtain detailed data needed to verify performance or provide sufficient information to verify performance through further analysis. Testing can be conducted on final end products, breadboards, brassboards, or prototypes.

3.2. Mission Design Independent Requirements, Justifications, and Verification Plan

Designation	Requirement	Verification
MR1	The spacecraft's wet mass should not exceed 12 kg	Analysis
MR2	The spacecraft’s volume shall conform to the CubeSat Design Specification for a 6U CubeSat	Analysis

MR3	The spacecraft shall remain at least 75 km from Clipper at all times during the mission	Analysis
MR4	The spacecraft shall characterize the REASON beam pattern along the x and y axes ± 60° from the nadir point to collect data at 1 degree increments	Analysis
MR5	All calibration measurements shall occur between the end of the Clipper non-interference phase and the beginning of the Mars Gravity Assist	Analysis
MR6	The spacecraft's calibration trajectory should not require more than 12 continuous hours of REASON signal	Analysis

MR1

Justification: MR1 is derived directly from the CubeSat Design Specification, which gives a maximum of 2 kg per U [2]. Since CaliPER is a 6U CubeSat, the design should be under 12 kg to comply with this standard. JPL is able to grant small exceptions to this 2 kg/U requirement if necessary as CaliPER is a unique mission that will not be ridesharing with other CubeSats.

Verification: Analysis will be done by the Bus subteam via mass properties in the fully integrated CAD model to verify this requirement. Since physical integration of flight parts did not happen in this project, this cannot be done with physical tests. For future iterations on this project where all subcomponents are manufactured and flight ready, a physical measurement test will be done to verify this requirement.

MR2

Justification: MR2 is derived directly from the CubeSat Design Specification which mandates outer dimensions and tolerances [2]. These are standardized so that CubeSat deployment systems can have unified designs to be compatible with all 6U CubeSats. Although last year's work designed CaliPER as a 12U system, JPL has now mandated that CaliPER be downsized to 6U. As CaliPER will be using a commercial deployment system, it is critical that the spacecraft comply with all relevant standards. See the Bus subteam report for more information.

Verification: Like MR1, since this project did not involve flight hardware being manufactured and integrated, physical tests are impossible. Instead, analysis on the fully integrated CAD model will verify if CaliPER complies with the CubeSat design specifications.

MR3

Justification: MR3 is given by the JPL Clipper team. Clipper is the primary focus of this mission, so this separation distance exists to minimize any risk of collision between the two spacecraft. 75 km of separation distance was based on the minimum required distance in between geostationary satellites, which is approximately 73 km.

Verification: This will be verified through analysis of the mission timeline that is designed and outlined in this paper.

MR4

Justification: MR4 is given by the JPL Clipper team, as this range of data points is desired to properly calibrate REASON. JPL is interested in determining how the signal from REASON changes in intensity as position along *x* and *y* vary. These axes are visualized in Figure 3.1 and labeled as the "across track" and "along track" axes, intersecting at the point known as "nadir".

Verification: This will be verified through analysis of the designed calibration path and approval of the Europa Clipper team.

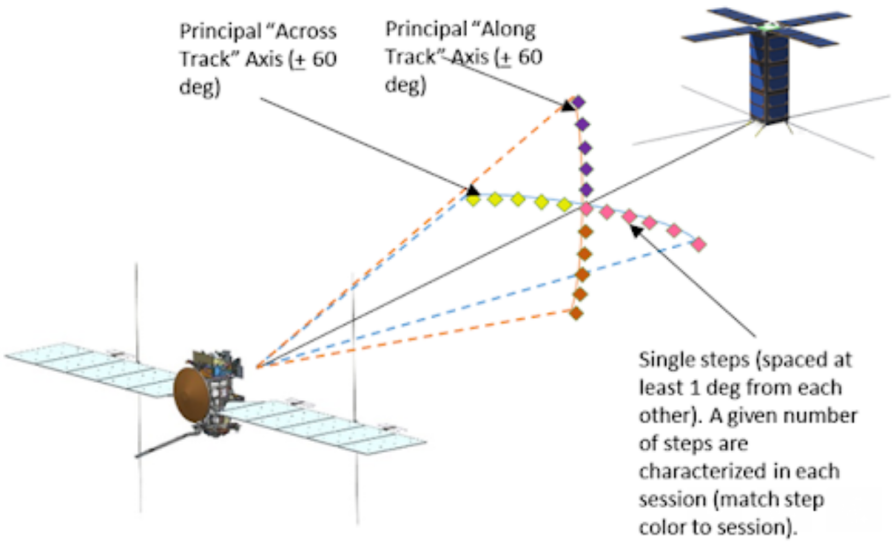

Figure 3.1: Representation of points ±60° with respect to Clipper that JPL has requested CaliPER collect data for calibration. The x axis is the "Across Track" and the y axis is the "Along Track". The origin is nadir relative to Clipper [23]

MR5

Justification: MR5 is given by the JPL Clipper team. CaliPER must wait until Clipper finishes its initialization, self-checkouts, and instrument deployments before interacting with Clipper to collect data. CaliPER must finish calibration measurements before the Mars Gravity Assist (MGA) since CaliPER will not follow Clipper through the MGA.

Verification: This will be verified through analysis of the mission timeline that is designed and outlined in this paper.

MR6

Justification: MR6 is given by the JPL Clipper team. Since Clipper will be performing other tasks while en route to Jupiter, it is unable to allot more than 12 hours at a time for beaming REASON signal to CaliPER. In other words, CaliPER cannot demand multiple days worth of continuous signal transmission. This requirement does allow for multiple 12 hour transmission periods split up between different days. Exact timing and total amount of time dedicated to CaliPER is subject to negotiations between JPL and the CaliPER team.

Verification: This will be verified through basic modeling of the mission plan to ensure timing is compliant.

3.3. Propulsion System Requirements, Justifications, and Verification Plan

3.3.1. Design Independent Technical Specifications

Designation	Requirement	Verification
PR1.1	Wet mass should be < 3.6 kg	Analysis
PR1.2	Propulsion system outer volume should be < 2U	Analysis
PR1.3	Power consumption during peak and standby usage shall not exceed power budget	Analysis
PR1.4	Propulsion systems shall have at least 3 inhibits to activation	Analysis
PR1.5	Propulsion system shall have the ability to rotate spacecraft about all 3 principal axes	Inspection
PR1.6	The propulsion system hardware shall have the ability to translate the spacecraft	Inspection
PR1.7	The thrusters shall all be independently activable	Inspection
PR1.8	The propulsion system shall have a minimum impulse bit no larger than 10% of the momentum storage capacity of the reaction wheels	Analysis
PR1.9	Commercial-off-the-shelf components shall be able to withstand a temperature range from at least -30 ℃ to 50 ℃	Inspection
PR1.10	The total delta-V capability of the system shall be no less than 52.21 m/s	Analysis and Test
PR1.11	End of life (EOL) thrust shall be >= 25 mN per axial nozzle	Analysis and Test

PR1.1

Justification: PR1.1 is derived from analogous CubeSat missions and discussions with the Bus subteam to divide mass between subteams. NASA's MarCO had a total mass of 13.7 kg with the wet mass of the propulsion system accounting for 3.49 kg of that. This is approximately 25% [3] [5]. Similarly, NASA's Lunar Flashlight has a total mass of 14kg, and its propulsion system has a wet mass of 5.5 kg, which is over 39% of the CubeSat's total mass [16] [15]. Using these other missions as a rough baseline since they had comparable delta-V budgets to CaliPER, the values were averaged to set the requirement.

Verification: Since this project does not include manufacturing the actual flight hardware, verification will be done via mass modeling on the CAD assembly at this stage.

PR1.2

Justification: PR1.2 is derived from discussions with the Bus subteam to properly divide volume between subteams. Exact dimensions are negotiable with Bus and other subteams with components required to be near the propulsion system. The goal of this requirement is just that the propulsion system fits in the spacecraft without physically interfering with other parts.

Verification: This requirement will be verified through analysis and extensive communication with the Bus team to ensure the propulsion unit does not interfere with other subassemblies.

PR1.3

Justification: PR1.3 derives from the power constraint set by the solar subteam. The propulsion system must comply with the power budget and draw as little power as to enable regular operation of all other power hungry subsystems, including communications with Earth, data intake from REASON, and an active GNC subsystem. The propulsion system must also comply with the power budget during peak usage so as not to dangerously drain battery reserves or demand more power than can be generated.

Verification: This requirement will be verified through power modeling of the propulsion system and its powered components as well as extensive communication with the solar subteam to ensure the propulsion unit is not drawing excessive power.

PR1.4

Justification: PR1.4 comes directly from CubeSat Design Specification 2.1.4. [2]. It is there to minimize the likelihood of a leak or misfire damaging the CubeSat or other payloads on the launch vehicle as well as for redundancy during mission operations.

Verification: This requirement will be verified through analysis of the system design to ensure that all 3 inhibits must be activated in order for the propulsion system to fire.

PR1.5

Justification: PR1.5 derives from the need to desaturate all reaction wheels which will be active on every principal axis. Without the ability to desaturate, the reaction wheels will eventually be unable to counter external torques on the spacecraft, rendering CaliPER uncontrollable.

Verification: This requirement will be verified through inspection that different combinations of nozzle activation produce a torque about each axis in both directions.

PR1.6

Justification: PR1.6 follows directly from MR4. In order to perform trajectory correction maneuvers (TCMs) and traverse relative to Clipper to collect REASON data, the propulsion system must have the ability to produce linear motion.

Verification: This requirement will be verified through inspection that firing certain nozzles produces a force and linear motion.

PR1.7

Justification: PR1.7 derives from the need to be able to control and command what type of motion the propulsion system generates. Having all nozzles be independently activable, combined with PR1.8, means it is possible to more finely tune and control the linear motion to reduce external torques generated.

Verification: This requirement will be verified through demonstration that each valve can be opened and closed independent from all other valves.

PR1.8

Justification: PR1.8 comes from the need to have enough precision to finely control impulse from the thrusters to precisely desaturate the momentum wheels. The GNC team is using reaction wheels with a momentum storage of 0.01 Nms, so the propulsion system shall have a minimum impulse bit no larger than 6.67 mNs, assuming a maximum moment arm of 15 cm.

Verification: This requirement will be verified through analysis of valve response time and thrust capabilities of the propulsion system.

PR1.9

Justification: All components must be able to survive the conditions of space. This range derives from standard temperature ranges considered by other spacecraft in literature and was confirmed with discussion from the Clipper team.

Verification: Component datasheets will be used to determine compliance with this requirement.

PR1.10

Justification: In order for the mission to be successful, the spacecraft must have enough propellant to impart enough impulse to complete all necessary translational maneuvers and desaturation of the reaction wheels. The exact amount of delta-V required is only determined by the mission calibration trajectory. The derivation of this number is discussed in greater detail in Section 4.3.

Verification: Since this project does not involve manufacturing of the flight unit, it is impossible to directly test the flight system to verify total delta-V capacity. In lieu of the full system test, specific impulse must be empirically measured on a modified testing unit and compared to the theoretical specific impulse to verify delta-V capacity will be as expected.

PR1.11

Justification: Due to the nature of coordinating between Clipper and CaliPER, some delta-V maneuvers must be completed within a timeframe. Namely, CaliPER must match certain trajectory correction maneuvers (TCMs) performed by Clipper. If CaliPER does not have sufficient thrust to roughly match the time it takes Clipper to perform these maneuvers, CaliPER may not exactly match Clipper's trajectory or otherwise require more delta-V for each TCM to maintain the proper position. In order to meet these timing requirements, the system must be able to produce a known minimum thrust in each nozzle throughout the entire mission. Since the CaliPER team could not be provided with specifics on Clipper's flight plan to determine this minimum thrust, this quantity was taken from the minimum thrust MarCO could achieve. Since MarCO also had to fly alongside a larger payload to Mars, the mission provides the best analog for what minimum thrust is acceptable in CaliPER's case. Since the TCMs are the driving factor behind this requirement and those only involve the axial nozzles, this requirement is technically only for axial thrusters.

Verification: Similar to PR1.10, this would ideally be verified through a full system test on the flight unit. However, since the flight unit will not be manufactured in this project, verification will happen through tests of a modified flight unit and analysis of how this compares to the expected theoretical results.

3.3.2. Design Dependent Technical Specifications

Designation	Requirement	Verification
PR2.1	The propulsion system shall be able to hold no less than 1.495 kg of R-236fa propellant.	Analysis
PR2.2	All valves should have a minimum cycle time of at most 13.5 ms	Inspection
PR2.3	The propulsion system shall have a means to measure properties of the propellant within the storage tank	Demonstration
PR2.4	Propellant storage tank shall be able to withstand 150 psia of internal pressure before yielding	Analysis
PR2.5	The propulsion system shall have the controlled ability to heat up the propellant	Demonstration

PR2.1

Justification: This requirement derives directly from PR1.11 and the requirement to be able to conduct all mission objectives. This mass is determined exactly by the rocket equation, or Eq. 2.7, which only involves the delta-V required, the spacecraft mass, and the specific impulse of the propellant. 1.495 kg was derived by the delta-V from PR1.11, a worst case spacecraft mass of 12 kg, and an assumed specific impulse of 40 seconds taken from the theoretical value and literature.

Verification: Ideally, PR2.1 would be verified through a system test on the flight unit to measure the maximum amount of mass it can contain. However, since the flight unit will not be manufactured in this project, verification will happen through analysis of the CAD to determine if the volume is large enough to store the required amount of propellant. It is assumed that the volume will be filled with liquid propellant such that the density is at least 1270 kg/m^3.

PR2.2

Justification: This requirement derives from the need for precision control of desaturation maneuvers. This response time is calculated from calculating the firing time required to desaturate 10% of the maximum momentum stored in the reaction wheels. Thrust is assumed to be the highest thrust possible under system constraints, meaning this thrust is calculated with a propellant pressure of 100 psi enacting a force 15 cm away from the center of

mass. The GNC team is using reaction wheels with 0.01 Nms of storage. Using equations found in Section 2.1.1.2, the thrust is predicted to be 0.247 N from a single thruster in worst case conditions at 50℃. Eq. 3.1 below shows this calculation for the length of the burn required to desaturate 10% of the capacity, accounting for two nozzles firing at once and assuming a constant maximum thrust. As such, this is a highly conservative result.

$$\frac{0.01Nms \cdot 0.1}{0.247N \cdot 2 \cdot 0.15m} = 13.5ms$$

Eq. 3.1

Verification: This requirement will be verified by inspecting the data sheet of the flight valves which include specifications on its response time.

PR2.3

Justification: PR2.3 derives from the requirement to have knowledge of the state of the propellant in order to inform precise control of delta-V maneuvers. Knowledge of the propellant pressure combined with performance characterization test prior to launch will provide accurate predictions of the expected level of thrust, which is essential in order to know how long each firing burst should be for mission operations.

Verification: This requirement will be verified through demonstration that sensors are installed and provide measurements inside the storage tank.

PR2.4

Justification: PR2.4 derives from the maximum operating pressure allowed for pressurized canisters on CubeSats before being subject to additional regulation, 100 psi. A safety factor of 1.5 was then applied to ensure the storage tank is never in danger of structurally failing.

Verification: This requirement will be verified through finite element analysis (FEA) of the designed tank by applying an internal pressure of 150 psi and ensuring no part of the tank yields.

PR2.5

Justification: PR2.5 derives from the requirement to control the temperature of the propellant to indirectly control the thrust output to meet mission objectives and firing maneuvers.

Verification: This requirement will be verified through a demonstration that the installed heater can be toggled on and off to heat up the propellant.

4. Mission Design

4.1. Mission Overview

The CaliPER mission is broken up into 4 distinct phases - deployment, chase, calibration, and disposal. The following sections will further investigate and explain these phases, outlining the trajectory design and plans for each phase. The deployment phase consists of the hours immediately after the spacecraft is deployed from the launch vehicle. The chase phase follows the deployment phase, and consists of CaliPER idling behind Clipper and catching up once the Clipper mission team gives CaliPER the go-ahead. Next, the calibration phase will consist of CaliPER maneuvering relative to Clipper to collect data from the REASON antenna. Finally, the disposal phase will last indefinitely as CaliPER enters a disposal orbit for the spacecraft to safely die.

As of January 2023, Europa Clipper is scheduled to launch on October 10th, 2024. Figure 4.1 below shows the path of Europa Clipper from Earth, to its Mars gravity assist, to its Earth gravity assist, and finally to its Jupiter insertion orbit. Given that CaliPER would be launched in the same launch vehicle as Europa Clipper, it will follow the same initial trajectory. All four of the aforementioned phases will occur between launch and the Mars gravity assist, which will occur on February 27th, 2025, 144 days after launch. Clipper will perform the Mars gravity assist and continue along the blue path by performing a trajectory correction maneuver, while CaliPER will not perform this correction and will instead enter a disposal orbit. During the period between deployment and Mars gravity assist, Clipper will always point its sun shield toward the Sun. This means that REASON will be facing directly away from the Sun and that CaliPER, during mission operations, will always be opposite the sun from Clipper.

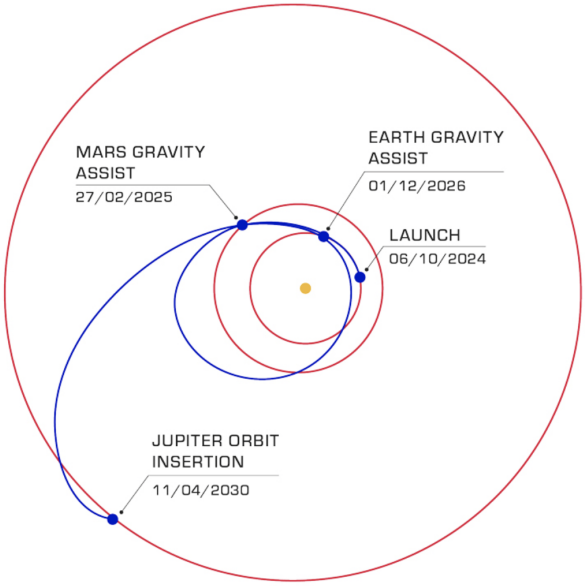

Figure 4.1: Clipper launch trajectory. Note that dates are listed in a DD/MM/YYYY format. [24]

In the following sections, the assumption will be made that all of CaliPER's delta-V maneuvers are sufficiently small such that they have no measurable impact on the larger trajectory. This assumption is valid due to the size of the delta-V maneuvers performed; as will be further described in the following sections, all bursts that only CaliPER performs will be <10 m/s and, in many cases, these changes in velocity will be immediately undone by a burst in of the same magnitude in the opposite direction. For comparison, the delta-V required for a Hohmann transfer to Mars is on the order of 1 km/s, which is three orders of magnitude larger than the size of the delta-V maneuvers CaliPER will be performing. Following this assumption, all velocity references will be made in Clipper's local frame of reference. As a consequence of this assumption, directions can be thought of as either parallel to the orbital path (in the direction of travel), or perpendicular to the orbital path.

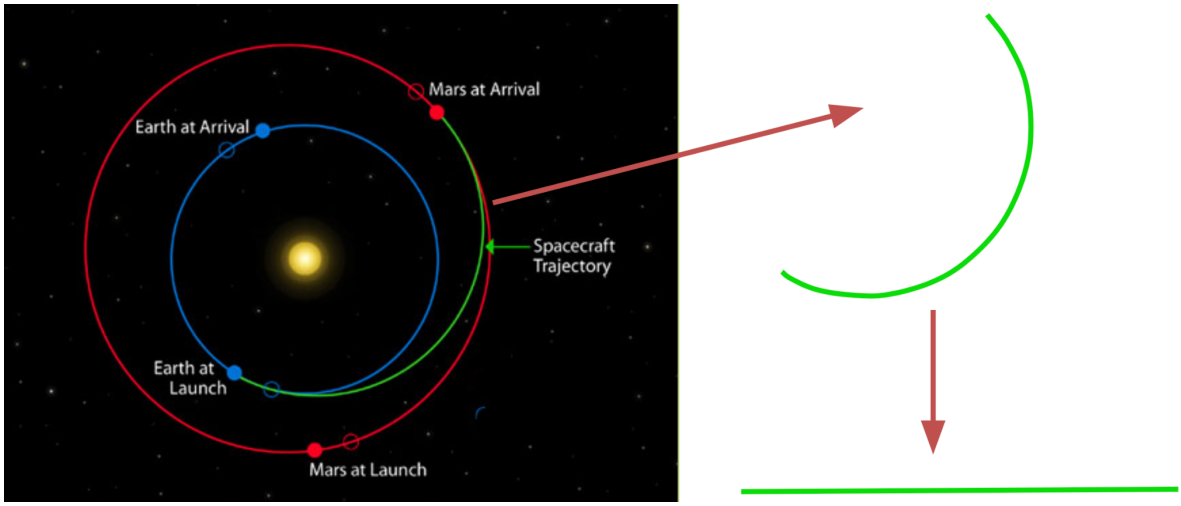

Figure 4.2: Sample Earth to Mars trajectory. The overall elliptical green trajectory can be approximated as linear in the Clipper's local frame of reference.

4.2. Trajectory Planning

The following sections will describe the delta-V firings throughout each phase of the mission, for which quantitative justifications will be found in Appendix A. All significant delta-V maneuvers will use the internal heater to warm the propellant to the appropriate temperature in order to increase thrust and efficiency. Details on the power required and timeline of heating can be found in Section 5.3.3 and 5.2.4.2.

4.2.1. Deployment Phase Design

Though Clipper and CaliPER will be deployed from the same launch vehicle, they will not be deployed at the same moment. In order to satisfy the separation distance requirement in MR3, CaliPER must be deployed some time after Clipper's deployment. According to the Clipper team, it can be assumed that deploying Clipper imparts a 2 m/s velocity relative to the launch vehicle. This means CaliPER must deploy no earlier than 10.42 hours after Clipper which will be when Clipper is 75 km in front of the launch vehicle.

As is standard for CubeSats, CaliPER will be deployed off of the side of the launch vehicle, rather than from the front with the primary payload. CaliPER is designed to integrate seamlessly with standard 6U commercial deployment systems. Like Clipper, deployment from the launch vehicle will give CaliPER some relative velocity which will be assumed to take on a value of 0.5 m/s perpendicular to the orbital path trajectory [25]. After the groundstation is able to establish communications with CaliPER, the spacecraft will be detumbled, the solar panels will deploy, and the spacecraft will slew to point to the Sun to collect power. Immediately following this maneuver, the propulsion system will perform a 2 m/s burn in the direction of the orbit path so that CaliPER and Clipper are traveling along the orbital path at the same speed.

This means that the component of separation distance along the direction of the orbital trajectory will now be constant and CaliPER will be completely stationary relative to Clipper.

Depending on which direction CaliPER is ejected from, the spacecraft may have to travel some distance to position itself on the side of Clipper opposite the Sun, where REASON is pointing and where CaliPER must traverse to collect REASON data. Conservatively assuming it takes 1 hour to gain control of the spacecraft, this distance could take on a value of up to 76.8 km. This number comes from 1.8 km of drift distance over 1 hour traveling 0.5 m/s and 75 km of perpendicular distance away from the orbit path in order to safely satisfy MR3 during the calibration phase. The total delta-V needed to move this worst-case scenario distance is 0.045 m/s in addition to the 0.5 m/s required to cancel the initial deployment velocity. Once CaliPER has moved to the appropriate side of Clipper and stopped itself, CaliPER is stationary relative to Clipper and will coast behind Clipper until the next mission milestone.

4.2.2. Chase Phase Design

After the previous maneuvers, CaliPER will remain on standby as it coasts behind Clipper, maintaining a constant distance. During this period of time, Clipper will be performing its own system checkouts and will not be ready to interact with CaliPER. According to JPL, this non-interference period will last at least 45 days after deployment. Once JPL informs the CaliPER team that Clipper is ready for REASON calibration, CaliPER will perform a 6.0 m/s burn in the direction of travel. This number is calculated as the speed required to coast through the entire calibration plane in 12 hours. Assuming CaliPER is 75 km behind Clipper in the direction along the orbital path, it will take approximately 4 hours to catch up to Clipper traveling at 6 m/s. Since CaliPER will simply be coasting until Clipper is ready for the calibration phase, the timing of this chase burn is extremely flexible and can be adjusted without issue based on when Clipper is available to use REASON.

4.2.3. Calibration Path Planning

The Calibration phase begins immediately after the initial 6.0 m/s burn. Due to the positioning of CaliPER after the deployment phase, this 6 m/s burn along the orbit path will mean CaliPER will fly past Clipper with a closest approach of 75 km when CaliPER is at nadir, the very center of the REASON beam pattern. Since CaliPER had to catch up to Clipper, there was freedom of design in determining the best path to minimize delta-V expenditures as the exact manner in which CaliPER caught up to Clipper could be altered to suit different paths. The calibration path chosen is seen below in Figures 4.3a and 4.3b. To comply with MR6, CaliPER must complete the *x* and *y* passes in 12 hours each, shown in green and red respectively in the figure below.

Given the perpendicular distance between CaliPER and Clipper, after the burn giving CaliPER an 6 m/s relative velocity to Clipper, CaliPER will coast the length of the *x*-axis (green)

in 12 hours. While CaliPER is coasting the spacecraft may slew in whatever orientation is necessary to collect REASON data and collect solar power. Data transmission back to Earth will happen at the conclusion of the 12-hour pass.

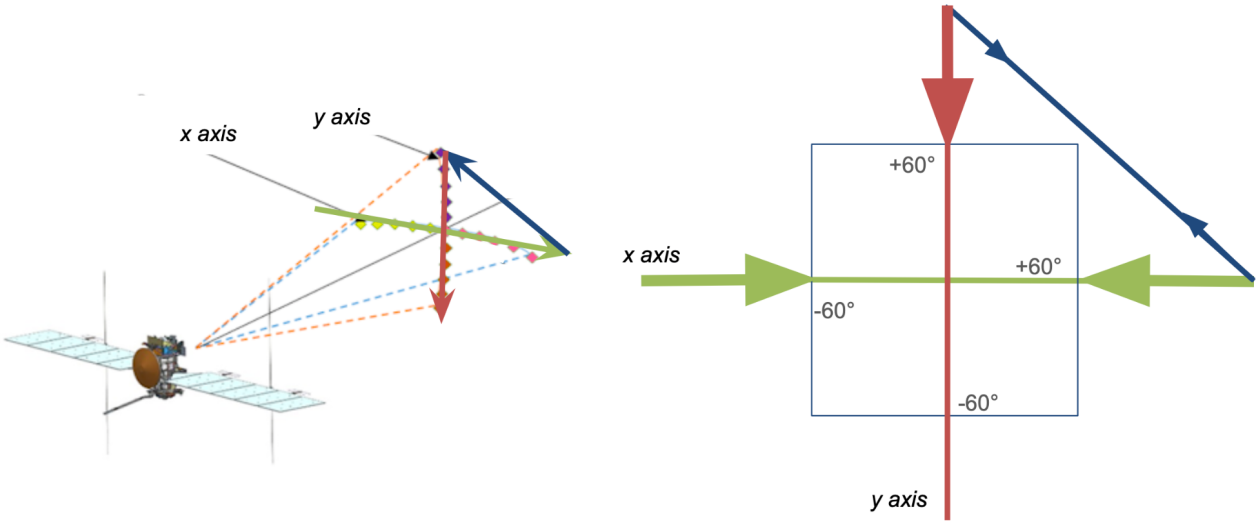

Figure 4.3a (left): "Connected Cross" calibration path with each segment color coded. Clipper is shown in the proper orientation during calibration. Arrows indicate the direction of travel. Figure 4.3b (right): Front view of calibration trajectory as seen from Clipper's perspective. Box delineates ± 60° calibration zone and arrows represent the direction and magnitude of velocity changes

After completing the first pass, CaliPER will immediately perform another 6 m/s burn opposite the direction of travel to counter the previous burn and remain at the intersection of the green and blue lines seen in Figure 4.3b, stationary relative to Clipper.

Once CaliPER is stationary with respect to Clipper again, CaliPER will slowly make its way to be in position for the second and final calibration pass down the *y*-axis. This path is seen in blue in Figures 4.2a and 4.2b. The precise amount of time to travel this path is subject to when Clipper is able to dedicate another 12 hours to calibration for CaliPER. Assuming this travel is allowed to take 40 days, this connecting path will require two burns of ~ 0.05 m/s each. Since there are over 90 days between the non-interference period and the Mars gravity assist, a 40 gap in between calibration passes is reasonable and is adjustable without significant cost to delta-V.

After traveling the length of the blue arrow in Figure 4.3b, CaliPER will position itself approximately 2120 km above the +60° mark on the *y* axis, which is at the intersection of the blue and red lines in Figure 4.3b. This is to provide the spacecraft with enough distance in which to accelerate to a coasting speed of 6 m/s before entering the calibration zone. Once CaliPER receives the go-ahead from the Clipper team, CaliPER will perform this final 6 m/s burn. Like

the *x*-axis calibration segment, CaliPER will coast through the calibration zone to collect REASON data. The calibration phase is now complete.

4.2.4. Disposal Phase

The disposal phase is the last phase of the mission. During this phase, the CubeSat will communicate any last data back to Earth, then continue in its eccentric heliocentric orbit indefinitely. The purpose of any disposal orbit is to ensure that the spacecraft has no risk of colliding with another planet. This is to protect the planet from any microbial life lingering on the satellite, which could contaminate the planet and interfere with future scientific observations. Fortunately for CaliPER, the initial launch trajectory is designed to not actually intersect with Mars for the gravity assist; instead, the launch trajectory is designed to narrowly miss Mars, so that in the event that JPL loses control of Clipper early in the mission, there is no risk of collision with Mars. This means that when Clipper approaches Mars, it must perform a trajectory correction maneuver (TCM) to place it on the correct path for a gravity assist flyby. Meanwhile, CaliPER will simply continue on its original orbit with no corrections and will therefore not collide with Mars.

The final delta-V maneuver of the calibration phase, the 6 m/s burn to coast through the *y* axis, will not significantly change the orbit path. As mentioned in the mission overview, REASON will always be pointing directly away from the sun. Therefore, the 6 m/s burn through the *y* axis is normal to the orbital plane, and only causes an inclination change. Eq. 4.1 is the equation for a simple plane change maneuver, which can be used for an order of magnitude approximation for the inclination change.

$$\Delta V = 2v sin\left(\frac{\theta}{2}\right)$$

Eq. 4.1

v is orbital speed and θ is the inclination change as a result of the delta-V maneuver. Approximating the orbit as circular and the orbital speed as Mars's orbital speed (24.07 km/s), one can rearrange to solve for the inclination change, θ, and find that the angle change is on the order of 0.01 degrees. This change is not of any concern to the safety of the disposal orbit.

4.2.5. Other Delta-V Expenditures

During all phases of the mission, CaliPER will experience a variety of external torques. It is the GNC subteam's responsibility to counter these external torques via the use of reaction wheels. However, as the reaction wheels counter torques from deployment and solar radiation, they will eventually require the use of the propulsion system to desaturate their reaction wheels, which will require approximately 1.5 m/s of delta-V. The full calculation can be found in

Appendix A. The amount of angular momentum the propulsion team is required to desaturate was provided to the propulsion team. Given the angular momentum the thrusters needed to impart and assuming the worst case moment arm, the delta-V required to impart this impulse was calculated.

Between deployment from the launch vehicle and the Mars gravity assist, Clipper will perform a series of trajectory correction maneuvers totaling 18.0 m/s. Delta-V is a mass-independent quantity, meaning CaliPER will have to match these maneuvers exactly in order to stay in the correct position with respect to Clipper. Due to ITAR restrictions, the exact timing and nature of these maneuvers could not be shared with the CaliPER team. However, because the bulk of CaliPER's mission will simply be coasting — only 24 hours of the 144-day mission is collecting REASON data — there is minimal concern about being able to schedule the TCMs within CaliPER's mission timeline.

4.3. Delta-V Budget

Phase	Maneuver	delta-V [m/s]	Rationale
Deployment	Match Clipper's Speed	2.0	Needed to match Clipper's deployment speed from launch vehicle
Deployment	Cancel Deployment Velocity	0.5	Needed to cancel CaliPER's deployment velocity
Deployment	Move to Position	0.045	Worst case delta-V needed to move 75 km away from Clipper on the side REASON
Calibration	Move through Connected Cross Path	18.14	Needed to catch up to Clipper, stop after the first calibration segment, move in position for the 2nd calibration segment, and then accelerate to coast through the 2nd calibration segment
All	GNC Desaturation	1.48	Needed to desaturate the reaction wheels over the course of deployment through disposal
All	Trajectory Correction Maneuvers	18.0	Europa Clipper will perform a series of TCMs between deployment and Mars gravity assist - the ΔV of a given trajectory is mass independent, so CaliPER must match these
Total with 1.3x safety factor: 52.21			

Table 4.1: Delta-V Budget

5. Propulsion System Design

5.1. System Overview

5.1.1. System Selection

As discussed in Section 2.1.2., each type of propulsion system has its own unique advantages and disadvantages. Discussed below are the relevant considerations.

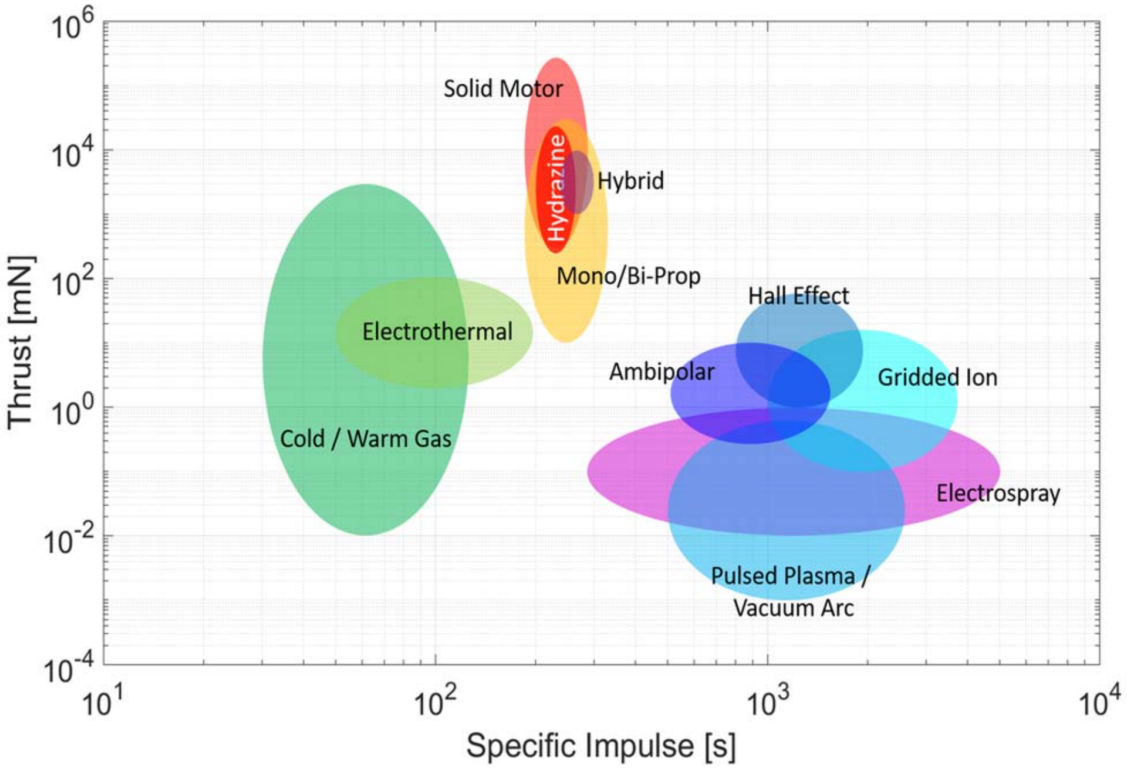

Figure 5.1: Various propulsion technologies plotted on a thrust vs specific impulse graph figured generated in [12]

Electric propulsion has the benefit of having a low mass of propellant and an extremely efficient means of accelerating this propellant. This gives electric propulsion systems a large specific impulse as can be seen in Figure 5.1. Unfortunately, it also has a very low thrust, meaning that acceleration will be very slow and burns will take very long. Additionally, these systems are extremely electronically complex and still undergoing active research to miniaturize the technology for the CubeSat scale. As this project is to satisfy the S.B. requirements for a Mechanical Engineering degree, electric propulsion falls too far outside of the field to be a realistic option.

Chemical propulsion has the benefit of large power output. The thrust that it produces is

greater than that of both electric and cold/warm gas propulsion, and its specific impulse still lies somewhere in the middle, as can be seen in Figure 5.1. However, these extremely exothermic chemical reactions pose more safety risks and would be limited by University rules and resources. In fact, Harvard does not allow students to test fire any rocket engines on campus, which would prevent any testing of the design. Additionally, using such volatile compounds poses a high risk to Clipper while in the launch vehicle.

Cold gas propulsion has the benefit of simplicity and heritage. The design is much more straightforward, and its propellant is easy to attain. Unfortunately, its specific impulse is rather limited, and its thrust is mediocre, as can be seen in Figure 5.1. However, these systems are feasible to design, construct, and test within the limited time frame and budget while still able to meet mission requirements. Ultimately, a cold gas propulsion design was chosen. Given the time frame, safety limitations, heritage, and necessary skills, it was the most logical decision. To reiterate, cold gas propulsion does not use any combustion whatsoever - simply the release of compressed gas. However, terms such as “firing” and “burn” are still used to refer to the expulsion of gas to produce thrust, and are not to be confused or associated with chemical combustion.

5.1.2. Propellant Considerations

R-236fa was chosen as the propellant for this cold gas system due to its flight heritage and high volumetric impulse. R-236fa is a readily available commercial refrigerant found in fire extinguishers, making it easily available to official research labs or EPA-certified technicians. It is non-toxic, inert, and simple to handle due to its low vapor pressures. As seen in Table 5.1 below, though R-236fa has the lowest specific impulse relative to the other cold gas propellants considered, it has the 2nd highest volumetric impulse only ~1% behind ammonia [19]. Because CubeSats are primarily volume-constrained systems, having a high volumetric impulse is the most critical characteristic. Ammonia was not chosen due to its complexity in handling, high causticity, and high vapor pressures.

Notably, R-236fa has significant flight heritage on satellite propulsion systems. For example, it was used in the MarCO, Bevo-2, BioSentinel, INSPIRE, and SunRISE propulsion systems demonstrating its reliability in propulsion systems.

Name	*M* [g/mol]	I_{sp} [s]	Density [kg/m^3]	I_{vol} [N-s/m^3]
R-236fa	152.04	46.9	1360	625 721
R-134a	102.03	49.3	1207	583 600
Butane	58.12	73.1	564	404 832
CO2	44.01	67.6	711	471 172
Ammonia	17.03	106.7	603	630 967
Nitrogen	14.00	77.6	113 *	85 641
Helium	4.00	177.3	16.4 *	28 525

Table 5.1: A comparison of the properties of various propellants [19]

To find the mass of propellant required to meet technical specification PR1.10, Eq. 2.9 can be used with values of 52.21 m/s for ΔV, 12 kg for m_0, and 40 seconds for I_{sp}. This value for I_{sp} is a theoretical estimation using the equations found in Sections 2.1.1.1 and 2.1.1.2 to calculate the expected value at propellant temperatures greater than 10℃ and assuming empirical efficiencies found in the literature [10]. Eq. 2.9 gives that 1.495 kg of propellant is necessary for the mission. Since R-236fa has a worst-case liquid density of 1270 g/cm^3 at 50℃, this requires a storage volume of 1.177 L based on the assumption that all propellant could be stored as a liquid. Detailed calculations can be found in Appendix A.

To contain such a large amount of propellant onboard, it is necessary to store it in a liquid phase. If the propellant was stored purely as a gas, the storage container would need to withstand unrealistically high pressures. Therefore, it is necessary to use a two-phase system. This means that the propellant is stored in the tank as a saturated liquid-vapor mixture. When firing, the valves will open and directly expose the 2-phase mixture to vacuum, causing the liquid to vaporize before expulsion.

5.1.3. System Map

Figure 5.2 shows a system diagram of the propulsion system.

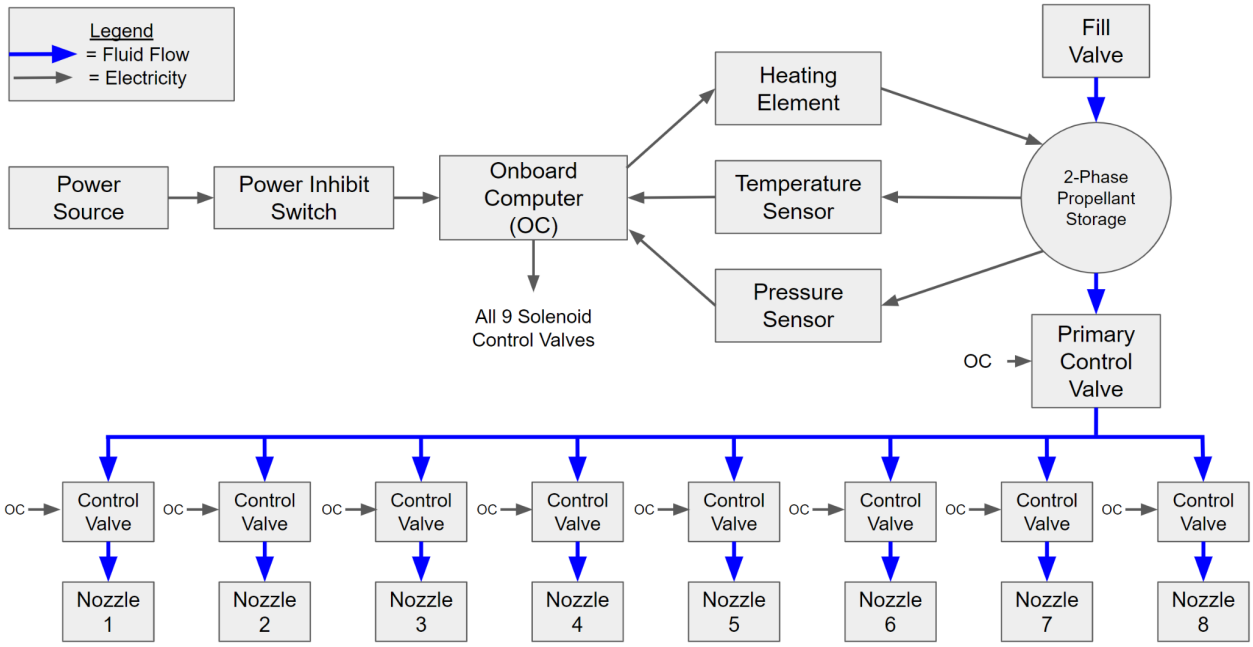

Figure 5.2: System diagram of propulsion system

As indicated by the legend in the top left corner of Figure 5.2, gray arrows indicate the flow of electrical signals and power, while blue arrows indicate the flow of fluid (the propellant) throughout the system.

The power inhibit switch is a mechanical switch that will prevent any power from entering the system until the CubeSat is deployed from its pod, which will be further discussed by the Bus subteam. Once power is connected to the system, the onboard computer (OC) will then control the propulsion system. The OC will receive data from the temperature and pressure sensors located within the propellant storage tank. It will then input this information into a simple control system, which then will selectively send power to the heater within the storage tank to raise the temperature to the desired level. This feedback control system is further discussed in Section 5.3.1. The OC will independently control each of the nine solenoid control valves in order to control the fluid flow throughout the system. The primary control valve is located directly outside the propellant storage tank, allowing it to prevent any fluid flow throughout the system. When the primary control valve is open, the fluid can flow up to each of the nozzles. However, the fluid can only flow through each nozzle when its respective control valve is opened. Therefore, the onboard computer can effectively independently control which nozzle(s) are thrusting at any given point.

5.1.4. Manufacturing Methods

Recent developments in additive manufacturing have made 3D printing a viable alternative to finding the right commercially available parts. Commercial-off-the-shelf (COTS) parts are generally desired because they are inexpensive relative to custom-designed parts and easy to procure. Buying from reputable suppliers also ensures that the products received have been properly tested and will conform to the standards supplied by the manufacturer. However, due to the very nature of COTS parts being generic, they may not be applicable to a specific application. Making requests for even slight alterations from the supplier can dramatically increase both the lead time and cost of the parts, if possible at all. In contrast, 3D printing allows for the extreme customization of each part without a significant price or lead time increase, but also without a guarantee of performance.

Given the extreme mass and volume constraints of CubeSats, commercial parts that fit the specific requirements were extremely difficult to procure. Most storage tanks that could hold the required volume were much too large to fit within our subsection of the CubeSat. Additionally, fitting and mounting all the valves and tubing around potential commercial solutions were not feasible in the limited space. Given these limitations, a primarily 3D-printed subsystem was chosen.

This approach of 3D printing propulsion systems already has successful flight heritage in CubeSats, as previously discussed in Section 2.2. Printing the storage tank allows for the full utilization of the limited space, making the system very volume efficient compared to the cylindrical COTS storage tanks. Unfortunately, since plastic is weaker than metal and the tank is not a conventional shape, FEA simulations and testing are required to ensure that it can handle the pressures. Both the tubing and nozzles can be integrated into the body of the 3D-printed tank, allowing for even greater packing efficiency. The heater, sensors, and solenoid valves are too complex to 3D print, so COTS parts will be selected for those components.

The 3D printing material chosen was Accura Bluestone. It is an SLA printing material with high printing accuracy and great thermal resistance. It has a high strength, high stiffness, and it is used often in “under the hood” automotive parts [26]. All four of the previously 3D printed propulsion systems discussed in Section 2.2 were printed in Accura Bluestone, which demonstrated excellent chemical compatibility with R-236fa propellant. The success of the systems also demonstrated the material’s ability to hold an airtight seal in a vacuum.

5.2. Mechanical Design

5.2.1. Body Design

5.2.1.1. Body Overview

The “body” refers to the single 3D-printed object, which contains the storage tank, nozzles, and internal tubing. Figure 5.3 displays the current CAD model of the entire propulsion system, where the body is displayed in blue. The Valve Assembly can be seen on the rear (-Z) face, and the slightly protruding tubes are the nozzles. The heater, thermistor, pressure sensor, and fill valve all enter through manifolds on the +Y face.

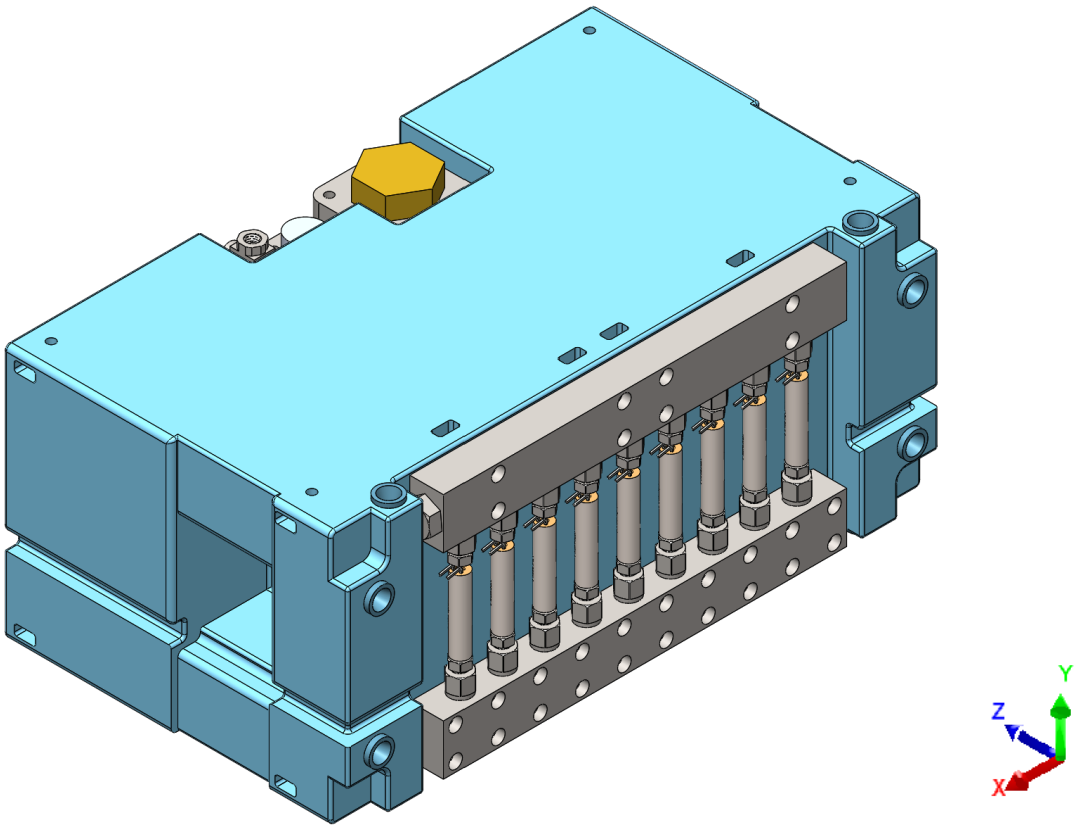

Figure 5.3: Full Propulsion system CAD

5.2.1.2. Internal Storage Tank and Tubing

Figure 5.4 shows a cross-sectional view of the propulsion system. The large cavity in the body is the storage tank for the propellant.

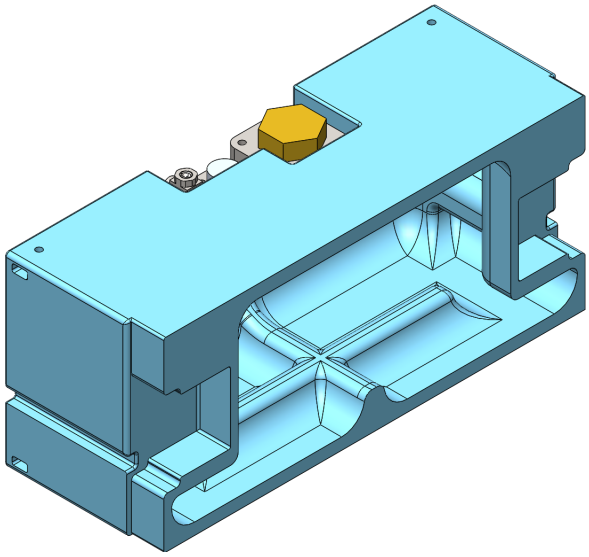

Figure 5.4: Cross sectional view of propulsion system CAD

The storage tank has a volume of 1.257 L, which surpasses the minimum required volume of 1.177 L needed to meet technical specification PR1.10, as is described in Section 5.1.2. This gives the system a delta-V of approximately 56 m/s assuming a specific impulse of 40 seconds. Figure 5.5 shows the internal volume of the storage tank.

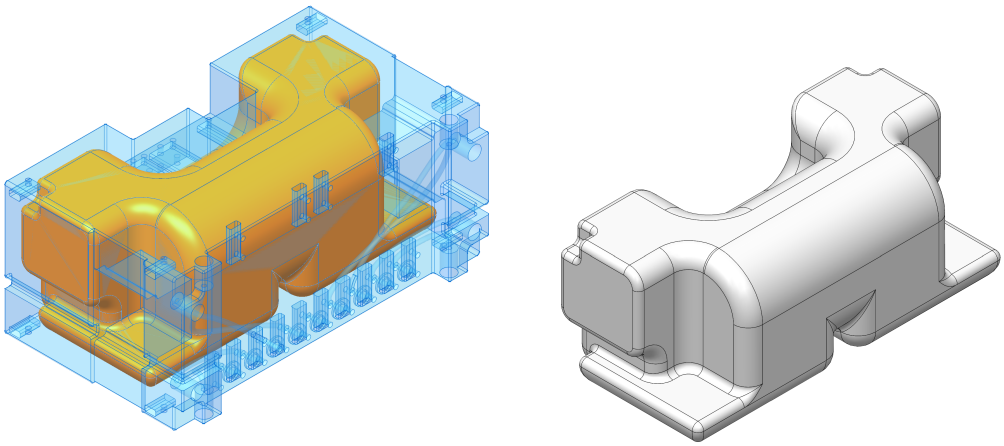

Figure 5.5a (left): Isometric view of the internal volume of the storage tank, shown in orange, within the larger propulsion system body, shown in translucent blue.
Figure 5.5b (right): Isometric view of the isolated negative volume of the storage tank

To meet technical specification PR2.4, this storage tank was designed to withstand an

internal pressure of 150 psi. Based on “back of the envelope” calculations, a default wall thickness of 4 mm was used to start, and walls were thickened in areas of structural weakness. A cross-beam was extruded from the -Y wall of the tank, seen at the bottom on Figure 5.4, in order to stiffen that face. Additionally, every corner in the storage tank was filleted to reduce stress concentrations. Corners where larger stress concentrations were found were given fillets with larger diameters.

As will be explained in Section 6.1 , this test model could not be built for testing, so the best way to verify technical specification PR2.4 was through finite element analysis. Solidworks Simulation was used to simulate a 150 psi pressure on the internal walls, and results are shown in Figure 5.6. The stress scale was manually adjusted so that any red coloration in the results indicates that the yield stress of Accura Bluestone, 67 MPa, has been reached.

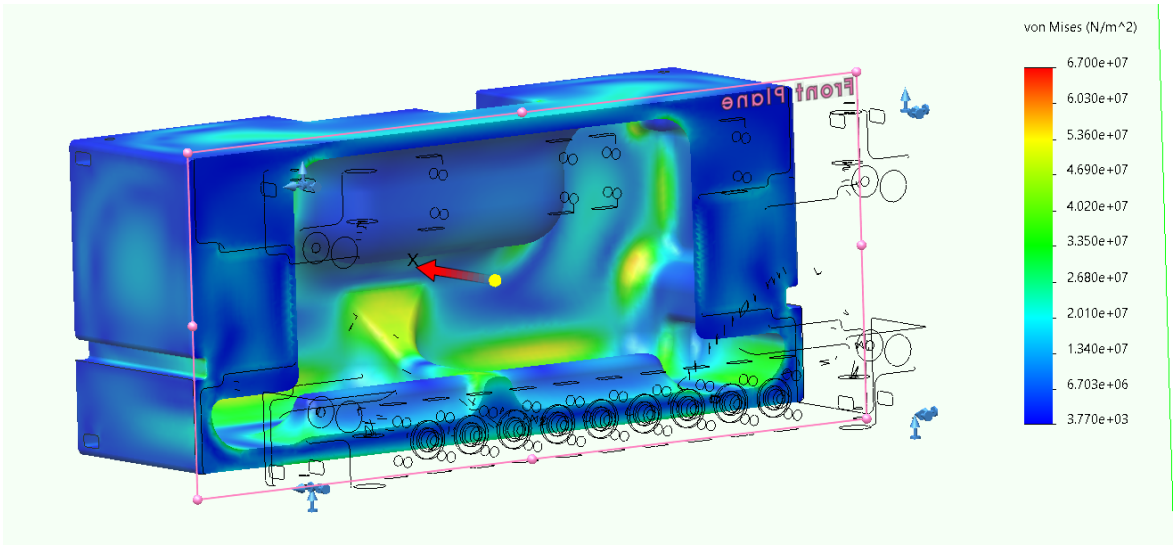

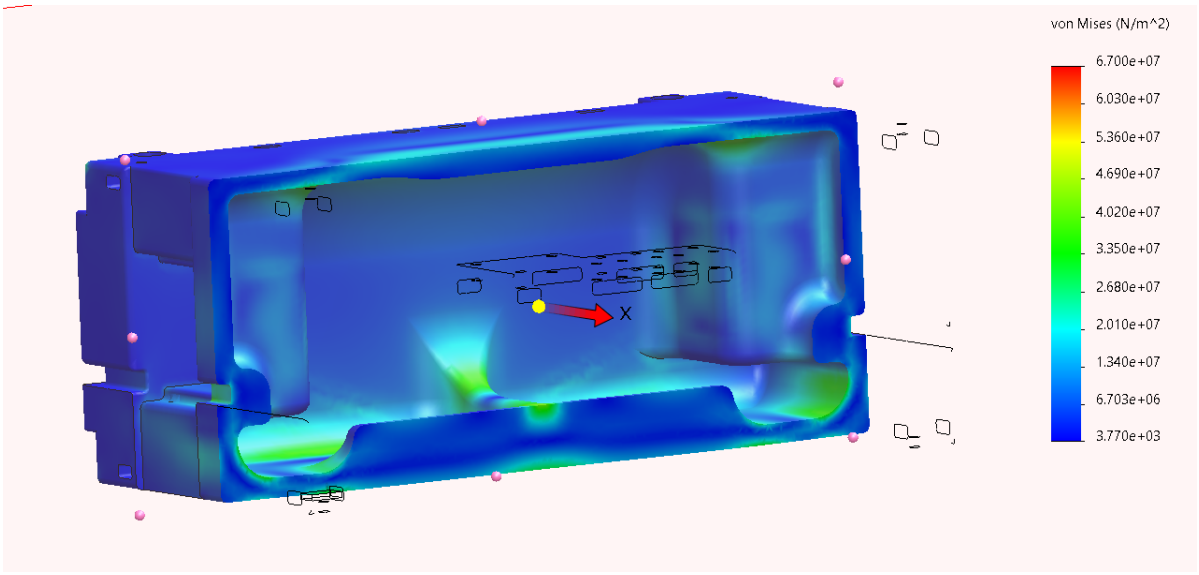

Figure 5.6a (top): Section view of FEA stress results
Figure 5.6b (bottom): Section view of FEA stress results, opposite view to 5.6a

As seen in Figure 5.6, there was no red coloration in the results, so the storage tank would not yield at 150 psi, therefore verifying technical specification PR2.4.

To allow fluid to flow throughout the system, internal tubes were cut within the body. This avoids the need for more external tubes and tube fittings, which take up valuable space and are potential causes of leaks. These internal tubes, seen in Figure 5.7, connected each of the nozzles directly to their respective ports on the -Z face.

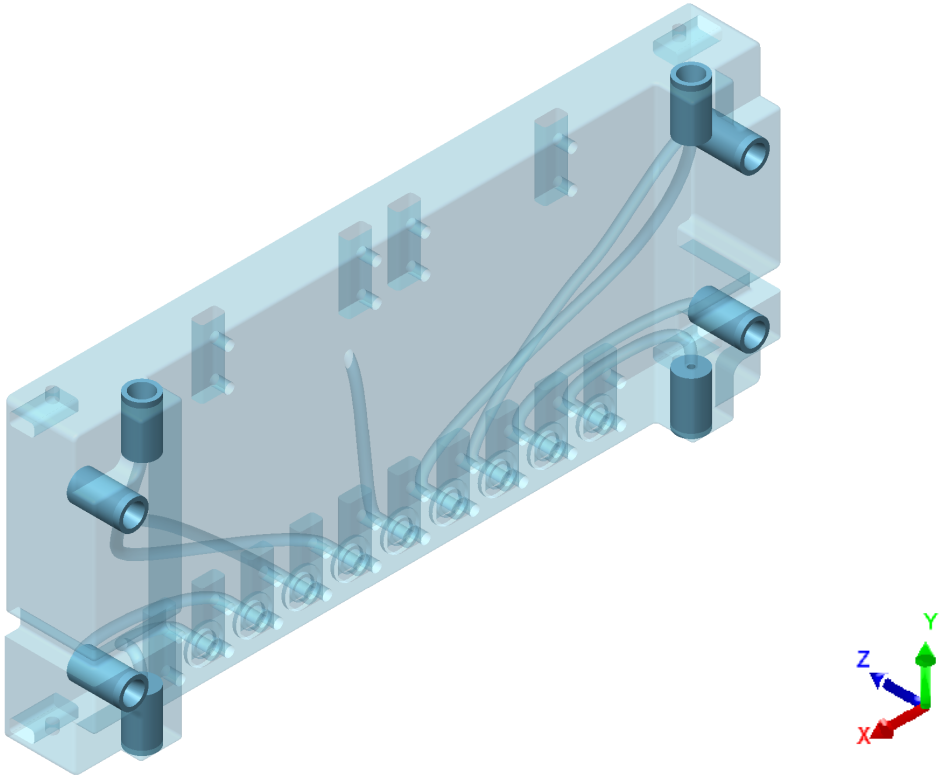

Figure 5.7: Cross sectional and translucent view of the body, displaying internal tubing

5.2.1.3. Body to Bus Integration

The propulsion system will sit in the “rear” of CaliPER, meaning on the -Z face. It is designed to fit snugly within the rails and the -Z facing nozzles are flush with the back plate. Figure 5.8 shows the propulsion system in relation to the bus.

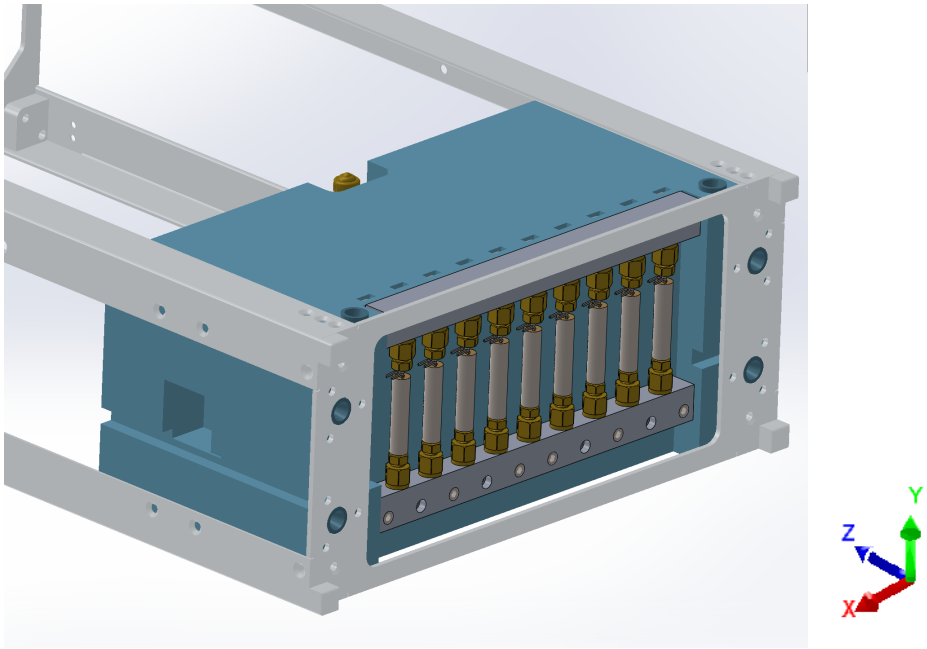

Figure 5.8: CAD of the propulsion system and the bus

The propulsion system will be mounted with eight screws. Countersunk holes will be drilled through the rails, through which 4-40 screws will stick that will mate with a nut stuck in the body of the propulsion system. Once all eight screws are tightened, the propulsion system will be fixed rigidly to the bus.

5.2.1.4. Exclusion Zones

The solar panels on CaliPER require a motor to alter their angle to maximize solar energy and this motor must be located in the same area occupied by the propulsion system. As a result, the propulsion system body has a cubic hole cut into the side of it where the motor can sit without collision. There is also a narrow line cut into the side of the body where wires can be routed. This ensures that the wires will remain within the confines of the CubeSat. Both the motor cutout and the wire cutout, referred to as exclusion zones, can be seen highlighted in blue in Figure 5.9.

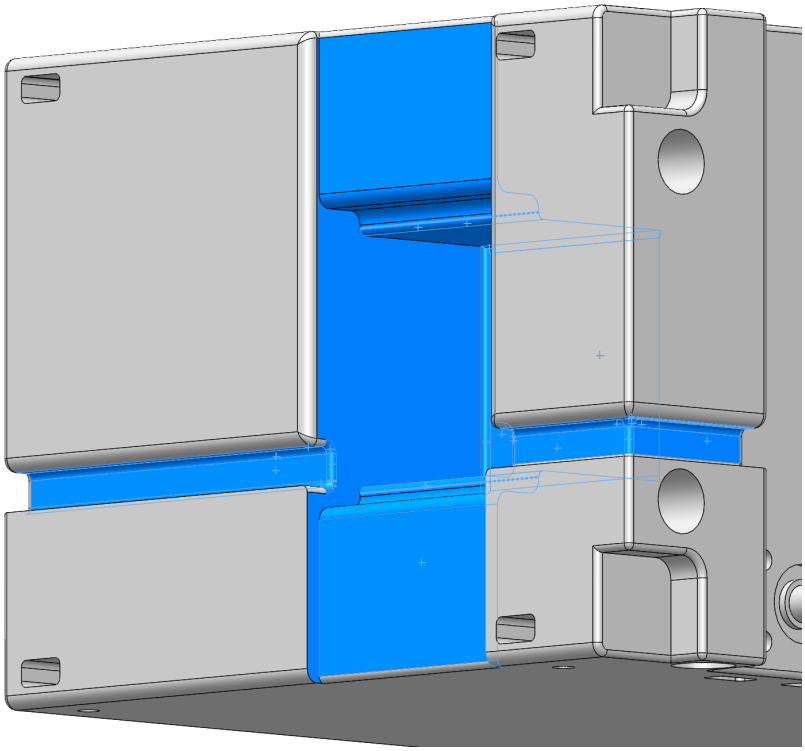

Figure 5.9: Body exclusion zones

5.2.2. Nozzles

5.2.2.1. Nozzle Design

Nozzle design is an extremely complex problem. Converging-Diverging nozzles were invented in the late 19th century, and are still being researched to this day to optimize the design. Due to the time limitations on the project, the team was advised to not spend large amounts of time on the nozzle and instead select a simple and proven design.

Converging-diverging nozzles feature three main sections. The first is the converging section, where the subsonic gas is rapidly compressed until it reaches the throat, which features the smallest cross-sectional area. As the gas passes through the throat, it is maximally compressed and, if choked, has a Mach number equal to one. The gas then continues through the diverging section, where it expands and accelerates to supersonic speeds and produces thrust. Figure 5.10 illustrates the sections of the nozzle.

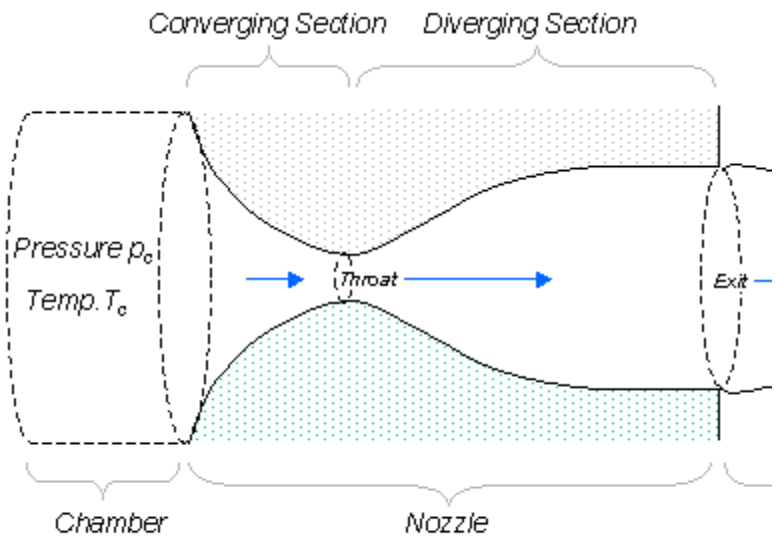

Figure 5.10: Illustration of a simple converging-diverging nozzle [27]

The design of the converging section does not significantly impact the thrust produced [9], so a simple conical shape was chosen for that section of our nozzle. The design of the diverging section has the largest effect on the thrust produced, so more focus was given to that design. Some common diverging nozzle variations are shown in Figure 5.11.

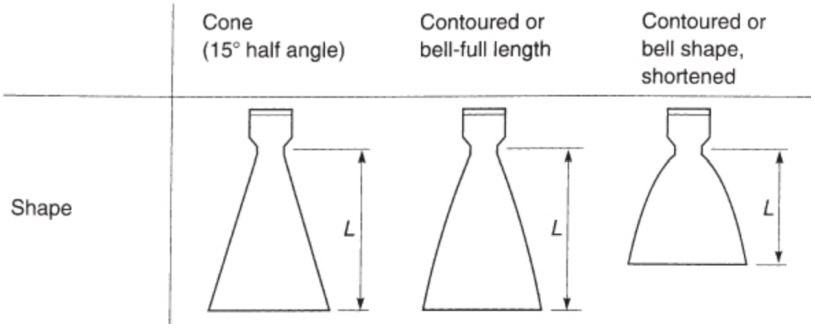

Figure 5.11: Illustration of common nozzle types [9]

Ultimately, the conical nozzle design was chosen. It is the simplest to design and fabricate and offers a performance similar to the more efficient bell-shaped nozzles. This performance can be described through a correction factor, λ, which signifies the nozzle's real performance relative to an ideal nozzle. Figure 5.12 displays data on three different nozzles, which shows that the conical nozzle and bell-shaped nozzle's correction factor differ by at most 0.5%.

Nozzle Exit Area Ratio	**10**	**25**	**50**
Cone (15° *Half Angle*)			
Length (100%)[a]	8.07	14.93	22.66
Correction factor λ	0.9829	0.9829	0.9829
80% Bell Contour			
Length[a]	6.45	11.94	18.12
Correction factor λ	0.985	0.987	0.988
Approximate half angle at inflection point and exit (degrees)	25/10	30/8	32/7.5
60% Bell Contour			
Length[a]	4.84	9.96	13.59
Correction factor λ	0.961	0.968	0.974
Approximate half angle at inflection point and exit (degrees)	32.5/14	36/17	39/18

Figure 5.12: Data on conical and bell-shaped nozzles [9]

Once the conical nozzle was chosen, the half angle, area ratio, and length of the cone then had to be determined.

The half angle is simply the angle between the centerline and the slope of the cone. According to the textbook *Rocket Propulsion Elements*, a half angle of 15 degrees has become the unofficial standard in the field [9]. As a result, 15 degrees was selected to be the half angle.

The area ratio of the nozzle is defined to be the ratio of the area of the nozzle throat to the area of the nozzle exit. Given a defined angle for the cone, the area ratio and the cone length are directly related through basic trigonometry. To select an appropriate area ratio for our application, we first calculated the theoretical performance of our nozzle using the equations described in Section 2.1.1.2, which directly depends on the area ratio of the nozzle. We then swept over a range of area ratios and plotted the resulting I_{sp} and delta-V, shown in Figure 5.13. The derivative of the Isp curve was plotted as well, shown in Figure 5.14.

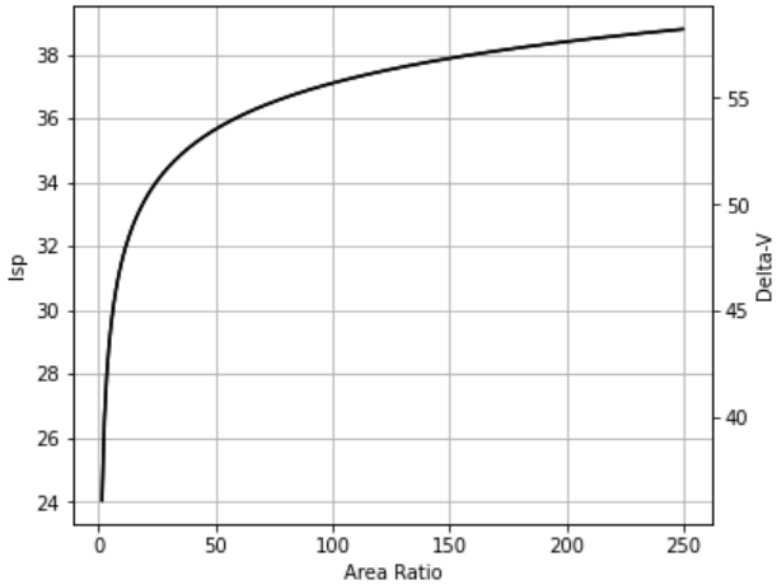

Figure 5.13: Graph of I_{sp} and delta-V vs Area Ratio

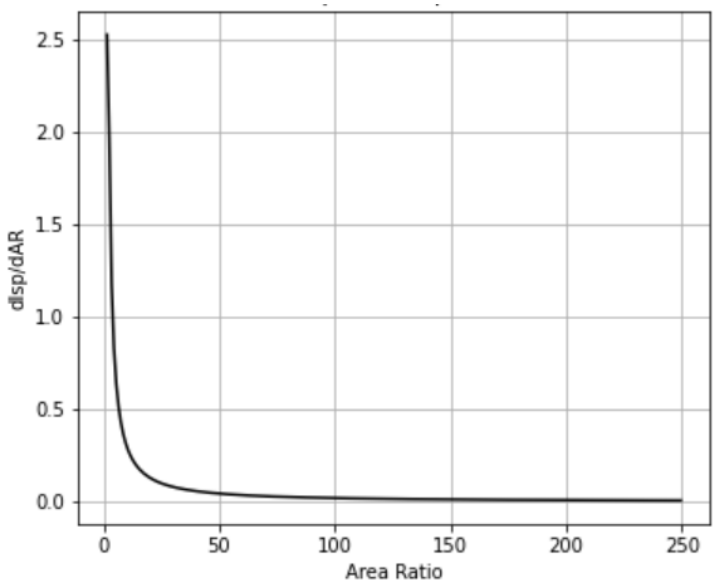

Figure 5.14: Graph of the derivative of I_{sp} vs Area Ratio

As can be seen in Figure 5.13, a larger area ratio corresponds to a larger I_{sp}, so it is always advantageous to maximize the area ratio in a vacuum setting. However, the marginal increase in I_{sp} is very small for an increase in the area ratio beyond 100, as seen in Figure 5.14. Additionally, there are size limitations that constrain the area ratio. Firstly, these nozzles will be printed on SLA printers, which generally have a minimum hole diameter of 0.5 mm. To maximize the area ratio, this minimum hole diameter of 0.5 mm was chosen to be the throat exit area. Secondly, due to the placement of the nozzles, which is discussed in Section 5.2.2.2, the

end diameter was limited to 1 cm, including the walls. To ensure the rigidity of the walls, they were chosen to be 1.5 mm thick, which gives an exit diameter of 7 mm and an area ratio of 196:1. This ratio is within the flat part of the I_{sp} curve, so slight variations in the area due to manufacturing should not significantly alter I_{sp} in either way, giving more predictable performance. This area ratio, along with the chosen half angle, means that the nozzle length must be approximately 13 mm. Shown below in Figure 5.15 is a cross-section of the nozzle design.

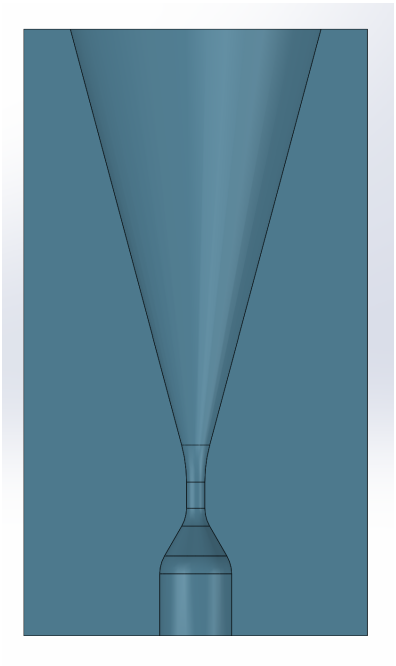

Figure 5.15: Cross section of nozzle

Now that the area ratio of the nozzle is known, the model introduced in Section 2.1.1.2 can be used to predict thrust values. Figure 5.15 shows the approximate thrust a single nozzle produces at a variety of chamber temperatures.

Chamber Temperature (deg C)	**Single Nozzle Thrust (mN)**
50	247
40	186
30	136
20	97
10	68

0	46
-10	30
-13	25
-20	18
-30	10

Table 5.2: Table of predicted thrust values for given temperatures

Note that at -13 degrees C, a single nozzle produces 25 mN of thrust, the threshold thrust for tech spec PR 1.11.

5.2.2.2. Nozzle Placement

As stated by PR1.5 and PR1.6, the propulsion system shall have the ability to rotate the spacecraft about all 3 principal axes and to translate the spacecraft. To ensure that this requirement is met, four nozzles were placed on the -Z face, two were placed on the +Y face, and two were placed on the -Y face. Figure 5.16 displays the location of the nozzles along with labels of 1 through 8, displayed in red. The blue translucent object is the "body" of the propulsion system, as discussed in Section 5.2.1.

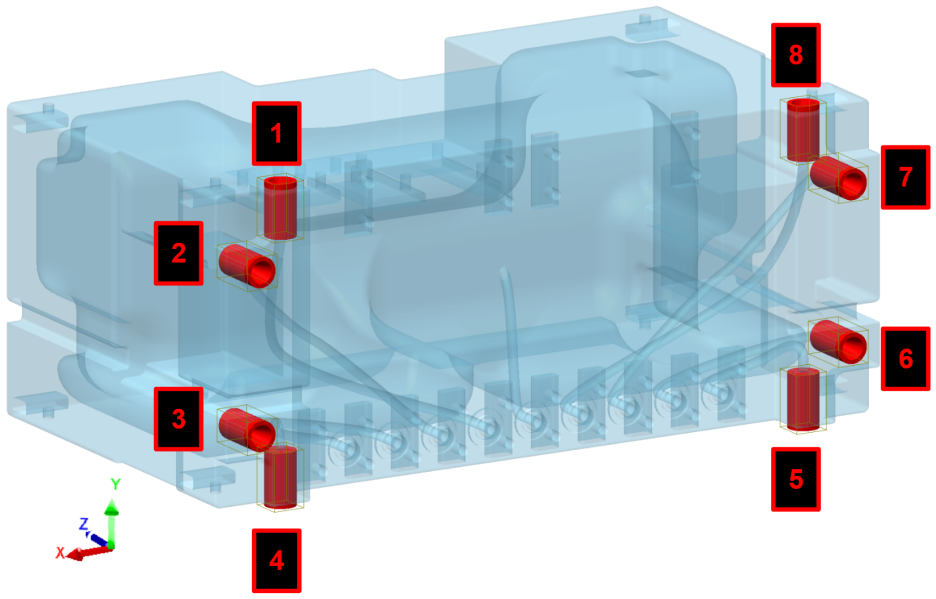

Figure 5.16: Location of all 8 nozzles

Firing nozzles 2, 3, 6, and 7, which are the four nozzles on the -Z face shown in Figure 5.17, allows the spacecraft to translate in the +Z direction.

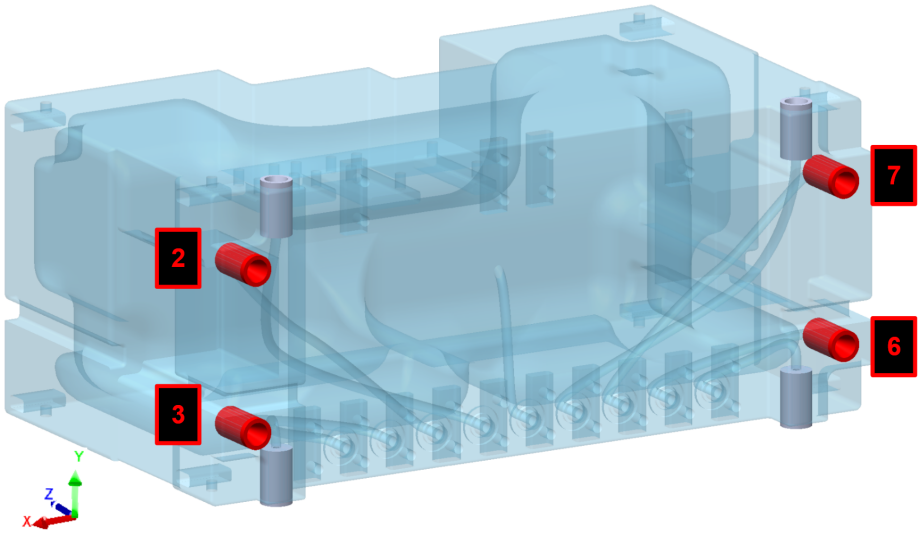

Figure 5.17: Nozzles fired for +Z axial motion

In order to rotate about the X axis, nozzles 1 and 8, or nozzles 4 and 5, can be fired. Figure 5.18 highlights nozzles 4 and 5, which can be fired to rotate the spacecraft in the +X direction.

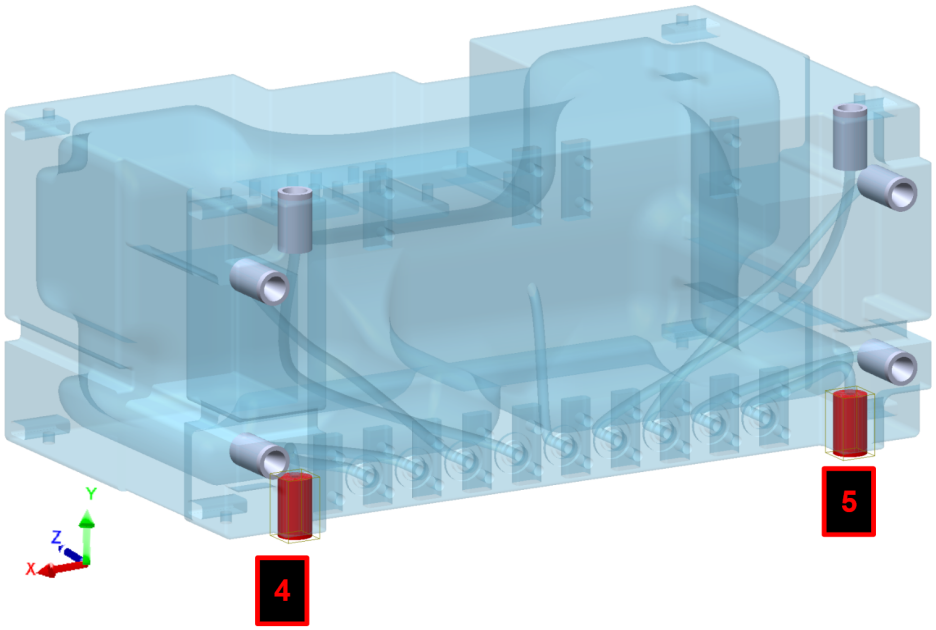

Figure 5.18: Nozzles fired for +X rotation

In order to rotate about the Y axis, nozzles 2 and 3, or nozzles 6 and 7, can be fired. Figure 5.19 highlights nozzles 6 and 7, which can be fired to rotate the spacecraft in the +Y direction.

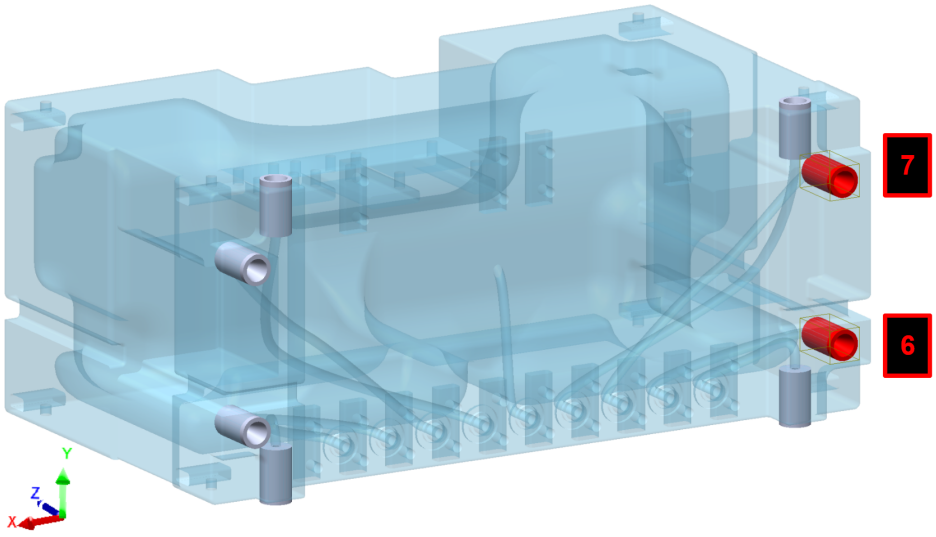

Figure 5.19: Nozzles fired for +Y rotation

In order to rotate about the Z axis, nozzles 1 and 5, or nozzles 4 and 8, can be fired. Figure 5.20 highlights nozzles 1 and 5, which can be fired to rotate the spacecraft in the -Z direction.

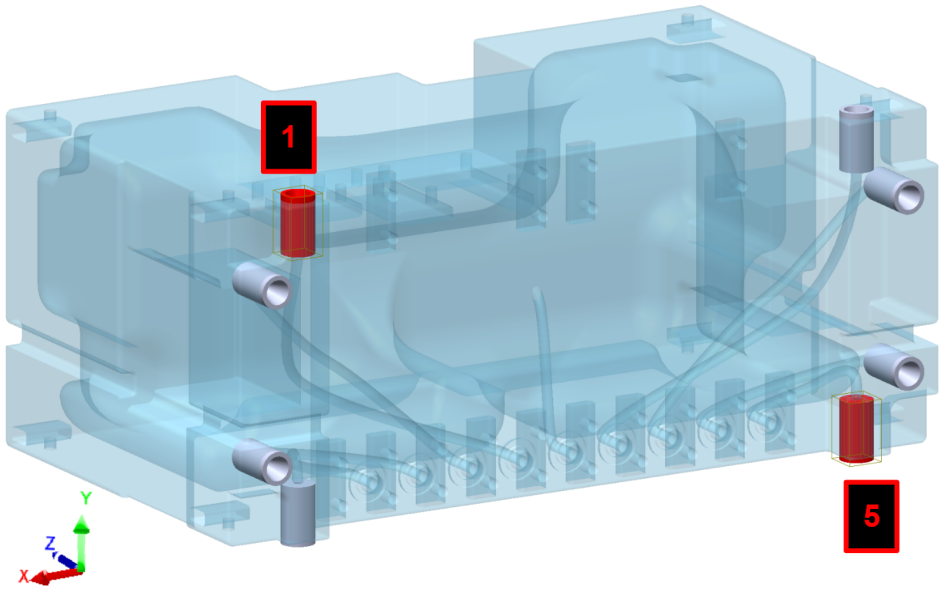

Figure 5.20: Nozzles fired for -Z rotation

5.2.3. Flow Control

5.2.3.1. Port-Manifold Interface

The purpose of the manifolds is to connect the fluid path from the plastic body to the metal fittings. There is a manifold wherever there is a connection from plastic to metal, and they all connect to the same fundamental port design. A "port", shown in Figure 5.21, is a section of the plastic body that consists of an alignment tube and an o-ring gland.

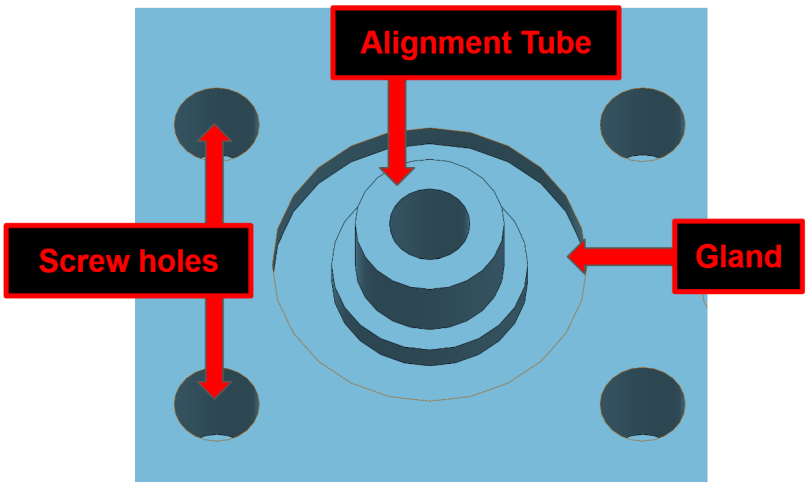

Figure 5.21: Diagram of a port

The alignment tube helps locate the hole on the manifold, making assembly easier. The hole leads directly to an internal tube or storage tank, whichever is needed for the exact port. Figure 5.22 shows a transparent manifold placed over the same port seen in Figure 5.21. Note that o-rings were not included in the CAD to decrease loading times and processing power required, but they sit within their designated glands.

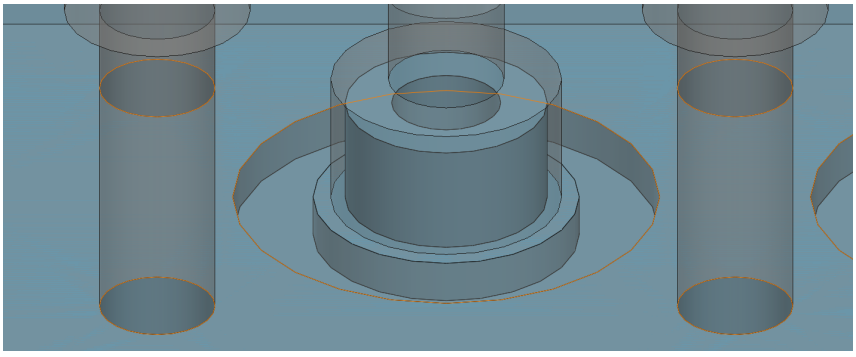

Figure 5.22: Transparent manifold over port (o-ring not included in image)

As can be seen in Figure 5.22, the manifold hole is slightly larger than the alignment tube, but smaller than the inner diameter of the o-ring gland. This means that the o-ring will be pressed up against the flat bottom face of the manifold to create a face seal. To ensure a good seal the gland is designed such that the gland depth is 75% of the O-ring thickness, the o-ring volume is 75% of the gland volume, and the o-ring has a 3% stretch [28]. Machine screws that pass through both the manifold and the screw holes in the body then mate with a nut and can be tightened to stabilize the manifold and sufficiently compress the o-ring to create a tight seal.

The o-rings chosen for this mission were made from Neoprene. Neoprene is specifically made to be resistant to refrigerants, so it will not react with our R-236fa propellant [29]. Additionally, Neoprene o-rings can withstand a temperature range of -45°F to +250°F, or -42.7°C to +121°C, which is more than the temperature range set for this mission.

5.2.3.2. Valve Selection

The valve chosen for this design was the "High Speed In-Line Solenoid Valve" by the Lee Company, which is shown in Figure 5.23.

Figure 5.23: Chosen solenoid valve, the High Speed In-Line Solenoid Valve by the Lee Company [30]

This valve is specifically manufactured for use in CubeSats. It functions in temperatures ranging from -29℃ to 49℃ and it can operate at up to 500 Hz, allowing short bursts for precise CubeSat control [30]. The mass is only 4.7 grams and the maximum diameter is 6.2 mm, which is useful for the compact nature of the project. Additionally, the holding power required is only 0.25W, so the power subsystem will not be drained much if the valve needs to remain open for a long period of time. These advantages have led to the use of this valve in other CubeSat propulsion systems, such as Bevo-2, Biosentinel, Sunrise, and Inspire, which are described in Section 2.2.

5.2.3.3. Valve Assembly

The valve assembly is responsible for allowing propellant to travel from the storage tank to each individual nozzle. This assembly has two manifolds, shown in Figure 5.24.

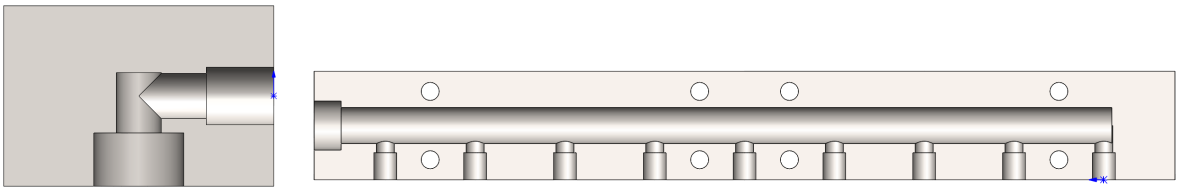

Figure 5.24a (left): Side section view of the outlet manifold
Figure 5.24b (right): Top section view of connector manifold

The outlet manifold interfaces with all the ports on the -Z face, allowing fluid to pass through the port and directly to the valve that is perpendicular to it. Each connection from port to valve is independent, and the cross section of this path can be seen above in Figure 5.24a. The connector manifold does not interface with any port. Instead, it connects all of the valves with one long hole cut through most of the manifold that is plugged at the end, as seen in Figure 5.24b. If any fluid flows into this manifold, it is directed out to all the other valves. This design eliminates nine plastic-to-metal interfaces, all of which are potential spots for leakages to occur. Both of these manifolds connect to the valves by way of a steel compression fitting. One end of the fitting screws into the manifold and the other end can form an airtight seal with the steel tubing on either end of the solenoid valves when properly tightened. Both of these manifolds are made of steel so that their threads remain intact and airtight, even if fittings are screwed in and out multiple times.

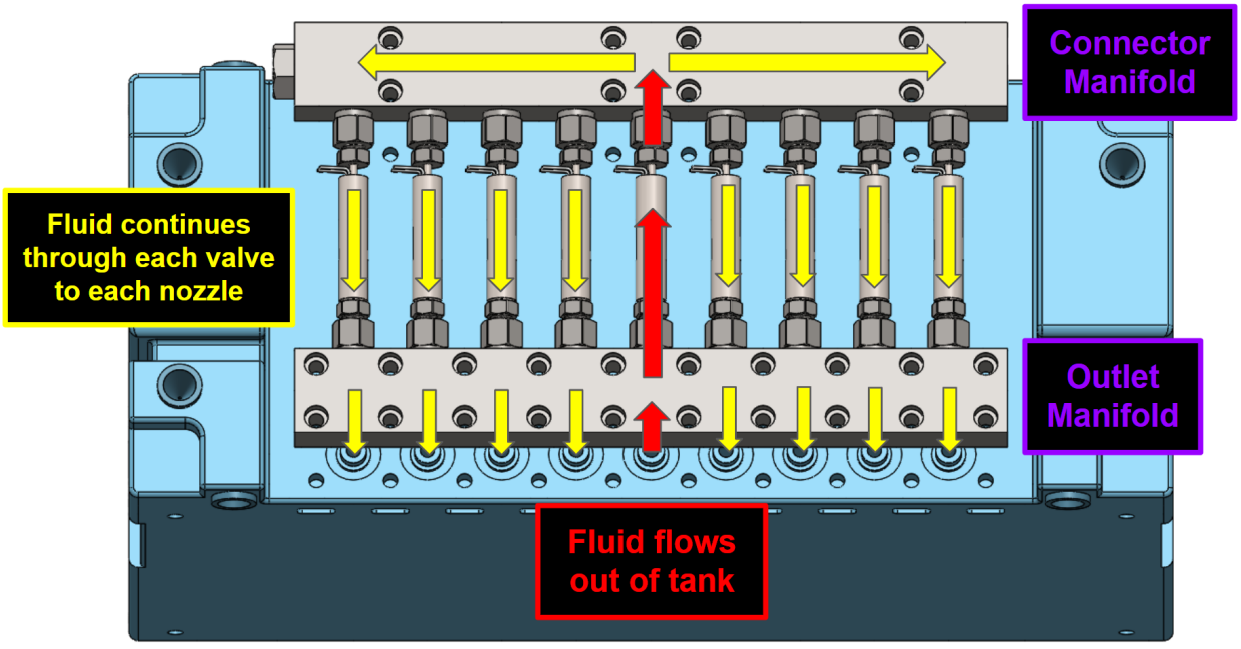

Figure 5.25: Flow Diagram of Valve Assembly

Shown above in Figure 5.25 is the flow diagram of the valve assembly. Fluid flows out

the tank through the central port, through the outlet manifold, and into the primary control valve (the central valve). When the primary control valve is opened, the fluid then flows into the connector manifold when it is distributed to each of the other eight valves. When one or more of those valves are opened, the fluid flows through the open valves, through the outlet manifold, and into one of the non-central ports. These eight ports are each connected through internal tubing directly to one of the eight nozzles, where the gas can finally escape.

5.2.3.4. Fill Valve

A manual valve from McMaster, part number 4668T51, was added to allow the user to fill the tank. This valve will only be opened to fill the tank, and then closed for the rest of the mission. The valve chosen was a miniature on/off ball valve that can withstand a temperature range of -60°F to +300° F [31].

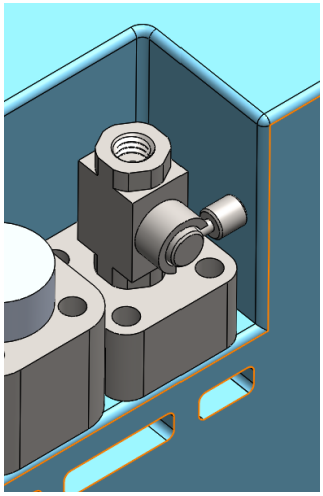

Figure 5.26: Fill valve and manifold

As seen in Figure 5.26, it is connected to the storage tank through a manifold interface. This valve is located on the +Y face of the propulsion system, so it can be accessed without removing the propulsion system from the bus and therefore allowing for multiple fillings during testing.

5.2.4. Thermal Consideration

5.2.4.1. Thermal Expansion

Since the system will potentially experience large temperature fluctuations, thermal expansion must be considered. The entire valve assembly is made of steel, so it will all expand/contract at equal rate. However, the main location where an issue may arise is the

interface between the steel manifold and the 3D-printed plastic body. The plastic has a much higher coefficient of thermal expansion (17.3 x 10^{-6} $°C^{-1}$ for stainless steel compared to 38 x 10^{-6} $°C^{-1}$ for Accura Bluestone), so the plastic alignment tube may expand more and push into the inner face of the hole in the manifold. To ensure that the plastic would not yield, a worst-case COMSOL simulation was done. The simulation began with the plastic already contacting the inside face of the steel hole. The temperature was then raised by 50℃ to match our temperature limit.

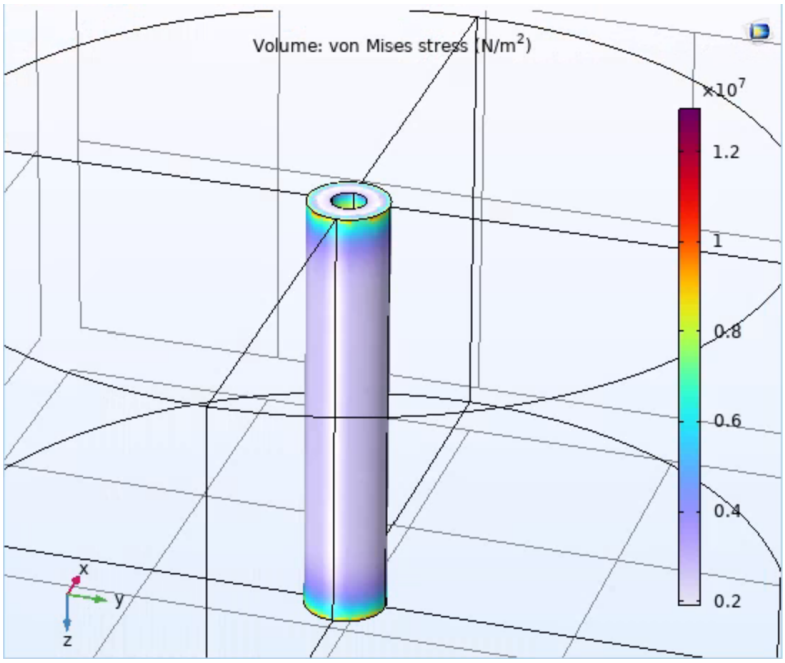

Figure 5.27: COMSOL stress results for thermal expansion of plastic into steel

The results of the simulation are shown above in Figure 5.27. Even with this extreme situation, the stress in the plastic was still under 15 MPa, which is well below the 67 MPa yield stress of the plastic. Therefore, thermal expansion should not be an issue for our design.

5.2.4.2. Propellant Heating

The largest single delta-V maneuver needed for this mission is 6 m/s, as described in Section 4.2.3. To achieve this delta-V, the propulsion system will need to thrust from all four axial nozzles for approximately 3.5 minutes. As the system fires, liquid propellant vaporizes and is expelled from the nozzles. Vaporization requires heat to occur, so heat is taken from the stored propellant as the firing continues. This lowers the temperature of the fluid in the chamber, therefore lowering the chamber pressure thrust. Figure 5.28 displays simulation results of firing for 3.5 minutes.

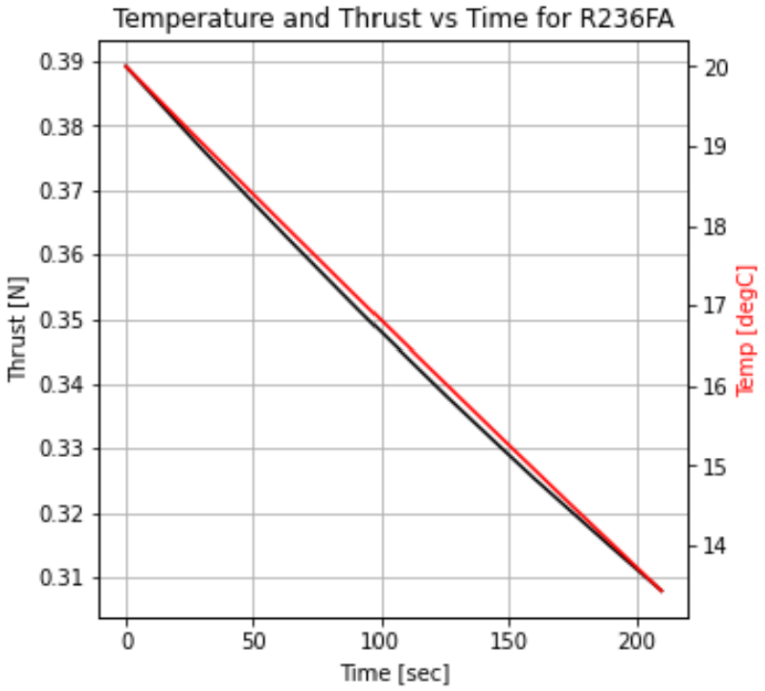

Figure 5.28: Graph of thrust and temp vs time

As can be seen in Figure 5.28, this 6 m/s maneuver drops the temperature from 20℃ to approximately 13℃ assuming there is no heating while firing. In order to control the temperature for each maneuver, the installed heater can be turned on prior to the maneuver. Higher temperatures increase both the thrust and specific impulse of the system, making it advantageous to keep the propellant as warm as possible during operations. To estimate the power required to heat up the propulsion system from one temperature to another, a conservative python script was included in the generated model (see Appendix C for the full code). It is a simple estimation that assumes that all propellant is in liquid form, since that has a higher specific heat capacity than gaseous R-236fa. Further, it assumes an extremely conservative efficiency factor of 50%, meaning that only half of the provided power actually enters the propellant. More details of the power required for different burns during the mission are discussed in Section 5.3.3.

5.3. Electrical Design

5.3.1. Control System

A control system was not within the scope of this project, so the topic was not investigated. Future work can further explore utilizing the data from GNC sensors to send commands to the propulsion system to achieve a specific maneuver given parameters on total impulse required and current propellant pressure conditions.

5.3.2. Additional Electrical Component Selection

In addition to the fill valve, all additional electrical components are located on the +Y face of the propulsion system, as seen in Figure 5.29.

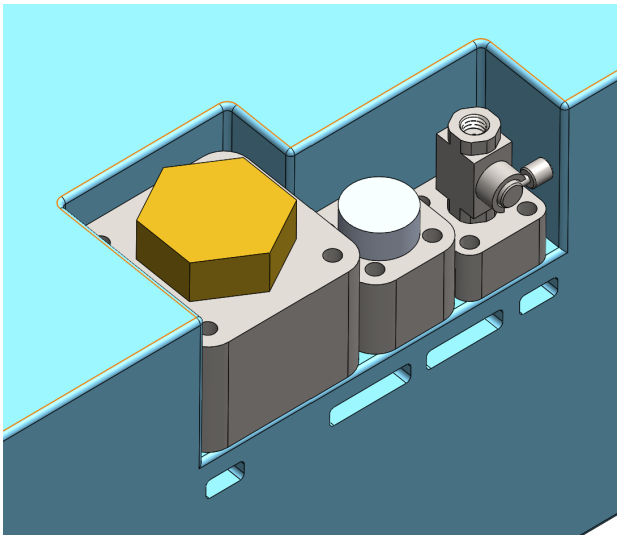

Figure 5.29: CAD of the wire passthrough, pressure transducer, fill valve, and their respective manifolds

This location allows these components to be replaced or otherwise accessed without the need to remove the propulsion system from the bus.

5.3.2.1. Pressure Sensor

To read the pressure within the storage tank, Omega's Subminiature Flush Diaphragm Pressure Transducer, part number PXM600MU-35BARGV, was chosen. As seen in Figure 5.30, the transducer is extremely compact, which is vital for this application.

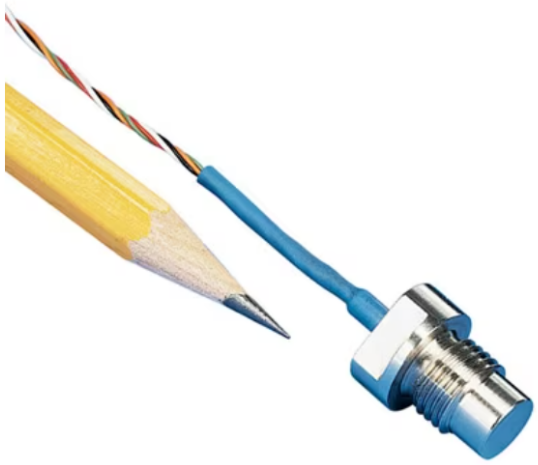

Figure 5.30: Chosen pressure transducer near a pencil

This transducer can measure pressures from 0 to 35 bar, and can operate in temperatures from -54°C to +121°C [32], making it suitable for this mission. It can be screwed directly into its manifold, creating an airtight seal.

5.3.2.2. Wire Passthrough

The temperature sensor and the heater have no threading and thus cannot be screwed into a manifold to create an airtight seal. To work around this issue, Omega's pressure NPT feedthrough will be used, part number PFT2NPT-1CU, as shown in Figure 5.31.

Figure 5.31: Wire Passthrough

This wire passthrough can be screwed into a manifold and create an airtight seal, while allowing up to four wires to pass through. These wires will be used for the temperature sensor and the heater. This feedthrough was chosen because it is chemically compatible with refrigerants, is operable from -40°C to 120°C, and is rated up to 120 psi [33].

5.3.2.3. Temperature Sensor

The temperature sensor chosen was a Minco miniature embedment RTD, part number S102951PD3E120AC1. This RTD is extremely small, with a diameter and length of less than a quarter inch. It is designed for harsh environments, with a temperature range of -50°C to 125°C [34]. There are several casing options available, with minor differences, shown below in Figure 5.32.

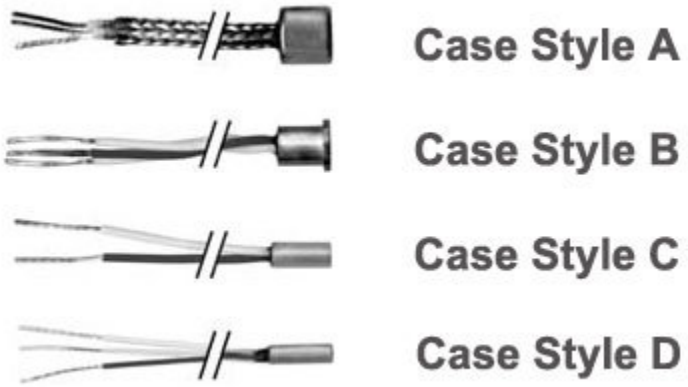

Figure 5.32: RTD casing options [34]

5.3.2.4. Heater selection

To heat the propellant in the storage tank, MINCO's Polyimide Thermofoil™ Heater, part number HK6910, was chosen. The heater can be seen in Figure 5.33. This heater was designed for use in satellite components, and it advertises NASA approval. Based on calculations in Section 5.3.3, a 42 W heater was chosen to satisfy the needs of heating the propellant up dramatically in only 2 hours. Since information on the TCMs is unavailable as well, an overestimate is safe. If once the detailed thermal analysis is performed it is determined that the heater is oversized, either a smaller heater can be chosen or the oversized heater can be run on a PWM circuit to reduce power output.

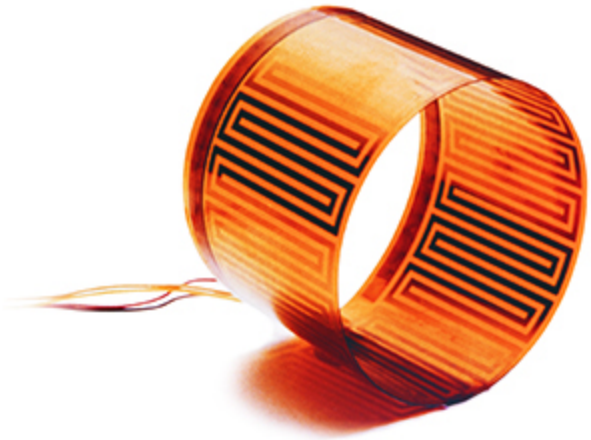

Figure 5.33: Polyimide Thermofoil™ Heater [35]

5.3.3. Power

Below is an estimation on power required during various stages of the mission. Because detailed thermal and heat transfer analysis was beyond the scope of this project, calculated powers are conservative over estimates. The table below is what the propulsion team provided the solar subteam for their extensive spacecraft power budget, which can be found in their report. During all burns, the power specified in this table is only the power required to hold the necessary valves open. However, all spare power should be sent to the heater to reduce performance loss during the burn. Temperature assumptions are listed in the right most column. This budget has been approved by the solar subteam, however, if the warm up power is too intense then the power required can be decreased at the expense of the length of time the propellant must be heater for.

Time	Propulsion	Description	Assumptions
ASAP After Deployment	1.25 W for 4 min	Clipper Catch Up 2m/s burn	No warm up, start at -10℃
ASAP After Deployment	1.25 W for 1 min,	Cancel 0.5 deployment vel + move to REASON side of Clipper	No warm up, start at -10℃
Day ~ 45	30 W for 2 hours	Catch up pre-heat	-20℃ to 30℃
Day 45 + 2 hours	1.25 W for 4 min	6 m/s calibration	30℃
Day 45 + 16 hours	12 W for 2 hours	6 m/s Slow down preheat	10℃ to 30℃

Day 45 + 18 hours	1.25 W for 4 min	6 m/s slowing down	30℃
Day ~ 46	1.25 W for 1 min	Move to y axis burn prep	No warm up, start at -10℃
Day ~ 85	1.25 W for 1 min	Stop in y axis to prep next burn	No warm up, start at -10℃
Day ~86	30 W for 2 hours	y axis calibration pre-heat	-20℃ to 30℃
Day 86 + 2 hours	1.25 W for 4 min	6 m/s calibration	30℃
Unknown	30 W for 2 hours, then 1.25W for x min (depending on size of TCM)	TCMs	-20℃ to 30℃ for warm up, then 30℃ for burn
Throughout Mission	0.75W for 4 min	Desaturation 2 m/s total	-10℃

Table 5.3: Estimated power budget

5.4. Overall Size

The CubeSat Design Specification states that a 6U CubeSat may extend up to 22.3 cm along the X axis, while the other dimensions remain at the standard of 10 cm per U. Therefore, to meet technical specification PR1.2, this propulsion system should have overall dimensions of 10 cm x 22.3 cm x 10 cm. This spec was not met, as the overall dimensions of the designed system are 10 cm x 22.3 cm x 13 cm, as shown below in Figure 5.34.

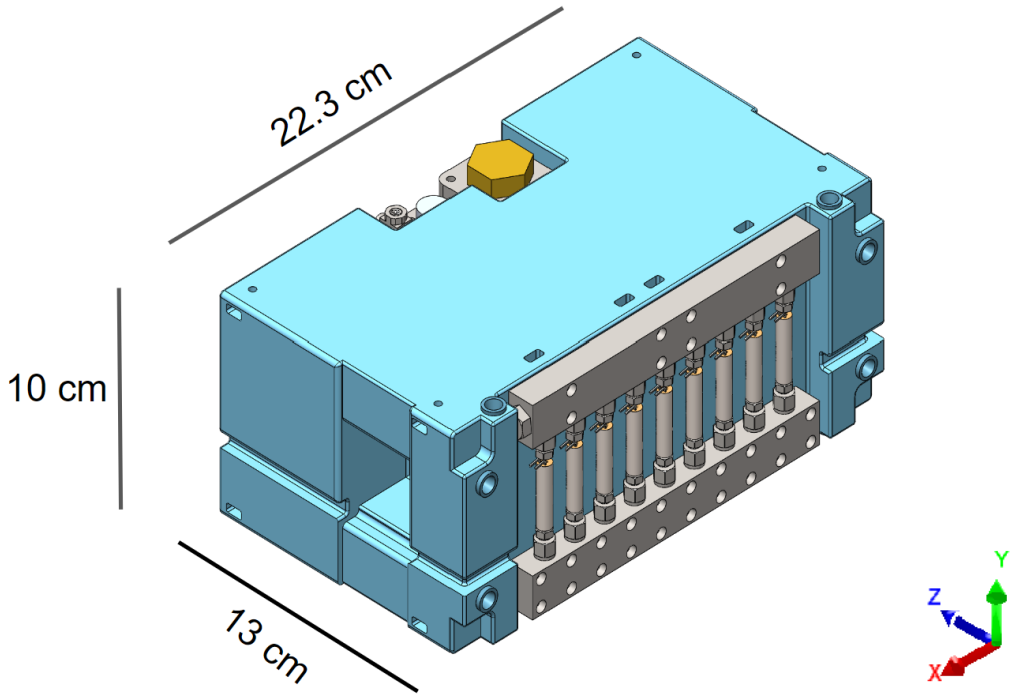

Figure 5.34: Overall dimensions of propulsion system

Similarly, to meet technical specification PR1.1, the wet mass of the system should be less than 3.6 kg. This spec was not met, as the system has a dry mass of 2.94 kg and a wet mass of 4.44 kg.

Technical specifications PR1.1 and PR1.2 were not met because tech spec PR2.1 and PR2.4 were prioritized over them. Tech spec PR2.1 must be met so that the system has enough propellant to complete the mission. Tech spec PR2.4 must be met so that there is a low risk of CaliPER damaging the primary launch payload, Clipper.

As described in Section 5.2.1.2, many internal fillings and fillets were necessary to design the tank to withstand an internal pressure of 150 psi for tech spec PR2.4. These changes occupied much space, decreasing the internal volume of the tank. In order to meet tech spec PR 2.1 as well, the body had to be extended along the Z axis.

This increased length and weight means the tech specs PR1.1 and PR1.2 were not met. However, further discussion with the Bus team has revealed that additional space and mass are available within the CubeSat, since some other subsystems were smaller than expected.

6. Build

6.1. Building Constraints

Thus far, the design that has been discussed in Section 5 has been the design that would meet all mission requirements and integrate into CaliPER. Henceforth, said design is referred to as the ‘flight’ or ‘ideal’ design. Unfortunately, building and testing this system would require funds and capabilities beyond the resources accessible to the team. Therefore, significant alterations were made to create a prototype system that is able to be tested in order to confirm the flight design while also fitting within the resources constraints.

6.1.1. 3D Printing Material and Capabilities

Accura Bluestone can only be printed with 3D System’s SLA 750 printer. Unfortunately, Harvard does not own or posses the ability to use this printer, meaning that printing and testing with the designed material is impossible. Furthermore, the resin 3D printers at the Harvard SEAS 3D printing core are not large enough to print the designed body, meaning an alternate test body must be designed.

6.1.2. Budget

In addition to the size and material constraints listed in Section 6.1.1, the Harvard printers are expensive, and printing the ideal system would cost around $1400. Therefore, a smaller body must be designed to fit within the budget of the project. Furthermore, the sensors and other COTS parts selected for the flight design are too expensive to be purchased to test with. For example, the High Speed In-Line Lee company solenoid valves cost $500 a piece, which is half of the allocated project budget alone. Detailed explanations of alternative selections are discussed below in Section 6.2.3.

6.1.3. Propellant

Despite R-236fa being inert and non-toxic, it is heavily regulated by the Environmental Protection Agency. Under Section 608 of the Clean Air Act, only EPA-certified technicians are able to purchase refrigerants [36]. This makes R-236fa unattainable for this team, so an alternative propellant must be used.

6.2. Prototype Build

6.2.1. Test Propellant Selection

Despite the EPA's strict regulations on the purchasing of refrigerants, there are a few exceptions. One of those exceptions is for R-134a, another commercial, inert, and non-toxic refrigerant that is commonly used in motor vehicle AC systems.

R-134a reaches a higher vapor pressure at a given temperature than R-236fa and it has a lower volumetric efficiency and specific impulse than R-236fa. Besides that, there are not many significant differences between the two refrigerants. They have similar chemical compatibility, and the R-134a comes stored as a liquid-vapor mixture, so it should closely mimic the behavior of the ideal propulsion system's liquid-vapor mixture. This makes it a useful analog for the ideal system and allows for the characterization of how well the system performs relative to its theoretical performance. As a result, all tests were conducted with R-134a.

6.2.2. Test 3D Printing Material and Methodology

Since it was not possible to 3D print using Accura Bluestone, alternative options from the Harvard SEAS 3D printing core were considered. Ultimately, Visijet Clear material printed on the 3D SYSTEMS MJP 2500 printer was chosen for numerous reasons. This printer is the most precise in the 3D printing core, with a minimum recommended feature size of 100 microns. The smallest feature in the propulsion system is the throat of the nozzles, which is 500 microns wide, so this precision is more than enough. The printer uses a dissolvable wax as a support material, allowing it to make complex inner geometries, which is necessary for the internal tubing in the body and the large storage tank cavity. The Visijet Clear material is watertight and similar to Accura Bluestone with a yield strength of 50 MPa. Additionally, the material is translucent, making it easier to check that the inner tubing is clear and look for any other possible defects. All of these reasons led the manager of the 3D printing core to recommend this printer and material combination for our application.

6.2.3. Alternate COTS Components

6.2.3.1. Valves

The valve chosen in Section 5.2.3.2 costs over $500, much too expensive to fit within the project's limited budget. Instead, a cheaper DC electric brass solenoid valve from electricsolenoidvalves.com, part number RSSM-2-110VAC, was used. It has a temperature range of -10 to 120°C, a pressure range of 0 - 145 PSI (with no minimum), and NPT fittings to create an airtight seal [37]. It is much larger than the ideal solenoid and it requires a greater amount of power, but this is not a concern when testing in the lab, as space and power are abundant. The

valve is shown below in Figure 6.1.

Figure 6.1: Solenoid Valve [37]

6.2.3.2. Pressure Sensor

The pressure sensor chosen in Section 5.3.2.1. cost over $700, so a cheaper alternative was chosen. This alternative was part M3234-000005-100PG, made by TE Connectivity, shown in Figure 6.2. It can operate in temperatures ranging from -40°C to 125°C and can measure pressures from 0 to 100 psi, making it the ideal choice for this application [38]. Additionally, it has a quarter-inch NPT port, allowing it to maintain the airtight seal in the storage tank.

Figure 6.2: Pressure sensor [38]

6.2.3.3. Temperature Sensor

The temperature sensor and pressure NPT feedthrough that are discussed in Section 5.3.2 each cost hundreds of dollars, making them too expensive for testing. Instead, an inexpensive RTD Probe from McMaster-Carr, part number 3866K19, was chosen. The RTD is shown in Figure 6.3.

Figure 6.3: RTD probe [39]

It can measure temperatures ranging from -55°C to 400°C and has NPT fittings to create a tight seal [39], so a separate NPT feedthrough will not be necessary. It is much larger than the ideal RTD, but volume is not an issue when testing in the lab.

6.2.3.4. Heater

Similar to the temperature sensor, the ideal heater that was chosen requires a NPT feedthrough, which is prohibitively expensive. In its place, a screw-plug immersion heater from McMaster-Carr with part number 4668T51, will be used. The heater is shown in Figure 6.4.

Figure 6.4: Screw-Plug Immersion Heater [40]

This heater has an NPT fitting to create an airtight seal, so the NPT feedthrough will not be necessary. It is much larger than our ideal heater, but volume is not an issue when testing in the lab.

6.2.4. CAD

6.2.4.1. Test Body Design

The body of the test system was designed specifically for the testing setup available and can be seen in Figure 6.5. The footprint of the body was 5.4” by 5.4”, which fits perfectly on the bed of the scale. Only four nozzles were included, as that is all that was needed to complete the tests described in Section 7. All four nozzles were centrally located on the top face so that the thrust produced would be centrally located on the scale as well, in order to get maximum measurement accuracy. An overhang sticks out near the nozzles so that any tubing that passes by can be tucked under the overhang to ensure that it does not bend over the nozzles and disrupt the airflow.

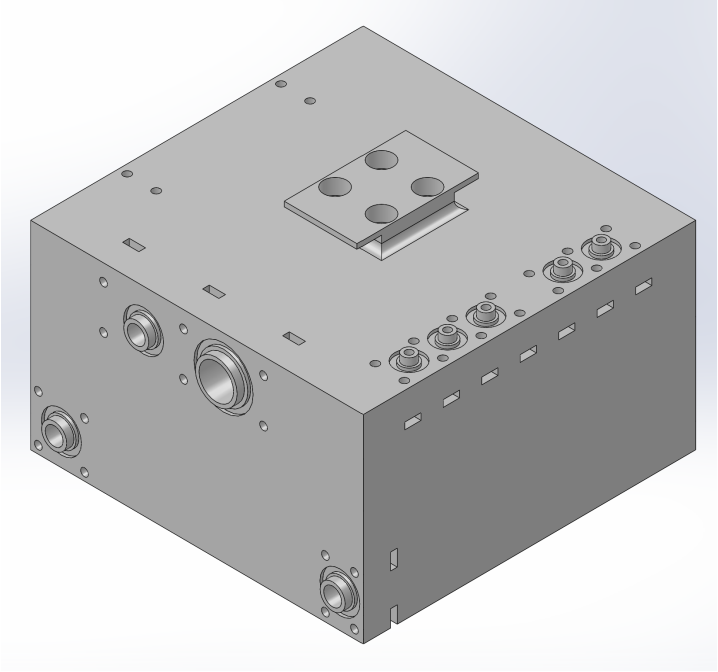

Figure 6.5: Test body

As can be seen in Figure 6.5 above, the test body has the same type of ports as the ideal body. The ports on the top face are exactly the same, and ports on the side are simply scaled up for larger components. This means that the plastic to metal interface will be the same as the ideal model, so any leaks can be seen.

Similar to the ideal body, the test body has an internal tubing and an internal storage tank. The internal tubing paths were two dimensional, traveling from the ports to the nozzles just as they would in the ideal body. Figure 6.6 shows a top-down cross section of the test body, which displays the internal tubing.

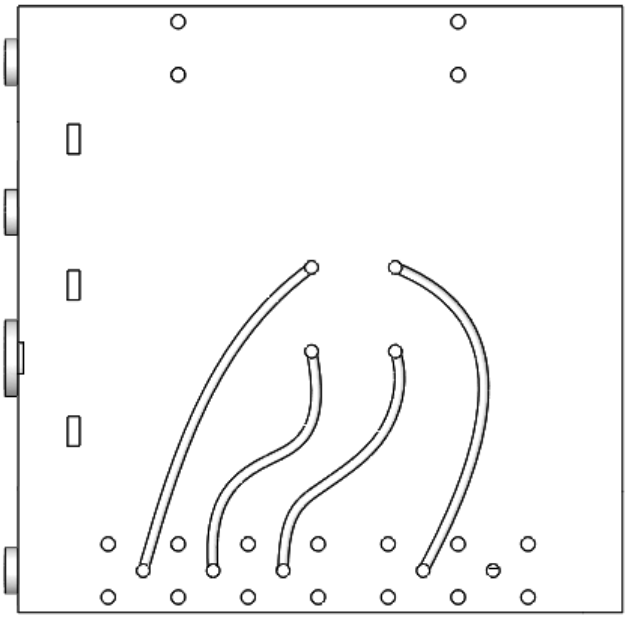

Figure 6.6: Cross section of test body that shows internal tubing

The test body also contained an internal storage tank, which can be seen below in Figure 6.7.

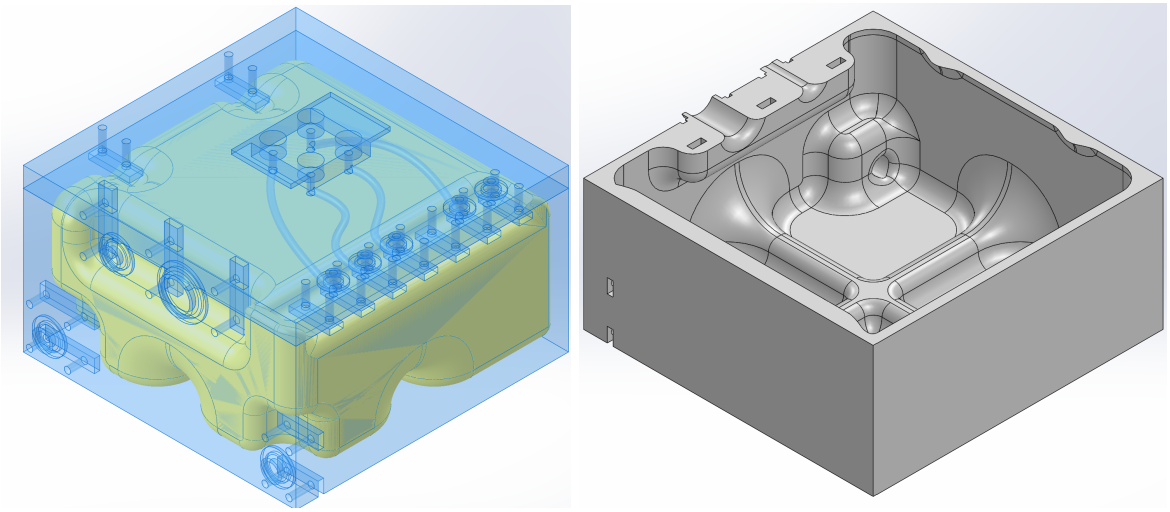

Figure 6.7 a (left): Isometric view of the internal volume of the storage tank, shown in yellow, within the test body, shown in translucent blue.
Figure 6.7b (right): Section view of the storage tank from a different angle than 6.7a

To strengthen the storage tank, a cross beam was extruded from the base of the tank, Additionally, every corner in the storage tank was filleted to reduce stress concentrations. Corners where larger stress concentrations were found were given fillets with larger diameters.

To ensure that this storage tank was safe to test with, finite element analysis was done with a pressure of 120 psi applied to every internal face of the tank. Results can be seen below in Figure 6.8.

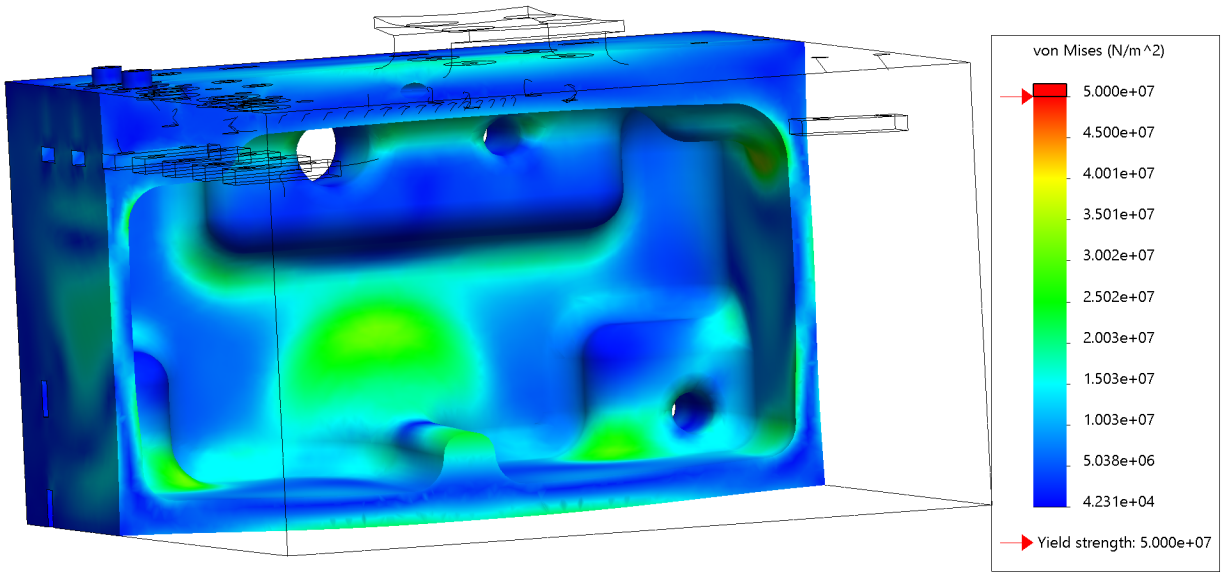

Figure 6.8: Cross section of FEA results

Any red coloration would indicate that a stress greater than or equal to the yield stress of 50 MPa, so the lack thereof indicates that this structure can support this pressure. Structural stability at 120 psi means there was a safety factor of 1.5, since the internal pressure of the tank was pushed greater than 80 psi when testing.

6.2.4.2. Test Nozzles Design

The nozzles designed for the ideal system were meant for use in a vacuum, where the pressure difference between the exit pressure and the ambient pressure is positive, and the total thrust is positive. However, when fired in an ambient pressure of one atm, those nozzles should actually produce a negative thrust since they are massively overexpanded. This is because the ambient pressure is much greater than the exit pressure of the nozzle, which causes the overall thrust term to be negative.

To test nozzles that would actually produce a positive thrust, it was necessary to lower the area ratio. A lower area ratio means that the gas is accelerated less and therefore has a higher exit pressure. The ideal nozzle had an area ratio of 196, as discussed in Section 5.2.2.1, and it was necessary to drop the area down to 4 for the test nozzle. The resultant nozzle is shown in Figure 6.9 below, where the bottom of the photo is where the internal tubing leads and the top of the photo is the exit of the nozzle.

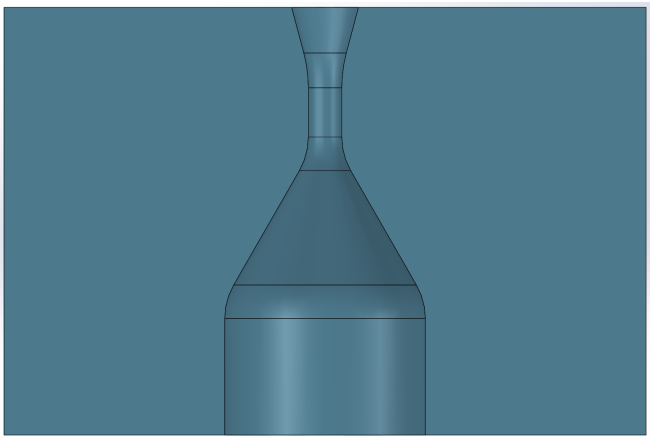

Figure 6.9: Cross section of the test nozzle

6.2.4.3. Complete Test Assembly

Other parts of the test system did not change significantly. The outlet and connector manifolds remained the same design, but were simply cut down to only have five holes rather than nine. The new electronic components required slightly different ports and manifolds, but they had the same base design as the ideal components. Therefore, when it is all put together, the entire assembly can be seen in Figure 6.10.

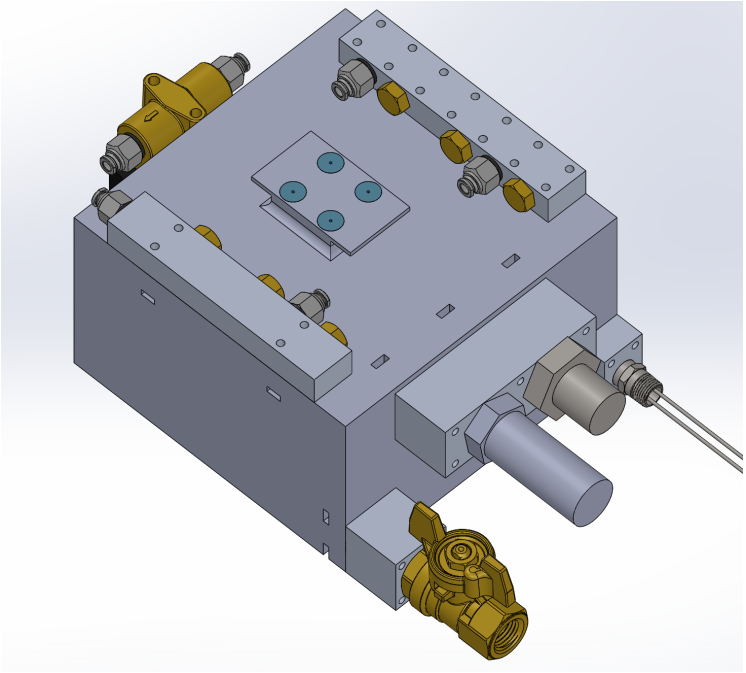

Figure 6.10: CAD of test system assembly

6.3. Build Execution

6.3.1. Manifolds

All manifolds were machined by propulsion team members in the Harvard SEC makerspace using CNC mills, seen below in Figure 6.11. CAD files were exported from SolidWorks to Fusion360 CAM software, and then uploaded to the CNC mill.

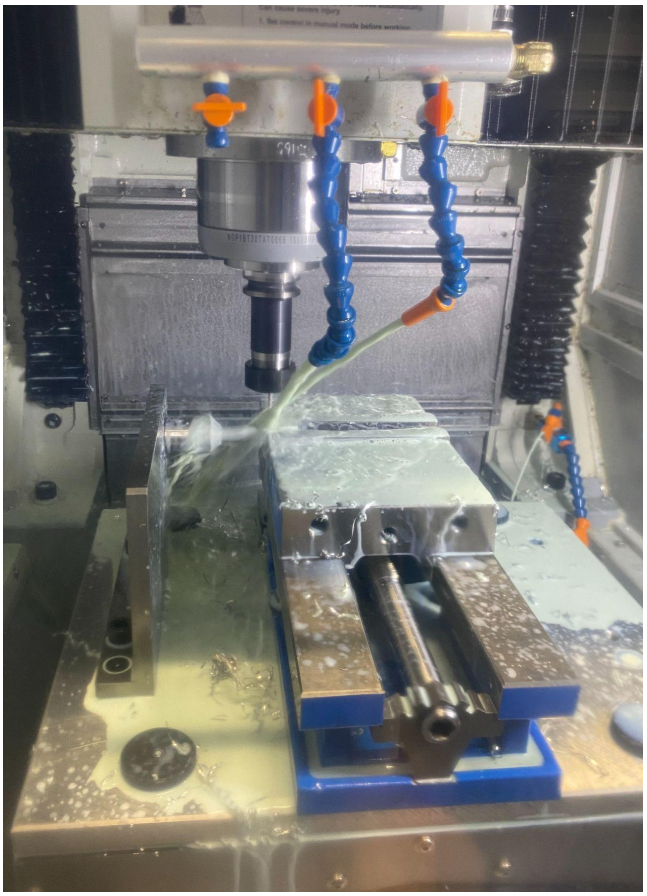

Figure 6.11: Machining a manifold in a CNC mill

Initially, all parts were manufactured out of 304 stainless steel, to replicate the ideal design. However, machining steel proved much more difficult and time consuming than expected, so the decision was made to switch to aluminum for the test. This made the process much faster and had no real drawbacks since testing did not include large temperature changes. To account for weaker threads in aluminum, careful planning was taken to ensure no component was ever unscrewed once it was screwed into the aluminum tapped hole. All completed aluminum manifolds can be seen below in Figure 6.12. Once the machining process was complete, all holes were tapped by hand.

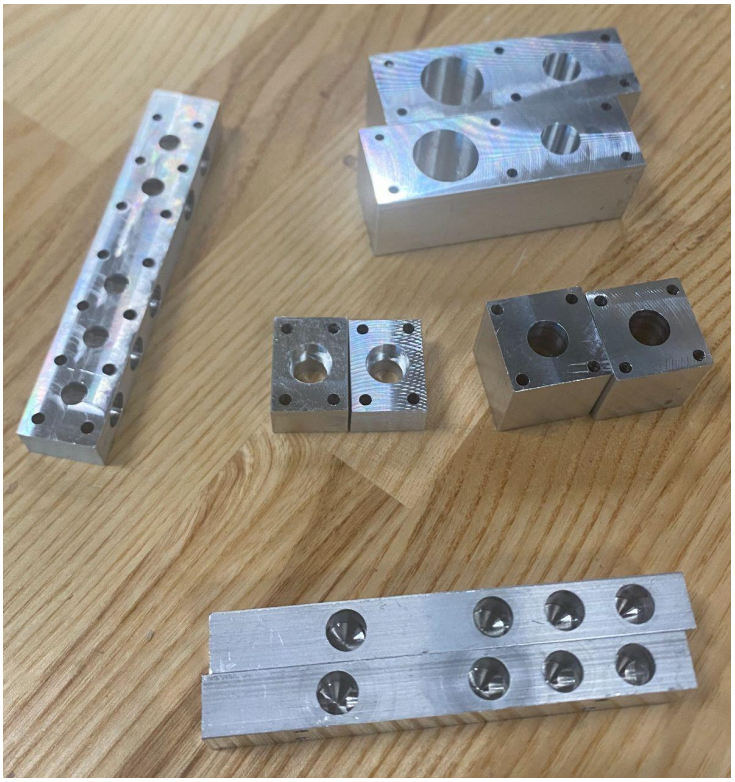

Figure 6.12: Completed manifolds

To achieve a face seal good enough to seal gas, the face of the manifold should have a surface finish of 16Ra. Unfortunately, there were no instruments to measure surface roughness available so each manifold was faced off to achieve the best surface finish possible.

6.3.2. 3D Print

Once design of the body was done and the FEA showed that the safety factor was met, the Harvard 3D printing core printed it, as seen below in Figure 6.13. Unfortunately, one of the ports had a broken slightly alignment tube, but this caused no functional issue since it could still be utilized to locate the manifold hole.

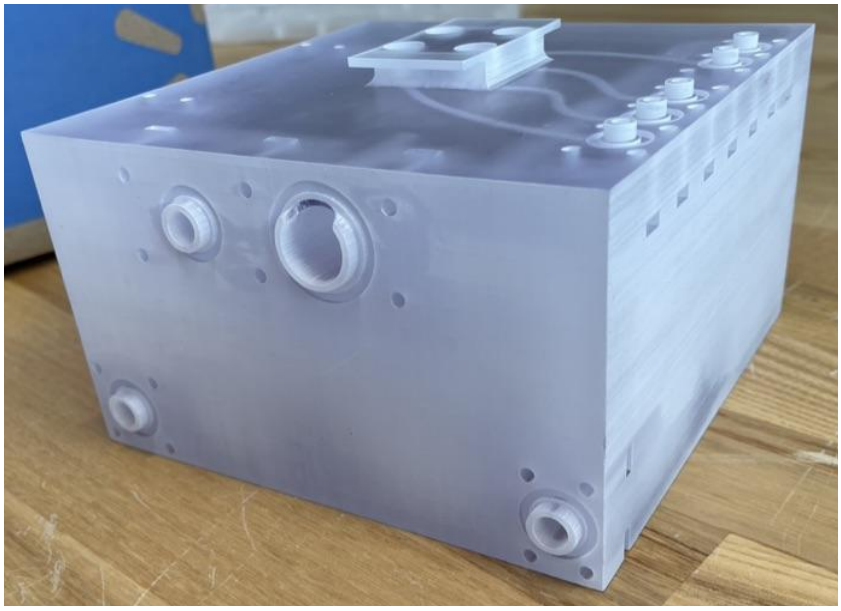

Figure 6.13: 3D print

Note that the nozzles were not printed with the body, as seen in Figure 6.14. Instead, a hole was left where the nozzles could be inserted later. This was done based on advice from the 3D printing core manager in order to reduce the risk of support material remaining in the internal tubing or clogging the narrow throat of the nozzle. This was effective, as the tubing was completely clear of support material.

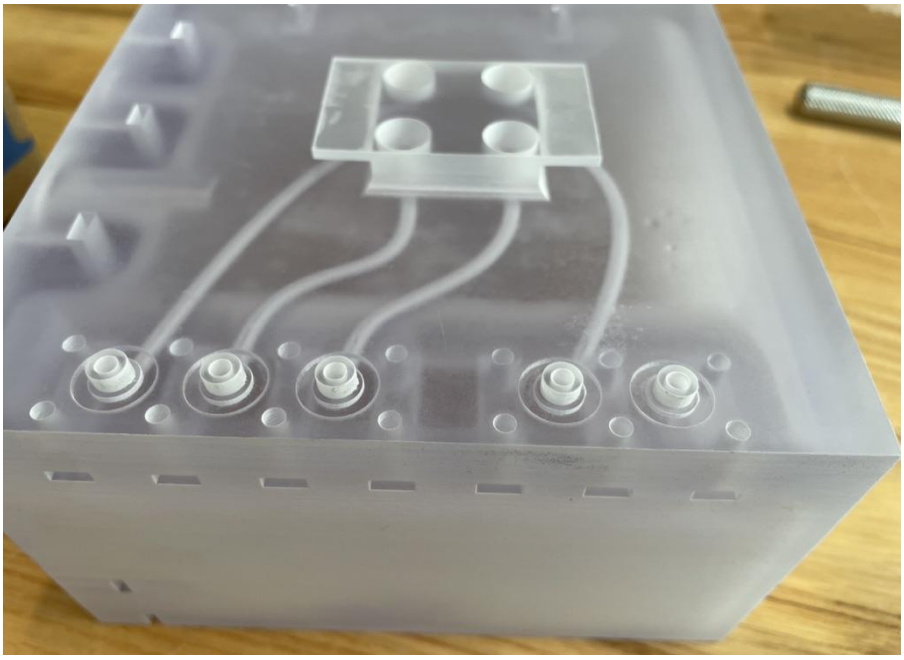

Figure 6.14: 3D print without nozzles

After printing separately, the nozzles were installed into the body. According to the manager of the 3D printing core, superglue effectively chemically bonds this type of resin. Therefore, superglue was spread around the outside on the nozzle and it was placed inside the cavity left for the nozzles and allowed to dry.

6.3.3. Assembly

Once both the manifolds and the 3D printed body were manufactured, assembly began. All components and push fittings were screwed into their respective manifolds before the manifolds were then attached to the body. Teflon tape was used on all threads and new o-rings were used for each connection. The assembled test system can be seen below in Figure 6.15, missing only the valve and external tubing.

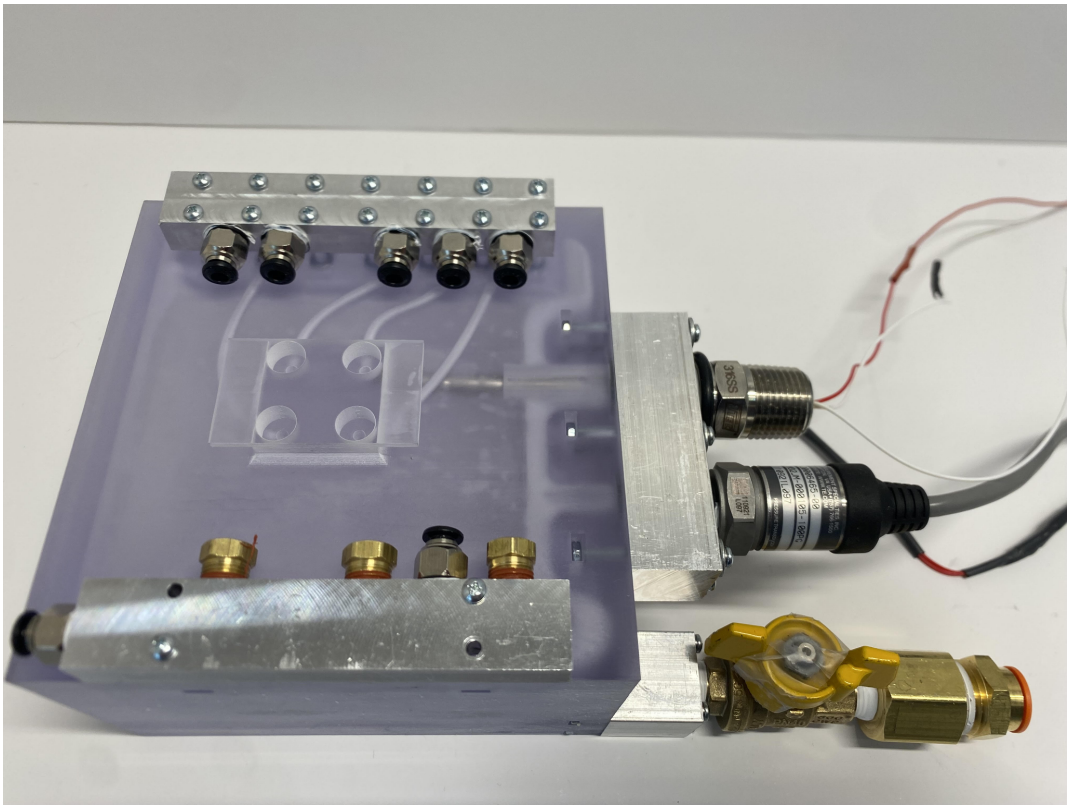

Figure 6.15: Assembled test system

When machining the manifolds, some additional facing operations were necessary. This decreased their overall thickness and made the screws slightly too long to properly clamp down on the manifolds. To remedy this, a variety of spacers were added under each screw head to account for the difference.

6.3.4. Leaks

In the process of assembling the system, a crack formed near the attachment point of the heater manifold, as seen in Figure 6.16. The exact origin of the crack is unknown, but the leading hypothesis is that some of the screws for the heater manifold were screwed in too tightly durings installation and a stress concentration formed at the inner corners of the nut cut outs.

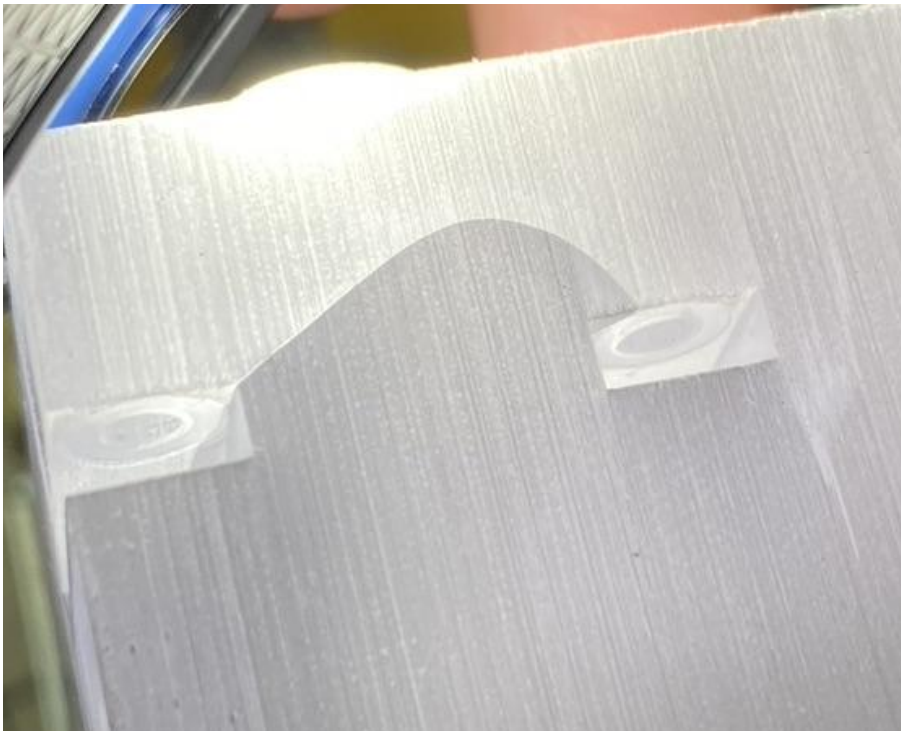

Figure 6.16: Crack in the system

Initially. superglue was used to fill in the crack (both internal and external) since it can bond to this particular resin. This fix did not work, and air immediately leaked through the crack once the tank was pressurized.

Fortunately, the crack only penetrated the tubing that led to the heater port, as seen in Figure 6.17.

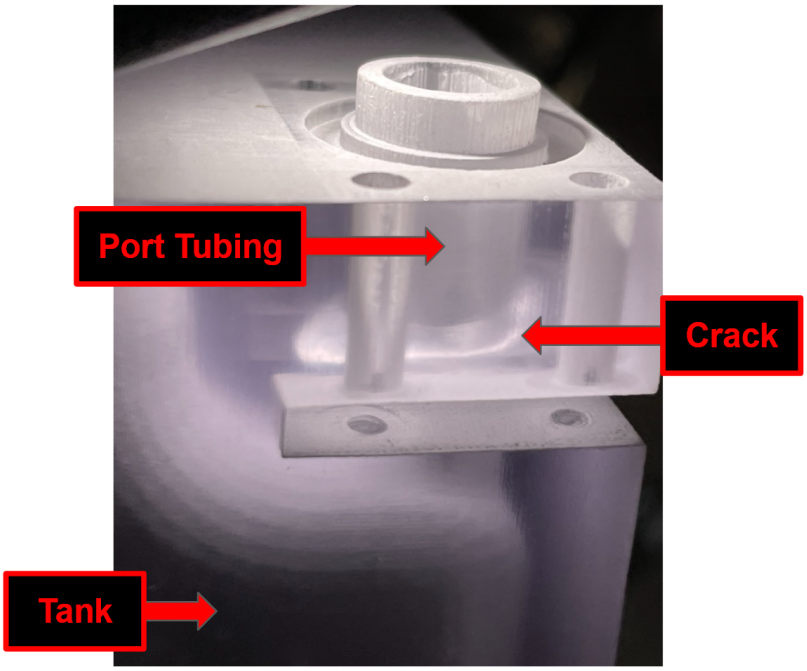

Figure 6.17: Crack misses the storage tank

Since the crack was isolated to the port tubing, this meant that there was an alternative solution: prevent the fluid from ever reaching the crack. To achieve this, the entire port and its tubing was filled with hot glue. Approximately two sticks of hot glue were poured into the port, the port was then sealed, and the whole propulsion system was oriented such that the molten glue would fall down and completely fill the tube. To seal the port, the heater was replaced with a NPT plug, and the manifold was screwed back on as normal. The fixed system can be seen in Figure 6.18.

Figure 6.18: Hot glue in storage tank

While this solution fixed the leak, it also meant that the port was no longer usable, so there would be no heater in the storage tank. This was unfortunate, but such a large leak would have prevented any testing from happening, so it was necessary.

Despite fixing the large leak, there were still some small leaks present in the storage tank. To find the leaks, the tank was pressurized with air to 80 psi and soapy water was left to sit along all interfaces, as seen in Figure 6.19.

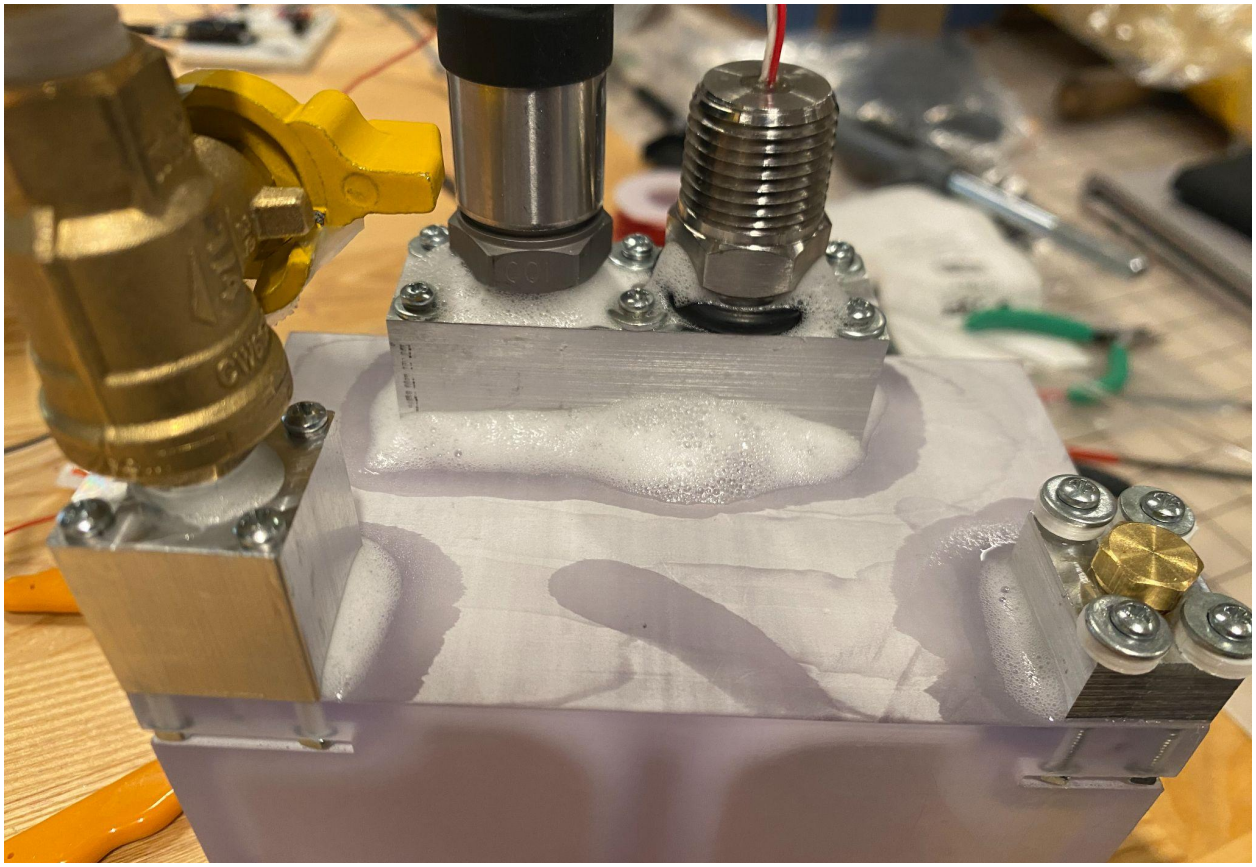

Figure 6.19: Finding leaks with bubbles

If a location produced a large amount of bubbles it was an indication of a leak, where more bubbles meant that more air was leaking from that interface. Once a leak was found, simple steps to correct that leak were taken, such as adding more teflon tape or screwing in a fitting more tightly. If a fitting needed to be removed to add more teflon tape, the o-ring was swapped out for a new one before the fitting was replaced. Once these fixes were implemented, the chamber was pressurized to 80 psi and then sealed while the pressure transducer continuously output data, as seen in Figure 6.20.

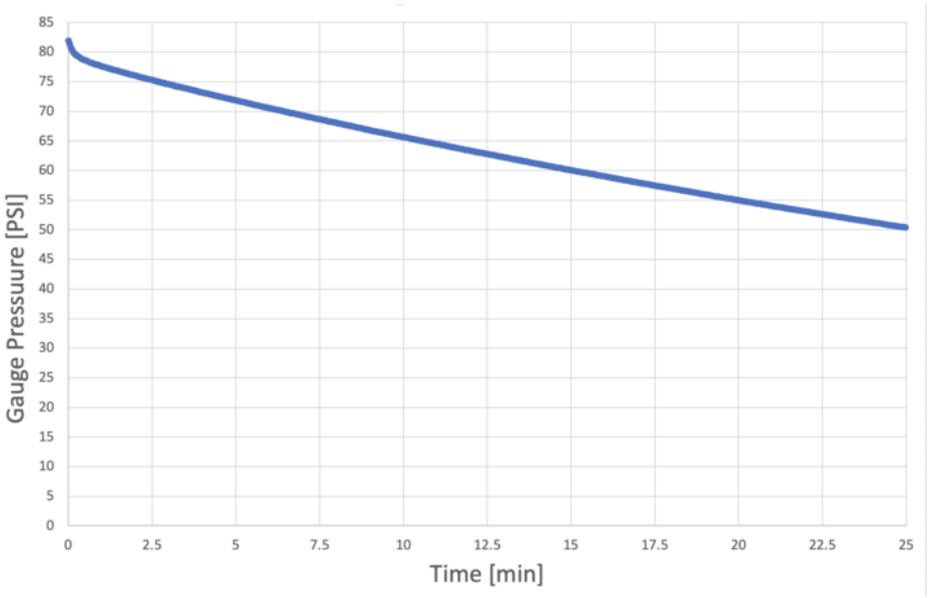

Figure 6.20: Storage tank gauge pressure vs time

Over 25 minutes, the gauge pressure dropped by approximately 32 psi. This equates to a pressure drop rate of 1.28 psi/minute, or approximately 0.021 psi/second. Since the testing trials were only five seconds in length and intentionally caused a much higher drop in pressure, this pressure drop rate was deemed acceptable to not greatly interfere with test results.

6.3.5. Propellant Loading

Once the leaks had been fixed, the next step was to load the tank with R-134a. Based on discussions with researchers from INSPIRE, it was determined that the best way to load the propellant would be to gravity feed it into the storage tank. The R-134a canisters were chilled prior to loading in order to increase the amount of propellant in the liquid state.

The setup to load the propellant is shown in Figure 6.21. To start the process, the valve to the R134a canister was closed and the valve to the pump was open. The pump pulled a vacuum of 25 inHg in the storage tank and its valve was then closed. The valve to the canister was then opened and the canister was lifted directly above the storage tank while being tilted upside-down. After one minute the valve to the canister was closed, finishing the loading process.

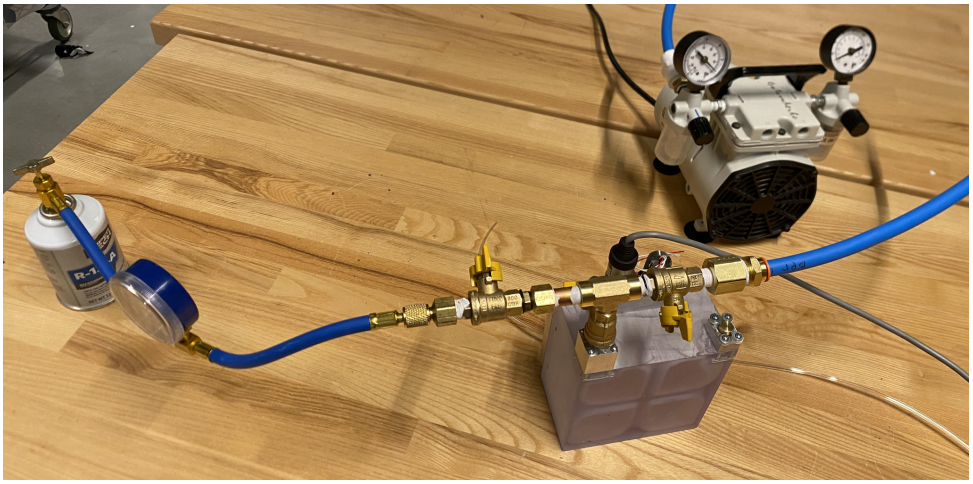

Figure 6.21: Propellant loading setup

Unfortunately, this process did not work very well, as only a small amount of liquid was transferred to the storage tank. The liquid propellant can be seen in Figure 6.22 below.

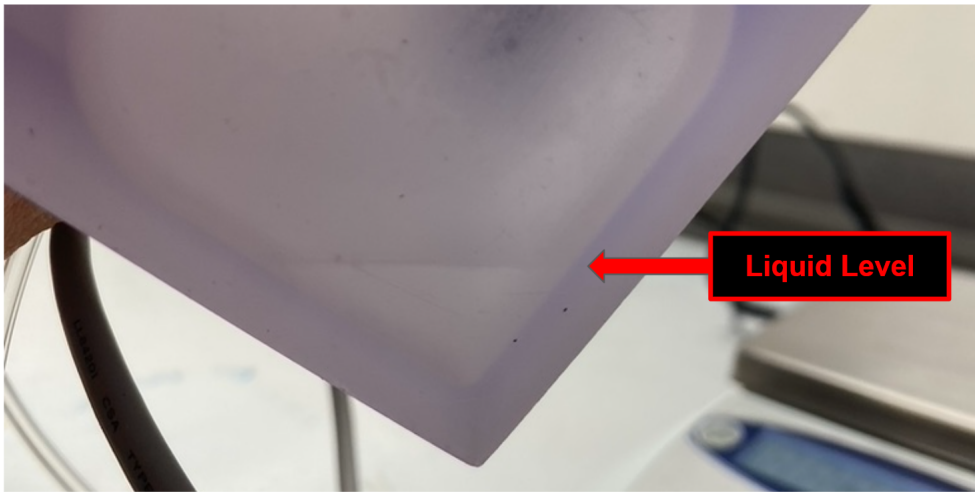

Figure 6.22: Liquid propellant in storage tank

The rest of the volume in the test storage tank is occupied by propellant vapor, so tests could still be performed. However, this would not effectively represent the ideal system since the behavior of the ideal system is based on the fact that the tank is filled with a two phase mixture, allowing the gas to be replenished by constantly vaporizing liquid. The small amount of liquid in the test storage tank was not nearly enough to replenish the vapor. Therefore, to more accurately mimic the behavior of the ideal system, the valve to the R134a canister was left open. This meant that the gas flowed from the canister into the storage tank, then into the manifolds and valves, then into the internal tubing, and out through the nozzles. This allowed the tests to correctly replicate the two phase mixture and also more closely replicate the path that the fluid would take before expulsion.

7. Test

7.1. Overview

System testing was divided into five stages. The first two collections of tests simply collected data on the 3D-printed nozzle performance independent of the fully 3D printed integrated system. These tests serve to verify the basic functionality of the fluid and propulsion system before including the full system. These tests had a 3D-printed nozzle with the same geometry as the fully 3D-printed system sealed to a stainless steel block that standard NPT components can thread into. Following these two tests, henceforth referred to as "benchtop tests", the fully integrated 3D-printed system will be put through three collections of tests. These tests will verify the basic fluid and structural design of the 3D-printed system, as well as provide more data on system performance. These last three tests are referred to as tests with the "test rig" or prototype system. Out of an abundance of caution, all tests took place within an active fume hood to properly dispose of the refrigerant and to protect against accidental spills or fluid getting on skin.

7.2. Data Collection Methodology and Basic Set Up

All tests used the same methodology for collecting thrust data. In each set up, the thrust producing component(s) were placed atop a TAJ 4001 scale, which was connected to an Arduino MKR Zero to collect the live scale output and send back commands. This scale had 0.1 g precision, thereby giving results precise to the nearest .981 mN. Before each firing, the scale was tared through the Arduino to ensure a consistent 0.0 g reading before each burst. Fluid was then released through the nozzle which produced a thrust and was read by the scale as additional weight. To control this timing, the Arduino sent a command to open a solenoid valve, then waited for five seconds until closing it. This five second opening time was kept standard for all short duration tests. This data was sent to the Arduino every ~60ms and written to a .csv file on a microSD card for post-processing. For some tests, a pressure sensor was also activated and also wrote gauge pressure data to a .csv file every 1 second. In cases where the pressure sensor could not be used to measure the chamber pressure, such as the benchtop tests, an analog pressure gauge was manually read before the valve was opened for each firing. Arduino code for testing can be found in Appendix D.

Some tests had a second TAJ 4001 scale placed under the canister of R134a propellant. Similarly, the scale was connected to an Arduino and mass data was exported to a .csv file. For the canister, data was sent every 1 second and the scale was only tared once at the beginning. This data was collected to read the mass lost for each thrust test.

All scales were calibrated at the beginning of each testing day with two known 1000 g weights. Each scale was also leveled using the built in gauge prior to testing per the operating

instructions included with the scale. Known masses were placed on all four corners of the scale to test how the scale handled off center loading. Figure 7.1 shows the results, demonstrating the scale reads mass accurately from all positions on the load plate.

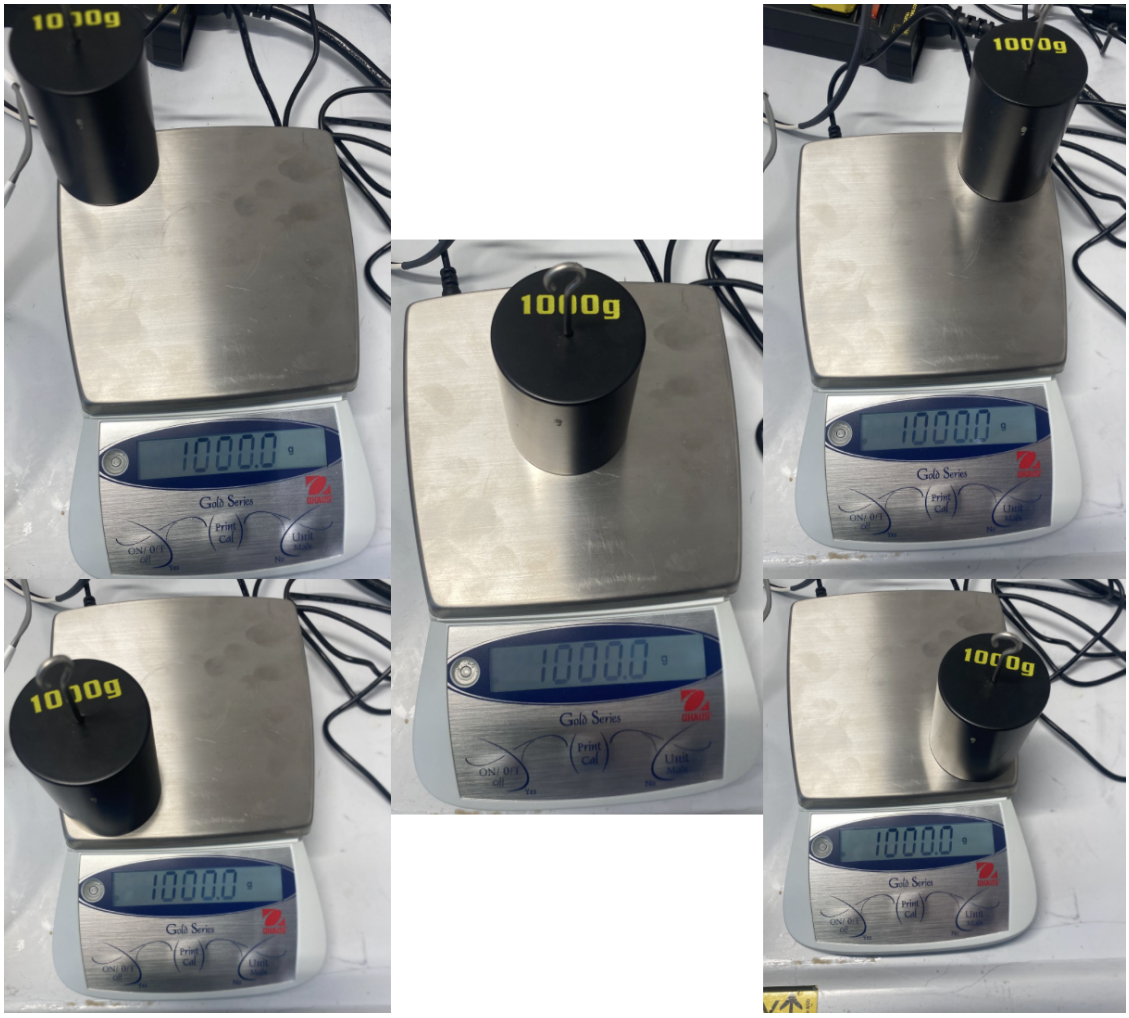

Figure 7.1: Five loading cases on the OHAUS TAJ 4001 scale showing it accurately reads mass everywhere on the loading plate.

An electrical schematic can be seen below in Figure 7.2. This figure includes the 100 Ω resistance temperature detector (RTD) that did not get used in the actual testing due to the sensor being inadequately calibrated, leading to temperature errors up to 10 ℃. The figure also includes wiring to additional components, such as the separate boards required to interface with the scale, and the relay used to actuate the DC solenoid valve.

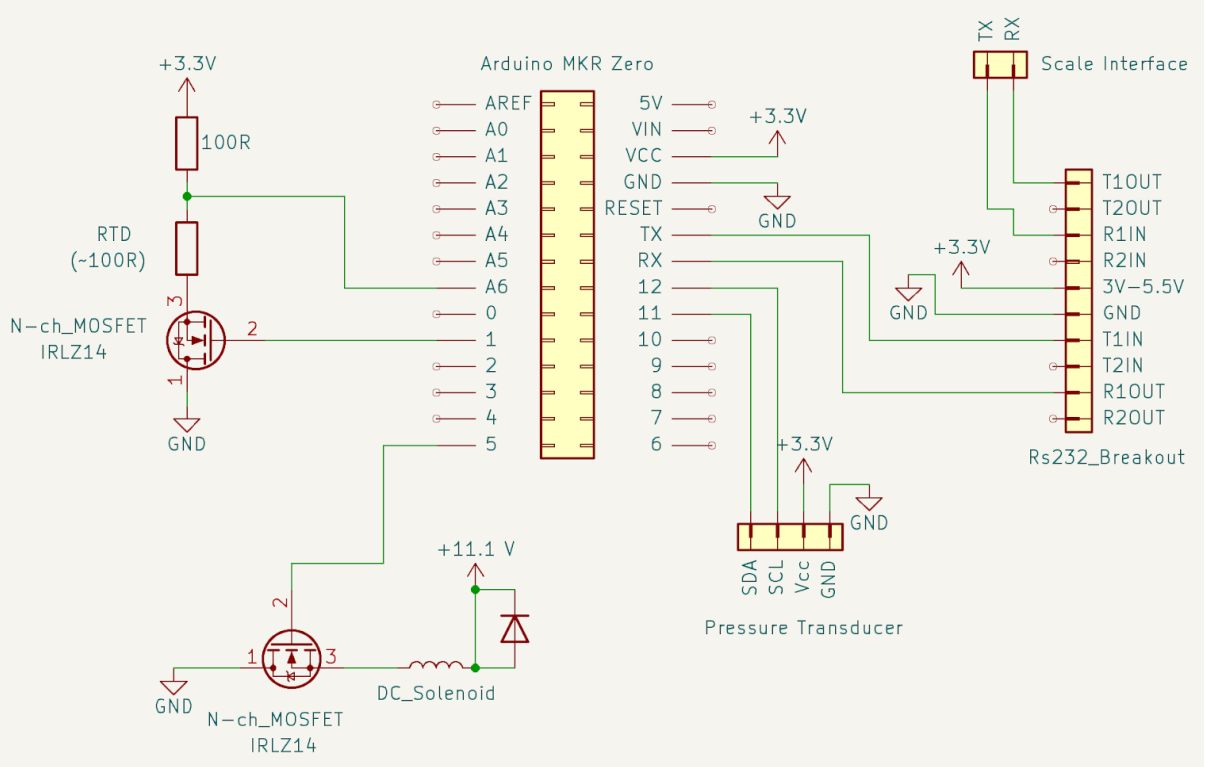

Figure 7.2: Electrical wiring diagram of Arduino MKR Zero and all associated electronic sensors and actuators used in testing

For both benchtop tests, nozzles were face-sealed in the same fashion as all other plastic-to-metal interfaces. As seen in Figure 7.3 below, a Neoprene O-ring was placed in a gland around the port in the same manner as described in Section 5.2.3.1. Custom manifolds were designed and machined for these benchtop tests to connect the nozzle to the flexible tubing push connect fitting.

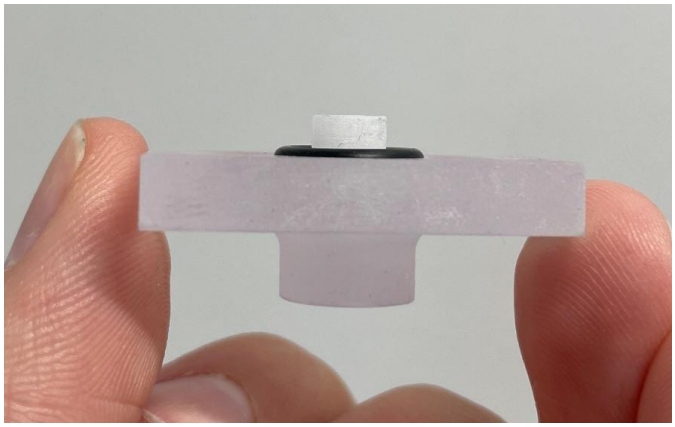

Figure 7.3: 3D-Printed nozzle for benchtop testing

7.3. Testing

7.3.1. Test 1: Benchtop Single Nozzle

7.3.1.1. Summary and Setup

The goal of this test was to characterize the performance of a single nozzle to verify basic functionality of the fluid system and performance against theoretical results. A more detailed description of the setup of this test is seen below in Section 7.3.1.3, but the basic setup consisted of a single 3D-printed nozzle mounted to a machined stainless-steel manifold connected to a canister of R-134a. The nozzle-manifold system was placed atop a precision scale which output the mass of the system as it produced thrust.

A picture of the test set up is seen below in Figure 7.4. The canister of R-134a was submerged in a water bath at room temperature. The water acted as a heat source to help the refrigerant minimize temperature and pressure loss as it cooled during vaporization. The canister system was placed on a digital scale which recorded the mass change over time as propellant was expelled. The canister was connected to a pressure gauge, then to an Arduino controlled 12V DC solenoid valve, and then to a stainless steel manifold with face sealed 3D-printed nozzle.

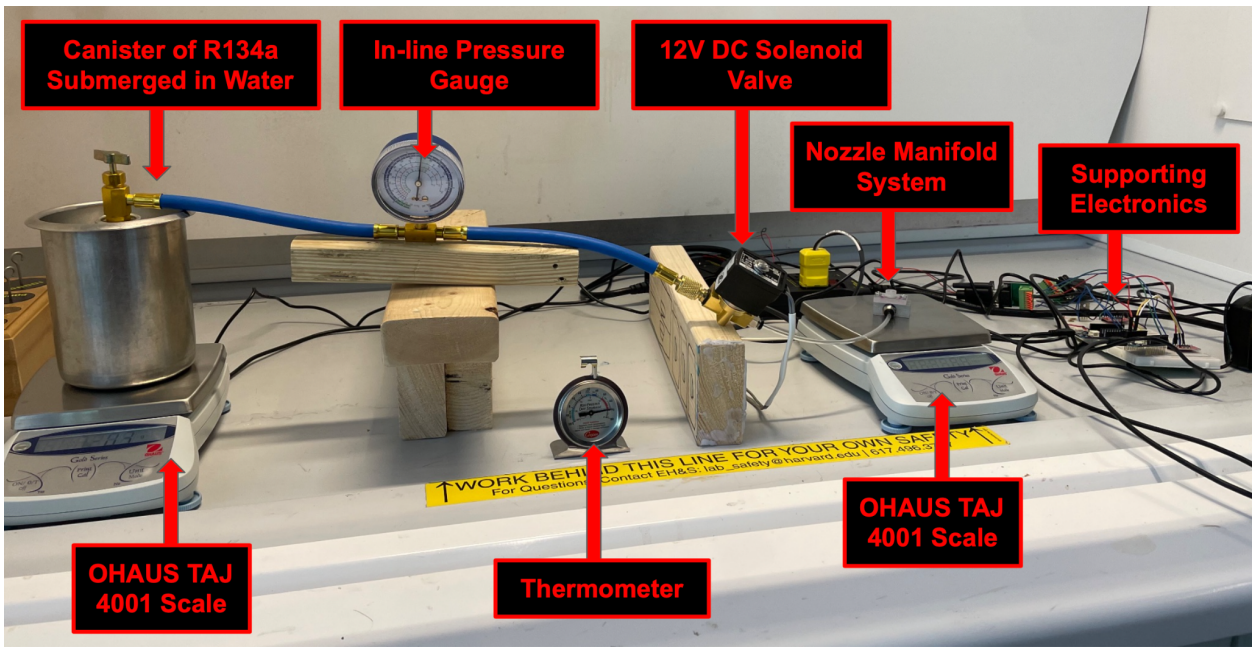

Figure 7.4: Test 1 setup with all major components labeled

7.3.1.2. Measurements

This test collected data on the thrust produced by a single nozzle reported at ~60 ms

intervals, the chamber pressure of the refrigerant before each firing, and the mass of the refrigerant canister reported every one second. Four nozzles were printed, and all were subjected to tests.

7.3.1.3. Procedure

1. Place benchtop testing setup in fume hood.
2. Record pressure of R134a.
3. Send an Arduino command to open the nozzle for five-seconds and record mass data. Record any anomalies or abnormal behavior.
4. Repeat steps 2. and 3. 25 times, waiting ~30 seconds between each firing to allow for the canister's pressure to stabilize between each run.
5. Change the nozzle and repeat steps 3., 4., and 5. three more times in order to collect data on all four printed nozzles.
6. Repeat steps 3., 4., 5., and 6. in order to collect a second set of 25 trials for each of the four nozzles.

7.3.2. Test 2: Benchtop Dual-Nozzle

7.3.2.1. Summary and Setup

The goal of this test was to characterize the performance of two nozzles firing at the same time to compare if thrusting out of two nozzles at once affects performance. The basic setup was identical to Test 1, except the solenoid valve opened to allow fluid to flow into both nozzles at once and each nozzle had its own dedicated scale. This difference is seen below in Figure 7.5.

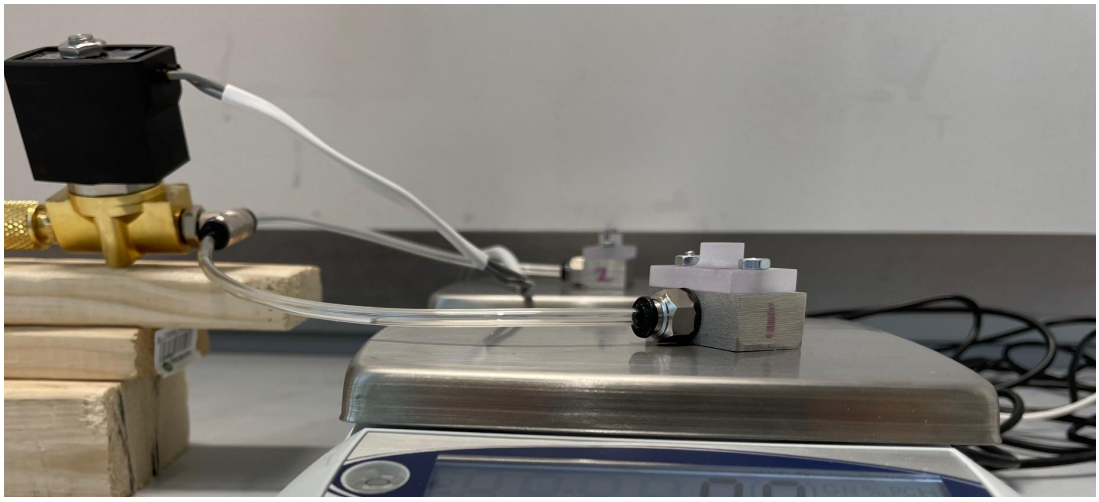

Figure 7.5: Dual-nozzle set up for Test 2

Following occasional issues with the solenoid valve continuing to let fluid pass through even after closing, a manual valve was added in line for redundancy in the event the solenoid valve got stuck open. This manual valve and the necessary adapters are seen below in Figure 7.6.

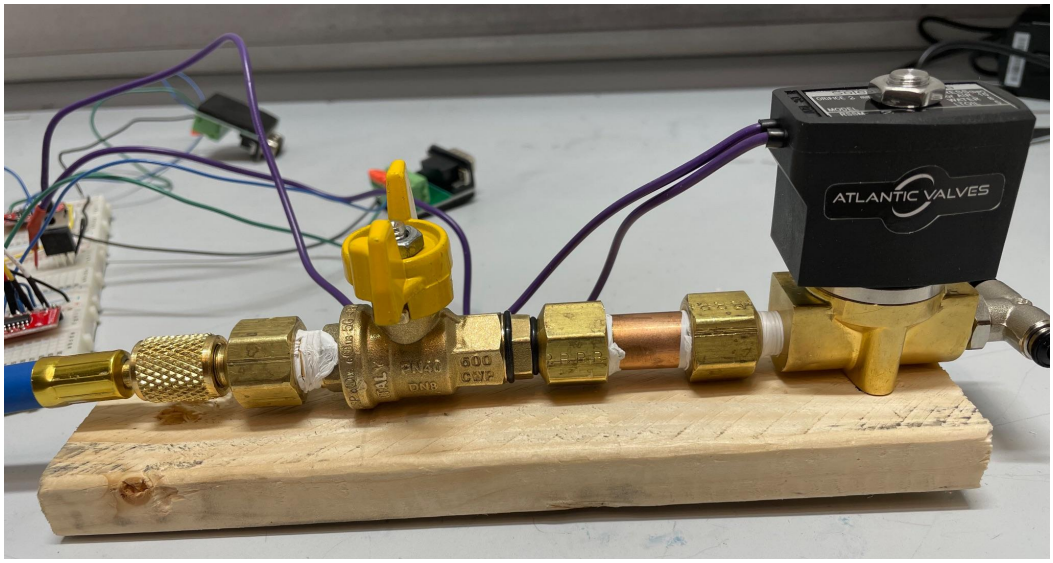

Figure 7.6: Added inline manual shut-off valve

7.3.2.2. Measurements

This test collected data on the thrust produced by both nozzles reported at ~60 ms intervals, and the chamber pressure of the refrigerant before each firing. Four nozzles were printed, and all were subjected to tests. Mass data of the propellant was not collected. All six combinations of pairs of nozzles were tested.

7.3.2.3. Procedure

1. Place benchtop testing setup in fume hood.
2. Record pressure of R134a.
3. Send an Arduino command to open the nozzle for five-seconds and record mass data. Record any anomalies or abnormal behavior.
4. Repeat steps 2. and 3. 10 times, waiting ~30 seconds between each firing to allow for the canister's pressure to stabilize between each run.
5. Change the nozzles and repeat steps 3., 4., and 5. five more times in order to collect data on all six combinations of the four printed nozzles.

7.3.3. Test 3: Prototype Single Nozzle

7.3.3.1. Summary and Setup

The goal of this test was to validate the basic functionality of the fully 3D-printed design as well as to characterize the performance of each of the four nozzles within the fully 3D-printed prototype system. Each nozzle on the prototype was tested individually. As discussed in Section 6.3.5, the tank could not be successfully loaded with enough liquid propellant so these tests were run in a similar fashion to the benchtop tests; the canister was attached to the fill port of the test rig to provide a direct path from the stored propellant in the canister, through the inner tank, through the manifold, through the solenoid valve, through the internal tubing to exit the nozzle. Prior to the beginning of the test, the vacuum pump brought the pressure inside the tank down to -25 inHg in order to remove as much ambient air as possible. The vacuum pump was then sealed off and the canister was opened to allow the pressure to equalize. The overall setup can be seen below in Figure 7.7. A diagram of just the test rig atop the scale can be seen in Figure 7.8.

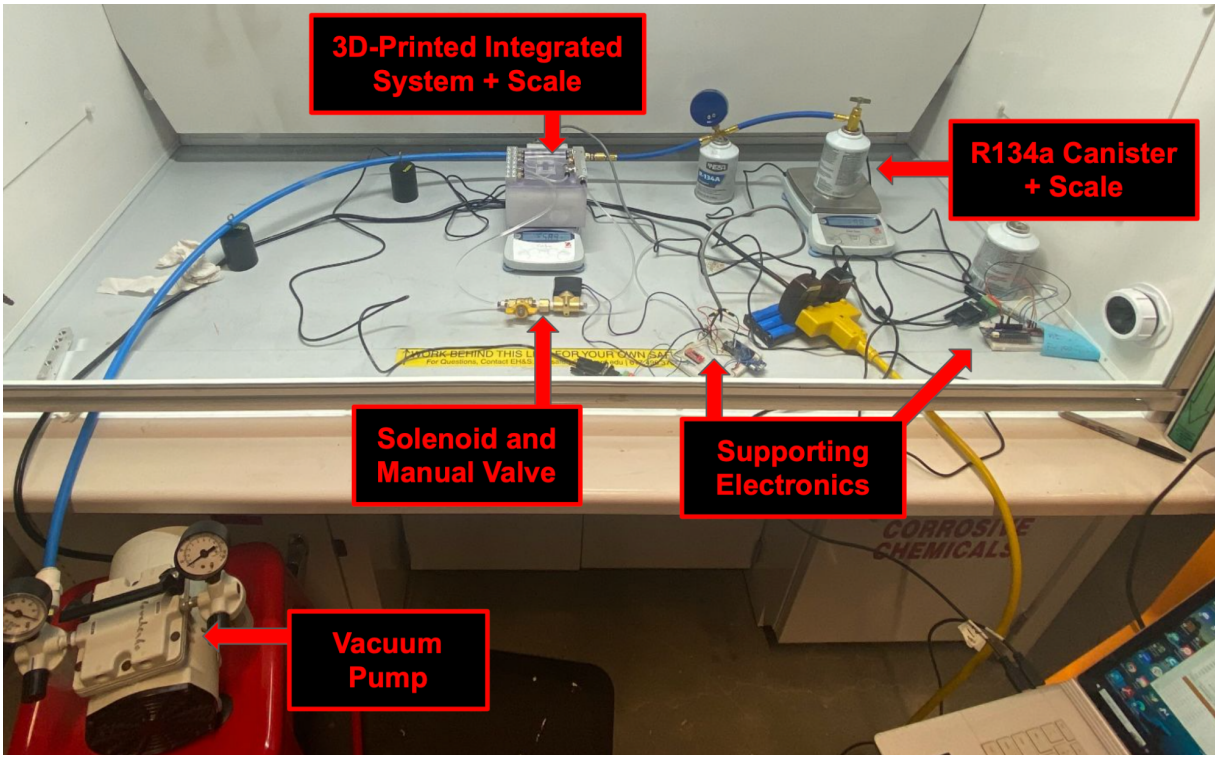

Figure 7.7: Labeled test setup for Test 3

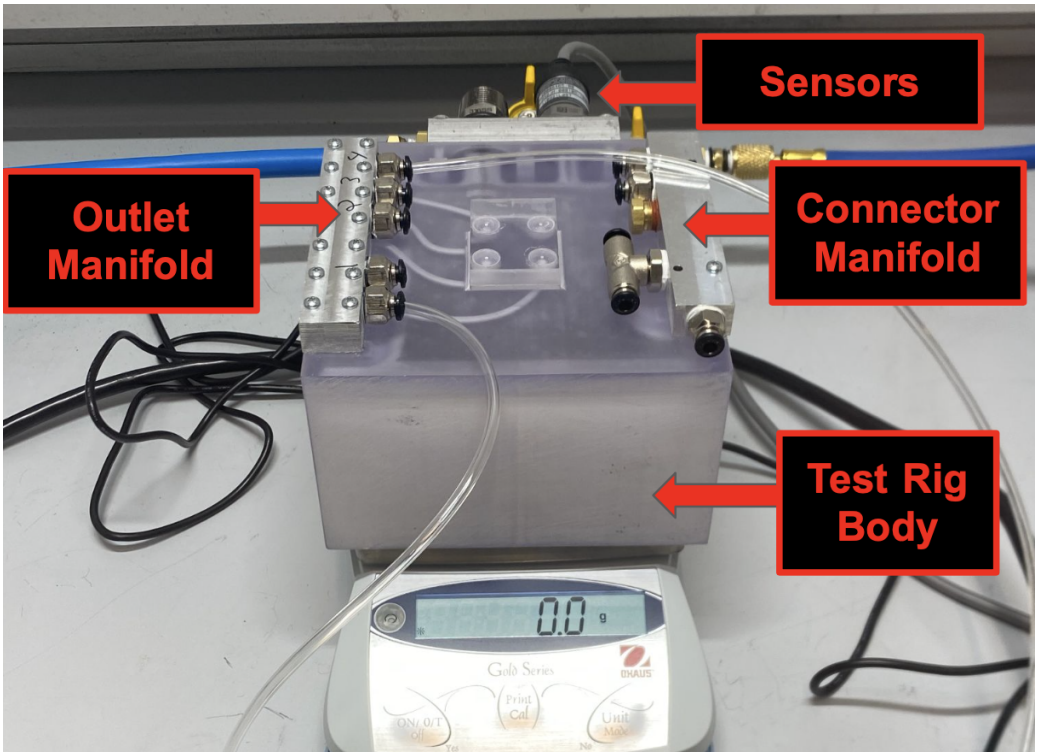

Figure 7.8: Labeled test rig setup for Test 3

7.3.3.2. Measurements

This test collected data on the thrust produced by a single nozzle reported at ~60 ms intervals, the tank pressure reported every 1 second, and the mass of the refrigerant canister reported every one second. All four printed nozzles were tested.

7.3.3.3. Procedure

1. Place prototype testing setup in fume hood.
2. Isolate canister fluid line and apply vacuum to remove excess air inside the tank.
3. Isolate vacuum pump and open propellant valve to allow the refrigerant to fill the tank
4. Send an Arduino command to open the nozzle for five-seconds and record mass data. Record any anomalies or abnormal behavior.
5. Repeat step 4. 15 times, waiting ~30 seconds between each firing to allow for the pressure to stabilize between each run.
6. Change the tubing to connect to different nozzles and repeat steps, 4. and 5. three more times in order to collect data on all four nozzles.

7.3.4. Test 4: Prototype Quad-Nozzle

7.3.4.1. Summary and Setup

The goal of this test was to characterize the performance of firing four nozzles at once within the fully 3D-printed prototype system. The set up was identical to Test 4, except that the connector manifold was used to divert the flow to all four nozzles. This is seen below in Figure 7.9.

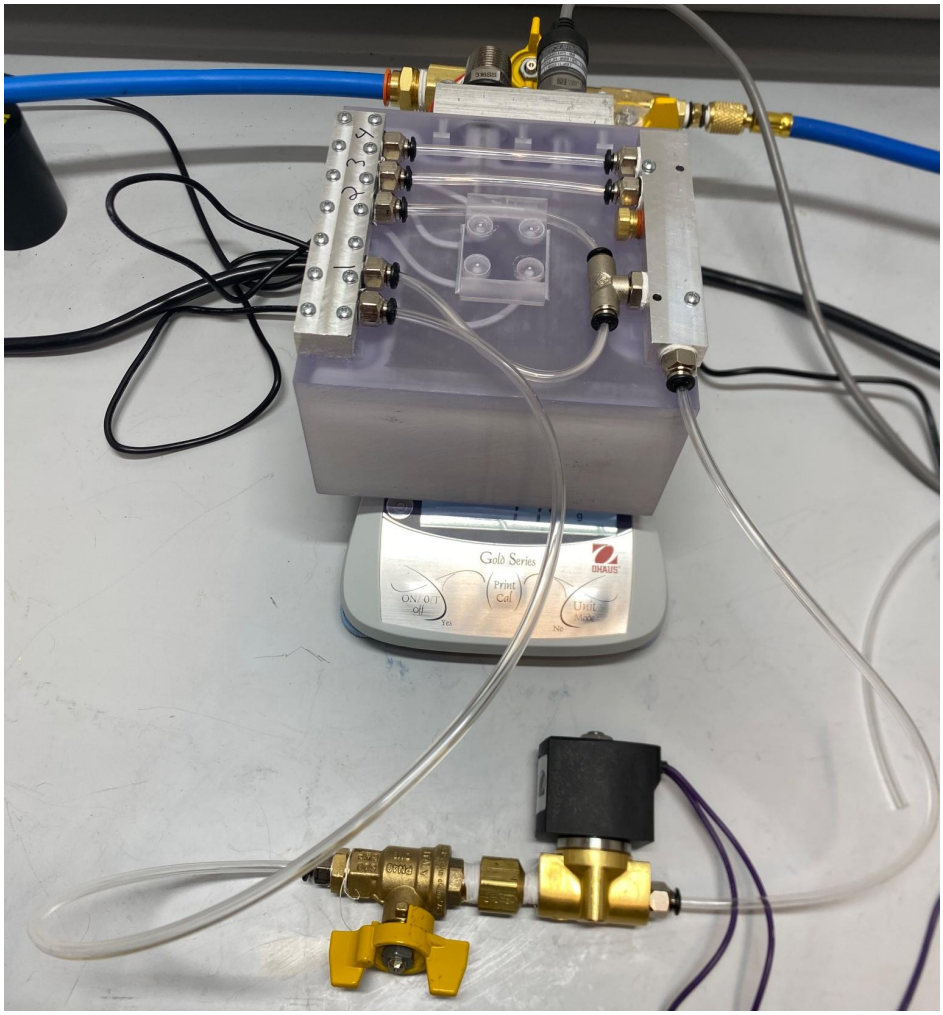

Figure 7.9: Test rig set up for Test 4 with all nozzles connected

7.3.4.2. Measurements

This test collected data on the thrust produced by all four nozzles reported at ~60 ms intervals, the tank pressure reported every one second, and the mass of the refrigerant canister reported every one second.

7.3.4.3. Procedure

1. Place prototype testing setup in fume hood.
2. Isolate canister fluid line and apply vacuum to remove excess air inside the tank.
3. Isolate vacuum pump and open propellant valve to allow the refrigerant to fill the tank
4. Send an Arduino command to open the nozzle for five-seconds and record mass data. Record any anomalies or abnormal behavior.
5. Repeat step 4. 20 times, waiting ~30 seconds between each firing to allow for the pressure to stabilize between each run.
6. Repeat steps 4. and 5. a second time to collect another set of 20 trials.

7.3.5. Test 5: Prototype Quad-Nozzle Long Duration

7.3.5.1. Summary and Setup

The goal of this test was to characterize the performance of firing four nozzles at once over a long duration to measure the thrust and pressure over time. The set up was identical to Test 4. The only difference was in the duration the valve was held open.

7.3.5.2. Measurements

This test collected data on the thrust produced by all four nozzles reported at ~60 ms intervals, the tank pressure reported every one second, and the mass of the refrigerant canister reported every one second.

7.3.5.3. Procedure

1. Place prototype testing setup in fume hood.
2. Isolate canister fluid line and apply vacuum to remove excess air inside the tank.
3. Isolate vacuum pump and open propellant valve to allow the refrigerant to fill the tank
4. Send an Arduino command to open the nozzle for 15 seconds and record mass data. Record any anomalies or abnormal behavior.
5. Repeat step 4. five times, waiting one minute between each firing to allow for the pressure to stabilize between each run.
6. Repeat steps 4. and 5. a second time with 30-second firing duration to collect another set of 20 trials.

8. Results and Analysis

8.1. Specific Impulse

Specific impulse can be experimentally measured by using Eq. 2.5:

$$I_t = I_{sp} m_p g_0$$

Eq. 2.5

As described in Section 7.3, the scale used during testing captured mass of the nozzle over time during each nozzle firing. Converting the mass units to force units then numerically integrating this force vs time data yields the total impulse. By then examining the other scale and finding the mass difference of the canister before and after these bursts, it is possible to extract an estimate for the propellant mass lost as well. Rearranging Eq. 2.5 will then yield specific impulse.

For every valid five-second firing trial in Tests 1, 3, and 4 (the only tests where mass data was collected for the five-second bursts), the specific impulse was calculated. In total, 243 trials were able to be used to calculate specific impulse. Section 8.1.2 will discuss sources of error in this analysis, including why some trials were unable to produce a value for specific impulse. Figure 8.1 shows a histogram of the results.

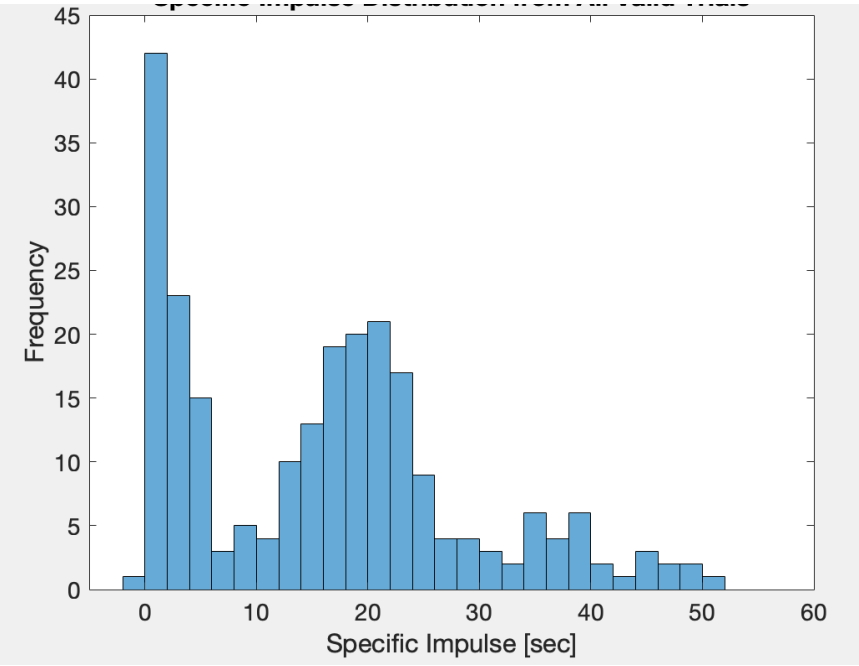

Figure 8.1: Distribution of calculated specific impulse (Isp [sec]) values from n = 243 trials. Mean of 16.14 sec; Standard deviation of 13.17 sec

Looking at the distribution, it appears to be bimodal and span a wide range of values. This data comes from all valid tests, ranging from the individual benchtop nozzle trials to the quad-nozzle tests with the fully 3D-printed system. Splitting the data into two histograms based on whether the trials were a part of a benchtop test or a test rig test yields the following two distributions, seen in Figure 8.3 and 8.4.

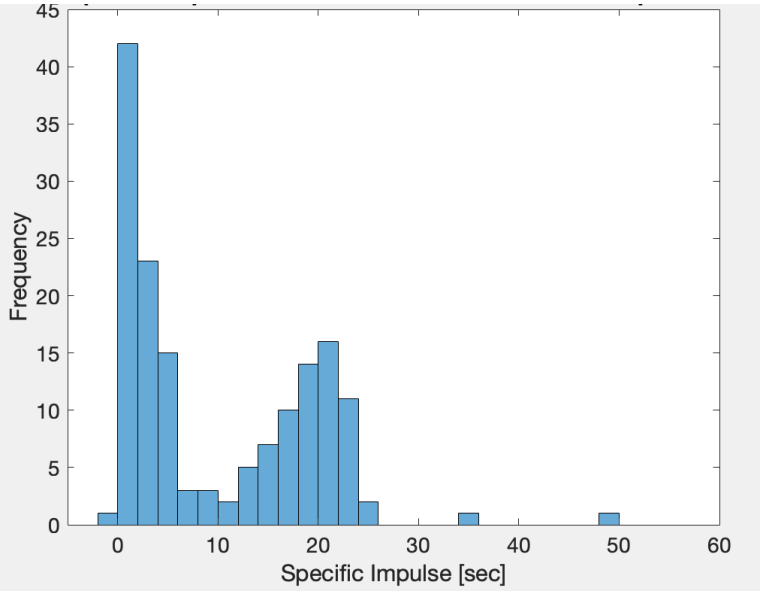

Figure 8.2: Distribution of calculated specific impulse values from n = 156 benchtop trials. Mean of 10.13 sec; Standard deviation of 9.33 sec

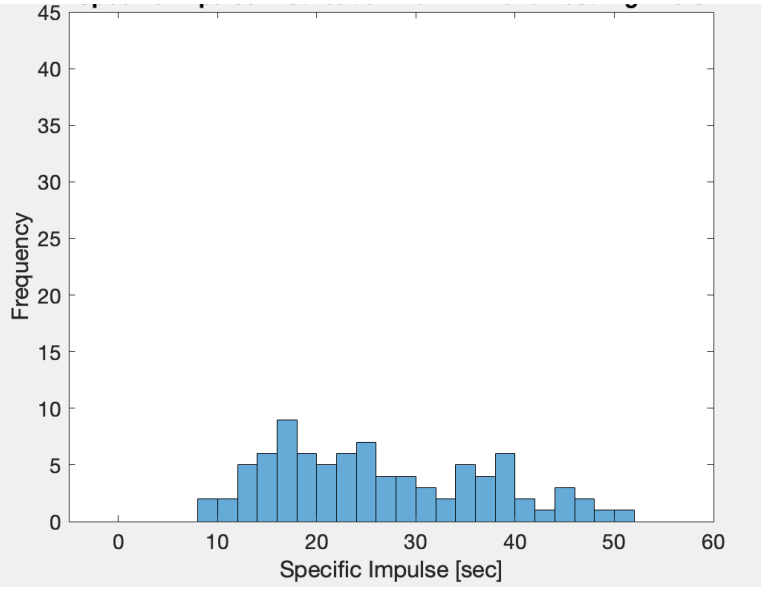

Figure 8.3: Distribution of calculated specific impulse values from n = 87 test rig trials. Mean of 26.93 sec; Standard deviation of 12.15 sec

Breaking the data set down by which tests the data originate from leads to distinctly different looking distributions. The results from the benchtop tests show a clear bimodality and have a much smaller mean (10.13 seconds) than the flatter distribution from the test rig (mean of 26.93 seconds).

Examining the raw data behind the distribution in Figure 8.3 shows the reason for a higher mean. A representative sample of a thrust over time graph for a test rig trial is shown below in Figure 8.4a.

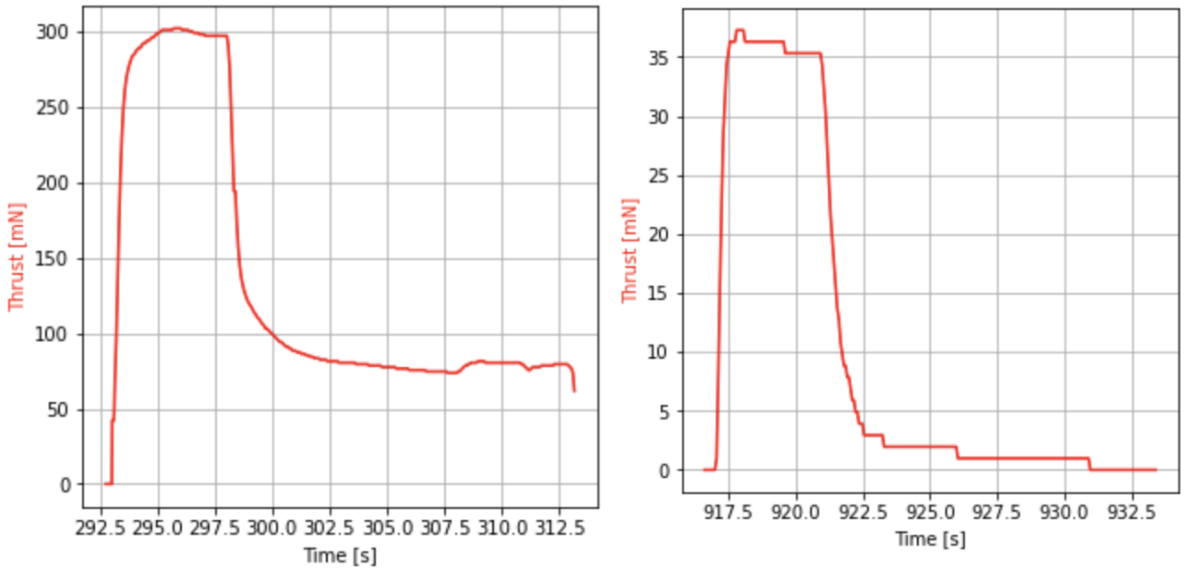

Figure 8.4a (left): A representative thrust vs time trial from a quad-nozzle test rig test. It is apparent that the scale did not properly drop back down to zero after the nozzle stopped firing. Figure 8.4b (right): A representative thrust vs time trial from a single nozzle benchtop test. In these trials, the scale properly identified zero thrust after the nozzle stopped firing.

As seen in the graph, after the five second release of propellant the thrust does not return to zero as expected. Instead, the scale continues to read a ghost offset value of approximately 75 mN. This unphysical offset is the likely culprit of higher specific impulse values since total impulse, or the integral of force over time, is directly proportional to specific impulse. Since the scale is either reading a value that is too high or is not properly dropping to zero, total impulse is artificially high, shifting the distribution's mean to the right. Additionally, this offset shift may have started during the firing, therefore causing all future values to be artificially high. A representative thrust over time graph for a benchtop test is shown below in Figure 8.4b to highlight this difference in offset.

Examining the raw data behind Figure 8.2 reveals the cause of the bimodal distribution. As mentioned in Section 7.3, tests were performed collecting sets of between 15-20 trials for each nozzle. In Test 1, two independent sets of trials were done for each nozzle. Figure 8.2 is the distribution of all trials from all benchtop testing sets. However, isolating and graphing each set

of trials reveals that each set either fell into the lower half of the distribution in Figure 8.2 centered near 3 seconds, or into the right half of the distribution centered near 19 seconds. Figure 8.5a and 8.5b displays representative distributions from two different sets in Test 1.

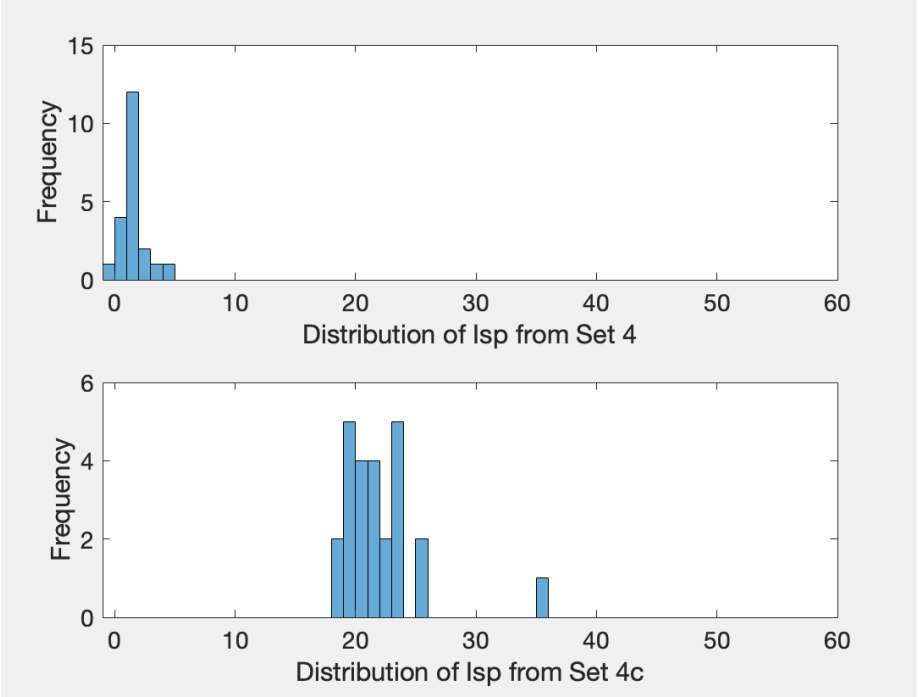

Figure 8.5a: All trials from Set 1 of Test 1 Nozzle 4 (top) have Isp values unrealistically near or below 0.

Figure 8.5b:All trials from Set 2 of Test 1 Nozzle 4 (bottom) have Isp values distributed near 22 seconds.

Causes for this difference are further discussed in Section 8.1.2. Graphing the distribution of trials from sets that are not unrealistically centered at or near 0 yields the histogram seen in Figure 8.6.

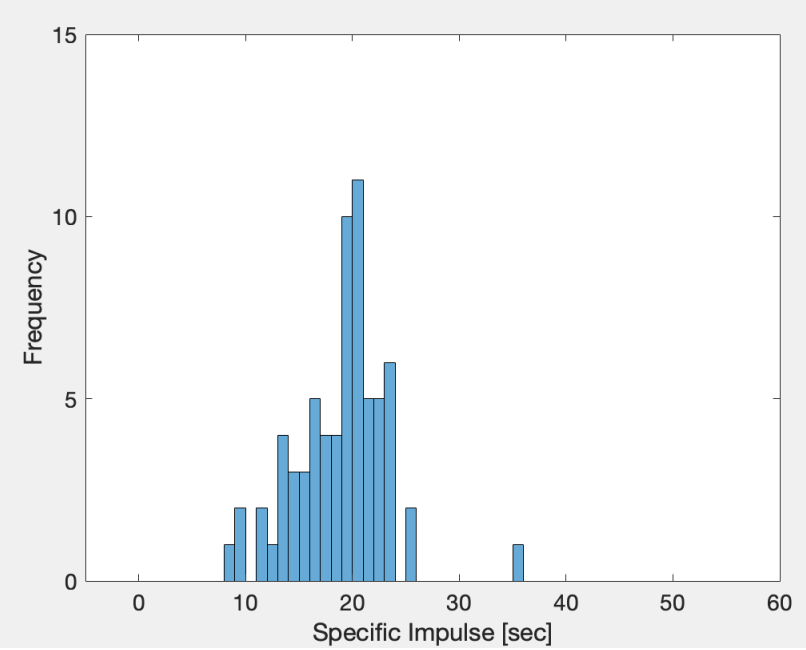

Figure 8.6: Distribution of calculated specific impulse values from n = 69 filtered trials. Mean of 18.81 sec; Standard deviation of 4.47 sec

After filtering the data to just these trials, the distribution has a mean of 18.81 seconds and a standard deviation of 4.47 seconds. As discussed above, test rig trials were ignored due to the offset error, and some sets of benchtop trials were ignored due to the consistent unrealistically low Isp. Comparing these results to the entire dataset present in Figure 8.1, the means are still remarkably close, only different by ~14%.

Specific impulse is theoretically determined by the governing equations in Section 2.1.1. Using the python model we created to solve these governing equations (see Appendix D for full code), it is possible to predict the specific impulse for any propellant with any nozzle geometry under any conditions. Using the parameters of the test set up, including nozzle geometry and the temperature and pressure range that was tested of the propellant, and incorporating experimental efficiency correct factors empirically measured from literature [10], between 17℃ and 22℃, R134a should have a specific impulse between 18.9 and 21.6 seconds. This range of values is within one standard deviation above the mean of both the filtered distribution in Figure 8.6 and the naive unfiltered total distribution in Figure 8.1.

This is an incredibly promising result: the empirical results from testing the system support the python model's prediction. Since the performance of the propulsion system designed in this report was built off of information and assumptions dictated by the model, experimental confirmation of the predictions made by the model support the idea that the propulsion system will perform as expected. In particular, this includes confirmation that the specific impulse of the flight system is likely to be as predicted, meaning the mass of propellant needed is realistic.

8.2. Dual Nozzle Tests

In addition to specific impulse, the python model will also return the theoretical thrust a propulsion system should generate. In order to determine the effects of adding a second nozzle firing at the same time, the thrust results from each trial can be normalized to the theoretical thrust level given the system's chamber pressure and temperature. To compare results between each trial, the peak thrust level of each trial in Test 1 and 2 was divided by the theoretical thrust. These normalized thrust values were then averaged for each valid nozzle set in Tests 1 and 2. Sets of Test 1 that were identified to have unphysical specific impulse in the above section were neglected in this analysis. This means that nozzle 1 could not be analyzed, as both sets involving nozzle 1 alone had unphysical results. Figures 8.7, 8.8, and 8.9 show the average normalized peak thrust for all valid individual nozzle tests and relevant double nozzle tests

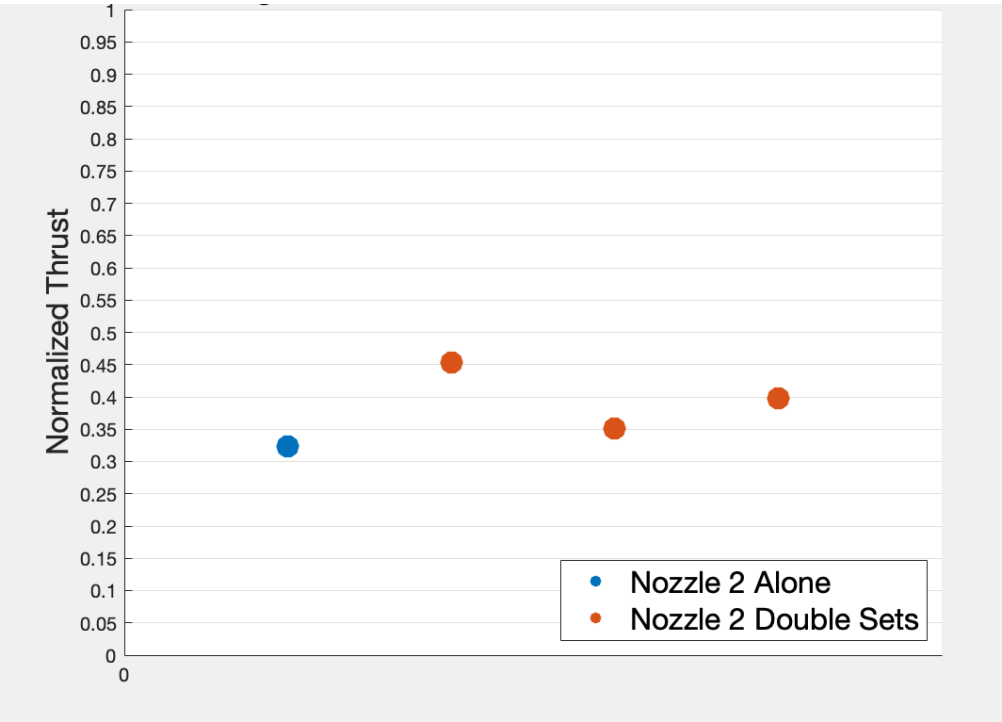

Figure 8.7: Average peak normalized thrust for nozzle 2 alone and three double nozzle sets involving nozzle 2

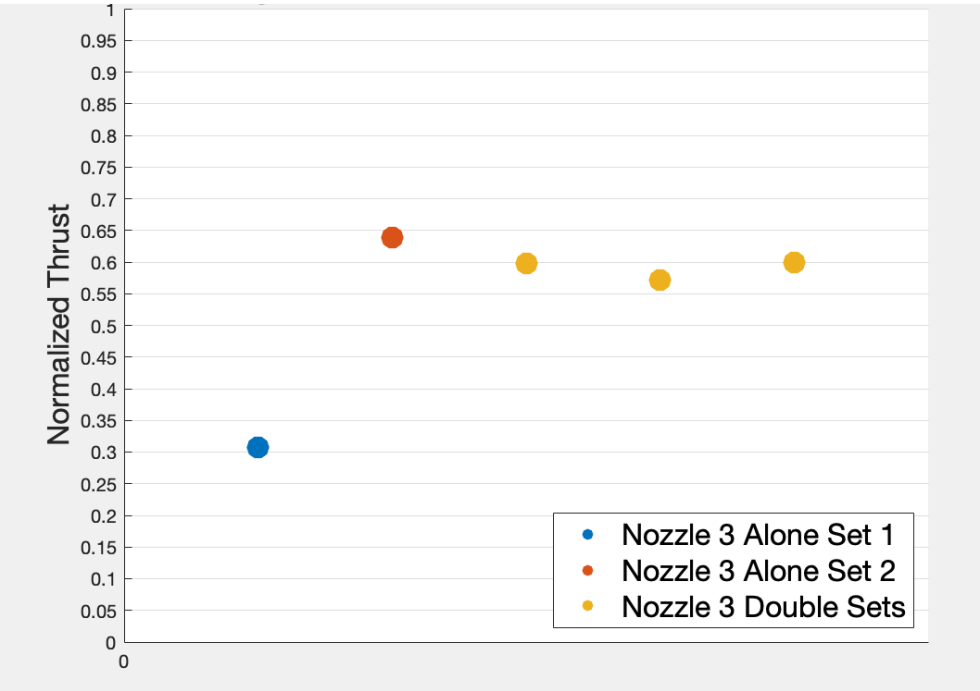

Figure 8.8: Average peak normalized thrust for two sets of nozzle 3 alone and three double nozzle sets involving nozzle 3

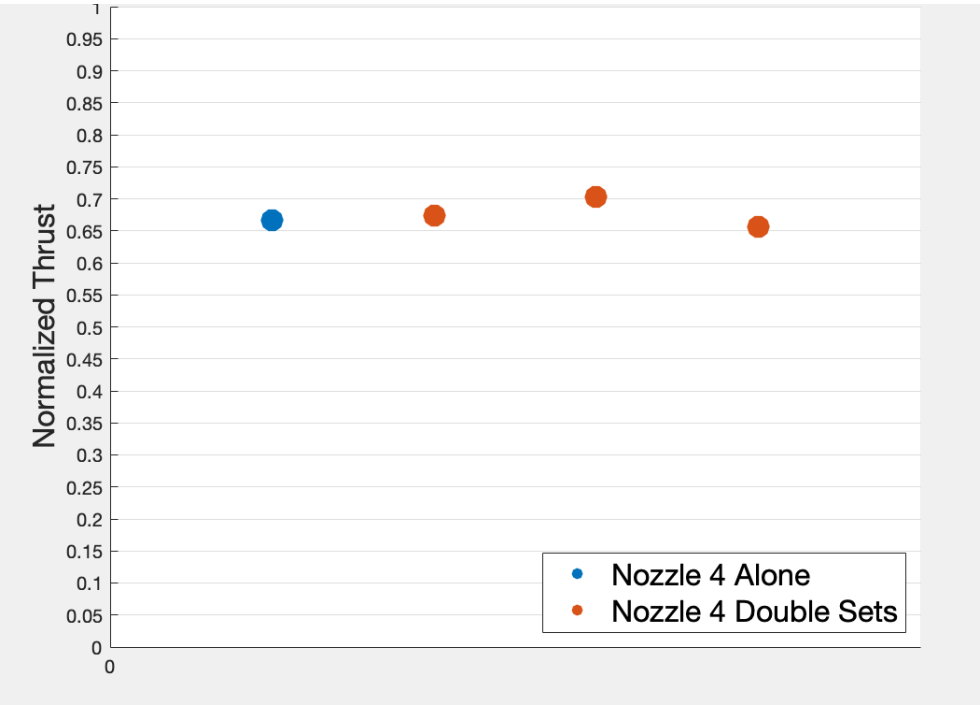

Figure 8.9: Average peak normalized thrust for one sets of nozzle 4 alone and three double nozzle sets involving nozzle 4

Taking the ratio of each double nozzle data point to its corresponding single nozzle data

point(s) yields the graph seen in Figure 8.10.

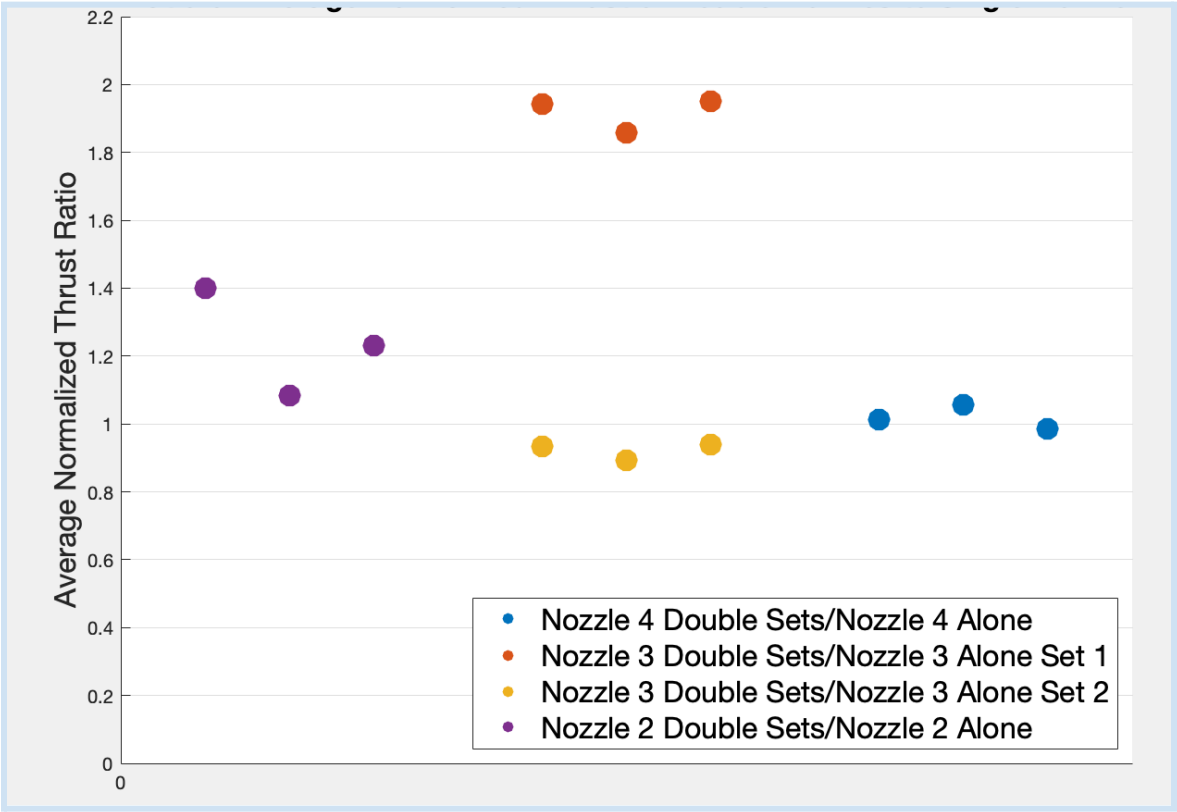

Figure 8.10: Ratio of the average peak normalized thrust of each double nozzle set to its corresponding single nozzle test. Nozzle 3 had two valid single nozzle tests so there are two triplets of ratios shown in the graph. A ratio above 1 means that the average peak normalized thrust was higher in the double nozzle set than the single nozzle.

None of the analyzed nozzles saw the thrust drop by more than 15% when adding a second nozzle. As seen in the graph above, the peak thrust was generally about the same or larger in the double nozzle set up than in the single nozzle set up. The data are not strong enough to make any quantifiable inference about how exactly doubling the nozzle count affects thrust performance. However, the data does support the hypothesis that adding additional nozzles does not split the thrust and mass flow between the nozzles. Further testing is required to fully determine the relationship beyond experimental error, but these preliminary results do not raise any doubts about the assumed behavior of adding more nozzles in parallel to increase total thrust output.

One peculiarity the data shows is the relative performance of each nozzle. Comparing the results in Figure 8.7 to Figure 8.8 and 8.9, it is apparent that nozzle 2 had consistently lower thrust performance than nozzles 3 and 4. This consistent difference across different data sets implies that nozzle 2 could have had a defective 3D print. Since the throat diameter was 0.5 mm and the minimum recommended feature size was 0.1 mm, small variations in this dimension are

likely and can have a significant effect on performance. More testing would be required for the flight prints to experimentally determine print consistency.

8.3. Long Duration Thrust over Time

Test 5 tracked the pressure drop of the propellant over the 15 or 30-second duration of all four nozzles firing. The constructed Python model produces a conservative estimation of what this theoretical pressure and temperature drop over time should look like. This drop comes from the fact that liquid propellant vaporizes to produce the gas used for propulsion. This vaporization requires energy, which is drawn from the surrounding propellant, thus lowering the temperature as it produces thrust. The model assumes that all energy to vaporize comes from the surrounding refrigerant gas since the gas has the lower heat capacity, and thus will have a greater temperature drop than the liquid given the same amount of energy. This unphysical assumption provides a conservative bound for analyzing performance drop over time. Given a 30-second burn with our test starting at room temperature, the model predicts the pressure should drop from ~69 psig to ~60 psig, or approximately 3℃. The temperature and thrust vs time graph the model predicts is seen below in Figure 8.11.

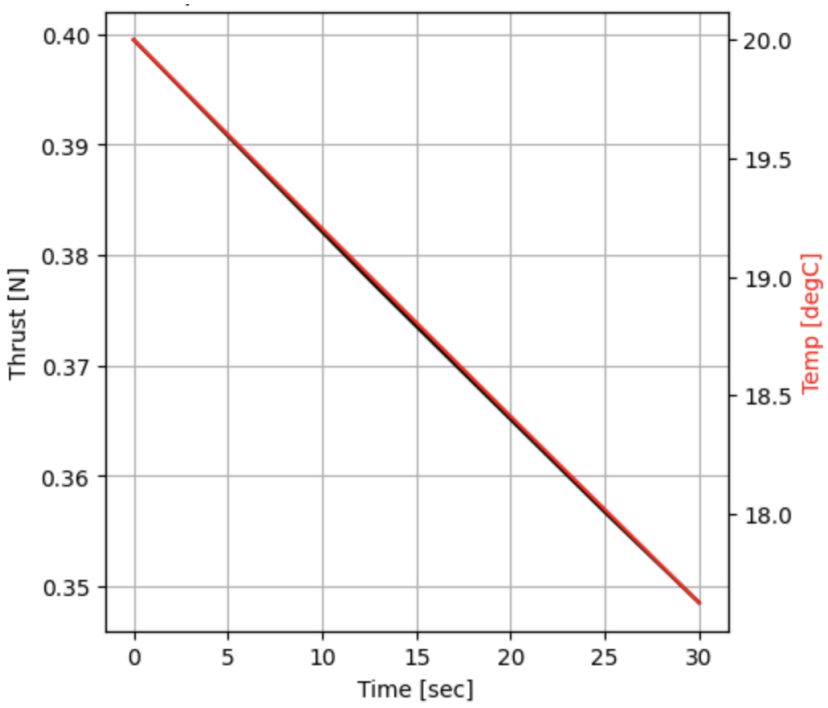

Figure 8.11: Thrust and Temperature vs time graph for a 30 second firing of R134a.

The experimental data for this starting pressure is seen in Figure 8.12.

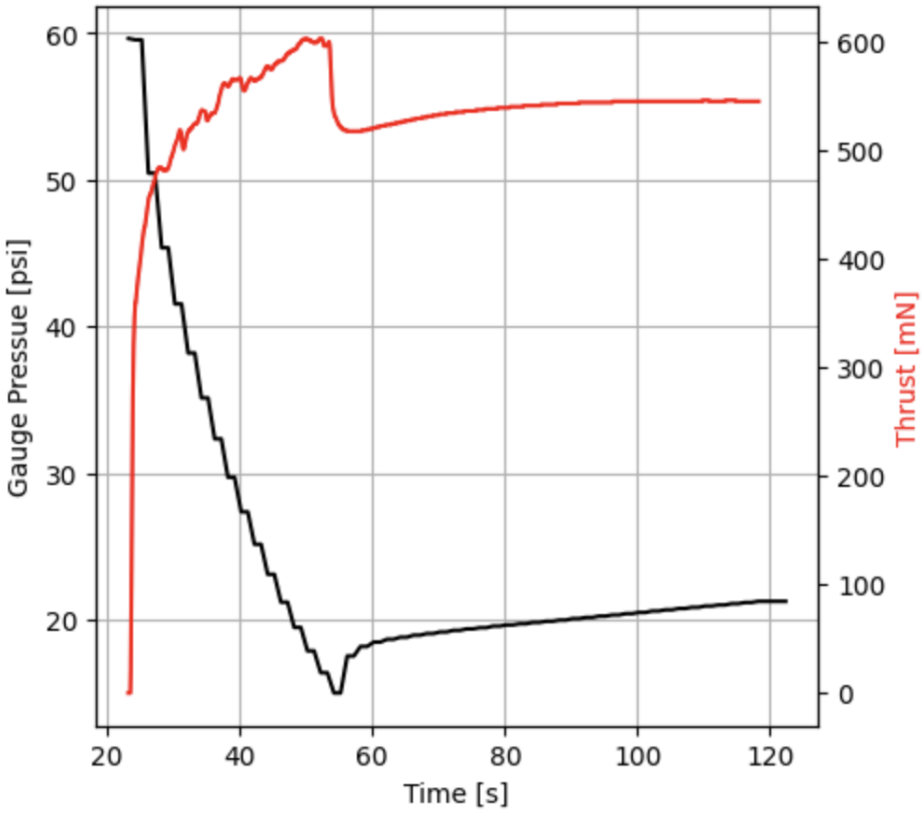

Figure 8.12: Pressure and thrust data over time for a 30-second fire trial

This data is dramatically different than expected results. The thrust continues to increase over time even as the pressure decreases. After the valve closed, there was a large mass offset similar to the offset discussed in Section 8.1. Also, the pressure dropped by around 40 psi whereas the model only predicted a 10 psi drop. Looking at other trials, the data is equally messy. Figures 8.13 through 8.17 show all other 30-second trials

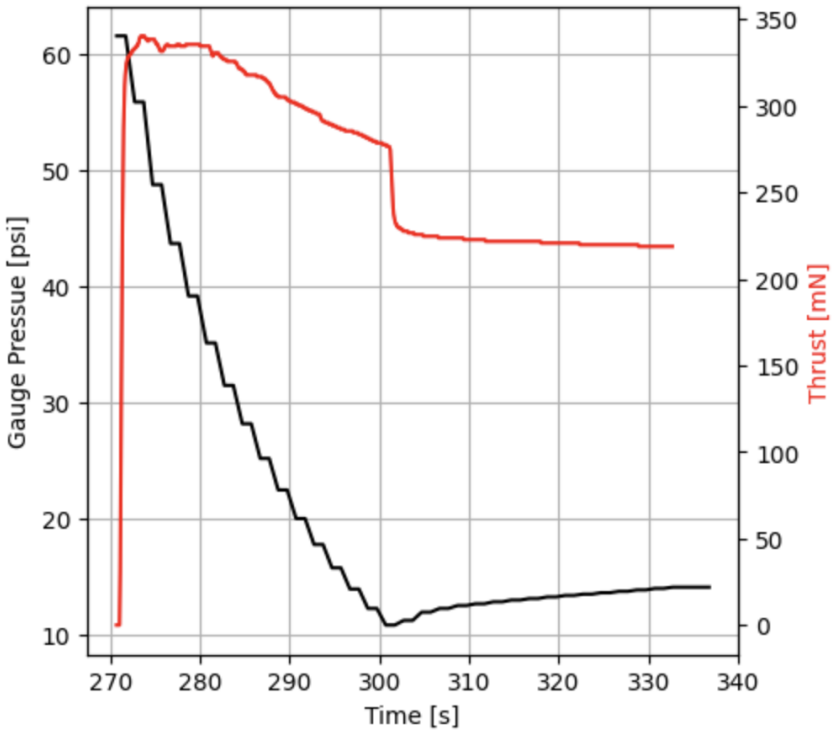

Figure 8.13: Pressure and thrust data over time for a 30-second fire trial

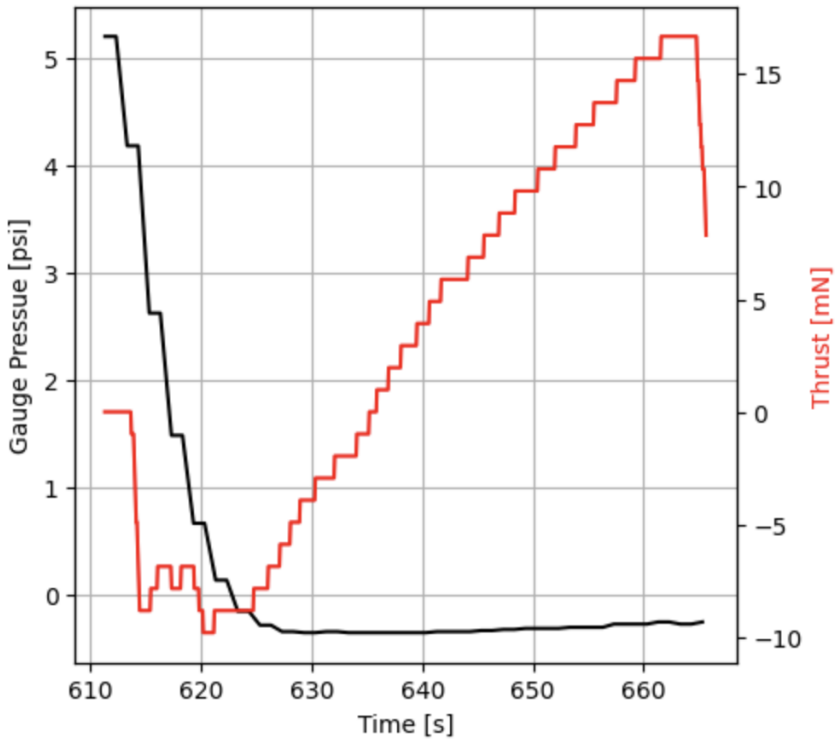

Figure 8.14: Pressure and thrust data over time for a 30-second fire trial

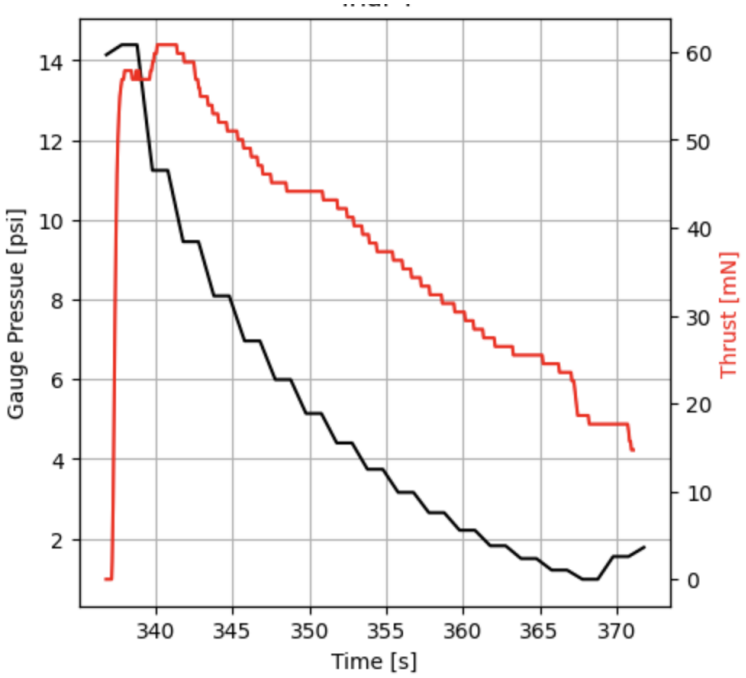

Figure 8.15: Pressure and thrust data over time for a 30-second fire trial

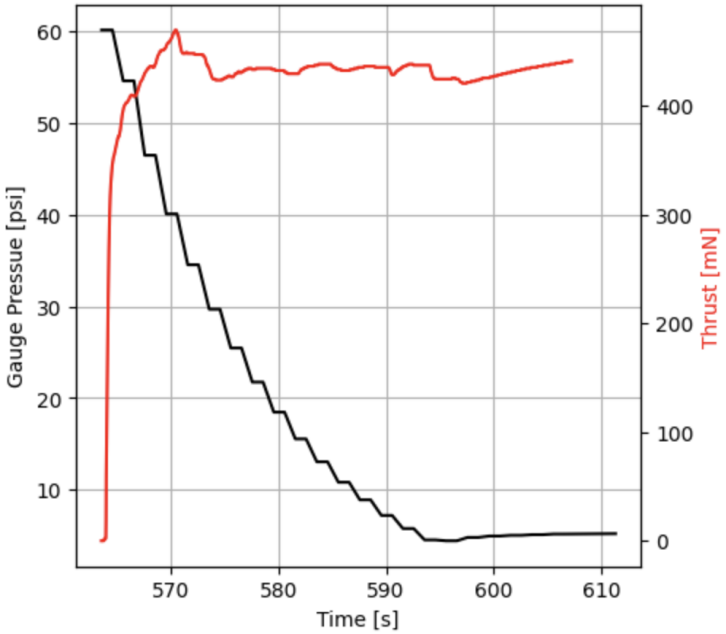

Figure 8.16: Pressure and thrust data over time for a 30-second fire trial

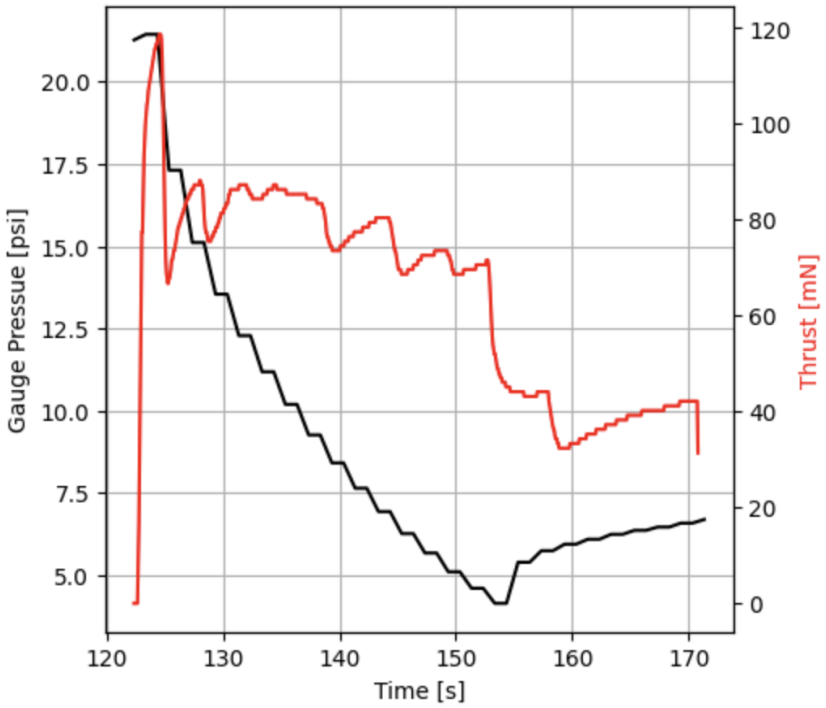

Figure 8.17: Pressure and thrust data over time for a 30-second fire trial

Clearly, the data is extremely inconsistent between trials and is quite far off from theoretical expectations. Due to the messiness of this data, it is not possible to draw a definitive conclusion or to gain any insight from this test. Further testing is necessary to investigate the relationship between the Python model and reality.

8.4. Sources of Error

8.4.1. Manufacturing Errors and Leaks

No fluid system is 100% leak proof, and these complex testing setups were no exception. Since all tests were conducted inside of a closed fume hood and the propellant is colorless, leaks are incredibly difficult to detect. The fans of the fume hood hide any sound of a small or medium leak, the fume hood blocks any air flow to the outside making it impossible to feel a leak blowing air, and the colorless gas makes it impossible to visually detect a leak. Any leak in the system will affect apparent specific impulse performance negatively, as propellant lost to the environment will increase the apparent mass loss between each firing. If the leak is substantial enough, not enough propellant could make it to the nozzle, driving down thrust substantially.

A large leak is the most likely explanation for the discrepancy in specific impulse values seen across sets of the benchtop nozzles trials in Test 1 discussed in Section 8.1. This hypothesis is supported by the fact that all trials within that set were ruined and it was not random trials between sets that were problematic. Furthermore, it was noticed that sometimes the flexible

tubing was not fully pushed into the push connect fittings, which caused a massive leak. This problem was noticed during data collection for Test 2, and extra care was taken after that to plug them in all the way. This would also account for why this behavior of ruined sets only appeared in Test 1 and not afterwards, as tests were conducted in numerical order.

Other sources of leaks include the valve itself. Five trials in Test 1 were completely neglected because after the solenoid valve appeared to close, gas was still flowing strongly through the nozzle. Only after repeatedly opening and closing the solenoid valve did the gas finally stop. This is the reason a manual valve was added in line with the solenoid valve in later tests. Dissection of the solenoid valve did not reveal any underlying causes. The best explanation is that the canister of propellant had particulate inside that prevented the valve from closing properly. It is possible that in other trials the valve could not close completely and remained open enough to let a small amount of gas through.

In the fully 3D-printed body, other sources of potential leaks were cracks in the body and small leaks in the manifold face seals and threaded fittings. As discussed in greater detail in Section 6.3.4., the crack was sealed with hot glue and a leak test was done to determine the magnitude of leaks in the system. Though results were deemed small enough to proceed with testing, the leaks could still have impacted results. Leaks in the tapped holes for the fittings could have occurred due to imprecise tapping. Since the NPT standard was used, all tapped holes were tapered and tapped by hand. It is therefore possible for the holes to have been tapped too deep and have too large of a taper for the fitting, or not tapped deep enough and have too small of a taper. Both results could impact the sealing properties of fittings screwed into these holes.

The final manufacturing issue that could have contributed to error in the results were the 3D printed nozzles. As discussed in Section 8 2, some nozzles appeared to have consistently lower thrust than others, which is possibly the result of inconsistencies in the print quality between nozzles. The throat and exit diameters could have been significantly smaller or larger than expected, which would affect the area ratio input in the python script, affecting results. Due to the tiny size of the nozzles, it was not possible to measure these features using hand tools. Furthermore, if the print surface finish was too rough in the diverging part of the nozzle, fluid friction with the walls could induce turbulence or energy losses, decreasing overall thrust.

8.4.2. Human Error

As always, human error in every step of testing could have contributed to errors. As previously mentioned in Section 8.4.1, the tubes were not always fully engaged with the push connect fittings, which could lead to leaks in the system. Other human errors include data recording and processing. For all benchtop tests, pressure was read off manually from the analogue gauge which only had tick marks for every 1 psi, creating the potential for human error in reading and recording this pressure. For reading the mass difference in the propellant canister, values had to be manually determined from the csv data by examining the stabilized pressure before and after each drop. This calculation was not done automatically due to the messiness of

the raw data. Again, manual data entry and value inspection creates ample opportunity for mistakes and typos. Finally, to format the files in such a way for a program to easily read in the files, manual data pre-processing was done to ensure each trial start was correctly flagged and associated with the proper mass drop and chamber pressure.

8.4.3. Scale Errors

As previously mentioned, the scales used to collect mass data to measure thrust appeared to have many inconsistencies. The scales purchased are marketed for jewelers in order to precisely mass jewelry. As such, they are designed to accurately measure dynamic mass changes that continuously vary. The scale has a built in stability indicator and would generally take on the order of 1 second to stabilize for regular test masses - much longer than the timescale of mass changes of the nozzle system.

As seen in both Section 8.1 and 8.3, tests involving the test rig were far more susceptible to scale offset errors. Since the test rig on its own weighed around 2 kg and the scale's maximum load was 4 kg, it is likely that the scale lost precision and the ability to consistently fall back to 0 due to this load. It was very common for trials involving the 3D-printed body to stabilize to a value on the same order of magnitude as the peak thrust, as seen in Sections 8.1 and 8.3. These offset errors are substantial enough to generate some doubt in all of the data in Tests 3, 4, and 5 since it is possible that all thrust and total impulse values were artificially high due to this offset.

Low thrust trials on the benchtop tests had the opposite offset issue, so this was substantially rarer. In some trials with the benchtop tests, the scale would return to a negative mass after the thrusting stopped. This could have tended to artificially lower the total impulse since the numerical integration could have included some of these negative mass values.

Similar issues existed with the scale used to track propellant mass in the canister over time. While the nozzle was firing, the scale registered a sharp decrease in mass of the canister, then stabilized to a higher value after the valve closed. For the majority of trials, the stabilized mass after the firing would be lower than the stable mass before. However, some trials inexplicably had masses greater than or equal to the mass before the thrust. Figure 8.18 shows an example of a set with this behavior.

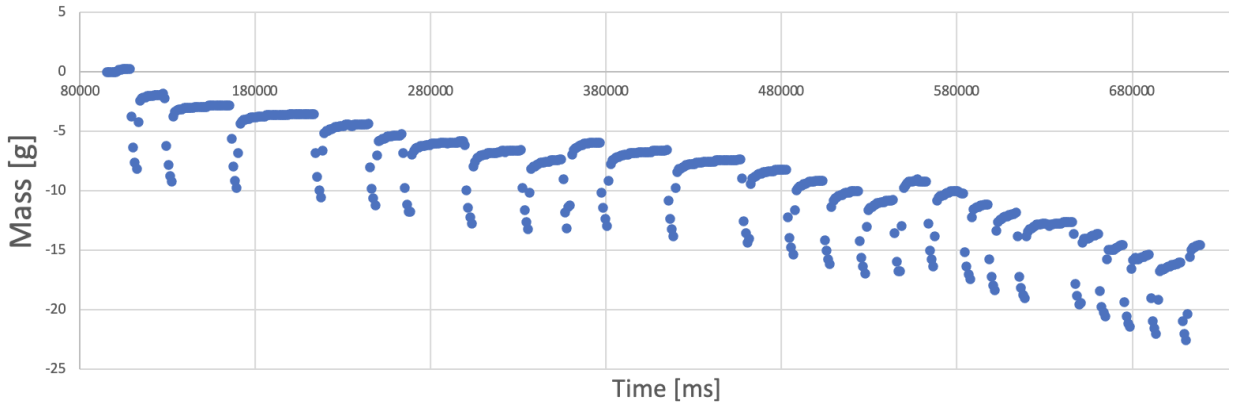

Figure 8.18: Propellant canister mass data for Test 1 Nozzle 1 Set 2. As seen in the latter half of the graph, after some trials, the mass of the canister goes up or hardly changes.

This behavior causes additional variance and uncertainty in the mass lost data, thereby propagating through to the calculations for specific impulse, since specific impulse and mass loss are inversely related. All trials with this behavior were rejected from specific impulse analysis, but this pattern raises some doubts about the accuracy of other propellant mass data points.

Additionally, the scale may have been not perfectly calibrated. 1000 g labeled masses from a test mass kit were used to calibrate the scales each day, but the kit's mass precision is unknown which could have caused a small systematic error in all measurements. Furthermore, it is possible the scale was not perfectly leveled which could generate some error. These factors are likely to not be large contributors to error relative to other sources mentioned in this section, but should be acknowledged nonetheless.

8.4.4. Propulsion System Behavior

Anomalies within the propulsion system and assumptions made during analysis are also cause for errors. Firstly, at high psi values, typically around 75 psig and above, the nozzles exhibited a phenomenon known as sputtering. Sputter occurs when liquid propellant is released through the nozzle in addition to the gaseous propellant. This is undesirable, as liquid propellant cannot convert its internal energy to kinetic energy as the gaseous propellant can through adiabatic expansion through the converging diverging nozzles. The most likely explanation for this behavior at high psi values is that the rapidly flowing gas dragged liquid through the system and out of the nozzle before the fluid had a chance to vaporize due to the sudden drop in pressure. Figure 8.19 below shows an image of a trial in which liquid came out of the nozzle.

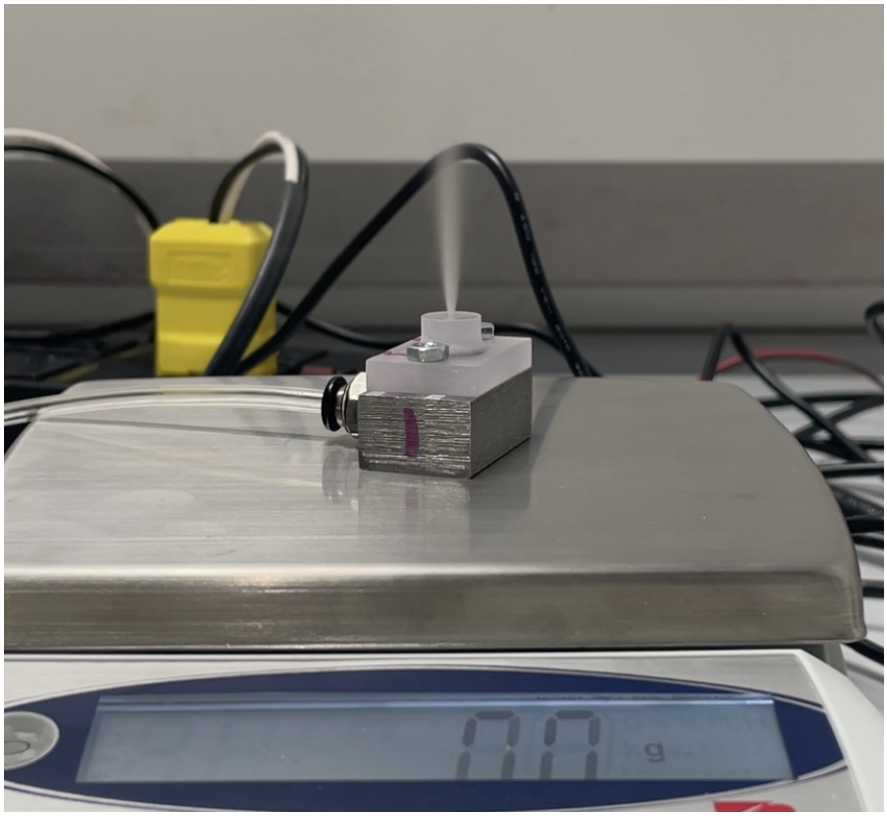

Figure 8.19: Sputtering of a nozzle as the exhaust is a misty vapor containing droplets of liquid R134a. The chamber pressure was 83 psig.

All trials in which sputtering was visually observed were flagged and not considered during analysis of the data. However, it is likely that there were some trials with sputtering not visually detectable. These trials would have a lower specific impulse since the mass was lost but not converted to thrust in the most efficient way.

Similarly, many trials continued to produce a little bit of thrust even after the valve closed. When this happened, there appeared to be liquid in the clear tubing before the nozzle but after the valve that would continue to vaporize after the valve closed. To account for this extra thrust generated, total impulse was calculated by integrating six seconds from the start of the trial, rather than exactly five, which is how long the valve was open for. Choosing a six second window balanced accounting for some of this extra thrust at the cost of potentially incorporating an incorrect scale offset as thrust as discussed in Section 8.4.3.

The analysis did not account for any pressure losses through the system before reaching the nozzle. It was assumed that the pressure was constant from the location of the pressure sensor to the nozzle inlet and from the tank outlet. This is an ideal approximation which introduced error, as the true static pressure at the nozzle is certainly lower than at the pressure sensor to due viscous effects as the fluid travels through small tubing.

Another behavior not considered in analysis was how the canister behaved as it began to run out of propellant. When the canister neared empty, the pressure would drop significantly

faster as there is no longer liquid inside to evaporate - everything is simply compressed gas when it is near empty. This means the thrust would not have been as high as predicted since the pressure quickly dropped as the gas expands without liquid to provide the vapor pressure to maintain pressurization.

Finally, the process for connecting to the 3D-printed tank did not remove all air from inside the tank before filling it with R134a. A vacuum was pulled to remove as much air as possible in order to keep the fuel as pure as possible, but the pump used could of course not create a perfect vacuum meaning the test rig tests were expelling a mixture of air and refrigerant. The model assumes that only one propellant was used and does not account for how a mixing of propellants would affect the results.

9. Tech Spec Verification

9.1. Mission Design Independent Tech Specs

Designation	Requirement	Verification
MR1	The spacecraft's wet mass should not exceed 12 kg	**N/A**
MR2	The spacecraft’s volume shall conform to the CubeSat Design Specification for a 6U CubeSat	**N/A**
MR3	The spacecraft shall remain at least 75 km from Clipper at all times during the mission	**Met**
MR4	The spacecraft shall characterize the REASON beam pattern along the x and y axes ± 60° from the nadir point to collect data at 1 degree increments	**Met**
MR5	All calibration measurements shall occur between the end of the Clipper non-interference phase and the beginning of the Mars Gravity Assist	**Met**
MR6	The spacecraft’s calibration trajectory should not require more than 12 continuous hours of REASON signal	**Met**

9.1.1. MR1

This tech spec verification was not applicable to this team. Verification of this spec is the responsibility of the Bus team.

9.1.2. MR2

This tech spec verification was not applicable to this team. Verification of this spec is the responsibility of the Bus team.

9.1.3. MR3

This tech spec was met. The path of CaliPER was designed so that it is at least 75 km away from Clipper at all times, as described in Section 4.2. Thus, this spec was verified through analysis of CaliPER's path.

9.1.4. MR4

This tech spec was met. The calibration path of CaliPER was designed to trace the x and y axes for 60 degrees, as described in Section 4.2.3. Thus, this spec was verified through analysis of the calibration path.

9.1.5. MR5

This tech spec was met. As described in Section 4.2.3, the calibration path of CaliPER can be completed in mere days, which is much less than the available calibration time window. Thus, this spec was verified through analysis of the calibration path.

9.1.6. MR6

This tech spec was met. As described in Section 4.2.3, each calibration pass takes only 12 hours. Thus, this spec was verified through analysis of the calibration path.

9.2. Propulsion System Design Independent Tech Specs

Designation	Requirement	Verification
PR1.1	Wet mass should be < 3.6kg	Not met
PR1.2	Propulsion system outer volume should be < 2U	Not met
PR1.3	Power consumption during peak and standby usage shall not exceed power budget	Met
PR1.4	Propulsion systems shall have at least 3 inhibits to activation	Met
PR1.5	Propulsion system shall have the ability to rotate spacecraft about all 3 principal axes	Met
PR1.6	The propulsion system hardware shall have the ability to translate the spacecraft	Met
PR1.7	The thrusters shall all be independently activable	Met
PR1.8	The propulsion system shall have a minimum impulse bit no larger than 10% of the momentum storage capacity of the reaction wheels	Met
PR1.9	Commercial-off-the-shelf components shall be able to withstand a temperature range from at least -30 ℃ to 50 ℃	Inconclusive
PR1.10	The total delta-V capability of the system shall be no less than 52.21 m/s	Inconclusive
PR1.11	End of life (EOL) thrust shall be >= 25 mN per axial nozzle	Inconclusive

9.2.1. PR1.1

This tech spec was not met. As further described in Section 5.4, additional mass had to be added to the storage tank to strengthen it, causing the system to be overweight. Thus, this spec was verified through analysis of the system CAD.

9.2.2. PR1.2

This tech spec was not met. As further described in Section 5.4, additional volume had to be added to the storage tank to store enough propellant, causing the system to be oversized. Thus, this spec was verified through analysis of the system CAD.

9.2.3. PR1.3

This tech spec was met. As seen in Section 5.3.3, analysis of the schedules reveals that peak power draw never surpasses 30, yet the solar arrays can supply roughly double that.

9.2.4. PR1.4

This tech spec was met. As shown in Section 5.1.3, the system has a power inhibit switch as well as two layers of control valves, summing to three in total. Thus, this spec was verified through analysis of the system design.

9.2.5. PR1.5

This tech spec was met. As shown in Section 5.2.2.2, the propulsion system has the ability to create a torque along all three principal axes. Thus, this spec was verified by inspection of the nozzle placement.

9.2.6. PR1.6

This tech spec was met. As shown in Section 5.2.2.2, the propulsion system has the ability to create a force along the +Z axis. Thus, this spec was verified by inspection of the nozzle placement.

9.2.7. PR1.7

This tech spec was met. As explained in Section 5.1.3, all nine valves are independently controllable. Thus, this spec was verified through inspection of the system design.

9.2.8. PR1.8

This tech spec was met. As seen in Section 3.3, through analysis of this spec and of the propulsion system design, PR 2.2 was derived. Tech spec PR 2.2 was met, therefore this tech spec was met.

9.2.9. PR1.9

This tech spec was inconclusive. As seen in Section 5, the fill valve, pressure sensor, wire passthrough, temperature sensor, and heater all meet this spec. This can be verified through inspection of their spec sheets.

Only the solenoid valve, discussed in Section 5.2.3.2, does not meet the spec. The solenoid valve is meant for use in CubeSats and it has a temperature range of -29°C to 49°C, meaning that it fails the spec by only 1°C on either extreme. Further independent testing should be done to see whether the valve can handle this slightly extended temperature range. If not, this problem could likely be corrected by insulating or heating the valve, or by speaking with the manufacturer about the idea of a custom part with a slightly larger temperature range that can be produced.

9.2.10. PR1.10

This tech spec was inconclusive. Analysis from the model in Section 5.1.2 predicts that the propulsion system can achieve the delta-V needed. As seen in Section 8.1, the testing results support the idea that the model accurately predicts Isp values. However, more testing must be done to conclusively determine whether this tech spec was met.

9.2.11. PR1.11

This tech spec was inconclusive. As shown in Section 5.2.2.1, analysis from the model predicts that a single nozzle can produce 25 mN of thrust when the chamber temperature is -13 degrees C or higher. Since the solar panels will always be producing excess power, the energy to heat up the chamber will always be present. However, testing results in Section 8.2 show that the actual thrust values are lower than predicted. Therefore, more testing must be done to accurately determine the temperature at which a single nozzle produces 25 mN of thrust.

9.3. Propulsion System Design Dependent Tech Specs

Designation	Requirement	Verification
PR2.1	The propulsion system shall be able to hold no less than 1.495 kg of R236fa propellant.	Met
PR2.2	All valves should have a minimum cycle time of at most 13.5 ms	Met
PR2.3	The propulsion system shall have a means to	Met

	measure properties of the propellant within the storage tank	
PR2.4	Propellant storage tank shall be able to withstand 150 psi of internal pressure before yielding	Met
PR2.5	The propulsion system shall have the controlled ability to heat up the propellant	Met

9.3.1. PR2.1

This tech spec was met. As discussed in Section 5.1.2, based on the assumption that all propellant could initially be stored as a liquid, a volume of 1.177L was needed to store this mass. The designed propulsion system had a storage capacity of 1.257L, surpassing the goal.

9.3.2. PR2.2

This tech spec was met. Inspection of the spec sheet of the “High Speed In-Line Solenoid Valve” by the Lee company reveals that it can operate at up to 500 Hz, meaning it can cycle within 2 ms, which is much faster than necessary.

9.3.3. PR2.3

This tech spec was met. Once the test system was built, pressure and temperature measurements were output to the arduino as programmed. Thus, this spec was verified by demonstration of the pressure and temperature data output.

9.3.4. PR2.4

This tech spec was met. As discussed in Section 5.2.1.2, finite element analysis verified that the storage tank can withstand a pressure of 150 psi internally.

9.3.5. PR2.5

This tech spec was met. Although the heater port was eventually filled by hot glue, the heater did demonstrate its ability to function.

10. Conclusion and Future Work

10.1. Future Work

10.1.1. Discovered Issues

As discussed extensively in Section 6.3 and 8.4, many problems arose during the course of the project. These issues were addressed where possible during the course of the project, but merit further dedicated investigations in the future.

10.1.1.1. Propellant Loading

As discussed in Section 6.3.5, the liquid propellant was unable to be fully loaded into the tank. This is a solvable problem - companies and manufacturers must have a way to pump refrigerants into constant volume containers, and the researchers who worked on INSPIRE were able to describe their method to this team. Given the limited time and material resources available, other methods of loading the liquid propellant were not tested. Determining a reliable method for loading the tank with entirely liquid propellant is a critical next task, as failing to load enough mass into the system means it cannot produce the required delta-V.

10.1.1.2. Testing Parameters

As mentioned in Section 8.3, the data from the long duration tests were inconclusive. This means that verification of the model's predictions for thrust and pressure over long periods of time could not be experimentally verified. Since the CaliPER mission requires delta-V maneuvers of over 3 minutes at once, understanding this behavior is crucial to the completion of the project. Future work on further testing on long duration burns is absolutely necessary.

Secondly, as discussed in Section 6.3.4, in order to patch the leak in the system, hot glue was used to fill in the port in question. Since the port that was filled was where the heater went, tests on how the fluid temperature responses to heat inputs could not be experimentally verified. Future work on this project must involve testing on the heating up of the propellant, as this is another crucial aspect of the project that must be understood in order to characterize the system as a whole.

Next, due to the fact that the tank was unable to be loaded properly, testing in the vacuum chamber was not feasible. While the tank was able to contain some amount of liquid, it was not enough to make isolating the test rig inside a vacuum chamber worth testing. Once the issue with loading the tank properly is resolved, then the system can undergo testing in a vacuum chamber. Removing or reducing the effects of the atmosphere on the system is crucial to testing the system in conditions more closely mimicking flight.

Finally, due to the resource constraints outlined in Section 6.1, testing of the flight hardware was impossible for this project. After completing the above testing, it all must be repeated for the flight system with the space rated hardware and flight units. All prior testing works to build confidence in the next iteration of the design, so the logical progression is that after extensively testing cheaper prototype systems to understand and characterize the base design, testing must happen on the real propellant and 3D print to have full confidence in the system.

10.1.1.3. Measurement Strategy

As discussed extensively in 8.4.3, there were a lot of issues discovered with using the scale for this case, particularly when the test involved the test rig thrusting into the scale. For future tests, investigation should be done into the root cause of some of the quirks of the purchased scales. Depending on the results from that find, new scales may have to be purchased, or alternate means of measuring force may have to be used. Strain gauges and load cells were considered for this purpose in this project, but time constraints led to the decision of the simple and straightforward scale.

10.1.1.4. Fluid Issues

As discussed in Section 8.4.4, the testing revealed issues with the fluids system involving leaks, cracks, sputtering, and abnormal valve behavior. While these issues were able to be worked around while testing, moving forward they must be addressed in full to prevent them from happening on future prototypes.

As was mentioned, sputtering was only observed at high psi values. Fortunately, the real propellant, R-236fa, has a substantially lower vapor pressure that the test propellant used. Based on the sputtering only appearing at high pressures, this might imply sputtering will not be an issue on the real system. Furthermore, sputtering may not be as common in a vacuum since the liquid requires less energy to vaporize. However, the fact that sputtering was observed at all demonstrates that even in a warm environment (at least compared to space) some of the liquid still does not vaporize before exiting. This could mean that despite the lower vapor pressure and operating in a vacuum, sputtering is still a potential issue. In either case, continued testing is necessary to identify how, when, and why this is an issue and to identify potential solutions. If sputtering persists, some ideas to investigate in future projects could be:

1. Adding a vaporization plenum to prevent liquid build up before leaving to the nozzles.
2. Instead of the entire tank being filled with liquid to vaporize, the tank should store the liquid-vapor mixture at its critical density at the start
3. Apply a larger safety factor to the delta-V budget to account for losses in efficiencies by bringing more spare propellant.

These are just a few potential solutions - ultimately further testing is required to identify the best method of prevention, if necessary at all.

Cracks and leaks in the 3D printed system is of course a significant issue for the flight system. Crack propagation should be reduced by adding fillets to the outside edges, which was not done on the test rig body. Additionally, analysis on the torque loading conditions of the screws clamping down the manifolds could be used to help standardize the face seals. Pursuing further testing of tapping the NPT hotels to the correct depth could help reduce leaks at those interfaces. After discussion with a researcher who worked on the INSPIRE mission, o-rings with a square cross section may be better than the circular o-rings used in this design since square o-rings will have more surface area in contact with the manifold and plastic. They also used EPDM instead of neoprene, which should also be investigated and compared to the current o-rings. Lastly, standardizing the surface roughness of the manifold and 3D print body could help decrease leaks at those boundaries as well - the INSPIRE researcher said they used a surface roughness of 16 Ra. Further testing should be done to investigate the best ways to seal each and every boundary.

10.1.2. Expanding Project Scope

This project was a massive undertaking and had countless subcomponents that merit an entire project all on their own. The following sections are descriptions of topics that were not investigated or considered, but that should definitely be given attention if this design and mission are to progress and move forward.

10.1.2.1. Orbit Analysis

Trajectory and path design was completed by hand and with only the limited information provided by JPL. Once given information regarding:

1. The precise launch trajectory of Clipper
2. The exact timing, duration, and delta-V of all Clipper TCMs
3. The exact times that the Clipper team wants CaliPER to calibrate REASON

then a more formal orbital analysis can be done. Softwares such as Ansys's STK (System Tool Kit) or JPL's MONTE (Mission analysis, Operations and Navigation Toolkit Environment) python package can be used to numerically solve and visualize the flight path of both Clipper and CaliPER. MONTE is the software JPL uses for actual mission design, so that is the gold standard as far as flight planning is concerned. Doing these formal analyses with numerical solvers will demonstrate the exact maneuvers CaliPER must perform.

10.1.2.2. Thermal

No team during this year's ES100 project took on the role as the system's thermal engineer. A full scale, spacecraft level thermal analysis must be done to ensure all sensitive components stay within their temperature ranges. This analysis will depend on the result of the orbit analysis in Section 10.2.1, as that simulation will output exactly where the sun is relative to CaliPER at any given time.

The spacecraft-level thermal analysis can be used to adjust design features of the propulsion system. Since hotter propellant means a more efficient system, it is to the propulsion system's advantage to soak up as much solar energy as possible to minimize reliance on onboard power to heat the propellant. If the thermal analysis shows that the exposed valves on the -Z face get too hot or cold, there is room on that face to install insulation material or other auxiliary components to maintain a desirable thermal state.

Within the propulsion system, full thermal analysis needs to be done to account for temperature losses from the refrigerant as it moves through the valves and tubing to potentially adjust design parameters. This project assumed the propellant was isothermal until reaching the nozzle, which is an assumption that would need to be adjusted as the project grows in technical readiness.

Furthermore, heat transfer and fluid dynamics analysis must be done to fully understand the patch heater inside the tank. This project assumed a blanket 50% efficiency in power into the heater vs power out to the propellant, so this could be refined to more properly size the heater. Additionally, thermal-fluid simulations would have to be done to understand the behavior of two-phase systems in a microgravity environment.

10.1.2.3. Controls

This project focused on the design, build, test, and characterization of the propulsion system. It did not attempt to integrate the propulsion system within the context of a central on board computer or closed-loop flight controller to remotely control the propulsion system to impart a specific amount of impulse. This is a crucial part of the next steps of this project, and is currently being investigated by another student for their ES100 project. This control algorithm will unite the GNC and propulsion subsystems, and will rely on a deep experimental understanding of how the system performs under various conditions in order to accurately predict performance. This flight controller PCB could even be located inside the storage tank to provide bonus heat to the propellant as the flight electronics are powered. This was actually done on MarCO's system, so this strategy has demonstrated flight heritage and electronic compatibility with R-236fa.

10.1.2.4. Mechanical Optimization

This project focused on the prototype design and build of the propulsion system. This means that no work was done to optimize the geometry of the 3D printed tank and manifolds to reduce mass while maintaining structural integrity. Filets and material were added inside the tank until FEA simulations demonstrated the tank could hold the internal pressure without yielding. Significant work could be done to reduce excess mass of the 3D print while increasing strength of the tank. Similarly, the manifolds were designed as simply as possible to fit the needs of the system. There is definitely room to remove a substantial amount of steel without compromising the structural integrity of the manifolds. Working to minimize the 3D print and the manifolds could significantly reduce the dry mass of the system, making the mission cheaper and/or allowing other subsystems more mass allocation if need be.

Nozzle geometries were discussed in brief in Section 5.2.2.1. As nozzles are complex enough to warrant their own dedicated project, this project chose a design rooted in simplicity and basic functionality. Other geometries, such as a bell-shaped nozzle rather than a conical shaped nozzle, could increase the performance of the propulsion system with little to no cost.

10.2. Impact and Conclusion

Ultimately, CaliPER will not fly with Europa Clipper given the timeline of this project and the expected October 2024 launch date of Clipper. However, work done on this project will serve as a baseline, proof-of-concept for future auxiliary CubeSats to support flagship NASA missions. Past flagship missions, such as DART and InSight have already proven the ability for CubeSats to complement primary mission operations by providing non-mission critical support. Given the success of these secondary CubeSat missions, CaliPER being able to provide mission essential functionality by properly calibrating a primary instrument is the next progression of the technology. CaliPER paves the way for CubeSats to enhance, support, and augment the mission priorities of future exploration missions.

Additionally, the propulsion system proposed in this paper, after continued testing and iteration, has the potential to dramatically enhance CubeSat propulsion systems. As of this writing, this prototyped warm gas CubeSat propulsion system has the highest theoretical delta-V capacity of a CubeSat to date. There is of course a long way to go from the proof of concept proposed here to a functional and space-rated propulsion system, but the groundwork has been set for this project to continue development and iteration. Other CubeSat missions with interplanetary delta-V capacities have the potential to further increase the abilities of these small, high risk spacecraft to explore and produce science. Beyond space, developments in cold gas propulsion systems even have terrestrial applications, such as controlling high altitude weather balloons [41].

Out of the 20 applicable technical specifications for this project, 15 were met, 3 were inconclusive, and 2 were not met. For the 2 requirements that were not met, the volume and mass requirements, there exists a clear path forward to adjust the design or reevaluate the requirement with the systems engineering to fully comply with set requirements. For the 3 requirements that were inconclusive, current data points towards compliance, but further testing is required to confidently say the design meets specifications.

Results from the proof of concept testing of this propulsion system proved to be extremely promising. The Python model, which was derived directly from governing physics equations, accurately predicted the thrust and specific impulse performance of the test system. This further supports the claim that the Python model can accurately predict the performance of the ideal flight system as well, which suggests that this ideal system truly is a viable design for the CaliPER mission. Of course, much more rigorous testing of the flight system is required, but this project has successfully charted a path forward for developing a custom propulsion unit for an auxiliary CubeSat for the Europa Clipper mission.

11. References

[1] E. Kulu, “Nanosats Database,” Nanosats Database. https://www.nanosats.eu

[2] “CubeSat Design Specification REV 14.1 CP-CDS-R14.1,” The CubeSat Program, Cal Poly SLO. [Online]. Available: https://static1.squarespace.com/static/5418c831e4b0fa4ecac1bacd/t/62193b7fc9e72e0053f00910/1645820809779/CDS+REV14_1+2022-02-09.pdf

[3] “JPL MarCO - Micro CubeSat Propulsion System Data Sheet,” VACCO. [Online]. Available: https://cubesat-propulsion.com/wp-content/uploads/2015/11/X14102000-01_2019update.pdf

[4] https://jpl.nasa.gov, “Mars Cube One (MarCO),” NASA Jet Propulsion Laboratory (JPL), 2018. https://www.jpl.nasa.gov/missions/mars-cube-one-marco

[5] T. J. Martin-Mur and B. Young, “Navigating MarCO, the First Interplanetary CubeSats,” Jet Propulsion Laboratory, California Institute of Technology. [Online]. Available: https://trs.jpl.nasa.gov/bitstream/handle/2014/49242/CL%2318-7451.pdf?sequence=1&isAllowed=y

[6] “CanX-4 and 5,” www.eoportal.org. https://www.eoportal.org/satellite-missions/canx-4-5#cnaps-canadian-nanosatellite-advanced-propulsion-system (accessed Sep. 09, 2022).

[7] Elizabeth Howell, “Europa: Facts About Jupiter’s Icy Moon and Its Ocean,” Space.com, Mar. 22, 2018. https://www.space.com/15498-europa-sdcmp.html

[8] J. Daigle, J. Hintz, M. LoPresti, S. Rolland, O. Ejikeme, and J. Johnson, “CaliPER: Calibration Post-Earth for REASON,” Apr. 2022.

[9] G. P. Sutton and O. Biblarz, Rocket propulsion elements. Hoboken, New Jersey: John Wiley & Sons Inc, 2017.

[10] C. Seubert, “Scholars’ Mine Masters Theses and Dissertations Refrigerant-based propulsion system for small spacecraft,” 2007. Accessed: Nov. 18, 2022. [Online]. Available: https://scholarsmine.mst.edu/cgi/viewcontent.cgi?article=7826&context=masters_theses

[11] K. Lemmer, “Propulsion for cubesats,” Acta Astronautica, vol. 134, pp. 231–243, May 2017. Doi: 10.1016/j.actaastro.2017.01.048.

[12] “State-of-the-Art Small Spacecraft Technology,” NASA Ames. Accessed: Oct. 2020. [Online]. Available: https://www.nasa.gov/sites/default/files/atoms/files/soa2020_final8_0.pdf

[13] “Cubesat Propulsion Systems Overview,” VACCO Industries. https://cubesat-propulsion.com/vacco-systems/

[14]“Table 4-5: Cold and Warm Gas Propulsion Manufacturer Product Propellant Thrust (Quantity).” [Online]. Available: https://www.nasa.gov/sites/default/files/atoms/files/table_4-5-_cold_and_warm_gas_propulsion.pdf

[15] “NASA - NSSDCA - Spacecraft - Details,” nssdc.gsfc.nasa.gov. https://nssdc.gsfc.nasa.gov/nmc/spacecraft/display.action?id=L-FLASHLT (accessed Sep. 09,

2022).

[16] D. Andrews and E. Glenn Lightsey, “Design of a Green Monopropellant Propulsion System for the Lunar Flashlight Mission,” 2019. [Online]. Available: https://ssdl.gatech.edu/sites/default/files/ssdl-files/papers/mastersProjects/AndrewsD-8900.pdf

[17] S. Arestie, E. Lightsey, and B. Hudson, “Development of A Modular, Cold Gas Propulsion System for Small Satellite Applications.” Accessed: Sep. 28, 2022. [Online]. Available: https://jossonline.com/storage/2021/08/0102-Arestie-Development-of-A-Modular-Cold-Gas-Propulsion-System-for-Small-Satellite-Applications.pdf

[18] T. Imken, T. Stevenson, and E. Lightsey, “Design and Testing of a Cold Gas Thruster for an Interplanetary CubeSat Mission,” JoSS, vol. 4, no. 2, pp. 371–386, 2015, [Online]. Available: https://jossonline.com/wp-content/uploads/2015/12/Final-Design-and-Testing-of-a-Cold-Gas-Thruster-for-an-Interplanetary-CubeSat-Mission.pdf

[19] E. Glenn Lightsey, T. Stevenson and M. Sorgenfrei, "Development and Testing of a 3-D-Printed Cold Gas Thruster for an Interplanetary CubeSat," in Proceedings of the IEEE, vol. 106, no. 3, pp. 379-390, March 2018, doi: 10.1109/JPROC.2018.2799898.

[20] https://www.jpl.nasa.gov, “SunRISE,” NASA Jet Propulsion Laboratory (JPL). https://www.jpl.nasa.gov/missions/sun-radio-interferometer-space-experiment

[21] L. Skidmore and E. Lightsey, “Design of a Cold Gas Propulsion System for the SunRISE Mission.” Accessed: Jan. 20, 2023. [Online]. Available: https://ssdl.gatech.edu/sites/default/files/ssdl-files/papers/mastersProjects/Skidmore_AE_8900.pdf

[22] “NASA SYSTEMS ENGINEERING HANDBOOK.” [Online]. Available: https://www.nasa.gov/sites/default/files/atoms/files/nasa_systems_engineering_handbook_0.pdf

[23] N. JPL, Reason calibration image as provided by nasa jpl, Oct. 19, 2021.

[24] “About | Mission – NASA’s Europa Clipper,” NASA’s Europa Clipper, Oct. 2019. https://europa.nasa.gov/mission/about/

[25] “NanoRacks DoubleWide Deployer (NRDD) System Interface Definition Document (IDD),” Nanoracks, Sep. 20, 2017. https://nanoracks.com/wp-content/uploads/Nanoracks-DoubleWide-Deployer-NRCSD-IDD.pdf (accessed Oct. 29, 2022).

[26] “Accura Bluestone (SLA),” 3D Systems, Jun. 21, 2016. https://www.3dsystems.com/materials/accura-bluestone (accessed Jan. 30, 2023).

[27] “Converging Diverging Nozzle,” www.engapplets.vt.edu. https://www.engapplets.vt.edu/fluids/CDnozzle/cdinfo.html

[28] “O-Ring Design Considerations | Marco Rubber & Plastics | Custom O-Rings Supplier,” www.marcorubber.com. https://www.marcorubber.com/o-ring-groove-design-considerations.htm

[29] T. of S. V.-T. H. Group and A. S. C. · REPLY, “Which O-ring material is right for my application? - Parker Distributor,” The Hope Group - Largest Parker Distributor in New England, Aug. 18, 2020. https://www.thehopegroup.com/blog/2020/08/o-ring-material-guide/

[30] D. Impulse, “High Speed In-Line Solenoid Valve,” The Lee Co. https://www.theleeco.com/product/high-speed-in-line-solenoid-valves/#cad-envelopes (accessed Jan. 30, 2023).

[31]“McMaster-Carr,” www.mcmaster.com. https://www.mcmaster.com/4059K36/ (accessed Mar. 29, 2023).

[32] “Subminiature, Flush Diaphragm Pressure Transducers | Omega,” www.omega.com. https://www.omega.com/en-us/pressure-measurement/pressure-transducers/px600/p/PXM600MU-35BARGV (accessed Mar. 29, 2023).

[33] “Vacuum & Pressure NPT Feedthroughs for Sealing Wire & Cable,” www.omega.com. https://www.omega.com/en-us/temperature-measurement/temperature-connectors-panels-and-block-assemblies/feedthroughs/pft2/p/PFT2NPT-1CU?gclid=CjwKCAiAp7GcBhA0EiwA9U0mtkSAdgzMO8yO7BgrtDSzblfy4kQFmWDeJP4ju-OKVJYI5cGB_DlITBoCK88QAvD_BwE&gclsrc=aw.ds (accessed Jan. 30, 2023).

[34] “CDS Catalog,” Minco. https://www.minco.com/catalog/?catalogpage=product&cid=1_7_1-embedment-rtds&id=S102951PD3E120AC1&unit=english (accessed Jan. 30, 2023).

[35]“CDS Catalog,” Minco. https://www.minco.com/catalog/?catalogpage=search&cid=3_1-polyimide-thermofoil-heaters (accessed Jan. 30, 2023).

[36] O. US EPA, “Refrigerant Sales Restriction,” US EPA, Oct. 09, 2015. https://www.epa.gov/section608/refrigerant-sales-restriction

[37] “1/8" 110V AC Electric Brass Solenoid Valve,” Electricsolenoidvalves.com. https://www.electricsolenoidvalves.com/1-8-110-120-volts-ac-electric-brass-solenoid-valve/ (accessed Mar. 30, 2023).

[38] Mouser, “TE Connectivity M3234-000005-100PG,” Mouser Electronics, 2023. https://www.mouser.com/ProductDetail/Measurement-Specialties/M3234-000005-100PG?qs=lc2O%252BfHJPVYMORecjPeMTA%3D%3D (accessed Jan. 30, 2023).

[39] “McMaster-Carr,” www.mcmaster.com. https://www.mcmaster.com/3866K19/ (accessed Jan. 30, 2023).

[40] “McMaster-Carr,” www.mcmaster.com. https://www.mcmaster.com/4668T51/ (accessed Jan. 30, 2023).

[41] R. Ranjan, S. K. Chou, F. Riaz, and K. Karthikeyan, “Cold gas micro propulsion development for satellite application,” Energy Procedia, vol. 143, pp. 754–761, Dec. 2017, doi: 10.1016/j.egypro.2017.12.758.

12. Appendix

A. Delta-V Budget Calculations

```
%matplotlib inline
import numpy as np
import matplotlib.pyplot as plt

def pathDeltaV(time, distance, thrust, mass):
 # Given the time allowed to travel a specified distance with a defined
thrust and spacecraft mass, what total change in velocity is required
 # assumes constant thrust that can be continuously fired for indefinite
periods
 a = thrust/mass
 deltaV = time*a - np.sqrt((time*a)**2 - 4*distance*a)
 totalAccelTime = 2*time - 4*distance/(deltaV)
  return deltaV, totalAccelTime

def massLost(Isp, dV, m0):
 #given a delta v maneuver, starting mass, and an assumed Isp calcuate
mass lost
 mloss = m0*(1-np.exp(-dV/(Isp*g0)))

 return mloss
```

Constants

```
#Spacecraft Constants and Assumptionss
m0 = 12 #kg
nozzleThrust = .025 #N
minDistance = 75000 #m
Isp = 40.0 #assumed Isp

#General constants
g0 = 9.8067 #m/s^2
```

GNC DeltaV Expenditures

```
m = m0 #at the start

#GNC variables (all from GNC team)
rxnWheelCap = .01 #Nms
phase1AngMomentum =  1.48 - rxnWheelCap #Nms in y or z axis
phase2AngMomentum = 0.028 - rxnWheelCap #Nms (x or y)
phase3AngMomentum = 0.035 - rxnWheelCap #Nms (x or y)

#nominal distances from geomtric center to each of the nozzles for the
moment arm
xDistNom = 366/2 #mm
yDistNom = 211.3/2 #mm
zDistNom = 173/2 #mm


#phase1: z is worst case scenario for us generating torque
#due to symmetry in nozzles, COM tolerance does not affect total torque
values (one nozzle gets worse, the other gets better)
phase1LinMomentum = (phase1AngMomentum)/(zDistNom/(1000))
mUsed1 = phase1LinMomentum/(Isp*g0)
GNCDeltaV = Isp*g0*np.log(m/(m-mUsed1))


#phase2+3: y is worst case scenario for us generating torque
# COM could be 4.5 cm closer to one side than the other, assume worst case
yDistWorst = yDistNom - 45 #mm
phase2LinMomentum = (phase2AngMomentum)/(yDistWorst/(1000))
phase3LinMomentum = (phase3AngMomentum)/(yDistWorst/(1000))
mUsed23 = phase2LinMomentum/(Isp*g0) + phase3LinMomentum/(Isp*g0)

GNCDeltaV = GNCDeltaV +  Isp*g0*np.log(m/(m-mUsed23))

#only subtract phase 1 mass since phasse 2 and 3 mass usage will be spread
out.
m = m - mUsed1

print("The total deltaV required for the GNC ssupport is " +
str(GNCDeltaV) + " m/s")
```

Deployment Phase Calculations

```
# Deployment variables
detubmleTime = 1 #hour
clipperRelV = 2 #m/s
caliperRelV = 0.5 #m/s
catchUpTime = 40 #days


#Delta-V required to cancel 2.0 m/s deployment from Clipper and 0.5 m/s
deployment from CaliPER
dV_deployCancel = clipperRelV + caliperRelV
m = m - massLost(Isp, dV_deployCancel,m) #update spacecraft mass after
maneuver


#CaliPER deploy time (in hours) after Clipper deploys
deployTime = minDistance/(clipperRelV*60*60) # hours


#Worst case delta-V required to get on opposite side of sun
perpDistance = detubmleTime*60*60*caliperRelV #m
travelDistance = perpDistance + minDistance #m
travelTime = catchUpTime*24*60*60 #sec

dV_perp, perpAccelTime  =
pathDeltaV(travelTime,travelDistance,4*nozzleThrust,m)


deployDeltaV = dV_deployCancel + dV_perp

print("The total deltaV required for the deployment phase is " +
str(deployDeltaV) + " m/s")
print("CaliPER will deploy " + str(deployTime) + " hours after Clipper")
#print("The acceleration time for the last maneuver " + str(perpAccelTime)
+ " sec, which is possible in 1 continous fire")
```

Calibration Phase Calculations

```
#Chase variables
caliTime = 12 #hours, time we get REASON
interimTime = 45 #days between calibration paths
```

```
#trig to determine length, using tricks with 30-60-90 triangle
caliLength = 2*minDistance*np.sqrt(3)
caliSpeed = caliLength/(caliTime*60*60)


#find travel distance to resting point before 2nd calibration path
--------->

#distance traveled while slowing down after 1st path, assuming constant
mass for conservative
driftDist1 = (caliSpeed**2)/(2*4*nozzleThrust/m)

#update spacecraft mass after 1st calibration maneuver
m = m - massLost(Isp, caliSpeed, m)

#distance traveled while accelerating to 2nd path, assuming no mass loss
during in between for conservative
accelDist2 = (caliSpeed**2)/(2*4*nozzleThrust/m)
interimDist = np.sqrt( (driftDist1+caliLength/2)**2 +
(accelDist2+caliLength/2)**2)

dV_interim, interimAccelTime  =
pathDeltaV(interimTime*24*60*60,interimDist,4*nozzleThrust,m)
m = m - massLost(Isp, dV_interim, m)


chaseDeltaV = 3*caliSpeed + dV_interim

print("The total deltaV required for the calibration phase is " +
str(chaseDeltaV) + " m/s")
```

Total DeltaV Expenditures

```
TCMDeltaV = 18 #given by JPL to match Clipper

totalDeltaV = 1.3*(TCMDeltaV+chaseDeltaV+deployDeltaV+GNCDeltaV)
massProp = massLost(Isp, totalDeltaV, m0)
propVol = massProp/(1270/1000) # 1270 is density of liquid at 50 degC with
units of kg/m^3, divide by 1000 to get to L
```

```
print("The total deltaV required for the mission, with a 30% safety
factor, is " + str(totalDeltaV) + " m/s")
print("The total propellant mass required for the mission, assuming an Isp
of " + str(Isp) + " sec, is " + str(massProp) + " kg")
print("The total volume required for the propellant, assuming it all
starts as a liquid, is " + str(propVol) + " L")
```

B. Thrust and Delta-V Relationship

The thrust produced by a given propulsion system is wholly independent of the total delta-V capacity of the same system. The latter is primarily determined by the total mass of propellant stored and the specific impulse of that system, while the former is primarily determined by the type of propulsion system used — such as cold gas, chemical, or ion — and the exact design of relevant components such as nozzle geometry and propellant pressurization. However, for a given path under a given time constraint, the delta-V required to complete the maneuver directly depends on the thrust of the system. To demonstrate why this dependence exists, compare the two cases of a system with infinite acceleration and a system with extremely low acceleration and the requirement that the system start and end with 0 velocity. The system with infinite acceleration could instantly accelerate to the necessary average velocity to travel the desired path, while a system with low acceleration would require continuous acceleration until its peak velocity doubles the required average velocity.

In geometric terms, consider a velocity-time graph of the spacecraft. The integral of this curve with respect to time is the distance traveled, d, which will be a fixed, known quantity. The starting time, t_0 we set equal to 0, and the end time, t_f is a known constraint of the system. In the instant acceleration case, the graph forms a rectangle with a height equal to v_{rect} , and in the minimum acceleration case, the graph forms an isosceles triangle with a height v_{tri}. For simplicity, in both cases we assume total mass to be constant, and the slope of the graph to be

$$\frac{dv}{dt} = a = \frac{F_t}{m_0}$$

(4.1)

where F_t is the thrust produced and m_0 is the wet mass of the spacecraft. By simple geometric arguments, if both shapes have the same area and base length, then $v_{tri} = 2v_{rect}$. By definition of delta-V, the required delta-V of each maneuver will be twice the height. Therefore the minimum acceleration case will require twice the delta-V budget of the infinite acceleration case.

However, real systems will operate somewhere in between these two extremes, making it necessary to derive an analytical relationship between thrust generated by the system and delta-V required to complete the path. The problem can then be interpreted as the following geometric problem: given an isosceles trapezoid with known area, d, known big base length, t_f, and known interior angle, θ where

$$tan(\theta) = \frac{v_{max}}{t_a}$$

(4.2)

and v_{max} is the maximum velocity and t_a is the time for one segment of the acceleration , determine the height, v_{max}. For convenience define the top base of the trapezoid to be t_c for the time in which the spacecraft coasts. From the area and geometry of a trapezoid and the definition of variables, we then know that

$$d = \frac{v_{max}(t_f + t_c)}{2}$$

(4.3)

and,

$$2t_a + t_c = t_f$$

(4.4)

and,

$$\Delta V = 2v_{max}$$

(4.5)

With the equations 4.1, 4.2, 4.3, 4.4, and 4.5 you can rearrange to find that:

$$\Delta V = \frac{F_t}{m_0}\left(t_f - \sqrt{t_f^2 - \frac{4dm_0}{F_t}}\right)$$

(4.6)

C. Isentropic Flow Analytical Modeling

```
%matplotlib inline
import numpy as np
import matplotlib.pyplot as plt
```

```
from google.colab import files
import io
import pandas as pd

uploaded = files.upload()
#upload csv of R236FA
```

```
#General Constants
g = 9.81   #m/s^2          #gravity
Po = 0.00001               #atmospheric pressure           #should be
vacuum
a = 15 #degrees          #half angle of nozzle



#R236fa Constants
R = 52.7 #J/(kg*K)         #specific gas constant
gam = 1.083                #specific heat ratio  #gamma
Cvl = 1000* 1.21 #J/(kg*K)   specific heat for liquid [BQ]
Cpg = 1000* 0.81
Cvg = Cpg/gam
# Temp (C) | Pressure (kPa) | Latent Heat (kJ/Kg) | Liquid Density
(kg/m^3) | Vapor density (kg/m^3)
# temp goes from -50 to 59 C. Row # = T + 50
pd236fa = pd.read_csv(io.BytesIO(uploaded['R236FA.csv']))
np236fa = pd.DataFrame.to_numpy(pd236fa)
#print(pd236fa)



#Correction factors: from [10]
Ccone= 0.983
Cmdot= 1.075
CIsp = 0.92
Ct = CIsp * Cmdot
```

```
#find Me
def MeFind(r, gam):
```

```
 MeList = np.arange(0.1, 10, 0.0005)
 dummy = 0
 mindiff = 10000

 for Me in MeList:
   dummy = ((gam +1)/2)**(-(gam+1)/(2*(gam-1))) * ((1+
0.5*(gam-1)*Me**2)**((gam+1)/(2*(gam-1)))/Me)
   diff = abs(r - dummy)
   if diff < mindiff:
     bestMe = Me
     bestdummy = dummy
     mindiff = diff
 '''
 print(bestMe)
 print(mindiff)
 print(bestdummy)
 '''

 return(bestMe)



#calculate Pe = exit pressure
def PeFind(Pc,gam,Me):
 exitpressure = Pc*(1+((gam-1)/2)*Me**2)**(-(gam)/(gam-1))

 return exitpressure



#calculate Te =  exit temperature
def TeFind(Tc,gam,Me):
 exittemp = Tc*(1+((gam-1)/2)*Me**2)**(-1)
  return exittemp
```

```
#calculate Ve =  exit velocity
def VeFind(Me,gam,Te):
 exitV = Me*np.sqrt(gam*R*Te)

 return exitV



#calculate mdot  = mass flow rate
def mdotFind(At, Pc, Tc, gam):
 mflowrate = ((At * Pc)/np.sqrt(Tc)) *
np.sqrt(gam/R)*((gam+1)/2)**(-(gam+1)/(2*(gam-1)))
  return mflowrate



# calculate thrust
def thrustFind(mdot, Ve, Pe, Po, Ae):
 F = mdot* Ve + (Pe-Po)*Ae
  return F



# calc Isp
def IspFind(thrust, mdot):
  isp = thrust/(mdot *g)
   return isp



#calc delta V
def dvFind(Isp, mtotal, mprop):
```

```
 dv = Isp*g*np.log(mtotal/(mtotal-mprop))
 return dv



#calc heat loss power. lhe = latent heat
def heatlossrate(lhe, mdot):
 hlr = lhe * mdot
 return hlr
```

```
#full calc

def fullcalc(r, Dt, Pc, Tc, mtotal, mprop, lhe):
  At = np.pi  * (Dt/2)**2  #meters^2   #throat area
 Ae = r * At
 rt = Dt/2   #radius of throat
 re = rt * np.sqrt(r)   #radius of exit



 Me = MeFind(r, gam)
 Pe = PeFind(Pc,gam,Me)
 Te = TeFind(Tc,gam,Me)
 Ve = Ccone*VeFind(Me,gam,Te)                          #corrected for
conical nozzle from ideal ideal
 mdot = mdotFind(At, Pc, Tc, gam)
 thrust = thrustFind(mdot, Ve, Pe, Po, Ae)
 Isp = IspFind(thrust, mdot)
 DeltaV = dvFind(Isp,mtotal, mprop)

 #add correction factors
 thrust = Ct*thrust
 Isp = CIsp*Isp
 mdot = Cmdot*mdot

 hlr = heatlossrate(lhe, mdot)
```

```
 '''
print("Me = "+str(Me))
print("Ve = "+str(Ve))
print("Mass flow rate = "+str(mdot))
print("Thrust = "+str(thrust))
print("Isp = "+str(Isp))
print("DeltaV = "+str(DeltaV))
'''


return thrust, mdot, hlr
```

```
def interp(x, x1, x2, y1, y2):
 m = (y2-y1)/(x2-x1)
 y = m*(x-x1) + y1
 return y
```

```
#tStart in deg C, burntime in sec, masses in kg
#assumed r236fa
def tempLoss (tStart, mprop, mtotal, burntime):
 # Initial Conditions:
 Tc = tStart # deg C
 Pc = 1000* np236fa[Tc+50, 1] #Pa
 lhe = 1000* np236fa[Tc+50, 2] # latent heat of vapoization at Tc, J/kg

 mpropStart = mprop
 mtotalStart = mtotal

 dt = 1 #sec

 tlist = np.arange(0,burntime+dt,dt)
 thrustarray = np.array(np.zeros(np.size(tlist)))
 temparray = np.array(np.zeros(np.size(tlist)))
```

```
 totalImp = 0

 #iterate through time steps
 # assume all energy to vaporize comes from gas propellant, so use Cvg for
gas
 # assuming all prop is liquid always (change this later?)
 for i in range(np.size(tlist)): #np.size(tlist):

   thrust, mdot, hlr = fullcalc(196, 0.0005, Pc, Tc + 273.15, mtotal,
mprop, lhe)

   # 4 nozzles, so 4x thrust and 4x mass flow
   #thrust = thrust * 4
   #mdot = mdot * 4

   thrustarray[i] = thrust
   temparray[i] = Tc

   Tc = Tc - (hlr * dt)/(mprop * Cvg)
   #print(Tc)
   Pc = 1000* interp(Tc, np.floor(Tc), np.ceil(Tc),
np236fa[int(np.floor(Tc)+50), 1], np236fa[int(np.ceil(Tc)+50), 1])
   lhe = 1000* interp(Tc, np.floor(Tc), np.ceil(Tc),
np236fa[int(np.floor(Tc)+50), 2], np236fa[int(np.ceil(Tc)+50), 2])
   mprop = mprop - mdot*dt
   mtotal = mtotal - mdot*dt

   totalImp = totalImp + thrust*dt

 #print(thrustarray)
 #print(temparray)

 deltaV =
totalImp/(mpropStart-mprop)*np.log(mtotalStart/(mtotalStart-mpropStart+mpr
op))
```

```
 print(mpropStart-mprop)
  fig, ax1 = plt.subplots()

 fig.set_size_inches(5, 5)

 plt.grid(True)

 ax2 = ax1.twinx()
 ax1.plot(tlist, thrustarray, 'black')
 ax2.plot(tlist, temparray, 'red')

 ax1.set_xlabel('Time [sec]')
 ax1.set_ylabel('Thrust [N]', color='black')
 ax2.set_ylabel('Temp [degC]', color='red')

 plt.title("Temperature and Thrust vs Time for R236FA")
 plt.show()
  return thrust
```

```
# assume worst case, everything is liquid (higher heat capacity)
# temps assumed to be in deg C, mprop is in kg, and Cvl in J/kg (for a
liquid)
def simpleHeatUpEnergy (tStart, tEnd, mprop, Cvl):
 energy = mprop*Cvl*(tEnd - tStart) #in J
 return energy

energy = 2*simpleHeatUpEnergy(-20, 30, 1.5, Cvl) #Joules
power = energy/(2*60*60) #Watts

print(power)
```

```
deltaV = tempLoss(30, 1.5, 12, 2*60*60)
print(deltaV)
```

D. Test Arduino Code

```
#include<Wire.h>
#include <SD.h>

int heaterRelay = 6;              // Tells Arduino the relay is connected to pin 6
int valveRelay = 5;              // Tells Arduino the relay is connected to pin 7
int RTDmosfet = 1;
int RTDPin = A6;

unsigned long time;
unsigned long valvetime;
float valveopentime = 5.0;   //valve open time in s
float heaterontime = 10.0;    //heater on time in s
bool valvesearch = false;
bool heatersearch = false;
unsigned long heatertime;

int M3200address = 0x28;   // 0x28, 0x36 or 0x46, depending on the sensor.
float maxPressure = 100.0;   // pressure in PSI for this sensor, 100, 250, 500, ...
10k.
double M3200pressure;
double M3200temperature = false;
bool requestPressure = false;
int M3200freq = 1000; //ms in between readings

double RTDvalue;
double RTDvoltage;
float RTDtemp;
bool requestTemp = false;
int RTDfreq = 250; //ms in between readings



char byteRead;
String data1 = "";
String datatime1;
int length1;
```

```
int datatimenum1;
bool unstable1;

int datatime2 = 0;

int datatime3 = 0;

// String data2 = "";
// String datatime2;
// int length2;
// int datatimenum2;
// bool unstable2;

const int chipSelect = SDCARD_SS_PIN;

// for computer interface/2nd scale (pins 2 for Tx and 5 for Rx)
// #define PIN_SERIAL3_RX       (45ul)               // Pin description number for
PIO_SERCOM on D5
// #define PIN_SERIAL3_TX       (44ul)               // Pin description number for
PIO_SERCOM on D2
// #define PAD_SERIAL3_TX       (UART_TX_PAD_2)      // SERCOM pad 2
// #define PAD_SERIAL3_RX       (SERCOM_RX_PAD_3)    // SERCOM pad 3

// // Instantiate the Serial3 class for computer
// Uart Serial3(&sercom2, PIN_SERIAL3_RX, PIN_SERIAL3_TX, PAD_SERIAL3_RX,
PAD_SERIAL3_TX);

void setup() {

 // put your setup code here, to run once:
 pinMode(heaterRelay, OUTPUT);      // Initialize the pin as an output
 pinMode(valveRelay, OUTPUT);      // Initialize the pin as an output
 pinMode(RTDmosfet, OUTPUT);      // Initialize the pin as an output
 pinMode(LED_BUILTIN, OUTPUT);

 Wire.begin();
```

```
// open the serial port:
Serial.begin(9600);
Serial1.begin(19200,SERIAL_7N2);
analogReadResolution(12); // make 12 bit precision

delay(3*1000); //wait 3 sec
SD.begin(chipSelect);
Serial.println("Initializing SD card...");
// see if the card is present and can be initialized:
if (!SD.begin(chipSelect)) {
  Serial.println("Card failed, or not present");
  // don't do anything more:
  while (1);
}
Serial.println("card initialized.");



//set up lines for scale
Serial1.println("T"); // tare
Serial1.println("0M"); // turn on gram mode
Serial1.println("0S"); // print unstable data
digitalWrite(LED_BUILTIN, HIGH);
delay(1*1000); // wait 1 seconds before actually turning on data output and starting
the code
digitalWrite(LED_BUILTIN, LOW);
Serial1.println("CA"); // turn on continuous autoprint every 1 sec

// Serial3.println("T"); // tare
// Serial3.println("0M"); // turn on gram mode
// Serial3.println("0S"); // print unstable data
// // digitalWrite(LED_BUILTIN, HIGH);
// // digitalWrite(LED_BUILTIN, LOW);
// Serial3.println("1A"); // turn on autoprint every 1 sec

Serial.println("Test3 All Set Up");
```

```
}

void loop() {
 time = millis();

 // get serial data from the first scale
 while(Serial1.available() > 0) {
   // read in character
   byteRead = Serial1.read();

   if (byteRead == '\n'){
     // Serial.print(millis());
     // Serial.print(',');

     length1 = data1.length();
     data1.remove(length1-9);
     //Serial.println(data1);
     datatimenum1 = millis();
     datatime1 = String(datatimenum1);   //not sure if this is necessary but it can't
hurt?



     //File dataFile = SD.open("Test1RoomtempMan1Nozzle1.csv", FILE_WRITE);
     File dataFile = SD.open("datalog1.csv", FILE_WRITE);

     if (dataFile) {
       dataFile.print(datatime1);
       dataFile.print(',');

       if (unstable1) {
         dataFile.print('1');
         dataFile.print(',');
         dataFile.print(data1);
         Serial.println(data1);
       } else {
         dataFile.print('0');
         dataFile.print(',');
```

```
        dataFile.print(data1);
        Serial.println(data1);

      }
      dataFile.close();
      unstable1 = false;
    }
    // if the file isn't open, pop up an error:
    else {
      Serial.println("error opening SD Card");
    }

    data1 = "";

    break;
  } else if (byteRead == ' ') {
    // do nothing so we ignore the spaces
  } else if (byteRead == 'g') {
    // do nothing so we ignore units since we know its g
  } else if (byteRead == '?') {
    unstable1 = true;
  } else {
    data1 += byteRead;
  }
}



//Pressure sensor (and bonus temp data!)
// from
https://forum.arduino.cc/t/interfacing-with-a-m3200-series-i2c-pressure-sensor/670139/
4
if (requestPressure || (time >= datatime2 + M3200freq)) {

  int n = Wire.requestFrom(M3200address, 4);    // request 4 bytes
//stop argument?
```

```
  if(n == 4) {
    digitalWrite(LED_BUILTIN, HIGH);

    uint16_t rawP;     // pressure data from sensor
    uint16_t rawT;     // temperature data from sensor


    rawP = (uint16_t) Wire.read();    // upper 8 bits
    rawP <<= 8;
    rawP |= (uint16_t) Wire.read();    // lower 8 bits
    rawT = (uint16_t)  Wire.read();    // upper 8 bits
    rawT <<= 8;
    rawT |= (uint16_t) Wire.read();   // lower 8 bits

    datatime2 = millis();   //not sure if this is necessary but it can't hurt?

    byte status = rawP >> 14;   // The status is 0, 1, 2 or 3
    rawP &= 0x3FFF;   // keep 14 bits, remove status bits

    rawT >>= 5;     // the lowest 5 bits are not used


    // Serial.print("rawP = ");
    // Serial.println(rawP);
    // Serial.print("rawT = ");
    // Serial.println(rawT);

    // The math could be done with integers,  but I choose float for now
    M3200pressure = ((rawP - 1000.0) / (15000.0 - 1000.0)) * maxPressure;
    M3200temperature = ((rawT*200.0)/2048.0) - 50.0;

    // Serial.print("Status = ");
    // Serial.print(status);
    Serial.print(", Pressure = ");
    Serial.print(M3200pressure);
    Serial.print(" psi, Temperature = ");
    Serial.print(M3200temperature);
```

```
    Serial.print(" *C");
    Serial.println();

    // write data to SD card
    //get timestamp too

    File dataFile = SD.open("datalog2.csv", FILE_WRITE);

    if (dataFile) {
      dataFile.print(String(datatime2));
      dataFile.print(',');
      dataFile.print(M3200pressure);
      dataFile.print(',');
      dataFile.println(M3200temperature);
      dataFile.close();
    }
    // if the file isn't open, pop up an error:
    else {
      Serial.println("error opening SD Card");
    }

  } else {
    Serial.println("Pressure sensor not found");
  }

  digitalWrite(LED_BUILTIN, LOW);
  requestPressure = false;

}



//RTD
// if (requestTemp || (time >= datatime3 + RTDfreq)) {
//   digitalWrite(LED_BUILTIN, HIGH);
//   digitalWrite(RTDmosfet, HIGH);   // Turn the relay on (HIGH is the voltage level
= 1)
```

```
//   Serial.println("Turning on RTD");

//   delay(5); // wait 5 ms before actually turning on data output and starting the
code
//   RTDvalue = analogRead(RTDPin);
//   datatime3 = millis();
//   RTDvoltage = RTDvalue * 3.3/4095.0;
//   //Serial.print("Meaured voltage: ");
//   Serial.println(RTDvoltage,5);
//   RTDtemp = 117.509517*pow(RTDvoltage,3) - 379.098639*pow(RTDvoltage,2) +
601.475415*RTDvoltage - 488.204210; // this is based on excatly 100 ohm assumption
//   Serial.print("Meaured temp: ");
//   Serial.println(RTDtemp,5);
//   digitalWrite(RTDmosfet, LOW);
//   digitalWrite(LED_BUILTIN, LOW);

//   File dataFile = SD.open("datalog3.csv", FILE_WRITE);

//     if (dataFile) {
//       dataFile.print(String(datatime3));
//       dataFile.print(',');
//       dataFile.println(RTDtemp);

//       dataFile.close();
//     }
//     // if the file isn't open, pop up an error:
//     else {
//       Serial.println("error opening SD Card");
//     }

//   requestTemp = false;
// }




//valve
if (valvesearch == true){         //if currently waiting to turn off valve
```

```
   if (time >= valvetime + 1000*valveopentime){
     digitalWrite(LED_BUILTIN, LOW);
     digitalWrite(valveRelay, LOW);    // Turn the relay off by making the voltage LOW
= 0
     valvesearch = false;
     Serial.println("Closing valve after waiting");

     File dataFile = SD.open("datalog1.csv", FILE_WRITE);

     if (dataFile) {
       dataFile.println(' ');
       dataFile.println("valve closed");
       dataFile.close();
     }
     // if the file isn't open, pop up an error:
     else {
       Serial.println("error opening SD Card");
     }


   }
 }


 // //heater
 // if (heatersearch == true){         //if currently waiting to turn off valve
 //   if (time >= heatertime + 1000*heaterontime){
 //     digitalWrite(LED_BUILTIN, LOW);
 //     digitalWrite(heaterRelay, LOW);    // Turn the relay off by making the voltage
LOW = 0
 //     heatersearch = false;
 //     Serial.println("Turning off heater");
 //   }
 // }


 // read in serial commands from user
```

```
 if (Serial.available() > 0) {


   // read incoming serial data:
   char command = Serial.read();


   //HEATER RELAY
   if (command == 'h') {
     digitalWrite(LED_BUILTIN, HIGH);
     digitalWrite(heaterRelay, HIGH);   // Turn the relay on (HIGH is the voltage
level = 1)
     heatersearch = true;
     heatertime = millis();
     Serial.print("Turning on heater for ");
     Serial.print(heaterontime);
     Serial.println(" seconds");
   }
   if (command == 'o') {         //open the valve
     digitalWrite(LED_BUILTIN, HIGH);
     digitalWrite(valveRelay, HIGH);   // Turn the relay on (HIGH is the voltage level
= 1)
     Serial.println("Opening valve");
   }
    if (command == 'c'){        //close the valve
     digitalWrite(LED_BUILTIN, LOW);
     digitalWrite(valveRelay, LOW);    // Turn the relay off by making the voltage LOW
= 0
     Serial.println("Closing valve");
   }
   if (command == 'v') {
     Serial1.println("T"); // tare


     File dataFile = SD.open("datalog1.csv", FILE_WRITE);


     if (dataFile) {


       dataFile.println(' ');
       dataFile.println("Trial start");
```

```
      dataFile.close();
    }
    // if the file isn't open, pop up an error:
    else {
      Serial.println("error opening SD Card");
    }

    delay(4000); // wait 4 sec to tare

    digitalWrite(LED_BUILTIN, HIGH);
    digitalWrite(valveRelay, HIGH);   // Turn the relay on (HIGH is the voltage level
= 1)
    Serial.print("Opening valve for ");
    Serial.print(valveopentime);
    Serial.println(" seconds");
    valvetime = millis();
    valvesearch = true;
  }
    if (command == 't') {
    Serial.println("checking RTD");

    requestTemp = true;
  }
    if (command == 'p') {
    Serial.println("checking m3200");
    requestPressure = true;
  }
 }
}

// void SERCOM2_Handler()    // Interrupt handler for SERCOM2
// {
//   Serial3.IrqHandler();
// }
```

E. Budget

BOM (Bill of Materials)	Unit Cost $	Unit	# of Units	Total $
1/8" solenoid valve AC	28.95	1	1	$28.95
R134a Canister	9.48	12oz	6	$56.88
R134a Rechrge	14.99	1	1	$14.99
Flexible tubing	7.5	25ft	1	$7.50
1/4 SAE to 1/8 NPT	1.41	1	2	$2.82
1/8" Universal Push connection	$2.52	1	10	$25.20
5/16" ID Oring	4.69	100 pack	1	$4.69
3/8" ID Oring	4.85	100 pack	1	$4.85
1/2" ID Oring	4.99	100 pack	1	$4.99
13/16" ID oring	13.39	100 pack	1	$13.39
3ft .5"x.75" Stainless Steel Stock	35.39	3ft	1	$35.39
1ft 1"x1" Aluminum Stock	12.05	1ft	1	$12.05
3ft .5"x.75" Aluinum Sstock	13.2	3ft	1	$13.20
13/16" ID Oring	3.1	100 pack	1	$3.10
1/4 npt Pressure Sensor	86.21	1	1	$86.21
1/8 npt Heater	102.71	1	1	$102.71
1/2 Temp sensor	68.4	1	1	$68.40
3D printed Test Unit	671	1	1	$671.00
3D printed nozzles	20	4	1	$20.00
3D printed nozzles round 2	16	4	1	$16.00
3D Printed Test Tubing	10	1	1	$10.00
1/8 Tube Cap	2.14	1	10	$21.40
1/8 Push connect tee	7.28	1	2	$14.56
1/4 male SAE to 1/4 male npt	1.64	1	2	$3.28
1/4 male to female tee	24	1	1	$24.00
1/4 male to female valve	13.09	1	3	$39.27

RS232 board for arduino	6.5	1	2	$13.00
1/4 NPT 100psi Pressure relief valve	16.73	1	1	$16.73
DC solenoid	28.95	1	1	$28.95
Male to Male DB9	8.28	1	2	$16.56
4 battery holder	1.49	1	2	$2.98
3 battery holder	0.86	1	2	$1.72
charger	11.99	1	1	$11.99
Nozzles for final test print	10	8	1	$10.00
1/4" drill bit	17.35	1	2	$34.70
RS232 Breakout board	17.5	1	2	$35.00
Scale	318.54	1	2	$637.08
RS232 Connector	186.69	1	2	$373.38

Please do your best to fill in the following details on your budget	**Total $**	**Exact or estimated?**
Total Development cost: everything that was spent on your project including prototypes, transportation to research locations, renting of equipment, orders from a lab you worked at, your own money etc...?etc...	$2,486.92	Estimated
What is the minimum cost to make one prototype of your project ($0 is an option)?	$1,750.21	Estimated
Total cost of items purchased through the *Active Learning Labs (ALL), if any*	$1,093.16	Estimated
Total cost covered by the *Harvard Research*Lab(s) you are affiliated with, if any	0	Exact

Total cost of items purchase personally, if any	$16.56	Estimated
Total cost covered by a *non-Harvard lab*and/or company, if any	0	Exact

F. Non-Technical Considerations

With any engineering project, a team must not only ask themselves whether they *could* complete a project, but whether they *should*. To answer this question, you must consider the ethical ramifications of your project, such as public health and safety, environmental factors, economic factors, and more.

As was discussed earlier in the paper, there are many different types of propulsion possibilities, ranging from chemical combustion to compressed gas. While considering the technical and physical properties of each of these options will be important, we must consider the health, safety, and environmental implications associated with handling and storing different types of propellants. For example, hypergolic propellants are extremely well suited for satellite applications as they combust upon contact and do not require the use of an ignition or spark. However, they are extraordinarily corrosive, toxic, and carcinogenic, making them extremely hazardous to work with [AL]. This also makes them harmful to the environment if an accidental discharge were to occur. Compressed gasses, while not toxic or corrosive like hypergolics, store a lot of energy under compression, making accidental leaks or explosions extremely dangerous to those working with them. These are just a few examples of how we must take into account the health and safety of those around us when approaching the design and test of our project.

While the goals of this project are ideally positive, being those of scientific discovery, we must also be aware of the economic reality we face. The money funding this project comes from NASA, and ultimately from Congressional budgeting. Rather than being budgeted for education, or welfare, or any other governmental programs, this money was spent here. Knowing this, it is our responsibility to minimize total cost, and do our best to maximize chances of success for the mission.

Finally, we must look beyond our planet and consider our impact on the solar system. If we were to discover life on a planet besides Earth, such a finding would be groundbreaking to our understanding of the universe and our place within it. Given the excitement it would cause, we would like to be as certain as we can that this truly is alien life. However, this discovery would be ruined if we had simply accidentally sent some Earthly life to that planet on a prior spacecraft. Additionally, if there actually is life on another planet, introducing Earthly biology could prove disastrous. As we have seen many times before, invasive species can quickly take over and dominate their new environment, killing any competition. To avoid any such scenarios, NASA typically assembles their spacecraft within a cleanroom, devoid of any contaminating organisms. However, our CubeSat will not be prepared in a cleanroom, so we must take care to

minimize the chance that it collides with any other planets. Specifically, we have budgeted extra propellant just to ensure we can escape Mars' gravitational pull and avoid the planet.

G. Product Data Sheets

McMASTER-CARR®

Miniature On/Off Valve

for Use with Water, T-Handle, 10-32 UNF Female

$101.25 Each
4059K36

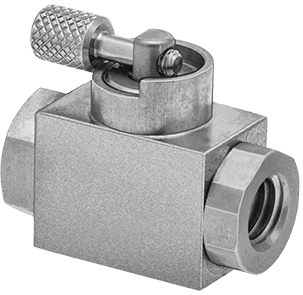

Valve Function	On/Off
Valve Type	Ball
Activation	Manual
Valve Operation	Handle
Handle Style	Lever
Handle Type	Standard
Fitting Type	Connector
For Use With	Water, Air, Argon, Helium, Krypton, Neon, Xenon
Connection Type	Pipe
Connection Style	Threaded
Thread Size	10-32
Gender	Female
Thread Type	UNF
Flow Coefficient (Cv)	0.1
Maximum Pressure	250 psi @ 150° F
Temperature Range	-60° to 300° F
Vacuum Rating	25 in. of Hg
Body Material	303 Stainless Steel
Ball Material	316 Stainless Steel
Seal Material	EPDM Rubber
Seat Material	EPDM Rubber
Port Type	Standard
Shape	Straight
End-to-End Length	11/16"
Overall	
Height	9/16"
Length	11/16"
Chemical Resistance	
Excellent	Acetone, Air, Ammonia, Argon, Carbon Dioxide, Citric Acid (100% Concentration), Citric Acid (25% Concentration), Citric Acid (50% Concentration), Ethanol, Ethylene Glycol, Helium, Hydrochloric Acid (25% Concentration), Hydrochloric Acid (37% Concentration), Isopropyl Alcohol, Krypton, Methanol, Methyl Ethyl Ketone, Neon, Nitrogen, Oxygen, Phosphoric Acid (100% Concentration), Phosphoric Acid (25% Concentration), Phosphoric Acid (50% Concentration), Salt Water, Soap Solutions, Sodium Hydroxide (100% Concentration), Sodium Hydroxide (25% Concentration), Sodium Hydroxide (50% Concentration), Sodium Hydroxide (75% Concentration), Sodium Hypochlorite (100% Concentration), Sodium Hypochlorite (25% Concentration), Sodium Hypochlorite (50% Concentration), Water, Xenon
Moderate	Beverage, Deionized Water, Drinking Water, Food

Poor	Butane, Chlorine, Diesel Fuel, Fuel Oil, Gasoline, Hydrochloric Acid (100% Concentration), Kerosene, Mineral Spirits, Natural Gas, Nitric Acid (100% Concentration), Nitric Acid (25% Concentration), Nitric Acid (50% Concentration), Oil, Propane, Sulfuric Acid, Toluene, Xylene
Warning Message	Chemical compatibility must be determined by the customer based on the conditions in which the product is being used, including the presence of other chemicals, temperature, and consistency.
RoHS	RoHS 3 (2015/863/EU) Compliant
REACH	REACH (EC 1907/2006) (01/17/2023, 233 SVHC) Compliant
DFARS	Specialty Metals COTS-Exempt
Country of Origin	United States
USMCA Qualifying	No
Schedule B	848180.3070
ECCN	2B999

With 10-32 UNF threads and a body less than 3/4" long, these valves are often used to control flow in miniature pipelines. They have a 303 stainless steel body for good corrosion resistance. All are standard port, so they slightly restrict flow.

Flow coefficient (Cv) is the amount of water (in gallons per minute) at 60° F that will flow through a fully open valve with a difference of 1 psi between the inlet and the outlet.

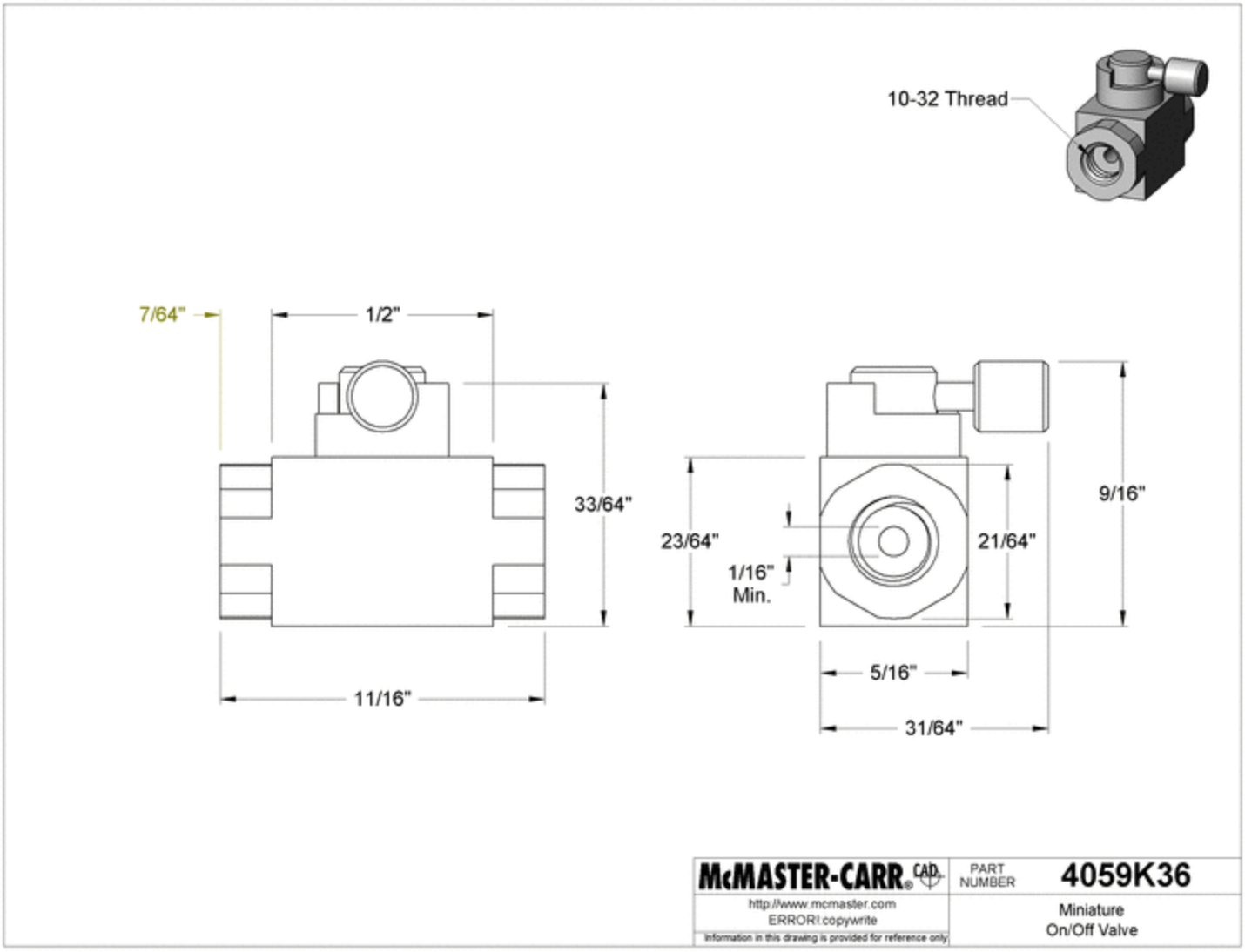

The information in this 3-D model is provided for reference only.

M3200

Pressure Transducer

SPECIFICATIONS

- **Analog Output**
- **14-Bit Digital Pressure with 11-Bit Temperature Output**
- **CE Compliant**
- **Weatherproof**
- **±1.5 %Span Accuracy**

The M3200 pressure transducer from the Microfused line of TE is suitable for measurement of liquid or gas pressure, even for difficult media such as contaminated water, steam, and mildly corrosive fluids.

The transducer pressure cavity is machined from a solid piece of 17-4PH stainless steel. The standard version includes a 1/4 NPT pipe thread allowing a leak-proof, all metal sealed system. With excellent durability, there are no O-rings, welds or organics exposed to the pressure media.

TE's proprietary Microfused technology, derived from demanding aerospace applications, employs micromachined silicon piezoresistive strain gages fused with high temperature glass to a stainless-steel diaphragm. This approach achieves media compatibility simply and elegantly while providing an exceptionally stable sensor without the PN junctions of conventional micromachined sensors.

This product is geared towards industrial and commercial OEMs for small to high volume applications. Standard configurations are suitable for many applications. Please contact factory for your customization needs.

FEATURES

- One Piece Stainless Steel Construction
- Digital Pressure and Temperature Output or Analog mV/Amplified Output
- Compact
- 17-4PH Stainless Steel
- Customizable

APPLICATIONS

- Pumps and Compressors
- Hydraulic/Pneumatic Systems
- Automotive Test Systems
- Energy and Water Management
- Medical Gas Pressure
- Leak Detection
- Remote Measuring Systems
- General Pressure Measurements

STANDARD RANGES

Range (psi)	Range (bar)	Gage/Compound
0 to 100	0 to 007	•
0 to 250	0 to 017	•
0 to 500	0 to 035	•
0 to 01k	0 to 070	•
0 to 2k5	0 to 170	•
0 to 05k	0 to 350	•

PERFORMANCE SPECIFICATIONS (ANALOG)

Unless otherwise specified: All parameters measured at 25°C

PARAMETERS	MIN	TYP	MAX	UNITS	NOTES
Accuracy	-0.25		0.25	% F.S BFSL	
Pressure Cycles	1.0E+6			0~F.S. Cycles	
Proof Pressure	2X			Rated	
Burst Pressure	5X			Rated	≤20kpsi
Isolation, Body to Any Lead	50			MΩ	@ 250V_{DC}
Load Resistance ($R_>$)	>100			kΩ	Voltage Output
Load Resistance	<(Supply Voltage-9V)/0.02A			Ω	Current Output
Current Consumption			5	mA	Voltage Output
Dielectric Strength			2	mA	@500 V_{AC} 1 min
Long Term Stability (1 year)	-0.25		0.25	%Span	
Total Error Band (for non-mv output)	-1.5		1.5	%F.S.	Over comp. temp
Thermal Zero Shift (for mv output)	-3		3	%F.S.	
Thermal Span Shift (for mv output)	-2		2	%F.S.	
Zero Offset & Span Tolerance (for mv output)	-2		2	%F.S.	@ 25°C
Compensated Temperature	0		55	°C	mV Output
	-20		85	°C	Non-mV Output
Operating Temperature	-40		125	°C	Except Cable 105°C max
Storage Temperature	-40		125	°C	Except Cable 105°C max
Weather proof Rating	IP67 for cable type, IP66 for Packard type, IP65 for Form C type				3
Rise Time (10% - 90%)	<2 ms (mV Output); <3ms (mA Output)				
Wetted Material	17-4PH Stainless Steel				
Shock	50g, 11 msec Half Sine Shock per MIL-STD-202G, Method 213B, Condition A				
Vibration	±20g, MIL-STD-810C, Procedure 514.2-2, Curve L				

Compliances[6]

EN 55022 Emissions Class A & B
IEC 61000-4-2 Electrostatic discharge immunity (4kv contact / 8kv air discharge)
IEC 61000-4-3 Radiated, Radio-Frequency Electromagnetic field immunity (10 V/m; 80M-1GHz; 3 V/m, 1.4 – 2.0GHz; 1 V/m, 2.0 – 2.7GHz)
IEC 61000-4-4 Electrical Fast Transient/Burst Immunity (±1kV)
IEC 61000-4-5 Surge (line to line: ±1.0kV/42Ω; Line to case: ±1.0kV/42Ω
IEC 61000-4-6 Immunity to conducted disturbances, induced by radio-frequency fields (150k-80MHz, $3V_{RMS}$ for current output model, $10V_{RMS}$ for voltage model)

PERFORMANCE SPECIFICATIONS (DIGITAL)

Unless otherwise specified: All parameters measured at 25°C

PARAMETERS	MIN	TYP	MAX	UNITS	NOTES
Output at Zero Pressure	750	1000	1250	Count	
Output at FS Pressure	14720	15000	15250	Count	
Current Consumption			3.5	mA	
Current Consumption (sleep mode)			5	µA	
Supply Voltage	2.7		5.0	V	
Proof Pressure	2X			Rated	
Burst Pressure	5X			Rated	No More than 20kpsi
Isolation, Body to Any Lead	50			MΩ	@ 250V_{DC}
Pressure Cycles	1.00E+6			0~F.S. Cycles	
Pressure Accuracy (RSS combined Non-Linearity, Hysteresis & Repeatability)	-0.25		0.25	%F.S. BFSL	@ 25°C
Temperature Accuracy	-3		3	°C	4
Long Term Stability (1 year)	-0.25		0.25	%F.S.	
Total Error Band	-1.5		1.5	%F.S.	Over comp Temp.
Compensated Temperature	0		55	°C	
Compensated Temperature Output	512		1075	Count	For reference
Operating Temperature	-20		+85	°C	
Storage Temperature	-40		+85	°C	
Response time			3	ms @ 4MHz	Non-sleep mode, 5
Response time			8.4	ms @ 4MHz	Sleep mode, 5
Wetted Material (except elastomer seal)	17-4PH Stainless Steel				
Shock	50g, 11 msec Half Sine Shock per MIL-STD-202G, Method 213B, Condition A				
Weather proof Rating[3]	IP67				
Vibration	±20g, MIL-STD-810C, Procedure 514.2-2, Curve L				

Compliance[6]

EN 55011 Emissions Class A & B
IEC 61000-4-2 Electrostatic Discharge Immunity (4kV contact/8kV air discharge)
IEC 61000-4-3 Radiated Radio-Frequency Electromagnetic Field Immunity (1V/m, 80M-1GHz; 3 V/m, 1.4 – 2.0GHz; 1V/m, 2.0-2.7GHz)
IEC 61000-4-4 Electrical Fast Transient/Burst Immunity (±1kV)
IEC 61000-4-6 immunity to conducted disturbances, induced by radio-frequency fields (150k-80MHz, 3V_{RMS})

Notes

1. mV Output is only available for cable connections
2. The mV output is only for the following range: 100P(7B), 250P(17B), 500P(35B), 1000P(70B), 2500P(170B), 5000P(350B)
3. Weather-proof ratings are met when the mating connectors are properly installed and cable termination to dry and clean area.
4. Reflect pressure port diaphragm temperature over the compensated temperature range.
5. Response time is from power on to reading measurement data.
6. For all CE compliance test, max allowed output deviation is ±1.5%F.S.
7. All Configurations are built with Voltage Reverse and output Short-Circuit Protections.
8. For communication and interfacing, refer to document ‘Interfacing to MEAS Digital Pressure Modules’ online

DIMENSIONS

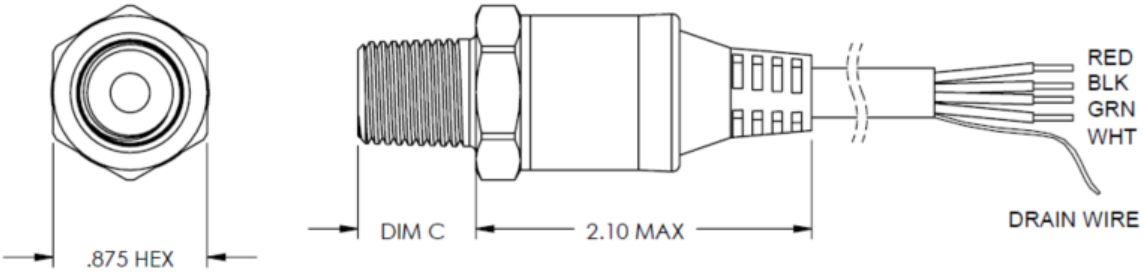

FORM C

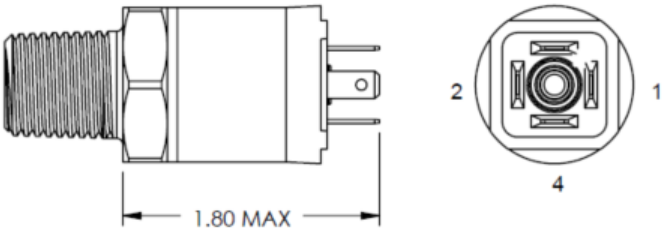

Digital Output Connection (Cable Type)

Mode	RED	BLACK	WHITE	GREEN
I^2C	+SUPPLY	-SUPPLY	SCL	SDA

Current Output Wiring

Connection	+Supply	-Supply	NC. Pins	P_{REF} Vent
Packard	A	B	C	Hole through connector
Form C	1	2	3, 4	Thread through connector
Cable	Red	Black	-	In Cable

PACKARD CONNECTOR

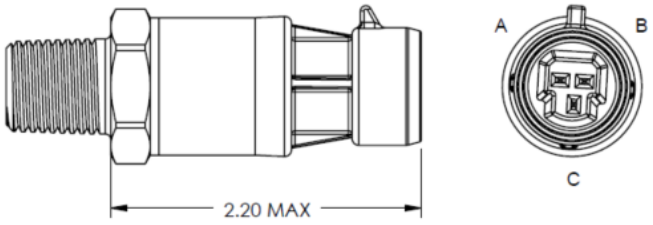

Voltage Output Wiring							
Connection		**+Supply**	**-Supply**	**+Output**	**-Output**	**NC. Pins***	**P_{REF} Vent**
Packard		A	B	C	-	-	Hole through Connector
Form C		1	2	3	-	4	Thread through Connector
Cable	mV Output	Red	Black	White	Green	-	In Cable
	V Output	Red	Black	White	Not connected	-	In Cable

Notes:

*NC. Pins are reserved for factory use only. **DO NOT CONNECT.**
**For cable connections, drain wire is internally terminated to pressure port.
Transmitter of gage pressure type requires vent to atmosphere on the pressure reference side.

- Accomplished via cable from transmitter or through customer mating connector/cable assembly which has internal vent path (end of cable should be terminated to clean & dry area)

Weather-proof Ratings are met when Mating Connectors are installed properly and cable termination is to try and clean area.

PRESSURE PORTS

Code	Pressure Port	Dim C	Recommended Torque [Nm]
2	1/4-19 BSPP	0.47 [11.94]	30-35
4	7/16-20 UNF Male SAE J1926-2 Straight Thread O-Ring BUNA-N 90SH ID8.92xW1.83mm	0.45 [11.43]	18-20
5	1/4-18 NPT	0.65 [16.51]	2-3 TFFT*
6	1/8-27 NPT	0.53 [13.46]	2-3 TFFT*
E	1/4-19 BSPT	0.50 [12.70]	2-3 TFFT*
P	7/16-20 UNF Female SAE J513 Straight Thread w/ Integral Valve Depressor	0.43 [10.92]	15-16

*Turn From Finger Tight

PRESSURE OUTPUT

% Output	Digital Counts (Decimal)	Digital Counts (Hex)
0%	1000	0x3E8
5%	1700	0X6A4
10%	2400	0X960
50%	8000	0X1F40
90%	13600	0X3520
95%	14300	0X37DC
100%	15000	0X3A98

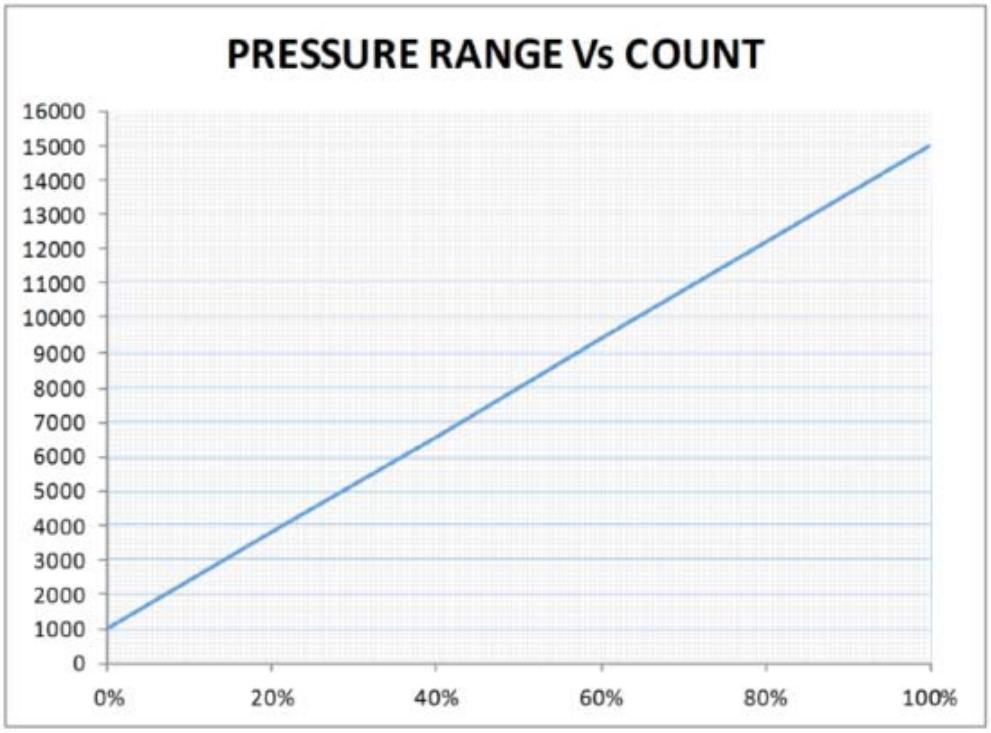

$$\text{OUTPUT (DECIMAL COUNTS)} = \frac{15000-1000}{\text{Pmax-Pmin}} X \ (\text{Papplied-Pmin}) + 1000$$

TEMPERATURE OUTPUT

Output °C	Digital Counts (Decimal)	Digital counts
0	512	0x200
10	614	0x266
25	767	0x2FF
40	921	0x399
55	1075	0x433

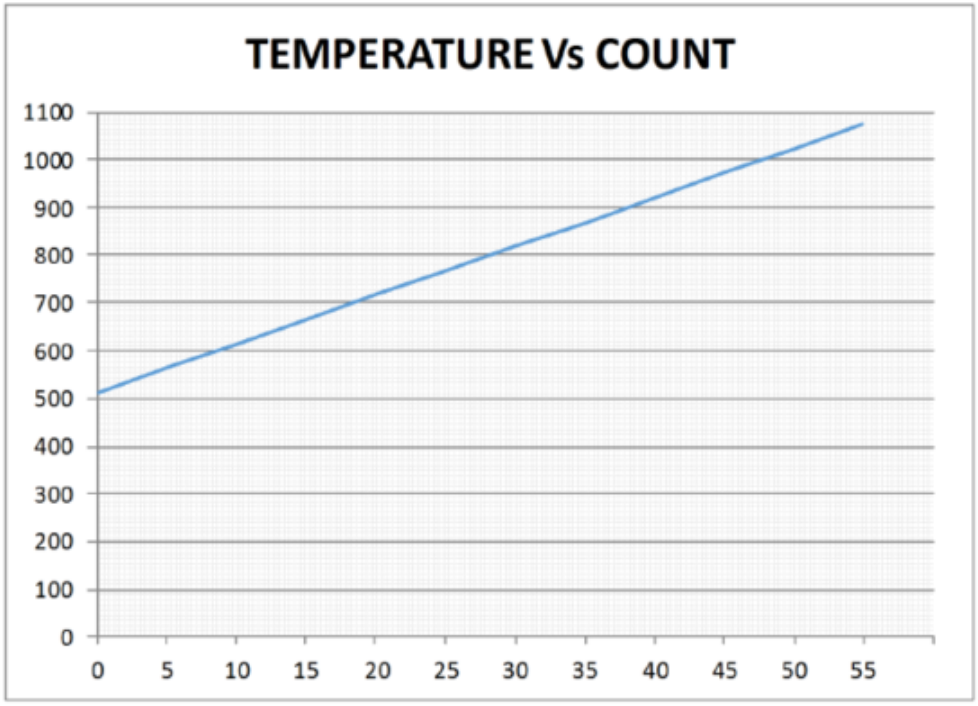

$$\text{OUTPUT (DECIMAL COUNTS)} = \frac{(\text{OUTPUT}^{\circ}\text{C}+50^{\circ}\text{C})\text{X}2048}{150^{\circ}\text{C}-(-50^{\circ}\text{C})}$$

OUTPUT (ANALOG)

Code	Output	Supply	Ratiometricity	Red	Black	Green	White
2	0 – 100mV	5V	Yes	+Supply	-Supply	-Output	+Output
3	0.5 – 4.5V	5 ± 0.25V	Yes	+Supply	Common	Not connected	+Output
5	4 – 20mA	9 – 30V	No	+Supply	-Supply	Not connected	Not connected
6	0 – 5 V	8 – 30V	No	+Supply	-Supply	Not connected	+Output
7	0 – 10 V	12 – 30 V	No	+Supply	-Supply	Not connected	+Output

OUTPUT (DIGITAL)

Code	Output	Supply	Red	Black	Green	White
J	I^2C	2.7 – 5.0V	+Supply	-Supply	SDA	SCL

ORDERING INFORMATION

For Analog Output:

M32 3 4 – 00000 4 – 250P G

Output	
Code	Output
2	0-100mV*
3	0.5-4.5V
5	4-20mA
6	0-5V
7	0-10V

Connection	
4	Packard Connector
6	Form C with Mating Connector
B	Form C without Mating Connector
L	Cable 0.5m
M	Cable 1m
N	Cable 2m
P	Cable 5m

Pressure Port	
Code	Description
2	1/4-19 BSPP
4	7/16-20 UNF Male SAE J1926-2 Straight Thread O-ring BUNA-N 90SH ID8.92xW1.83mm
5	1/4-18 NPT
6	1/8-27 NPT
E	1/4-19 BSPT
P	7/16-20 UNF Female SAE J513 Straight Thread with Integral Valve Depressor

Pressure Type	
G	Gage
C	Compound

Compound pressure range is -14.7 to XXX psig or -1 to XXX barg.
i.e. 200PC: -14.7 to 200psig, 020BC: -1 to 20 barg

Pressure Range	
psi STD	**bar STD**
100P	**007B**
250P	**017B**
500P	**035B**
01KP	**070B**
2K5P	**170B**
05KP	**350B**

Non-mV Output Pressure Ranges between 100-5000psi (7-350bar) are all available.
Change Pressure Number Accordingly

*Available for Cable Connections only, intermediate Pressure Ranges Not Available
For Digital Output, see “For Digital Output” Ordering Information
All Configurations are built with Voltage Reverse and Output Short-Circuit Protections.
Click here for Torque Recommendation

For Digital Output:

M32 J L – 000 0 0 4 – 250P G

Output	
Code	Output
J	I^2C

Connection	
L	Cable 0.5m
M	Cable 1m

Sleep Mode (Digital ONLY)	
0	Non-Sleep Mode
1	Sleep Mode

Digital Address (Digital ONLY)	
0	0X28H
1	0X36H
2	0X46H
3	0X48H
4	0X51H

Pressure Port	
Code	Description
2	1/4-19 BSPP
4	7/16-20 UNF Male SAE J1926-2 Straight Thread O-ring BUNA-N 90SH ID8.92xW1.83mm
5	1/4-18 NPT
6	1/8-27 NPT
E	1/4-19 BSPT
P	7/16-20 UNF Female SAE J513 Straight Thread with Integral Valve Depressor

Pressure Type	
G	Gage
C	Compound

Compound pressure range is -14.7 to XXX psig or -1 to XXX barg.
Ex. 200PC: -14.7 to 200psig, 020BC: -1 to 20 barg

Pressure Range	
psi STD	**bar STD**
100P	**007B**
250P	**017B**
500P	**035B**
01KP	**070B**
2K5P	**170B**
05KP	**350B**

All Configurations are built with Voltage Reverse and Output Short-Circuit Protections.
Click here for Torque Recommendation

NORTH AMERICA
Measurement Specialties, Inc.,
a TE Connectivity Company
Phone: +1 800-522-6752
Email: customercare.frmt@te.com

EUROPE
Measurement Specialties (Europe), Ltd.,
a TE Connectivity Company
Phone: +31 73 624 6999
Email: customercare.lcsb@te.com

ASIA
Measurement Specialties (China), Ltd.,
a TE Connectivity Company
Phone: +86 0400-820-6015
Email: customercare.shzn@te.com

TE.com/sensorsolutions

McMASTER-CARR®

RTD Probe for Liquids and Gases

Threaded, 304 Stainless Steel with 3 Wires, 3" Probe Length

$68.40 Each
3866K19

RTD Type	100 ohms
Temperature Range	-55° to 400° F
Probe	
Length	3"
Diameter	1/4"
Accuracy	±0.12%
Response Time	10 sec.
For Use With	Liquids, Gases
Connection Type	Wire Leads
Mount Type	Threaded
Probe Connection	
Pipe Size	1/2
Thread Type	NPT
Gender	Male
Maximum Pressure	Not Rated
Probe Material	304 Stainless Steel
Wire	
Lead Length	3"
Gauge	24
Number of Wires	3
Wire Color	Red/White
RoHS	RoHS 3 (2015/863/EU) Compliant
REACH	REACH (EC 1907/2006) (01/17/2022, 223 SVHC) Compliant
DFARS	Specialty Metals COTS-Exempt
Country of Origin	United States
USMCA Qualifying	No
Schedule B	854430.0000
ECCN	EAR99

Often used to measure temperature in water lines and low-pressure steam lines, these RTDs have an NPT male probe connection for easy installation in pipes, tanks, and thermowells.

McMASTER-CARR®

Compact Screw-Plug Immersion Heater for Water

316 Stainless Steel Heating Element, 120V AC, 55W

$102.71 Each
4668T51

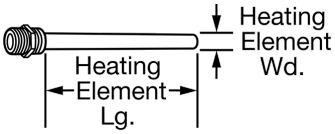

Heater Type	Immersion
Wattage	55 W
Watt Density	47 W/sq. in.
Voltage	120V AC
Electrical Phase	Single
Current	0.5 A
Heating Element	
Length	1 5/8"
Width	1/4"
Material	316 Stainless Steel
Unheated Length	1/4"
Heated Length	1 3/8"
Number of Heating Elements	1
Minimum Heating Element Coverage	Fully Covered
Temperature Control Type	None
Pipe Connection Type	Threaded
Pipe Size	1/8
Thread Type	NPT
Gender	Male
Power Source	Electric
Electrical Connection Type	Hardwire
Wire Connection Type	Wire Leads
Wire Lead Length	6"
Wire Lead OD	0.05"
Wire Lead Gauge	24
Body	
Diameter	1/4"
Length	7/8"
Material	316 Stainless Steel
Overall Length	2 1/2"
Hex Shoulder	
Length	1/8"
Width	7/16"
Maximum Pressure	100 psi
Conduit	
Connection Type	Threaded
Connection Thread Type	NPT

Mount Type	Screw Plug
Mounting Orientation	Horizontal, Vertical
For Use With	Water, Salt Water
Specifications Met	UL Recognized Component, CSA Certified
RoHS	RoHS 3 (2015/863/EU) Compliant
REACH	REACH (EC 1907/2006) (07/08/2021, 219 SVHC) Compliant
DFARS	Specialty Metals COTS-Exempt
Country of Origin	United States
USMCA Qualifying	Yes
Schedule B	851610.0080
ECCN	EAR99

Efficiently heat liquid in small containers. These immersion heaters install into threaded container openings or pipe couplings. All require a temperature switch or controller (sold separately) to regulate heat output. The heating element is 316 stainless steel for excellent corrosion resistance.

Note: Fully immerse the heating element in liquid to prevent heater failure.

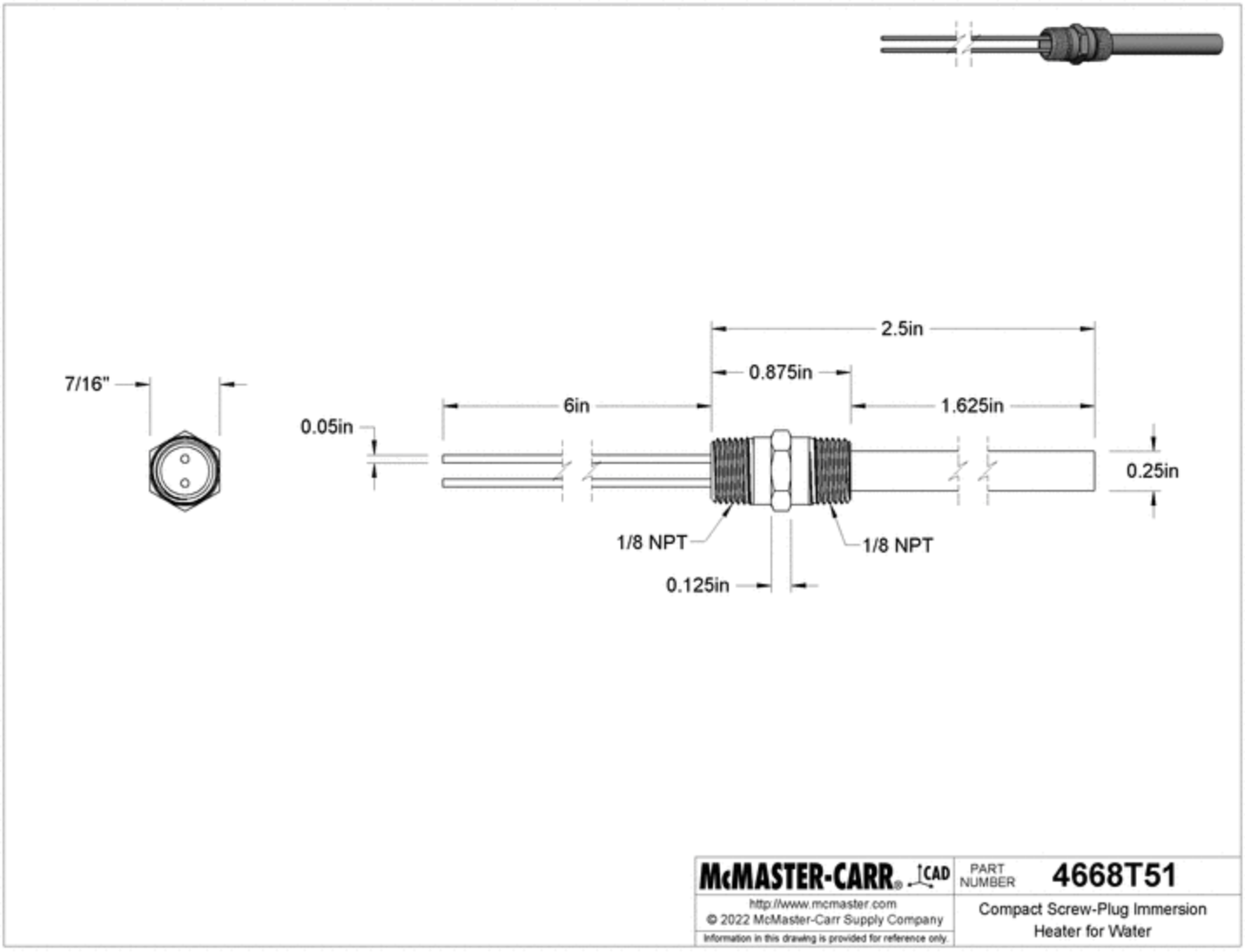

The information in this 3-D model is provided for reference only.

Actual product may not be shown

S102951PD3E120AC1

Category: **Embedment RTDs**

List Price: $343.30	Quantity: 1	ADD TO CART (https://shop.minco.com/handlers/addtocart.ashx?productId=S102951PD3E120AC1&stock=1&imageUrl=https://dpk3n3gg92jwt.cloudfront.r

Product Details

○ English ◉ Metric

Minco miniature embedment RTDs feature a variety of mounting methods, including: spring loading or potting in drilled holes and factory applied babbitt metal tip to reduce overheating of the senors when installed in babbitt layer. They also feature standard lead wire options of PTFE lead wire, PTFE lead wire with a stainless steel overbraid for added durability or PTFE lead wires with stainless steel overbraid and a Teflon sleeve filled with elastomer for rugged cable that prevents migration of oil along the cable.

Element Type	Platinum, Single
Resistance	100 Ω ±0.12% at 0°C (Meets EN60751, Class B)
TCR	0.00385 Ω/Ω/°C
Diameter (mm)	4.78
Length (mm)	6.35
Case Style	B

For applications requiring:

- Reliable and rapid response
- Installation in small space
- Rough handling and harsh environments
- Temperature range of -50 to 260°C (-58 to 500°F)

Lead Length (mm)	3,048
# Leads (each)	3
Lead Wire	AWG #24
Time Constant (seconds)	2.5 seconds typical, in moving water at 1 m/s
Lead Jacket	FEP over stainless steel braid, with\n elastomer fill and PTFE insulated leads
Accessory Description	Supplied with AC171 spring and AC172 series ring (case style B only)
Flange Diameter (mm)	6.4
Base Model	S102951
Element Code	PD
Approval Area	Zone 0 & 1
Temperature Range	-50 to 125°C (-58 to 257°F)
Intrinsically Safe	II 1 G Ex ia IIC T6...T3 Ga
Increased Safety	II 2 G Ex e IIC T6...T3 Gb

Documentation	
Technical Specification	MCTS Intrinsically Safe Increased Saf... (https://dpk3n3gg92jwt.cloudfront.net/domai Intrinsically Safe Increased Safety embedmer

SUBMINIATURE FLUSH DIAPHRAGM PRESSURE TRANSDUCER
WITH 3/8-24 THREAD

0-200 to 0-10,000 psi
0-13.8 to 0-689 bar

PX600 Series

NIST CE RoHS

Standard

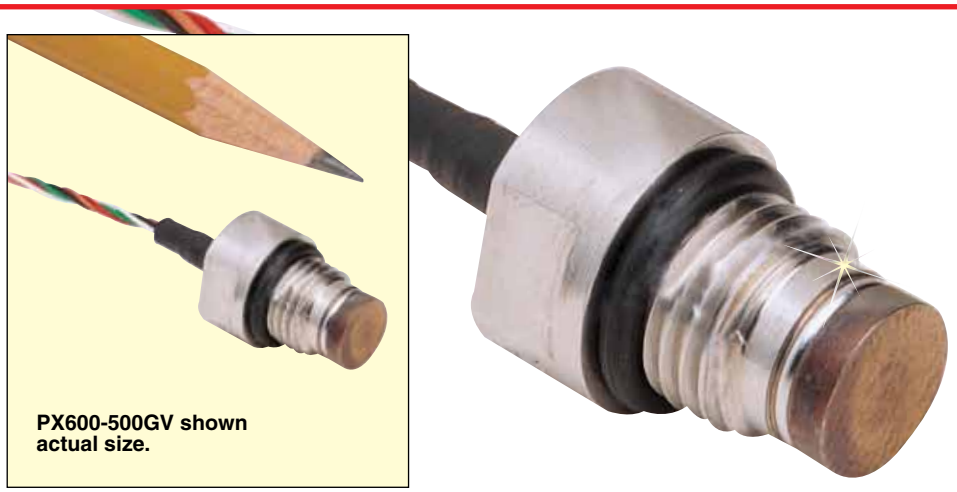

PX600-500GV shown actual size.

- **All Stainless Steel Diaphragm and Threaded Sidewall Construction**
- **Rugged Stainless Steel Case Protects Components in Industrial Environments**
- **Uses a Standard 5 Vdc Regulated Power Supply for Maximum Versatility**
- **Custom Subminiature Design Techniques Provide Small Size and Preserve Accuracy**

Dimensions: mm (inch)

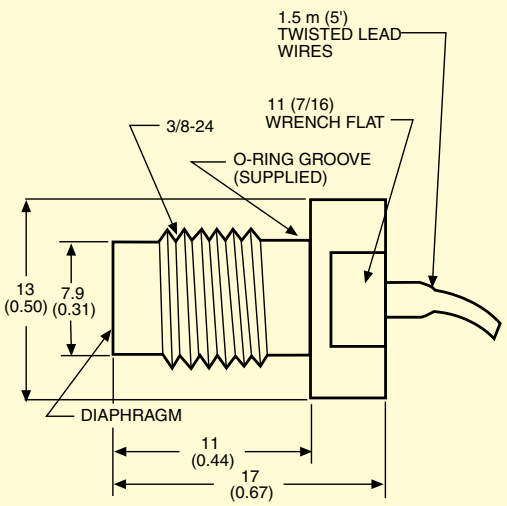

WIRING CODE

RED = +EXC
BLK = - EXC
GREEN = - OUT
WHITE = +OUT

SPECIFICATIONS

Excitation: 5 Vdc @15 mA
Output: 10 mV typical @ 5 Vdc
Sensitivity: 2 mV/V nominal
Input Impedance: 350 Ω min
Output Resistance: 350 Ω min
Insulation Resistance: 5 MΩ @ 75 Vdc
Accuracy: ±1% FS
(linearity and hysteresis combined)
Repeatability: ±0.1% FS
Zero Balance: ±3% FS
Operating Temperature Range:
-54 to 121°C (-65 to 250°F)
Compensated Temperature Range:
16 to 71°C (60 to 160°F)
Thermal Zero Effect: <±0.018% full scale/°C
Thermal Sensitivity Effect: ±0.036% reading/°C
Proof Pressure: 150% range
Burst Pressure: 400% range
Body and Diaphragm Material:
17-4 PH stainless steel
O-Ring: 2-011, FKM
Electrical Connection: 4-conductor cable
Weight: 14 g (0.5 oz)

To Order

RANGE		MODEL NO.	COMPATIBLE METERS
psig	bar		
0 to 200	0 to 13.8	**PX600-200GV**	DP41-S**, DP25B-S**, DP87**
0 to 500	0 to 34.5	**PX600-500GV**	DP41-S**, DP25B-S**, DP87**
0 to 1000	0 to 68.9	**PX600-1KGV**	DP41-S**, DP25B-S**, DP87**
0 to 2000	0 to138	**PX600-2KGV**	DP41-S**, DP25B-S**, DP87**
0 to 3000	0 to 207	**PX600-3KGV**	DP41-S**, DP25B-S**, DP87**
0 to 5000	0 to 345	**PX600-5KGV**	DP41-S**, DP25B-S**, DP87**
0 to 10,000	0 to 689	**PX600-10KGV**	DP41-S**, DP25B-S**, DP87**

ACCESSORIES

MODEL NO.	DESCRIPTION
2-011-P	Polyvinyl O-rings, 10 pack
2-011-V	FKM O-rings, 10 pack

Comes complete with 5-point calibration and FKM O-rings.
***** Meter excitation voltage requires field adjustment by customer to 5 Vdc.*
***Ordering Example: PX600-200GV,** 200 psig subminiature transducer.*

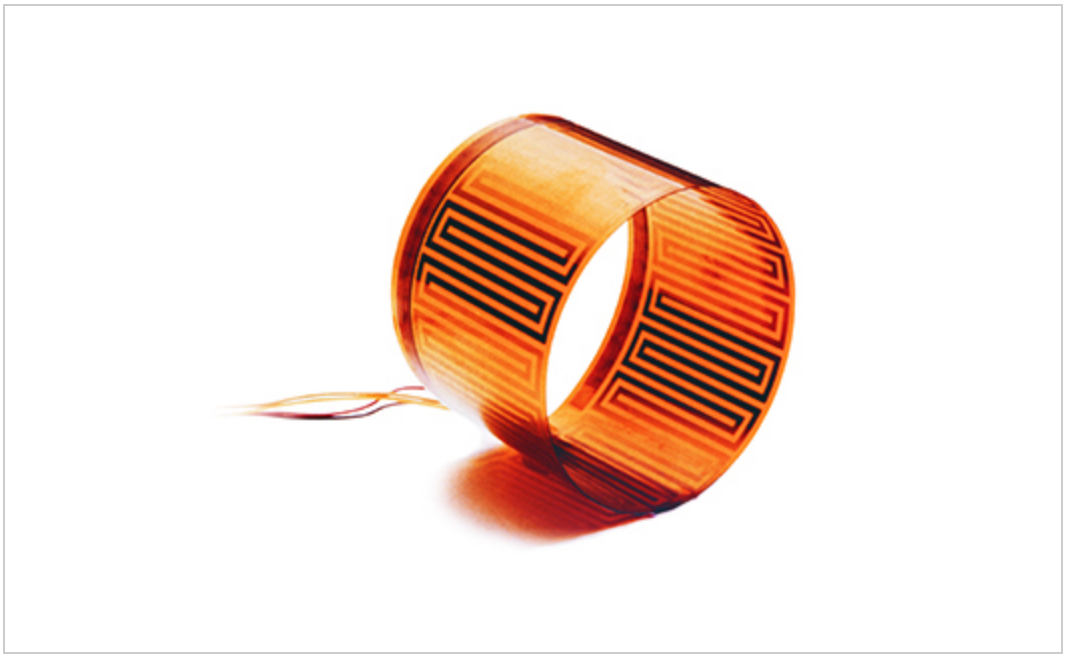

Actual product may not be shown

HK6910

Category: **Polyimide Thermofoil™ Heaters**

List Price: $89.15	Quantity: 1	ADD TO CART (https://shop.minco.com/handlers/addtocart.ashx?productId=HK6910&stock=1&imageUrl=https://dpk3n3gg92jwt.cloudfront.net/domains/mir

Product Details

○ English ◉ Metric

Provides heat where it's needed to reduce operating costs.

Fast and efficient thermal transfer. Uniform thermal performance by custom profiling. Customized options for turnkey thermal solutions.

Custom options:

- Customized options (i.e. SMT components, flex leads, connectors, and laminated to heatsinks) offer

Mounting	Acrylic Adhesive (PSA)
Thickness (mm)	1.52
Min Temp (°C)	-32
Max Temp (°C)	100
Weight (g)	2.27
Style	Etched Kapton/WA

turnkey solutions to drastically reduce assembly time and increase productivity
- Custom profiling gives uniform thermal performance of the heating output to improve processing yields and productivity
- Custom shapes and sizes:
  - Polyimide / FEP – 22" x 42" (560 x 1065 mm)
  - Polyimide / WA/ULA – 22 ” x 72” (560 x 1825 mm)
- Custom resistance:
  - Polyimide / FEP – 450 Ω/in^2 (70 Ω/cm^2)
  - Polyimide / WA/ULA – 1500 Ω/in^2 (233 Ω/cm^2)
- WA or ULA internal adhesive is more economical than FEP for most custom designs that operate below 150°C
- NASA approval is available in nearly all of the standard size Polyimide heaters
- TÜV or UL recognition marking is optional
- Tighter resistance tolerance
- RoHS compliance

X dim (mm)	25.4
Y dim (mm)	127.0
R (Ω)	18.65
AWG	26
Area (in^2)	4.2032
Volt	28.00
Watt	42.0
Watt Density (w/in^2)	10.00

Documentation	
Product Drawing	HK6910.pdf (https://dpk3n3gg92jwt.cloudfront.net/domains/m

Innovation in Miniature

LEE®

ELECTRO-FLUIDIC SYSTEMS

PRODUCT DATA SHEET

IEP EXTENDED PERFORMANCE SOLENOID VALVE

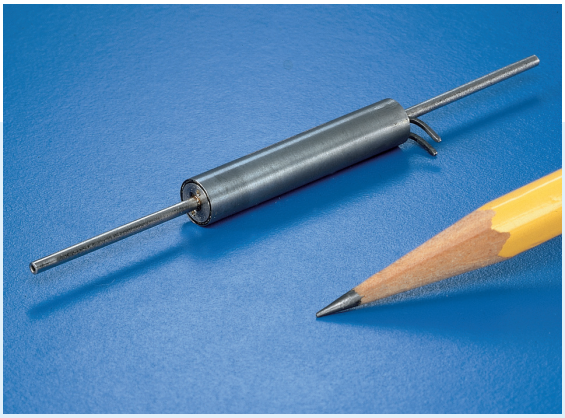

The Lee Company's IEP Series Extended Performance Solenoid Valve is designed to perform consistently under conditions that are far more demanding than typical high-speed dispensing applications. Available in a 2-way, normally closed, axial flow configuration, this compact solenoid valve expands on the operating pressure and temperature range capabilities of Lee's micro-dispense valves without compromising reliability.

Featuring welded stainless-steel construction and a wide selection of seal elastomers, this robust valve is suitable for flowing both gases and liquids in extreme environments. The valve design was optimized to achieve a perfect balance between switching and sealing performance making it ideal for a wide variety of applications such as CubeSat propulsion, precision combustion systems, gas chromatography, scanning electron microscopes, medical devices and other OEM applications.

Performance parameters can be optimized to meet specific application requirements. Contact your Lee Sales Engineer for additional technical assistance and application information.

- Compact size
- Light weight: 4.7 grams
- Low internal volume: 62 µL
- Operating pressures up to 800 psig
- Operating temperatures up to 275°F (135°C)
- Flow capacity: 4100 Lohms (54 SLPM @ 800 psid, air; 70°F, Ref. Cv = 0.005)
- Response time as fast as 0.5 ms
- Spike & hold drive required (reference Lee drawing number LFIX1002250A for schematic)
- Wetted materials: FeCr alloy, 316 SS and seal material
- Recommended filtration: 17 microns

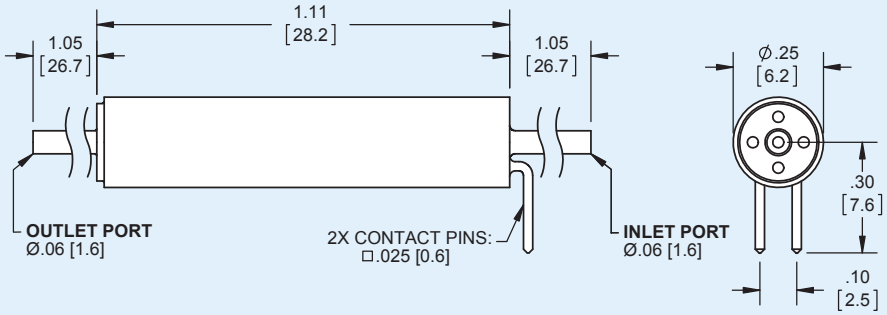

PART NUMBER	SPIKE VOLTAGE (Vdc)	HOLD VOLTAGE (Vdc)	POWER AT HOLDING VOLTAGE (mW)	OPERATING PRESSURE RANGE (psig)	AMBIENT TEMPERATURE RANGE	SEAL MATERIAL
IEPA1211541H	12	1.6	250	0-300	40 to 120°F (4 to 49°C)	FFKM
IEPA2411541H	24	3.0	250	0-300	40 to 120°F (4 to 49°C)	FFKM
IEPA1221541H	12	1.6	250	0-300	40 to 275°F (4 to 135°C)	FFKM
IEPA2421541H	24	3.0	250	0-300	40 to 275°F (4 to 135°C)	FFKM
IEPA1211241H	12	1.6	250	0-800	-20 to 120°F (-29 to 49°C)	EPDM
IEPA2411241H	24	3.0	250	0-800	-20 to 120°F (-29 to 49°C)	EPDM

**The Lohm is a measure of flow resistance. Additional information can be found on the reverse side and at www.theleeco.com.*

The Lee Company • 2 Pettipaug Road, PO Box 424, Westbrook, Connecticut 06498-0424
Tel: 860-399-6281 • Fax: 860-399-7037 • www.theleeco.com

LEE LOHM LAWS

The Lohm Laws are a simple system of defining the fluid resistance of Lee components. Just as the "Ohm" is used in the electrical industry, we can use the "Liquid Ohm" or "Lohm" to quantify the resistance to flow of any fluid control component. When using the Lohm system, you can forget about coefficients of discharge and dimensional tolerances on drilled holes. These factors are automatically compensated for in the Lohm calculations, and confirmed by testing each component to establish flow tolerances.

LOHM LAWS (liquids)

The Lohm has been selected so that a 1 Lohm restriction will permit a flow of 100 gallons per minute of water with a pressure drop of 25 psi at a temperature of 80°F.

The following formulas are presented to extend the use of the Lohm laws to many different liquids, operating over a wide range of pressure conditions.

These formulas introduce compensation factors for liquid density and viscosity. They are applicable to any liquid of known properties, with minimum restrictions on pressure levels or temperature.

The units constant (K) eliminates the need to convert pressure and flow parameters to special units.

Volumetric Flow Units $L = \frac{KV}{I}\sqrt{\frac{H}{S}}$

Gravimetric Flow Units $L = \frac{KV}{w}\sqrt{HS}$

LIQUID FLOW – UNITS CONSTANT K

VOLUMETRIC FLOW UNITS			
	Pressure Units		
Flow Units	psi	bar	kPa
GPM	20	76.2	7.62
L/min	75.7	288	28.8
ml/min	75700	288000	28800
in^3/min	4620	17600	1760

GRAVIMETRIC FLOW UNITS			
	Pressure Units		
Flow Units	psi	bar	kPa
PPH	10000	38100	3810
gm/min	75700	288000	28800

NOMENCLATURE, Liquids

- L = Lohms
- S = Specific gravity*
- H = Differential pressure
- V = Viscosity compensation factor**
- I = Liquid flow rate: Volumetric
- w = Liquid flow rate: Gravimetric
- K = Units Constant – Liquid (see chart left)
- *S = 1.0 for water at 80°F.
- **V = 1.0 for water at 80°F.

(For other fluids and temperatures, contact your Lee Sales Engineer or visit us at www.theleeco.com)

LOHM LAWS (gases)

The Lohm has been selected so that a 100 Lohm restriction will permit a flow of 250 standard liters per minute of nitrogen at a temperature of 59°F, and an upsteam pressure of 90 psia discharging to atmosphere.

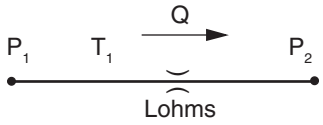

$$L = \frac{K\, f_T\, P_1}{Q} \quad \text{(Sonic region) i.e. } P_1/P_2 \geq 1.9$$

$$L = \frac{2\, K\, f_T \sqrt{\Delta P\, P_2}}{Q} \quad \text{(Subsonic region) i.e. } P_1/P_2 < 1.9$$

GAS FLOW – UNITS CONSTANT K

To eliminate the need to convert pressure and flow parameters into specific units such as "psia" and "std L/min.", the table below lists values of the Units Constant "K", which is used in the Gas Flow Lohm Formulas:

VOLUMETRIC FLOW UNITS							
Abs. Pres	psia			bar		kPa	mm.Hg
Flow	SLPM	SCFM	in^3/min	SLPM	SCFM	SLPM	mL/min
He	771	27.2	47100	11200	395	112	14900
N_2	276	9.73	16800	4000	141	40.0	5330
Air	271	9.56	16500	3930	139	39.3	5230
O_2	257	9.08	15700	3730	132	37.3	4970
CO_2	213	7.52	13000	3090	109	30.9	4110

For more information on Lohms, visit us at www.theleeco.com or contact your Lee Sales Engineer.

NOMENCLATURE, Gases

- L = Lohms
- K = Units Constant – Gas (see chart left)
- f_T = Temperature correction factor
- P_1 = Upstream absolute pressure
- P_2 = Downstream absolute pressure
- Q = Gas flow rate
- $\Delta P = P_1 - P_2$

1. Compute the P_1/P_2 pressure ratio.
2. Select the correct formula for the flow region.
3. Look up the value of "K" for the gas.
4. Determine the temperature correction factor, " f_T".
   f_T = 1.0 @ room temperature (70°F)

$$f_T = \sqrt{\frac{530}{T\,(°F) + 460}}$$

5. Use the formula to solve for the unknown.

The Lee Company • 2 Pettipaug Road, PO Box 424, Westbrook, Connecticut 06498-0424
Tel: 860-399-6281 • Fax: 860-399-7037 • www.theleeco.com

VisiJet® M2R-CL

Clear Plastic

ProJet MJP 2500

Rigid general-purpose plastic with translucent clear finish delivering a balance of strength and elongation with a moderate HDT

Similar to the VisiJet M2R-WT (white) and VisiJet M2R-GRY (gray), Visijet M2R-CL is a rigid material that is good for a broad range of concept models and functional prototypes. It is optically clear and has high feature fidelity, sharp corners and edges and smooth surface finish. It is a general-purpose material with high accuracy suitable for prototypes, printed assemblies, medical/dental applications and some end-use parts. Able to make extremely small and complex internal structures for microfluidics and flow visualization.

Note: Not all products and materials are available in all countries — please consult your local sales representative for availability.

APPLICATIONS

- Translucent functional prototypes and some end-use parts
- Rapid prototyping of plastic injection molded thermoplastic parts
- Able to be drilled, tapped and machined and can create moderate functional snap fits
- Functional printed assemblies and injection molded screw bosses
- Functional printed screw-threads and thin walls
- Medical/dental applications like surgical guides
- Translucent flow visualization and dye-tinted applications
- Optically clear sight windows in fixtures
- Excellent for microfluidics, capillary fluidics and lab-on-a-chip

BENEFITS

- High fidelity fine features, sharp edges and high accuracy
- Exceptional smooth and consistent surface finish
- Excellent optical clarity
- No surface cure inhibition of paints or silicones; no sanding required
- Excellent for painting or molding applications

FEATURES

- Moderate strength and stiffness, 20-30% elongation
- Able to make extremely small and complex internal structures
- High accuracy and watertight
- Biocompatible USP Class VI & ISO 10993

MATERIAL PROPERTIES

The full suite of mechanical properties is given per ASTM and ISO standards where applicable. Properties like flammability, dielectric properties and 24-hour water absorption are also provided for better understanding of material capabilities to help design decisions using the material. All parts are conditioned per ASTM recommended standards for a minimum of 40 hrs at 23°C, 50% RH.

Solid material properties reported were printed along the vertical axis (ZX-orientation). As detailed in the Isotropic Properties section, VisiJet material properties are relatively uniform across print orientations. Parts do not need to be oriented in a particular direction to exhibit these properties.

LIQUID MATERIAL	
Color	Clear

SOLID MATERIAL						
METRIC	ASTM METHOD	METRIC	ENGLISH	ISO METHOD	METRIC	ENGLISH
PHYSICAL				PHYSICAL		
Solid Density	ASTM D792	1.16 g/cm³	0.042 lb/in³	ISO 1183	1.16 g/cm³	0.042 lb/in³
24 Hour Water Absorption	ASTM D570	≤0.5%	≤0.5%	ISO 62	≤0.5%	≤0.5%
MECHANICAL				MECHANICAL		
Tensile Strength Ultimate	ASTM D638 Type IV	50 MPa	7200 psi	ISO 527 -1/2	43 MPa	6200 psi
Tensile Strength at Yield	ASTM D638 Type IV	50 MPa	7200 psi	ISO 527 -1/2	42.8 MPa	6200 psi
Tensile Modulus	ASTM D638 Type IV	2200 MPa	330 ksi	ISO 527 -1/2	2500 MPa	359 ksi
Elongation at Break	ASTM D638 Type IV	11 %	11 %	ISO 527 -1/2	18 %	18 %
Elongation at Yield	ASTM D638 Type IV	4.2 %	4.2 %	ISO 527 -1/2	4 %	4 %
Flex Strength	ASTM D790	65 MPa	9400 psi	ISO 178	60 MPa	8100 psi
Flex Modulus	ASTM D790	1900 MPa	270 ksi	ISO 178	2200 MPa	314 ksi
Izod Notched Impact	ASTM D256	15 J/m	0.3 ft-lb/in	ISO 180-A	1.9 kJ/m²	0.9 ft-lb/in²
Izod Unnotched impact	ASTM D4812	400 J/m	8 ft-lb/in	ISO 180-U		
Shore Hardness	ASTM D2240	79 D	79 D	ISO 7619	79 D	79 D
THERMAL				THERMAL		
Tg (DMA E")	ASTM E1640 (E"Peak)	40 C	111 F	ISO 6721-1/11 (E" Peak)	40 C	111 F
HDT 0.455MPa/66PSI	ASTM D648	49 C	119 F	ISO 75- 1/2 B	43 C	109 F
HDT 1.82MPa/264 PSI	ASTM D648	44 C	112 F	ISO 75-1/2 A	38 C	101 F
CTE -20 to 70C	ASTM E831	94 ppm/C	52 ppm/F	ISO 11359-2	94 ppm/K	52 ppm/F
CTE 95 to 180C	ASTM E831	181 ppm/C	101 ppm/F	ISO 11359-2	181 ppm/K	101 ppm/F
UL Flammability Rating		HB				
ELECTRICAL				ELECTRICAL		
Dielectric Strength (kV/mm) @ 3.0 mm thickness	ASTM D149	400				
Dielectric Constant @ 1 MHz	ASTM D150	3.15				
Dissipation Factor @ 1 MHz	ASTM D150	0.019				
Volume Resistivity (ohm-cm)	ASTM D257	6.94E+15				

ISOTROPIC PROPERTIES

MultiJet Printing (MJP) technology prints parts that are generally isotropic in mechanical properties meaning the parts printed along either the XYZ axis will give similar results.

Parts do not need to be oriented to get the highest mechanical properties, further improving the degree of freedom for part orientation for mechanical properties.

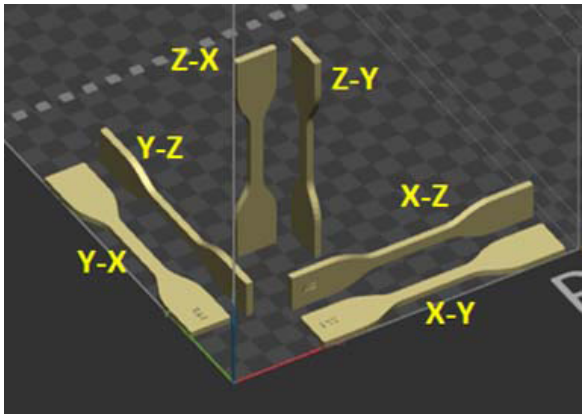

SOLID MATERIAL								
METRIC	METHOD	METRIC						
MECHANICAL								
		XY	XZ	YX	YZ	Z45	ZX	ZY
Tensile Strength Ultimate	ASTM D638 Type IV	50 MPa	44 MPa	42 MPa	39 MPa	40 MPa	36 MPa	34 MPa
Tensile Strength at Yield	ASTM D638 Type IV	50 MPa	45 MPa	41 MPa	40 MPa	41 MPa	37 MPa	33 MPa
Tensile Modulus	ASTM D638 Type IV	2200 MPa	2100 MPa	1980 MPa	2120 MPa	1750 MPa	1780 MPa	1700 MPa
Elongation at Break	ASTM D638 Type IV	11 %	14 %	16 %	18.5 %	23.1 %	14 %	15.4 %
Elongation at Yield	ASTM D638 Type IV	4.2 %	4.3 %	4.5 %	4.2 %	4.3 %	4.3 %	4.2 %
Flex Strength	ASTM D790	65 MPa	50 MPa	59 MPa	47 MPa	58 MPa	50 MPa	46 MPa
Flex Modulus	ASTM D790	1900 MPa	1460 MPa	1880 MPa	1400 MPa	1670 MPa	1420 MPa	1330 MPa
Izod Notched Impact	ASTM D256	15 J/m	16 J/m	16 J/m	16 J/m	13 J/m	16 J/m	16 J/m
Shore Hardness	ASTM D2240	79 D	78 D	76 D	78 D	78 D	78 D	78 D

STRESS-STRAIN CURVE

The graph represents the stress-strain curve for VisiJet M2R-CL per ASTM D638 testing.

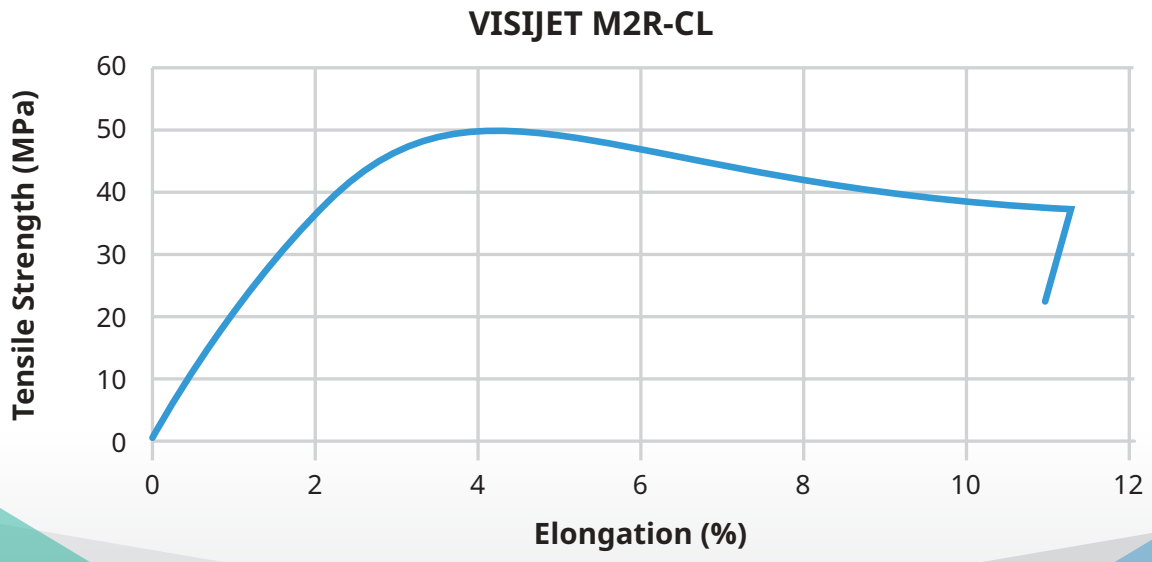

LONG TERM ENVIRONMENTAL STABILITY

VisiJet M2R-CL is engineered to give long-term environmental UV and humidity stability. This means the material is tested for the ability to retain a high percent of the initial mechanical properties over a given period of time. This provides real design conditions to consider for the application or part. **Actual data value is on Y-axis, and data points are % of initial value.**

INDOOR STABILITY

INDOOR STABILITY: Tested per ASTM D4329 standard method.

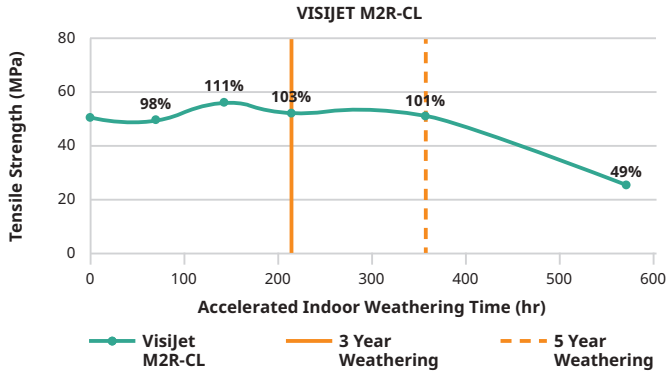

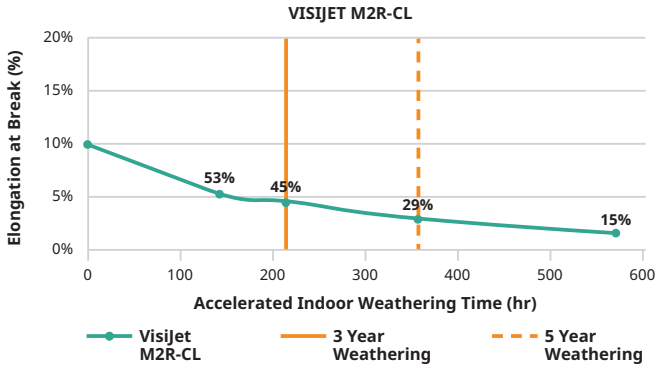

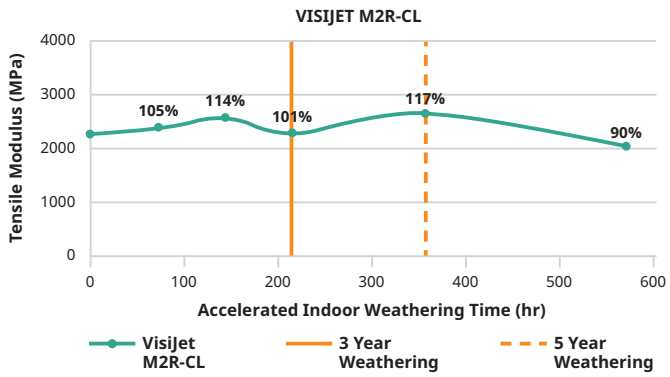

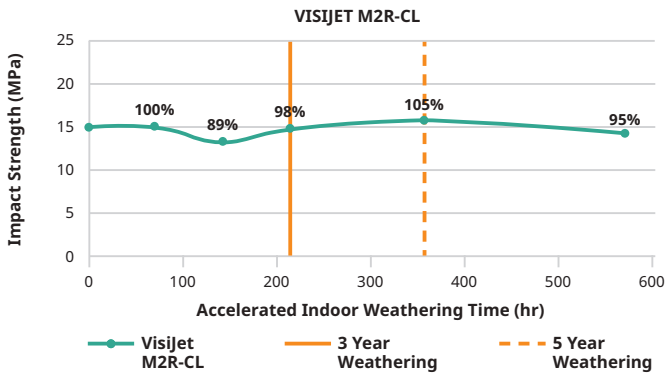

OUTDOOR STABILITY

OUTDOOR STABILITY: Tested per ASTM G154 standard method.

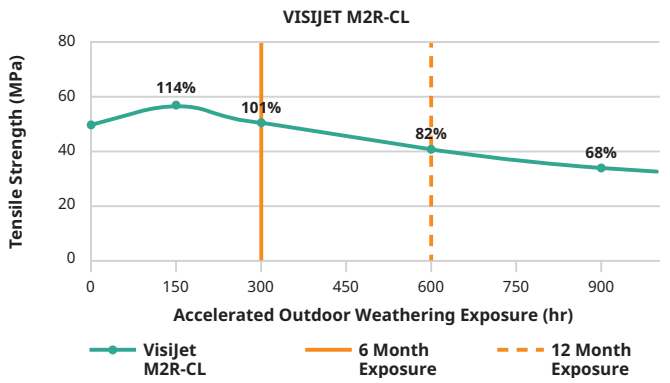

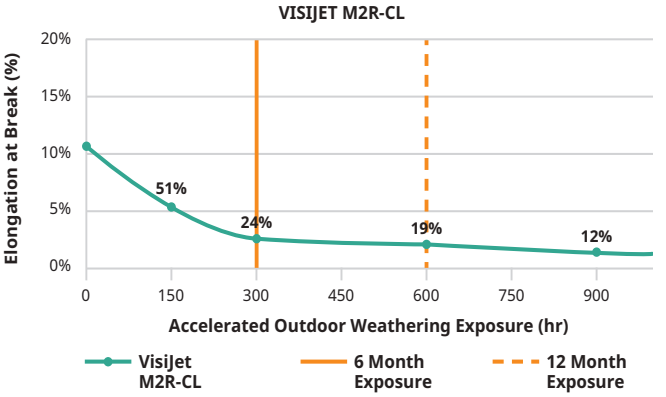

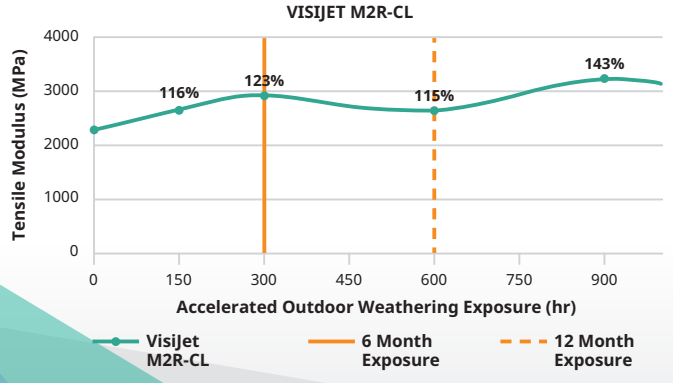

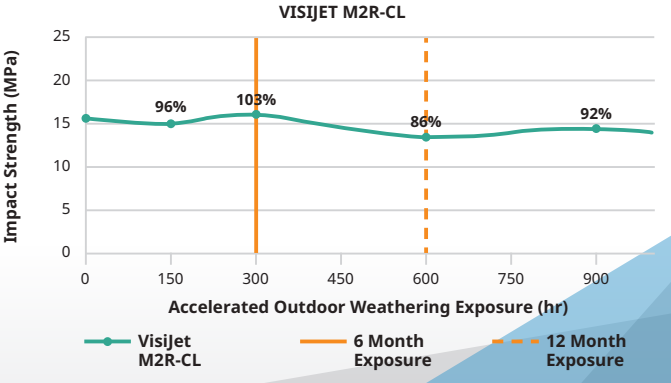

AUTOMOTIVE FLUID COMPATIBILITY

The compatibility of a material with hydrocarbons and cleaning chemicals is critical to part application. VisiJet M2R-CL parts were tested for sealed and surface contact compatibility per USCAR2 test conditions. The fluids below were tested in two different ways per the specs.

- Immerse for 7-days, then take mechanical property data for comparison.
- Immerse for 30-minutes, remove and take mechanical property data for comparison in 7-days.

Data reflects the measured value of properties over that period of time.

AUTOMOTIVE FLUIDS		
FLUID	**SPECIFICATION**	**TEST TEMP °C**
Gasoline	ISO 1817, liquid C	23 ± 5
Diesel Fuel	905 ISO 1817, Oil No. 3 + 10% p-xylene*	23 ± 5
Engine Oil	ISO 1817, Oil No. 2	50 ± 3
Ethanol	85% Ethanol + 15% ISO 1817 liquid C*	23 ± 5
Power Steering Fluid	ISO 1917, Oil No. 3	50 ± 3
Automative Transmission Fluid	Dexron VI (North American specific material)	50 ± 3
Engine Coolant	50% ethylene glycol + 50% distilled water*	50 ± 3
Brake Fluid	SAE RM66xx (Use latest available fluid for xx)	50 ± 3
Diesel Exhaust Fluid (DEF)	API certified per ISO 22241	23 ± 5

*Solutions are determined as percent by volume

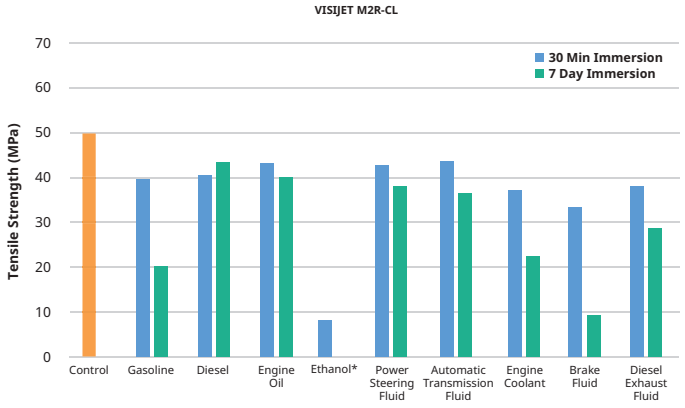

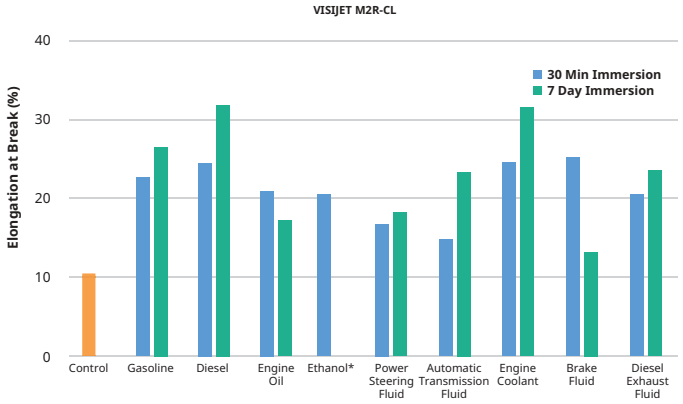

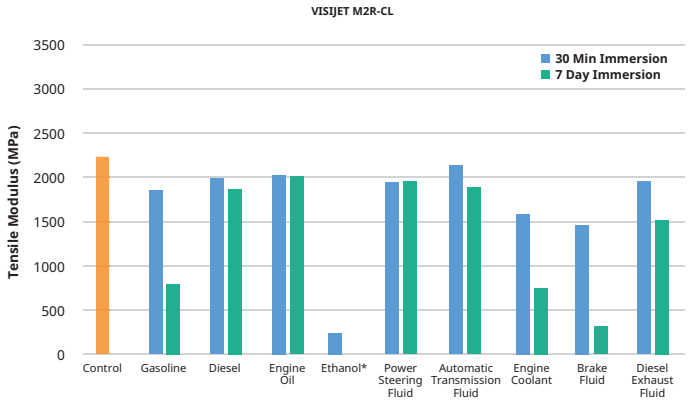

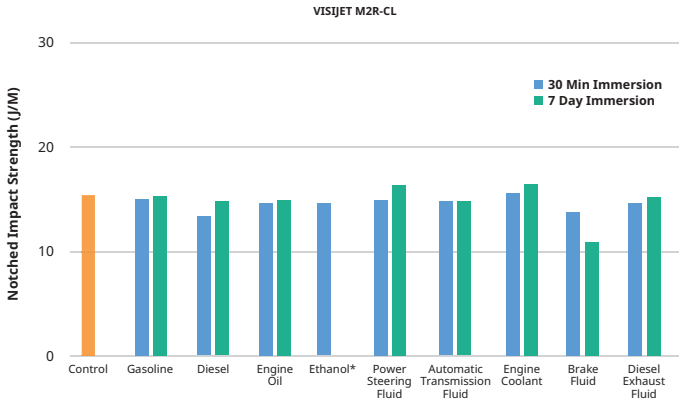

CHEMICAL COMPATIBILITY

The compatibility of a material with cleaning chemicals is critical to part application. VisiJet M2R-CL parts were tested for sealed and surface contact compatibility per ASTM D543 test conditions. The fluids below were tested in two different ways per the specs.

- Immerse for 7-days, then take mechanical property data for comparison.
- Immerse for 30-minutes, remove, and take mechanical property data for comparison in 7-days.

Data reflects the measured value of properties over that period of time.

*Denotes materials did not go through 7-day soak conditioning.

CHEMICAL COMPATIBILITY
6.3.3 Acetone
6.3.12 Detergent Solution, Heavy Duty
6.3.23 Hydrochloric Acid (10%)
6.3.38 Sodium Carbonate Solution (20%)
6.3.44 Sodium Hypochlorite Solution
6.3.46 Sulfuric Acid (30%)
6.3.42 Sodium Hydroxide Solution (10%)
6.3.15 Distilled Water

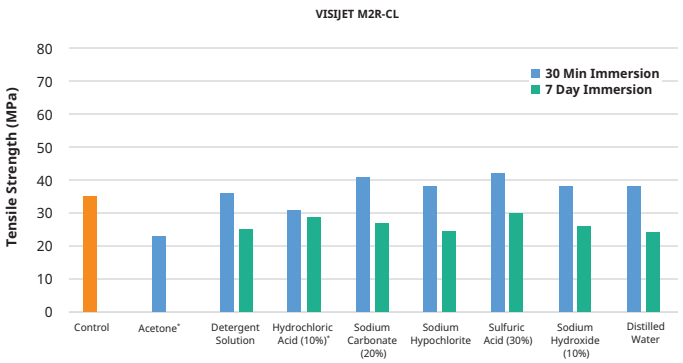

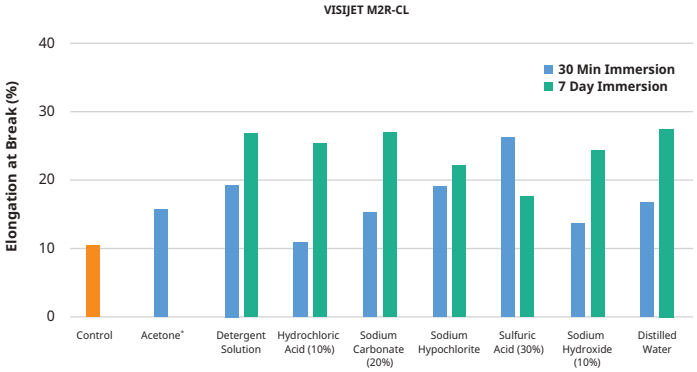

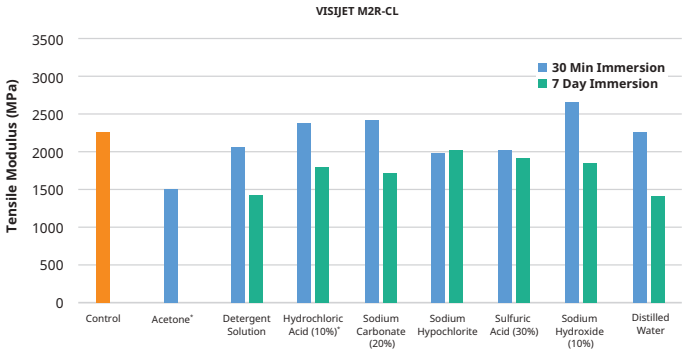

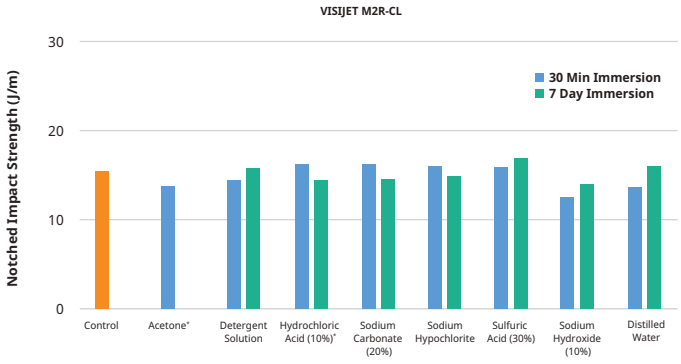

VISIJET M2R-CL BIOCOMPATIBILITY POST-PROCESS

- Remove wax support in an oven
- Clean with EZ Rinse-C or mineral oil
- Ethyl alcohol (ethanol) rinse with sonication
- Second fresh high purity ethanol rinse with sonication
- Air dry